ATTENTION: The Singapore Copyright Act applies to the use of this document. Nanyang Technological University Library

Structural Analysis and Design of Porous Media Materials

Kapil Mohan

School of Materials Science and Engineering

A thesis submitted to Nanyang Technological University
in partial fulfillment of the requirements
for the Degree of Doctor of Philosophy

March 2007

ATTENTION: The Singapore Copyright Act applies to the use of this document. Nanyang Technological University Library

Abstract

Metallic foams are a new class of cellular materials (composites) with attractive physical, mechanical, acoustical, thermal and electrical properties. These foams can be produced by a variety of manufacturing routes to relative densities as low as 3%. They have applications in light weight structural design, energy management devices as car bumpers, heat sinks, and noise absorbing devices. The structural performance of these metallic foams is enhanced by bonding them in between two strong and stiff face sheets. In this work, the mechanical performance of sandwich structures comprising of Aluminum alloy foam and a variety of face sheet materials was investigated under different loading conditions.

The elastic stiffness, failure load and mechanism of hybrid sandwich beams with (a) Al foam core and Alumina face sheets, and (b) Al foam core and carbon fiber reinforced polymer face sheets were measured through instrumented bending tests. For a range of beam geometries, materials properties of three competing failure modes: face sheet cracking, core shear and core local indentation, were identified. The failure loads were compared with the analytical formulae. The identified failure modes are also checked with finite element simulations. The phenomenon logical metal foam yield surface, which is a quadratic function of mean stress and effective stress, and is inbuilt in the ABAQUS commercial finite element package, was used to simulate the metal foam core yield behavior. For these sandwich beams, a failure mode map was generated in the normalized face sheet thickness and core thickness, (for a given thickness of face sheet and strength ratio of face sheet that of core). For a range of practical structural load indices, minimum weight design was obtained.

Secondly, the quasi-static indentation response of Aluminum foams with face sheets representing elastic (Alumia, CFRP), elastic-ideally plastic (Al) and elastic-plastic strain hardening (Stainless Steel) behavior was measured. Indentation tests were carried out using stiff tool steel flat and hemispherical indenters on the blocks of Aluminum foam with and without face sheets. The thickness of the face sheets was varied from 0.5 to 1.0 mm to evaluate the effect of thickness on the indentation behavior. Competing failure modes for the initiation of failure are discussed. Face sheet bending, face sheet cracking, face sheet yielding and local indentation were found to be the dominant failure modes occurring under indentation. Effect of the type of indenter on failure modes for those structures under

ATTENTION: The Singapore Copyright Act applies to the use of this document. Nanyang Technological University Library

indentation is also indicated. The results showed that the indentation behavior was strongly dependent on the type and thickness of face sheets used.

Thirdly, low velocity impact response of aluminum foams with face sheets representing elastic (Alumia, CFRP), elastic-ideally plastic (Al) and elastic-plastic strain hardening (Stainless Steel) behavior was measured experimentally. A steel spherical impactor of 2.65 kg and velocity 6.7 m/s was used to impact the rigidly fixed structures. The energy absorption of these structures was compared. Face sheet punching was found to be the only final failure mechanism for structure with different face sheets except Stainless Steel (SS), but the amount of energy absorption depends on the type of face sheet. Foam with SS face sheet absorbed almost all the impact energy and proved to be the best choice as an energy absorber in comparison to blocks with other face sheets. Also, the enhancement in energy absorption capability of foam filled rectangular tubes was studied under quasi-static compression load. In this case, Interaction effect between foam and tube and role of adhesive was also investigated in terms of energy absorption capability of those tubes.

Finally, an overview was established for different competing failure modes for sandwich columns with Alporas foams having Al face sheets under end compression loading. Euler buckling, core shear and face sheet yielding were found to be competitive failure mechanisms. Failure mode map design for these sandwich columns was constructed as a function of ratio of thickness of face sheet to core, and ratio of thickness of core to length of the beam, for a given ratio of Young's modulus of face sheet to strength of the foam, and shear modulus of foam to strength of the foam core. Minimum weight design calculations were carried out for a range of load carrying capacity.

ATTENTION: The Singapore Copyright Act applies to the use of this document. Nanyang Technological University Library

Acknowledgements

I am deeply grateful to my supervisor Asst. Prof. Dr. Yip Tick Hon for giving me the opportunity to work with him. I am indebted to him for his constant guidance, moral and academic support. His commitment to hard work and discipline has inspired me though the course of this study.

I would like to express my sincere thanks to Asst. Prof. Dr. Sridhar Idapalapati for helping me during crucial issues of my research. While working with him, I learned to explore new ideas as well as to trust my abilities and intuition. Not only his vast knowledge of the field, but his dedication to the research has been an inspiration to me.

Special thanks are due to all the technicians of School of MSE, especially Mr. Eric and Mr. Kek Koon for their assistance and support. I would also like to thank all the staffs of Materials Laboratory A and B, for providing a cheerful working environment during the progress of my research work.

I am short of words when it comes to thank my parents and brother Prashant for their continuous support and inspiration. Their sacrifices and a strong belief in me have helped me to achieve my goals. I want to thank specially to my wife Anjali who fill my life full of love and help me in fulfilling my goals of life. I thank my friends Shashi, Rama, Akhilesh, Vijay, Reju, Rakesh, Xu Cong, Qiaoyan, Ramki, and Madhu who made the research environment comfortable around me. I also heartily address the existence of God, and fully accept that without his mercy nothing would have been possible.

ATTENTION: The Singapore Copyright Act applies to the use of this document. Nanyang Technological University Library

Table of Contents

Abstract I
Acknowledgements III
Table of Contents IV
List of Figures X
List of Tables XV
List of Abbreviations and Symbols XVI
CHAPTER- 1 1
Introduction 1
1.1 Background and motivation 1
1.2 Objectives 2
1.3 Scope of the present work 3
1.4 Thesis organization 3
CHAPTER 2 5
Literature Review 5
2.1 Foam 5
2.2 Aluminum foams 6
2.2.1 Production methods of metal foams 6
2.2.2 Types of aluminum foams 7
2.2.3 Manufacturing process for Alporas foam 7
2.2.4 Manufacturing process for Cymat foam 8
2.2.5 Manufacturing process for open cell Duocel 8
2.2.6 Microstructure and cell morphology of aluminum foams 9
2.3 Mechanical behavior of aluminum foam 10
2.3.1 Deformation behavior under different loadings 10
2.3.2 Size effect on deformation behavior of aluminum foams 11
2.4 Surface characterization of Al foams with ultrasonic techniques 13
2.5 Ceramics and CFRP as face sheet material 13
2.5.1 Ceramic material 13
2.5.2 Carbon fiber reinforcement polymer composite material 14
2.6 Sandwich panels with Al foam as core materials 15
2.6.1 Failure of sandwich beams of Al foam core under bending 15
2.6.1.1 Face yield 17

ATTENTION: The Singapore Copyright Act applies to the use of this document. Nanyang Technological University Library

2.6.1.2 Core indentation 17
2.6.1.3 Core shear 18
2.6.2 Failure of sandwich comprising Al foam core on plastic foundation under indentation 19
2.6.3 Failure of sandwich comprising Al foam core under impact 21
2.6.4 Failure of sandwich columns with foam core under end compression 23
2.6.5 Performance of Al foams filled structures under end compression 24
2.7 Failure mechanisms map 26
2.8 Minimum weight design 28
2.9 Finite element analysis 31
2.9.1 Model for metallic foams 31
2.9.1.1 Elastic regime 31
2.9.1.2 Plastic regime 31
2.9.1.2.1 Classical J_2 plasticity: 32
2.9.1.2.2 Crushable foam model: 32
2.9.2 Model for brittle materials 34
2.9.2.1 Brittle cracking model for ceramics 35
2.9.2.2 Model for CFRP 36
2.10 Problem identification 36
CHAPTER-3 38
Characterization of materials 38
3.1 Introduction 38
3.2 Surfaces characterization of Al foams 39
3.2.1 Chemical composition 39
3.2.2 Relative density measurement 39
3.2.3 Cell size measurement 40
3.2.4 Morphology of foam cells 42
3.2.5 Ultrasonic measurement of Alporas Al foams 43
3.2.5.1 Response with ultrasonic testing 45
3.2.5.1.1 Pulse echo technique: 45
3.2.5.1.2 Through transmission technique: 45
3.3 Mechanical characterization of materials 47
3.3.1 The mechanical characterization of foams 48
3.3.1.1 Sample preparation 48

ATTENTION: The Singapore Copyright Act applies to the use of this document. Nanyang Technological University Library

3.3.1.2 Tensile testing 48
3.3.1.3 Uniaxial compression testing 50
3.3.1.4 Shear testing 51
3.3.1.5 Bending 54
3.3.2 Mechanical characterization of face sheets 58
3.3.2.1 Mechanical property of Aluminum and Stainless steel face sheet 59
3.3.2.1.1 Al sheets: 59
3.3.2.1.2 Stainless Steel sheets: 59
3.3.2.2 Mechanical property of alumina and CFRP face sheet 61
3.3.2.2.1 Alumina sheets: 61
3.3.2.2.2CFRP sheets: 62
Chapter- 4 66
Sandwich beam with Al foam core and alumina face sheet under four- point bending 66
4.1 Introduction 66
4.2 Sandwich beam with Al foam core and alumina face sheet under four – point bending 67
4.2.1 Analytical analysis of sandwich beams under four point bending 67
4.2.1.1 Elastic Stiffness 67
4.2.1.2. Estimation of failure loads 68
4.2.1.2.1. Face sheet cracking: 68
4.2.1.2.2 Core indentation: 69
4.2.1.2.3. Core shear: 70
4.2.2 Experimental procedure of testing of sandwich beams under four point bending. 72
4.2.3 Finite element modeling 73
4.2.3.1 Material constitutive modeling 74
4.2.3.2 FE modeling of sandwich beam 74
4.2.4. Comparison of analytical, simulated and experimental results 74
4.2.4.1 Failure mechanisms map for sandwich beam under four point bending 75
4.2.4.2 Face sheet cracking 75
4.2.4.3 Core indentation 80
4.2.4.4 Core shear 82
4.2.5 Minimum weight design 85
Chapter- 5 91
Sandwich beam with Al foam core and CFRP face sheet under three- point bending 91

ATTENTION: The Singapore Copyright Act applies to the use of this document. Nanyang Technological University Library

5.1 Introduction 91
5.2 Sandwich beam with Al foam core and CFRP face sheet under three – point bending 91
5.2.1 Analytical analysis of sandwich beams under three- point bending 92
5.2.1.1 Elastic Stiffness 92
5.2.1.2. Estimation of Failure loads 92
5.2.1.2.1. Face sheet cracking: 92
5.2.1.2.2 Core indentation: 93
5.2.1.2.3. Core shear: 93
5.2.2 Experimental procedure of sandwich beams under three- point bending 94
5.2.2.1 Materials 94
5.2.2.2 Sandwich beam 95
5.2.3 Finite element modeling 95
5.2.4 Failure mechanisms map for sandwich beam under three- point bending 96
5.2.5 Comparison of analytical, numerical results with experimental observations 98
5.2.5.1 Face sheet cracking 98
5.2.5.2 Core indentation 100
5.2.5.3 Core shear 102
5.2.6 Minimum weight design 104
Chapter-6 110
Indentation response of Al foams with different face sheets 110
6.1 Introduction 110
6.2. Sandwich structure with Al foam with and without different face sheets under static indentation 112
6.2.1 Materials for foam core and face sheets 112
6.2.2 Test specimen preparation and experimentation 112
6.2.3 Results and discussion 113
6.2.3.1 Indentation response with flat indenter 113
6.2.3.2. Indentation response with spherical indenter 120
6.2.3.3 Morphological aspects of damaged zones 127
6.2.3.4 Energy absorption 136
Chapter -7 137
Impact response of structures with Al foam and different face sheets 137
7.1 Introduction 137
7.2. Structure with Al foam with and without different face sheets under impact 138

ATTENTION: The Singapore Copyright Act applies to the use of this document. Nanyang Technological University Library

7.2.1 Materials for foam core and face sheets 138
7.2.2 Test specimen preparation and experimentation 138
7.2.3 Results and discussion 141
7.2.3.1 Impact response of Alporas foam 141
7.2.3.2 Impact response of Cymat foam 145
7.2.3.3 Impact response of Alporas foam with different face sheets 148
7.2.3.4 Impact response of Cymat foam with different face sheets 156
Chapter -8 162
Sandwich structure of Al foam core with Al face sheet and Al tube under compression 162
8.1 Introduction 162
8.2. Analytical analysis of sandwich column under end compression 162
8.2.1. Estimation of failure loads 163
8.2.1.1 Euler macro-buckling 164
8.2.1.2 Core shear 165
8.2.1.3 Face sheet yielding 165
8.2.1.4 Face sheet wrinkling 165
8.2.2. Experimental procedure for sandwich columns under end compression 165
8.2.3. Comparison of analytical and experimental results of end compression of sandwich columns with Al foams 166
8.2.3.1 Failure mechanisms map for sandwich column under end compression 166
8.2.3.2 Results and discussion 168
8.2.4 Minimum weight design 171
8.2.5 Compression of Alporas foam filled Al tubes 176
8.2.5.1 Experimental procedure 176
8.2.5.2 Energy absorption of Al foam with Al tube in compression 179
Chapter-9 186
Conclusions and Recommendations 186
9.1 Conclusions 186
9.2 Contributions 190
9.3 Recommendations for future research scope 191
References 193
Appendix A-1 207
A1-1 FE Geometry and materials properties: 207
A1-2 Contact interface: 208

ATTENTION: The Singapore Copyright Act applies to the use of this document. Nanyang Technological University Library

A1-3 Loading and boundary conditions: 209
A1-4 Mesh designing: 211
A1-5 Configuration of outputs: 212

ATTENTION: The Singapore Copyright Act applies to the use of this document. Nanyang Technological University Library

List of Figures

Figure2.1 All-possible dispersions of one phase of the matter into another. 5
Figure2.2 A schematic of processing techniques for cellular metals 6
Figure2.3 Manufacturing processes of Alporas 7
Figure2.4 Manufacturing processes of Cymat 8
Figure2.5 Micrographs of metallic foams. 9
Figure2.6 Nominal stress versus strain uniaxial response of Alporas foam 11
Figure2.7 Effect of ratio of length of specimen to cell size 12
Figure2.8 Stress –Strain curve under bending for aluminum oxide. 14
Figure2.9 Failure modes in sandwich beams. 16
Figure2.10 Indentation failure for a sandwich beam having metal foam core with metallic face sheet under bending. 18
Figure2.11 Competing collapse modes A and B for core shear of a sandwich beam in four-point bending 18
Figure2.12 Failure Mechanism map of sandwich beams subjected to four-point bending 27
Figure2.13 Failure Mechanism map for simply supported sandwich plate 28
Figure2.14 Optimum design with graphical method of optimization for sandwich having polyurethane core and aluminum face sheets 30
Figure2.15 Yield surface and flow potential for isotropic hardening model. 33
Figure 3.1 Frequency distribution of cell size measurement for Alporas foam. 41
Figure 3.2 Frequency distribution of cell size measurement for Cymat foam 42
Figure 3.3 Optical micrographs of Alporas foam 43
Figure 3.4 SEM images of Alporas foam 44
Figure 3.5 Schematic sketch of an ultrasonic test setup for through transmission technique. 45
Figure 3.6 Change in echo height for specimens of Alporas foam. 46
Figure 3.7 Possible paths of ultrasonic waves inside the Al foam specimen. 47
Figure 3.8 A specimen of Alporas foam during tensile testing. 49
Figure 3.9 Tensile stress strain curve of Alporas foam 49
Figure 3.10 Compressive stress-strain response of Alporas foam. 50
Figure 3.11 Compressive stress-strain curve of Cymat foam 51
Figure 3.12 Specimens preparation for shear testing 52
Figure 3.13 A specimen of Alporas foam undergoing double lap shear testing. 53
Figure 3.14 Shear stress –strain behavior of Alporas foam of different thicknesses. 54
Figure 3.15 Load-displacement behavior of Alporas foam under bending 56

ATTENTION: The Singapore Copyright Act applies to the use of this document. Nanyang Technological University Library

Figure 3.16 In-Situ picture of the Alporas foam specimens under three-point bending..... 57

Figure 3.17 In-Situ picture of the Alporas foam specimens under four-point bending..... 58

Figure 3.18 Tensile stress-strain responses of Al sheets..... 60

Figure 3.19 Tensile stress-strain response of strain hardened SS sheets. 61

Figure 3.20 Stress-strain responses of alumina face sheets under four-point bend tests. 62

Figure 3.21 Order of arrangement of the prepreg stack..... 63

Figure 3.22 Longitudinal tensile and compressive stresses of CFRP laminate. 64

Figure 4.1 Schematic of a sandwich beam under four-point bending 67

Figure 4.2 Indentation zone beneath loading indenter. 70

Figure 4.3 Two competing shear failure modes of sandwich beams (a) Mode-A (b) Mode-B. 71

Figure 4.4 Failure mechanisms map for sandwich beam having foam core..... 76

Figure 4.5 Load and displacement curves for the sandwich beam failed under face sheet cracking. 77

Figure 4.6 Effect of face sheet thickness t on the face sheet cracking failure. 77

Figure 4.7 In-Situ picture of the sandwich beam specimens expected to fail by face sheet cracking. 78

Figure 4.8 Stress contours in the sandwich beam at the failure.. 79

Figure 4.9 Load versus displacement responses under core indentation 81

Figure 4.10 In-situ picture of the sandwich beam specimens expected to fail by core indentation (geometry – 4)..... 82

Figure 4.11 In-situ picture of the sandwich beam specimens expected to fail by core indentation (geometry –5)..... 82

Figure 4.12 Load versus displacement responses under core shear..... 84

Figure 4.13 In-situ picture of the sandwich beam specimens expected to fail by core shear mode-B..... 84

Figure 4.14 Contours of the dimensionless mass index and structural load index in collapse mechanism map of sandwich beam of Alporas foam core with alumina face sheet. 87

Figure 4.15 Minimum weight design of sandwich beam with Alporas foam core and 2 mm thick alumina face sheet. 89

Figure 5.1 Schematic of a sandwich beam under three-point bending showing geometrical and material parameters. 92

Figure 5.2 Sandwich in core shear failure under Mode-A. 94

Figure 5.3 Failure mechanisms map for sandwich beam having foam core and unidirectional CFRP face sheet..... 97

Figure 5.4 Load and displacement curves for the sandwich beam failed under face sheet cracking. 99

ATTENTION: The Singapore Copyright Act applies to the use of this document. Nanyang Technological University Library

Figure 5.5 In-Situ picture of the sandwich beam specimen failed by face sheet cracking. .. 100

Figure 5.6 Stresses S11 contours in half sandwich beam showing face sheet cracking. 100

Figure 5.7 Comparison of load and displacement curve for sandwich beam failed under core indentation..... 101

Figure 5.8 Compressive stress (S22) contours in sandwich beam showing core indentation failure. 102

Figure 5.9 In-situ picture of the sandwich beam specimens failed by core indentation. 102

Figure 5.10 Load versus displacement responses under core shear for sandwich beam. 103

Figure 5.11 In-situ picture of the sandwich beam specimens failed by core Shear Mode-A 103

Figure 5.12 Shear stress (S12) contours in sandwich beam showing core shear mode-A failure 104

Figure 5.13 Contours of the dimensionless mass index and structural load index in collapse mechanism map of sandwich beam of Alporas foam core with CFRP face sheet. 106

Figure 5.14 Minimum weight design of sandwich beam with Alporas foam core and CFRP face sheet 108

Figure 6.1 Failure modes for sandwich beam under indentation loading..... 111

Figure 6.2 Comparison of experimental indentation behavior of Alporas foam with different face sheets with thickness of 0.5 mm under flat indenter. 115

Figure 6.3 Comparison of experimental indentation behavior of Alporas foam with different face sheets with thickness of 1mm under flat indenter. 117

Figure 6.4 Top view of the indented specimens with 0.5 mm thick face sheet under flat indenter. 119

Figure 6.5 Top view of the indented specimens with 1.0 mm thick face sheet under flat indenter. 120

Figure 6.6 Comparison of experimental indentation behavior of Alporas foam with different face sheets with thickness of 0.5mm under spherical indenter. 122

Figure 6.7 Comparison of experimental indentation behavior of Alporas foam with different face sheets with thickness of 1.0 mm under spherical indenter. 124

Figure 6.8 Top view of the indented specimens having 0.5 mm thick face sheet under spherical indenter 125

Figure 6.9 Top view of the indented specimens having 1.0 mm thick face sheet under spherical indenter. 126

Figure 6.10 Cross-sectional view of the indented foam blocks with Al face sheets under indentation..... 129

Figure 6.11 Cross-sectional view of the indented foam blocks with SS face sheets under indentation..... 130

Figure 6.12 Cross-sectional view of the indented foam blocks with alumina face sheets under indentation..... 133

ATTENTION: The Singapore Copyright Act applies to the use of this document. Nanyang Technological University Library

Figure 6.13 Cross-sectional view of the indented foam blocks with CFRP face sheets under indentation..... 134

Figure 6.14 Comparison of initial peak for indentation versus strength ratio of face sheet to core..... 135

Figure 6.15 Energy absorption by blocks with various face sheets..... 136

Figure 7.1 A schematic view of the Instron Dynatup 8250 testing machine..... 139

Figure 7.2 Punch through Al foam block of 30 mm thickness by impactor..... 140

Figure 7.3 Comparison of load-impactor penetration depth behavior of Alporas foam with different thicknesses under impact loading..... 141

Figure 7.4 Cross-sectional view of the impacted Alporas foam block with various thicknesses 142

Figure 7.5 Bottom views of the impacted Alporas foam specimens without face sheet 143

Figure 7.6 Absorbed energy and load as a function of time for impact of Alporas foam alone. 144

Figure 7.7 Normalized absorbed energy vs. thicknesses of Alporas foam under impact loading..... 144

Figure 7.8 Comparison of load-impactor penetration depth behavior of Cymat foam with thickness of 40mm under impact loading. 146

Figure 7.9 Bottom view of the impacted Cymat foam specimen with a thickness of 40mm. 146

Figure 7.10 Absorbed energy and load as a function of time for impact of Cymat foam alone with thickness of 40 mm. 147

Figure 7.11 Comparison of load-impactor penetration depth behavior of 30 mm thick Alporas foam with different face sheets of 0.5 mm thickness..... 148

Figure 7.12 Cross-sectional views of the impacted 30mm thick Alporas foam blocks with different face sheet of thickness 0.5 mm 149

Figure 7.13 Top views of the impacted 30 mm thick Alporas foam specimens with different face sheet of 0.5 mm thickness 150

Figure 7.14 Load-time for impact of Alporas foam of 30 mm thickness with out and with different face sheet under impact loading. 152

Figure 7.15 Absorbed energy and load as a function of time for impact of Alporas foam of 30 mm thickness with out and with different face sheet under impact loading..... 153

Figure 7.16 Comparison of load- impactor penetration depth behavior of Alporas foam of 40 mm thickness with different face sheets of 0.5 mm thickness under impact loading..... 154

Figure 7.17 Cross-sectional views of the impacted Alporas foam blocks with 40mm thickness with out and with different face sheet of thickness 0.5 mm. 155

Figure 7.18 Normalized absorbed energy vs. blocks of Alporas foam having thicknesses of 30 and 40 mm without and with different face sheet of 0.5mm thickness under impact loading..... 156

ATTENTION: The Singapore Copyright Act applies to the use of this document. Nanyang Technological University Library

Figure 7.19 Comparison of load- impactor penetration depth behavior of Cymat foam of 40 mm thickness with different face sheets of 0.5 mm thickness under impact loading..... 157

Figure 7.20 Comparison of load- impactor penetration depth behavior of Cymat foam of 40 mm thickness with different face sheets of 1.0 mm thickness under impact loading..... 158

Figure 7.21 Top views of the impacted Cymat foam specimens without and with different face sheet..... 160

Figure 7.22 Normalized absorbed energy vs. blocks of Cymat foam having thicknesses of 40 without and with different face sheet of 0.5mm and 1.0mm thicknesses under impact loading. 161

Figure 8.1 A sandwich column consisting of Alporas foam core and Al face sheets under end compression. 163

Figure 8.2 Failure modes in sandwich columns subjected to end compression 164

Figure 8.3 Failure mechanisms map for sandwich column having Alporas foam core and Al face sheets. 167

Figure 8.4 Load and displacement curves derived from analytical and experimental observations for the sandwich column..... 169

Figure 8.5 Snap shots of the sandwich column specimens failed by different mechanisms.. 170

Figure 8.6 Contours of the dimensionless mass index and structural load index in collapse mechanism map of sandwich column of Alporas foam core with Al face sheet..... 172

Figure 8.7 Minimum weight design of sandwich column with Alporas foam core and Al face sheet 175

Figure 8.8 A bonded Al tube filled with Alporas foam during compression testing..... 177

Figure 8.9 Comparison of load-displacement response of bonded Al tube filled with Alporas foam under compression with response of individual constituents. 179

Figure 8.10 Failure of specimens for various cases. 181

Figure 8.11 Comparison of load-displacement response of un-bonded Al tube filled with Alporas foam under compression with response of summation of responses of Al tube and Alporas foam together..... 183

Figure 8.12 Comparison of load-displacement response of bonded Al tube filled with Alporas foam under compression with response of un-bonded Al tube filled with Alporas foam. ... 184

Figure A1-1 Loading of sandwich beam consisting of Alporas foam core and alumina face sheets……..210

FigureA1-2 Typical finite elements mesh..... 211

ATTENTION: The Singapore Copyright Act applies to the use of this document. Nanyang Technological University Library

List of Tables

Table2.1 Commercially available aluminum foams 7
Table3.1 Chemical composition of Alporas foam 39
Table3.2 Relative density of Alporas foam with standard deviation 40
Table3.3 Relative density of Cymat foam with standard deviation 40
Table3.4 Cell size measurements for Alporas foam with standard deviation 41
Table3.5 Cell size measurements for Cymat foam with standard deviation 41
Table3.6 Details of specimens for Alporas foam tested under three and four-point bending 55
Table3. 7 Material properties of various metallic sheets of various thicknesses 59
Table3.8 Material properties of alumina sheets of various thicknesses 62
Table3.9 Composite laminate material properties under compression and tensile loading 65
Table4.1 Geometry of sandwich beams under four point bending 73
Table5.1 Geometry of sandwich beams under three-point bending 98
Table8.1 Geometry of sandwich columns under end compression 166
Table8. 2 Details of specimens tested under compression 176
Table8.3 Experimental results of tubes compression in various combinations 183
TableA1-1 Input data for Alporas and alumina sheet material 207
TableA1-2 Foam hardening data for Alporas foam 208

ATTENTION: The Singapore Copyright Act applies to the use of this document. Nanyang Technological University Library

List of Abbreviations and Symbols

AE	Absorbed energy
Al	Aluminum
ASTM	American Society for Testing of Materials
AIS	Analytical imaging station
θ	Angle of rotation
Ca	Calcium
CFRP	Carbon fiber reinforced polymer
C_{ij}	Compliance matrix
cs	Compressive displacement
P	Compressive force
c	Core thickness
A_i	Cross-sectional area of different materials
cl	Crushed length
m^3	Cubic meter
δ	Deflection
^0C	Degree centigrade
ρ_c, ρ_f, ρ_i	Density of foam core and face sheet, Density of different materials
d	Distance between central axis of upper face sheet and central axis of lower face sheet in a sandwich beam
s	Distance between inner loading spans in bending
l	Distance between outer loading spans in bending
I_{eff}	Effective second moment of area of sandwich structure
E, Es, E_f, E_c	Elastic modulus, Elastic modulus of solid material, Young's modulus of face sheet, Young's modulus of foam core
EDM	Electro discharge machine
$(EI)_{eqv.}$	Equivalent flexural rigidity of the sandwich structure
$(AG)_{eq}$	Equivalent shear rigidity of the sandwich structure
W_E, W_{ic}, W_{if}	External work done on the structure, Internal work done by the core and face sheet

ATTENTION: The Singapore Copyright Act applies to the use of this document. Nanyang Technological University Library

F_{CSA}, F_{CSB}	Failure load for core shear mode-A, core shear mode-B
F_E, F_{FSY}, F_{FSW}	Failure load for Euler buckling, face sheet yielding, face sheet wrinkling
F_{FSC}, F_{CI}, F_{CS}	Failure load for face sheet cracking, core indentation, core shear mode
F_e	Load in the elastic limit
FEM	Finite Element Model
FP	Flow potential compression to hydrostatic compression
GFRP	Glass fiber reinforced polymer
g	Gravitational acceleration
H_2	Hydrogen
G_{12}	In-plane shear modulus
σ_0	Initial residual stresses
σ_c^0	Initial stress in uniaxial compression
p_c^0	Initial yield stress in hydrostatic compression
J, MJ	Joule, Mega Joule
kHz, MHz	Kilo hertz and Mega hertz
λ	Length of core crush at one side of indenter
LF	Load at failure
$\sigma_{11}^{\ c}, \sigma_{22}^{\ c}$	Longitudinal, and transverse compressive strength
$\sigma_{11}^{\ t}, \sigma_{22}^{\ t}$	Longitudinal, and transverse tensile strength
$E_{11}^{\ c}$	Longitudinal compressive elastic modulus
$E_{11}^{\ t}$	Longitudinal tensile elastic modulus
υ_{12} , υ_{12} and υ_{12}	Major Poisson's ratio of material
M	Mass of the structure
m_t	Mass of the tube
M_{max}, M_f	Maximum moment applied on the structure and face sheet
S_f	Mean force efficiency
p	mean stress
Mpa, GPa	Mega Pascal, Gega Pascal
μm, mm, m, km	Micrometer, millimeter, meter, kilometer

ATTENTION: The Singapore Copyright Act applies to the use of this document. Nanyang Technological University Library

$\overline{M}_{\min}$	Minimum mass index
$\left(\overline{M}_{\min}\right)_{CI-CSB}$	Minimum mass index at the boundary between core indentation and core shear mode-B failures
$\left(\overline{M}_{\min}\right)_{CS-FSY}$	Minimum mass index at the boundary between core shear and face sheet yielding failures
$\left(\overline{M}_{\min}\right)_{CS-E}$	Minimum mass index at the boundary between Euler buckling and core shear failures
$\left(\overline{M}_{\min}\right)_{FSY-E}$	Minimum mass index at the boundary between Euler buckling and face sheet yielding failures
$\left(\overline{M}_{\min}\right)_{FSC-CI}$	Minimum mass index at the boundary between face sheet cracking and core indentation failures
$\left(\overline{M}_{\min}\right)_{FSC-CSB}$	Minimum mass index at the boundary between face sheet cracking and core shear mode-B failures
$\left(\overline{M}_{\min}\right)_{CI}$	Minimum mass index for core indentation failure zone
$\left(\overline{M}_{\min}\right)_{CS}$	Minimum mass index for core shear failure zone
$\left(\overline{M}_{\min}\right)_{CSA}$	Minimum mass index for core shear mode-A failure zone
$\left(\overline{M}_{\min}\right)_{CSB}$	Minimum mass index for core shear mode-B failure zone
$\left(\overline{M}_{\min}\right)_{E}$	Minimum mass index for Euler buckling failure zone
$\left(\overline{M}_{\min}\right)_{FSC}$	Minimum mass index for face sheet cracking failure zone
$\left(\overline{M}_{\min}\right)_{FSY}$	Minimum mass index for face sheet yielding failure zone
N, kN	Newton, Kilo Newton
$\bar{M}$	Non-dimensional mass index
$\overline{F}_{CSA}$, $\overline{F}_{CSB}$	Non-dimensional structural load index (for core shear mode-A and core shear mode-B respectively)
$\overline{F}_{E}$, $\overline{F}_{FSY}$, $\overline{F}_{CS}$	Non-dimensional structural load index (for Euler buckling, face sheet yielding and core shear respectively)
$\overline{F}_{FSC}$, $\overline{F}_{CI}$	Non-dimensional structural load index (for face sheet cracking and core indentation respectively)

ATTENTION: The Singapore Copyright Act applies to the use of this document. Nanyang Technological University Library

$\bar{c}, \bar{t}, \bar{s}, \bar{\sigma}, \bar{\rho}$	Non-dimensional terms (core thickness, face sheet thickness, span length strength and density)
c/R	Normalized sandwich core thickness
$\varepsilon, \varepsilon_0, \varepsilon_1^e$	Normal strain, Initial strains, Elastic strain
$\sigma, \sigma_{pl}, \sigma_{ys}$	Normal stress, Compressive plateau stress, Yield stress of solid material
G_{13} and G_{23}	Out-of-plane shear modulus
H	Overhang length in bending
%	Percentage
$\dot{\lambda}$	Plastic flow multiplier
Mp	Plastic moment
$\varepsilon^P, \varepsilon_{vol}^P$	Plastic strain, volumetric plastic strain
R	Plate radius
υ, υ_p	Poisson's ratio, Plastic Poisson's ratio
PEEK	Poly ether ether-ketone
PVC	Polymer vinyl chloride
$\sigma_1, \sigma_2, \sigma_3$	Principal stresses
r	Punch radius
K'	Ratio of initial yield stresses
ρ, ρ_s	Relative density, Relative density of solid
G, Gs, G_c	Shear modulus, Shear modulus of solid material, shear modulus of foam core
β	Shape of flow potential ellipse
α	Shape of the yield ellipse
γ	Shear strain
$\tau, \tau_y^c, \tau_{13}$	Shear stress, Shear strength of core, Interlaminar shear strength
B	Size of the (vertical) axis of the yield ellipse
L	Size of the specimen
S_e	Specific energy absorption
SS	Stainless steel

ATTENTION: The Singapore Copyright Act applies to the use of this document. Nanyang Technological University Library

σ_j	Stress tensor
St_e	Stroke efficiency
S_{st}	Stroke length (it is the length up to which the compression displacement is consider.
$\bar{F}$	Structural load index
SDA	Surface displacement analyzer
Π	Tearing energy of the foam
t	Thickness of face sheet
3D	Three dimensional
TiH_2	Titanium hydride
F, F_m, F_{max}	Total applied load, Mean applied force, Maximum applied force
$E_{22}{}^c$ and $E_{33}{}^c$	Transverse compressive elastic modulus
$E_{22}{}^t$ and $E_{33}{}^t$	Transverse tensile elastic modulus
2D	Two dimensional
Y	Uni-axial yield strength of the material
σ_e	Von –Misses effective stress
Wt	Weight
W	Weight of the structure
b	Width of the specimen
$f(\sigma_{ij})$	Yield function
P_c^0	Yield strength in hydro static compression
$\sigma_y^f, \sigma_y^c, \sigma_c$	Yield strength of face sheet and core, Compression strength of the foam
f	Yield surface

ATTENTION: The Singapore Copyright Act applies to the use of this document. Nanyang Technological University Library

CHAPTER- 1

Introduction

1.1 Background and motivation

The quest for advanced engineering materials with improved properties is unending. Great strides in modern technology increase demand for newer and improved materials. Metallic foams are known to have excellent combinations of physical and mechanical properties such as a high specific stiffness, strength combined with high noise & vibration absorber. Therefore metallic foams are currently the most important material with widespread applications in nearly every area of science and technology [1-11]. Some applications of metallic foams are in bonnets, boot lids of car, crash boxes or underride protectors for lorries, impact cushion for railway rolling stock, tailbooms of helicopters, floor and roof panel for building structures, elevator platforms, structural bulkheads in ships, space vehicle landing pads, fire doors, hatches, underside of an elevated expressway and tunnels.

Sandwich structure, as low-density core material, flanked between two high modulus face sheets is a lightweight structure with a very high stiffness to weight ratio. Because of high cross-sectional second moment of the area the sandwich structure can withstand higher bending and buckling loadings as compared to other structures. The face sheets carry the normal stresses and core resist the transverse shear loading. Nature also utilizes sandwich structures with low density core in skull of a human and wing of bird [10]. Honeycombs and polymer foams have been used for many years as core of sandwich structures in various applications [10]. But metallic foams have shown great potential in the applications as a core material in sandwich structures, over honeycombs and polymer foams as the latter two materials pose problems with durability, anisotropy, creep even at ambient temperature and evolution of toxic gases in fires [12]. A variety of metallic foams are available such as aluminum, nickel, Fe (steel), copper, Ti etc but aluminum foams are widely used due its recyclability, good corrosion resistance and light weight.

Sandwich structure with aluminum foam core offers following additional advantages over sandwich structures.

- Homogenous and nearly isotropic nature

ATTENTION: The Singapore Copyright Act applies to the use of this document. Nanyang Technological University Library

- Formability into curved shapes
- Usability at high temperature as well as fire retardation capability
- Easily recyclable [13,14]

In view of the advantages mentioned above of sandwich structures with Aluminum foam coupled with brittle materials, such as alumina or CFRP material, as face sheet can increase the stiffness and strength, thereby increasing the mechanical performance of the sandwich structure. In view of the limited studies on mechanical behavior of the sandwich structures with brittle face sheet and aluminum foam core, it would be significant to conduct the studies on this combination under bending. For optimal performance and improved properties of such a sandwich structure, it is necessary to understand the typical problems expected and competing failure modes under various loading conditions such as bending, end compression, local indentation and impact. Minimum weight design is very important aspect for a sandwich construction because it can enhance structural efficiency, meaning for a given loading conditions, the construction utilizes minimum possible material.

1.2 Objectives

The need for safe usage of structures with specific strength and stiffness having foam core is stimulated by the ever increasing demand of structures with light weight and high performance in real life. The evaluation of the performance of these structures with metal foam core under various loading conditions such as bending, end compression, indentation and impact is necessary for the practical use of these structures. Since these structures possess excellent mechanical properties, the main objective of this investigation is to obtain the design maps for these structures and make a good comparison of these structures with various combinations of face sheets as these structures are capable of achieving variety of high performances. The research effort combines analytical, numerical and experimental investigation to provide a better understanding of structures with Al metallic foams. The specific goals of the present research are as follows:

- To design high performance light weight and safe structure comprising of metal foam core under bending and end compression loading.
- To evaluate the performance of these structures coupled with various face sheets under quasi-static indentation loading.

ATTENTION: The Singapore Copyright Act applies to the use of this document. Nanyang Technological University Library

- To evaluate the performance of these structures under low velocity impact for safe usage in automobile and aerospace application.
- To investigate the energy absorption capacity of these light weight structures under compression.

1.3 Scope of the present work

Review of the literature related to the structure with Al foam revealed that the studies on a sandwich structure having aluminum foam core and brittle (ceramic or CFRP) face sheet have not been dealt adequately. The failure mechanisms maps and minimum weight design maps of these structures under bending would be quite important for its safe usage in real applications. The failure mechanism map will lead to an optimum solution in terms of geometrical parameters for a particular requirement such as collapse load or specific strength and/or stiffness. Designers can employ these solutions in various applications of structures. It would be interesting to develop an appropriate numerical simulation model to predict the deformation behavior of the sandwich beam with brittle face sheet such as alumina and CFRP (by considering the failure criteria for each material involved). The failure mechanisms map and minimum weight design map of structures with Al foam and Al face sheet under end compression would be important for designers for safe usage in real applications where long and light weight columns are required. Indentation behavior of structures with Al foams is not yet well researched. Therefore, failure analysis of structures comprising of Al foam core and various face sheets under quasi-static indentation should provide a good comparison among the performance of those structures, which can work as guidelines for designers to build those structures in various applications. Energy absorption characteristics of these structures will provide, an estimation of performance of those structures in high impact, and blast loading.

1.4 Thesis organization

In this report, the current status of the literature related to aluminum metallic foam, sandwich structure with aluminum foam and finite element models for aluminum foam core and brittle material are discussed in Chapter 2. Chapter 3 deals with surface and mechanical characterization of Al foams and the various face sheets materials involved in the study. Chapter 4 presents an in-depth investigation on the failure of sandwich beam with Alporas Al

ATTENTION: The Singapore Copyright Act applies to the use of this document. Nanyang Technological University Library

foam core and brittle alumina face sheet under four point bending. Chapter 5 analyses the sandwich beam with Alporas foam core and CFRP face sheet under three-point bending and also compares experimental results with analytical and numerical predictions. Failure analysis of structures with Al foam core and various face sheets including elastic, elastic-perfectly plastic and elastic-strain hardening behavior is presented in Chapter 6. In Chapter 7, performance of structure comprising of Al foam core with various face sheets is demonstrated under low velocity impact. Chapter 8 shows an in-depth analysis of sandwich column comprising of Alporas foam core and Al face sheet under end compression loading. Energy absorption capacity of Al rectangular tube filled with Al foam under compression is also dealt with. Chapter 9 is concluded with major conclusions based on the research work and scope for further research is outlined.

ATTENTION: The Singapore Copyright Act applies to the use of this document. Nanyang Technological University Library

CHAPTER 2

Literature Review

This chapter gives a brief overview of the work done on Al alloy foams covering its production, cell morphology, deformation behavior and effect of its morphology on mechanical properties. The structural analysis of sandwich panel consist of Al foam core under various loading such as bending, indentation, impact and end compression is also reported in terms of the possible failure modes and minimum weight design data. Finite element models for foam and face sheet materials including metals, ceramics, and CFRP are reviewed.

2.1 Foam

Figure 2.1 shows all-possible dispersions of one phase of the matter into another, where both phases can be the same. Foam is formed due to uniform dispersion of a gaseous phase in either a solid or a liquid.

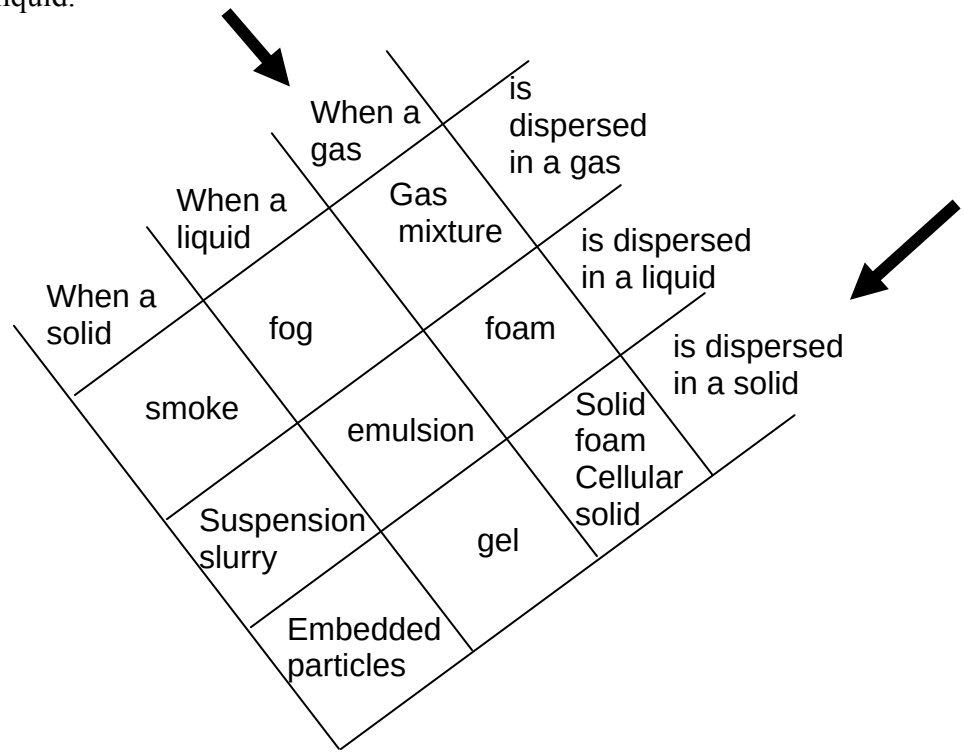

Figure2.1 All-possible dispersions of one phase of the matter into another [7].

Metallic foams as described in the following section, are a special class of cellular solids, under category of solid foams. A range of engineering alloys such as Al, nickel, iron (steel),

ATTENTION: The Singapore Copyright Act applies to the use of this document. Nanyang Technological University Library

copper, etc can be foamed but aluminum foams are widely used as structural foam due its recyclability, good corrosion resistance and light weight [7].

2.2 Aluminum foams

2.2.1 Production methods of metal foams

Various researchers have developed different techniques to produce metal foams [7, 11, 15]. The manufacturing methods for producing metal foams are classified broadly into four groups: those made from melts, from powders, by sputtering and by deposition [11]. An outline of these processing techniques is given in Figure 2.2. Each technique covers a characteristic range of density, cell size, cell morphology and end application of the produced metal foam.

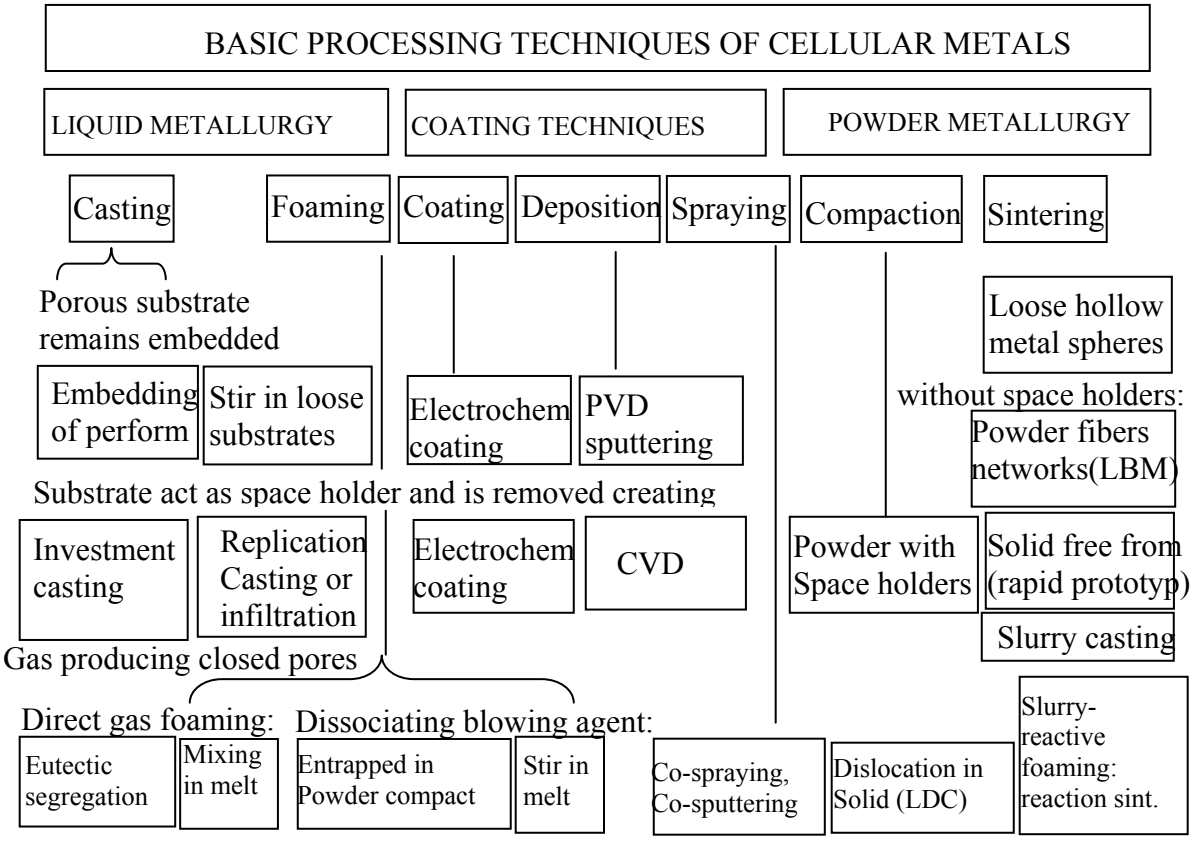

Figure2.2 A schematic of processing techniques for cellular metals [6].

Different combinations of processing, architecture and metal matrix make different types of products and prototypes. Due to the economical handling of the large quantities of metal, melt route is very attractive for the making of closed cell metal foams [7]. Foaming of metallic melts can be done by creating gas bubbles in the liquid. This can be either done by

ATTENTION: The Singapore Copyright Act applies to the use of this document. Nanyang Technological University Library

the injection of gas into the liquid metal from an external source or by in-situ gas formation in the liquid by a chemical decomposition of a foaming agent. Alporas Al foam made by foaming technique with blowing agent (as shown in Figure 2.2) is reported to be the most homogenous cellular structure [16].

2.2.2 Types of aluminum foams

Commercially available aluminum foams can be broadly classified into two categories based on cell structure as shown in Table 2.1, i) Open cell or ii) closed cell. Cells are connected through the open faces in open cell aluminum foam. If the faces are solid such that each cell is sealed off from its neighbor, it is called a closed cell aluminum foam.

Table2.1 Commercially available aluminum foams[9,17]

Open Cell	Closed Cell
ERG Duocel	Cymat, Hydro, Alulight (Mepura), Alporas, Alcan, Frounhofer(IFAM), Numan-Alu, Gesar, LKR

2.2.3 Manufacturing process for Alporas foam

The manufacturing process of closed cell aluminum foam (Alporas- trade name, patented by Shinko wire company, Japan) is shown systematically in Figure 2.3. It is made by a batch casting process with molten aluminum. Calcium by 1.5 wt % is mixed with molten aluminum at 680^0 C and stirred for 6 minutes at an ambient atmosphere.

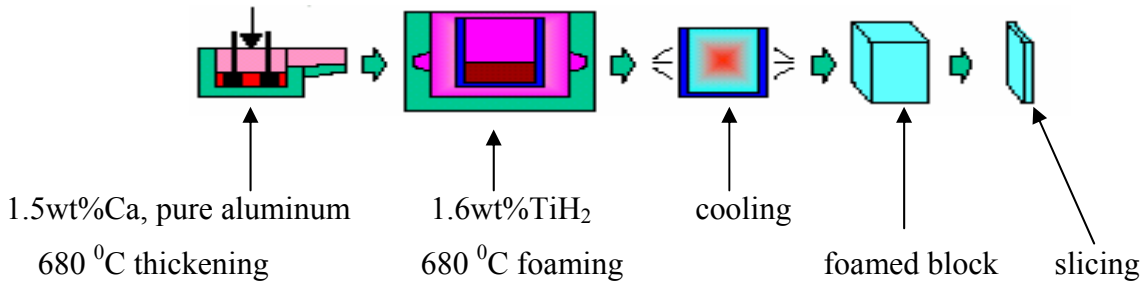

Figure2.3 Manufacturing processes of Alporas [18].

Calcium is used as a thickening agent to increase the viscosity of the melt and to prevent floatation of the bubbles. The addition and subsequent agitation of Calcium, facilitates the

ATTENTION: The Singapore Copyright Act applies to the use of this document. Nanyang Technological University Library

oxidation process on the surface of the molten aluminum. Molten aluminum is thickened by the formation of oxides (CaO, Al_2O_3, $CaAl_2O_4$ etc) [6, 18, 19 and 20]. This thickened Al is poured into a casting mold. It is stirred with a foaming agent of 1.6wt% of TiH_2 at 680^0C. Hydrogen gas evolves from the decomposition of TiH_2, in the form of bubbles. Molten material is cured for 15 mins after stirring. Due to the generation of gaseous bubbles, molten material expands and fills up the mold. These bubbles are responsible for creation of various pores whose faces are sealed by other oxides present and make this foam as closed cell one. This foamed molten material is cooled by fans so it solidifies in the casting mold. Cooled aluminum foam block is taken out from the mold and cut into the desired shape.

2.2.4 Manufacturing process for Cymat foam

The manufacturing process of closed cell aluminum foam (Alporas-trade name, licensed by Cymat Aluminum Corp.) is shown systematically in Figure 2.4 [15]. It is made by continuous casting process with metal matrix composite. A metal matrix composite (Al –wrought or Al-casting alloys and SiC or Al_2O_3 particles) is melted with foundry equipment and transfer to a tundish where air is introduced. The resulting liquid metal foam is removed on a conveyor belt as is shown in Figure 2.4.

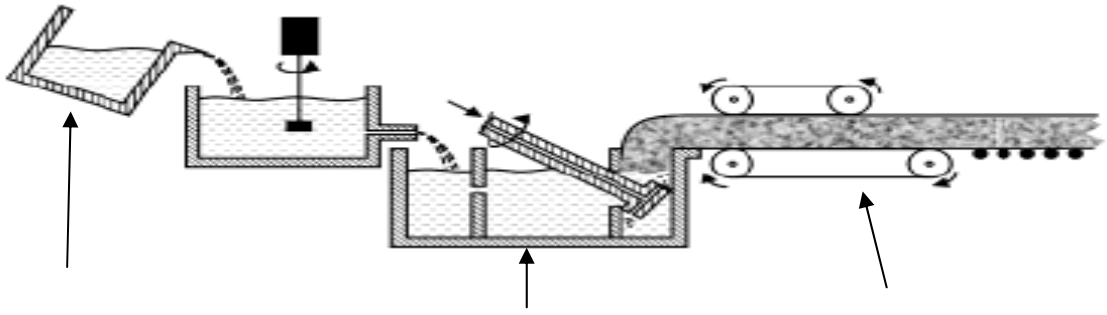

Figure2.4 Manufacturing processes of Cymat, consist of melting and holding furnaces, the foaming box, and foaming equipment and a twin-belt caster [15].

2.2.5 Manufacturing process for open cell Duocel

Open-cell polymer foam is filled with slurry of heat resistant material. After drying, this polymer is removed and a molten aluminum alloy (generally 6101) is cast into the resulting cavity which corresponds exactly to the original polymer foam structure. After directional

ATTENTION: The Singapore Copyright Act applies to the use of this document. Nanyang Technological University Library

solidification the mould material is mechanically removed and continuously connected, open-celled foam Duocel is formed [15].

2.2.6 Microstructure and cell morphology of aluminum foams

The microstructure of foams generally consists of an interconnected network of struts and plates that form the edges and faces of polyhedral cells. Special features of this microstructure of metallic foams are studied by several researchers [11, 16, 21-29]. Microstructures of some typical closed cell foams are shown in Figure 2.5 (a), (b), (c), (d). Here, the voids of the each cell are separated by solid faces. Figure 2.5(e) shows the microstructure of open cell foam. In these kinds of foams, cells are connected through the open faces [11].

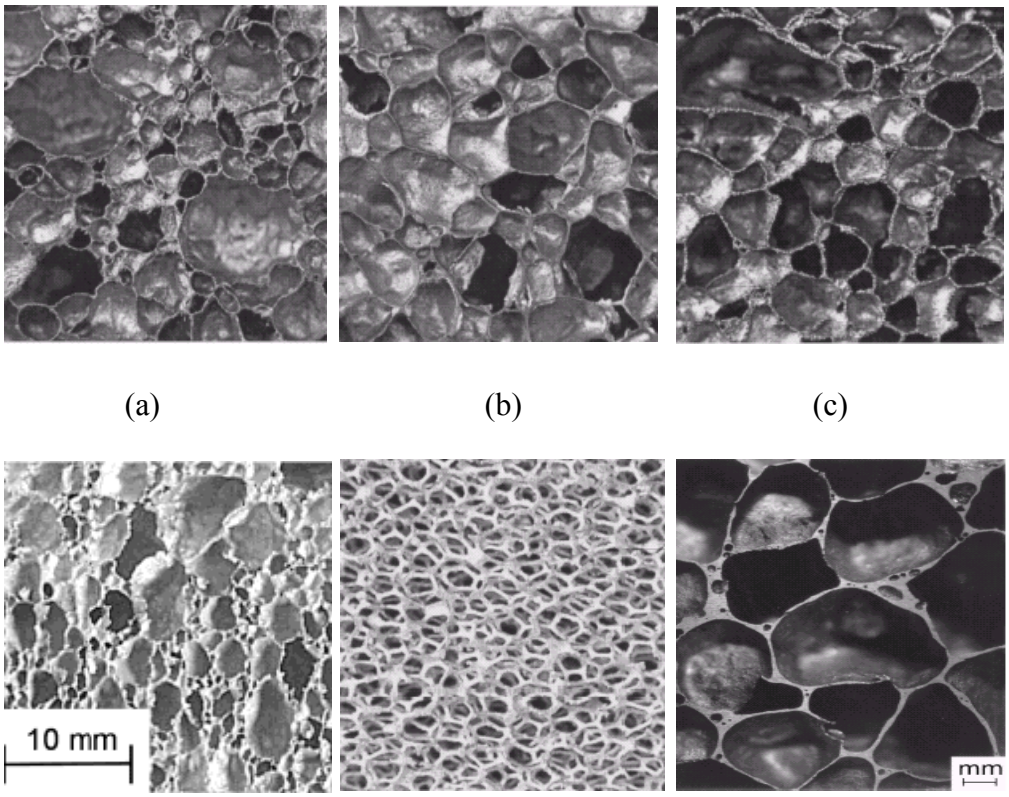

Figure2.5 Micrographs of metallic foams. (*a*) Alcan, (*b*) Alporas, (*c*) Alulight, (*d*) Cymat, (*e*) ERG Duocel (f) Alporas showing curvature of cell walls[25, 30].

The cell size of most metallic foams is in the range of 2 to 10 mm [16, 21]. Cell size for Alporas foam was measured, which varies from 1- 13 mm with a mean size of 3 mm. The mean cell size of Cymat foam depends upon the density and varies from 3 mm to 25 mm

ATTENTION: The Singapore Copyright Act applies to the use of this document. Nanyang Technological University Library

[15]. The shape of the cells of most metallic foams varies from equi-axed to ellipsoidal, with the ratio of major to minor axes length up to 1.5 [16]. A typical example of curve cell walls of Alporas Al foam is shown in Figure 2.5 (f).

2.3 Mechanical behavior of aluminum foam

Metallic foams, especially those of aluminum are of great industrial interest because they combine the advantages of a bulk metal with the structural advantages of the foam. It is well known that metals are strong, tough, deformable and conductive to both electricity and heat. Foams are light, stiff and have high surface to volume ratio and adjustable cell structure. Aluminum metallic foams with all these characteristics are used in various industries like automobile, aerospace, defense, building, shipbuilding, sports etc [7, 9].

The following list includes the most interesting properties of aluminum foams, which are important to automotive industries:

- Low density gives high specific stiffness and strength
- High energy absorption capacity during impact and blast loading
- Good mechanical and acoustic damping
- Ease in recycling and
- Good machinability

Mechanical behavior of aluminum foams [30-45], failure mechanisms [30-39] under different loading and effect on deformation behavior by relative density, cell size, cell wall curvature [10, 23-28, 37, 46] were studied extensively. Micro-mechanical models were also proposed to describe the uniaxial tensile, compressive, shear and bending behavior of these foams [11, 27, 47, 48].

2.3.1 Deformation behavior under different loadings

The stress-strain curves for aluminum foam (Alporas) under different monotonic loadings (like tensile, compression and shear) are shown in Figure 2.6 [44]. In tensile loading, strong hardening behavior is exhibited prior to tearing across the section at a nominal strain of only a few percent. The deformation is caused by bending of cell walls and stretching of faces for closed cell foam (like Alporas) under tensile loading. Deformation behavior of aluminum

ATTENTION: The Singapore Copyright Act applies to the use of this document. Nanyang Technological University Library

foams under compression loading shows high energy absorption capacity of these foams. In almost all Al foams the compression behavior can be divided into mainly three regions. The first region is the linear elastic region. The second region is known as the plateau in which cell collapse at almost constant stress. The third region is called densification region in which all the cells are collapsed. Quantitatively, the response under shear loading is similar to that in tensile loading. The peak stress in shear stress-strain curve is termed the shear strength. Fracture occurs due to initiation, growth and coalescences of tensile micro cracks. These tensile micro cracks exist along the mid-plane of the specimen in such a way that everyone is inclined at about 45^0 towards the shearing direction.

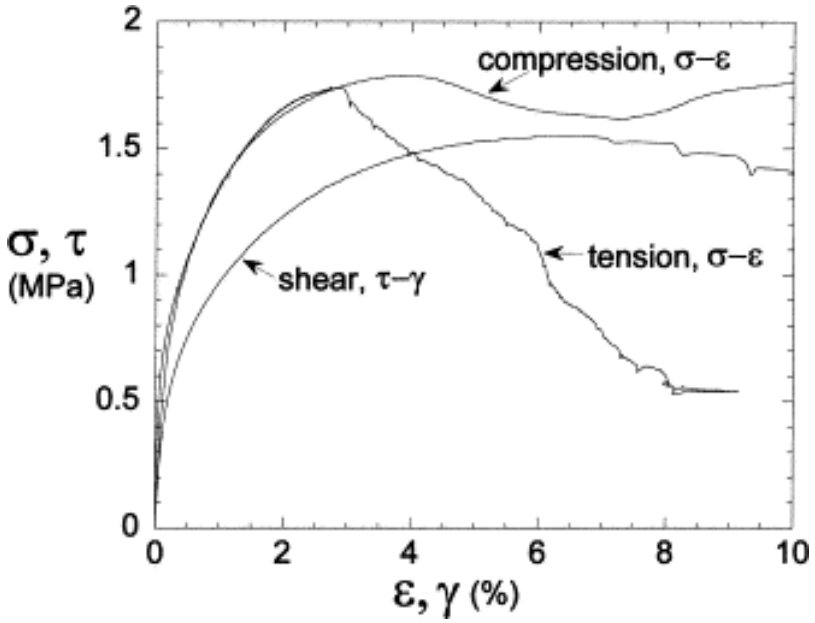

Figure2.6 Nominal stress versus strain uniaxial response of Alporas foam (relative density 11 %) [44].

2.3.2 Size effect on deformation behavior of aluminum foams

Various researchers have studied the effect of parameters such as cell size, cell structure, relative density of foam, loading rate, cell walls, composition etc on deformation behavior of metal foam, especially aluminum [9, 21, 25, 30,31, 48-51].

Cell walls near the free surface are less constrained than the ones in the bulk of the material, while cell walls far away from outer surface are as constrained as in the bulk of the specimen. Therefore, as the ratio of specimen size to cell size increases, normalized modulus (modulus of foam/modulus of bulk material) and normalized strength (strength of foam/strength of

ATTENTION: The Singapore Copyright Act applies to the use of this document. Nanyang Technological University Library

bulk material) also increase, which is shown by plots of normalized compressive Young's modulus, normalized compressive peak stress and normalized shear strength normalized against the ratio of specimen size to the cell size, as shown in Figure 2.7 (a), (b) and (c) respectively [25].

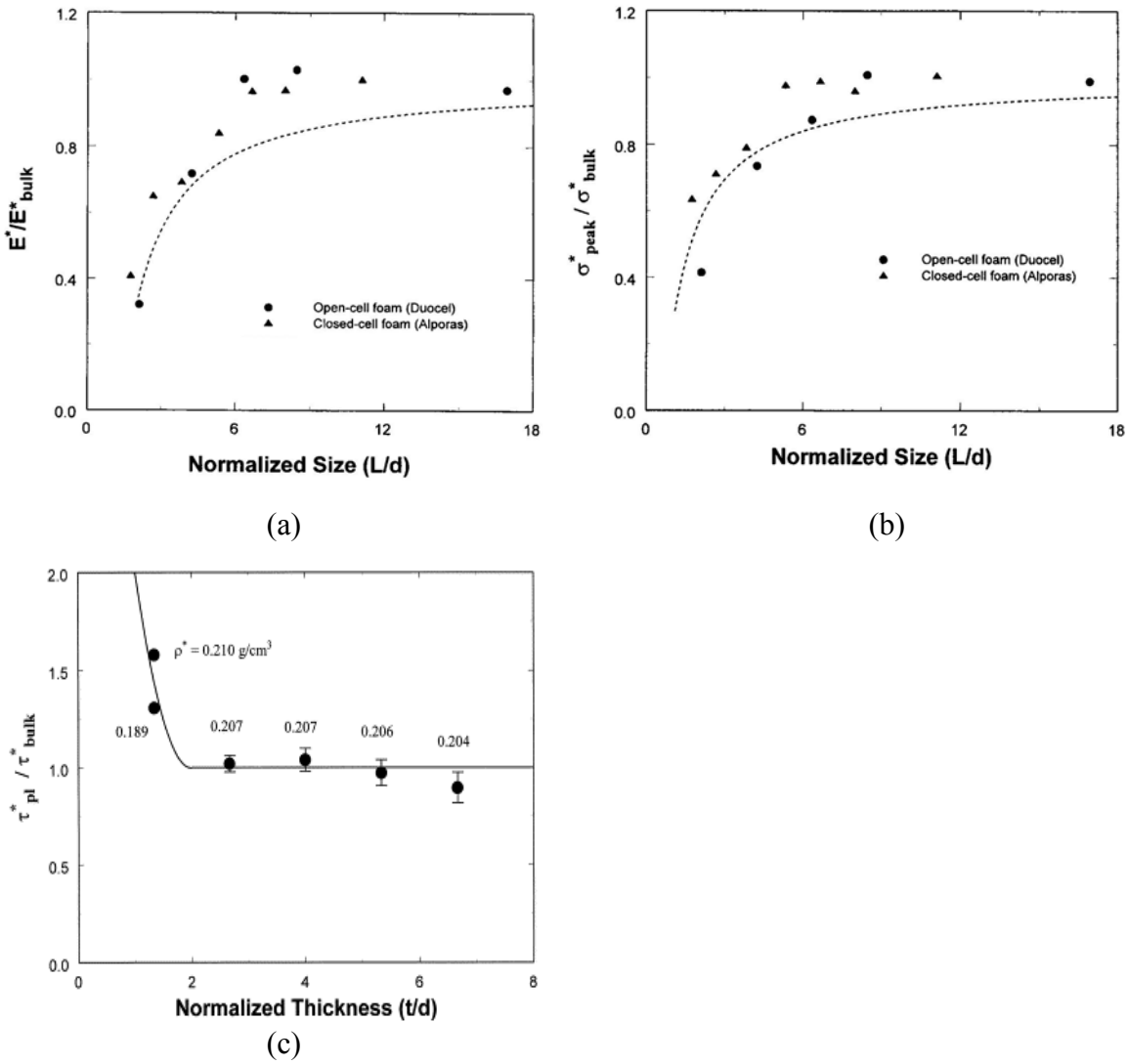

Figure2.7 Effect of ratio of length of specimen to cell size on (a) normalized Young's modulus (b) normalized compressive strength for Alporas and Duocel aluminum foams (relative density of around 8% and 7 % respectively) (c) shear strength for Alporas aluminum foams (relative density of around 8%) [25].

In shear testing, bonding of the foam specimen to stiff plates increases the constraints of the cell walls at the boundary, producing a stiffening effect. Thus, shear strength becomes independent of the specimen thickness for size ratio (thickness of specimen to cell size) more than 2.67. Effect of relative density on deformation behavior of Al foam is well studied and concluded that normalized Young's modulus and normalized compression strength increases

ATTENTION: The Singapore Copyright Act applies to the use of this document. Nanyang Technological University Library

with the relative density of aluminum foams [21]. Relative density of aluminum foam also influences tensile and shear strengths [25, 30, and 31].

2.4 Surface characterization of Al foams with ultrasonic techniques

Weaver [52] has investigated the ultrasonic measurement in open cell ERG foam in the frequency range of 200 kHz to 2 MHz. No back wall signal or reflection was detected by using pulse echo contact ultrasonic with transducer of 500 kHz. With a frequency of less than 100 KHz, waveform was received faster than for higher frequency using point source–point receiver configuration. Ultrasonic measurements on diffusivities, absorptivities and modal densities were found to be appropriate for high frequency regime. Propagation of ultrasonic wave in water saturated ERG Al foams using pulse transmission methods was demonstrated by Ji et al [53] Only low frequency waves are found to travel through the samples in the fast and slow wave modes, while the high-frequency portion of the input pulse has been strongly attenuated. Fellah et al [54] have proposed a method for measuring transport parameters in porous materials which is based on temporal model of direct and inverse scattering problems affecting the propagation of transient ultrasonic waves in a homogenous isotropic slab of porous material with a rigid frame. Acoustic parameters needed for ultrasonic propagation in porous material are estimated by reflection contributions from the first and second interface of the medium

2.5 Ceramics and CFRP as face sheet material

2.5.1 Ceramic material

Ceramic materials are inorganic and non-metallic materials. These materials are non-conductors of electricity and heat. They can withstand higher temperatures and a harsher environment than metals and polymers [55]. Alumina is the most matured high technology ceramic material. It is produced by compacting alumina powders into a shape and firing the powders at high temperatures to allow it to densify into a solid, polycrystalline, non-porous component [56].

Ceramic materials show catastrophic failure in a brittle manner with little energy absorption. Stress-strain behavior of ceramics (alumina) is usually determined by flexural test because of practical constraints in tensile testing. Compressive strength of these materials is usually 50%

ATTENTION: The Singapore Copyright Act applies to the use of this document. Nanyang Technological University Library

higher than the tensile strength. A typical stress-strain curve for alumina under bending is shown in Figure 2.8 [55].

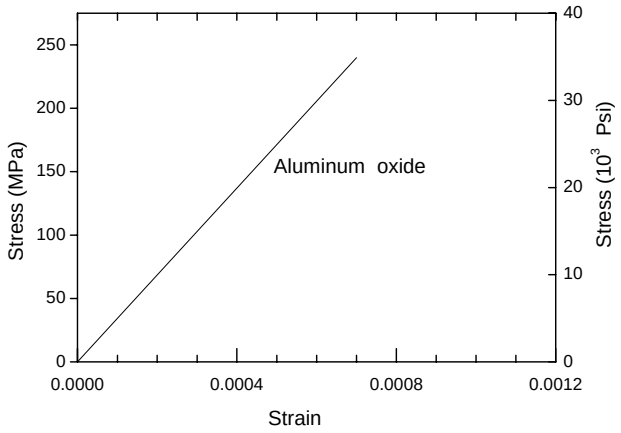

Figure2.8 Stress –Strain curve under bending for aluminum oxide [55].

2.5.2 Carbon fiber reinforcement polymer composite material

Composite materials are engineered materials made from two or more constituent materials that remain separate and distinct on a macroscopic level while forming a single component [57]. It consist of two or more clearly distinguishable constituents working together to achieve a blend of mechanical properties superior to the properties of the individual constituent. There are three commonly accepted types of composite materials: "fibrous composites" which consist of fibers in a matrix, "laminated composites" which consist of layers of various materials and "particulate composites" which are composed of particles in a matrix.

Carbon fiber reinforced polymer matrix (CFRP) composite is one type of fibrous composite material in which carbon is used as high performance fiber material and polymer resin as matrix material [55]. Carbon fibers are strong and stiff long reinforcing materials held together by epoxy or PEEK matrix. The roles of polymer matrix are to provide ductility, to protect the fibers from the mechanical abrasion or chemical reactions with the environment and to serve as a barrier to crack propagation by separating fibers and preventing the propagation of cracks from one fiber to another [55]. These composites are currently being utilized in various fields such as aircraft (military and commercial both) structural components, rocket motor cases, pressure vessels and sports equipments [55] because of several favorable properties such as low density, high specific strength and stiffness. In

ATTENTION: The Singapore Copyright Act applies to the use of this document. Nanyang Technological University Library

addition, the fatigue strength-weight ratios as well as fatigue damage tolerances of laminates made with these composite are excellent [58].

2.6 Sandwich panels with Al foam as core materials

A sandwich panel is normally a low-density core material sandwiched between two high modulus face sheets to produce a lightweight panel with a very high stiffness [59]. The face sheets act like flanges of I-beams carrying axial tensile and compressive loads. The core plays the role of the web, separating the face sheets and bears the shear loads [60, 61]. These structures are very efficient in bending and buckling loads because of the high inertia of the light-weight panel. These sandwich panels are used in applications like aircraft, automobile, sport equipments and portable structures, where weight saving is very important. Application of those sandwiches leads to investigation of their performance under various loadings such as bending, indentation, impact or end compression.

Metallic foams as a core of sandwich structure have lot of advantages over other materials like polymer foams, honeycomb. Its advantages are isotropy, high temperature sustenance and ease in obtaining doubly curved surfaces [9, 49].

The mechanical behavior of the sandwich panel not only depends upon the properties of core and face sheets but also upon the geometry of the sandwich. Specific applications of sandwich panels require minimal stiffness, load tolerance and lightweight. Sandwich panels with minimal weights and desired stiffness and strength can be achieved by optimization of different parameters like core materials and face sheets or design geometry of panel [10]. Size effect in sandwich panel can be induced or eliminated by choosing the appropriate dimension of the core foam. This is based on the fact that the size effect in the core material causes the panel to show the same size effect [49-51].

2.6.1 Failure of sandwich beams of Al foam core under bending

Some applications of the sandwich structures require studying the performance of the sandwiches under bending for safe usage. Various researchers investigate the sandwich beam with metallic foam core and metallic face sheets under bending and found that it can fail

ATTENTION: The Singapore Copyright Act applies to the use of this document. Nanyang Technological University Library

under various failure mechanisms such as i) face yield, ii) face wrinkling, iii) core shear, iv) core indentation, and v) delamination [12,62].

A sandwich beam having a core thickness of *'c'*, width of 'b', a face sheet thickness of '*t*', length of *'l'* ,Young's modulus of core and face sheet as 'E_c', 'E_f' and total applied loads *'F'*, can fail under three-point bending in any failure modes, as shown in Figure 2.9.

If the load required for failure under any mode is less than other failure mechanisms then the sandwich beam will fail under that particular failure mode. If bonding between face sheet and core is perfect then delamination can be avoided. Usually, failure due to face wrinkling is not found in sandwich beam with metal foam because load required for this failure is very high compare to other failure modes due to the presence of Youngs' modulus terms as shown in equation 2.1 [62].

$$LF = 2.28E_f^{1/3}E_c^{2/3}\frac{btc}{l} \tag{2.1}$$

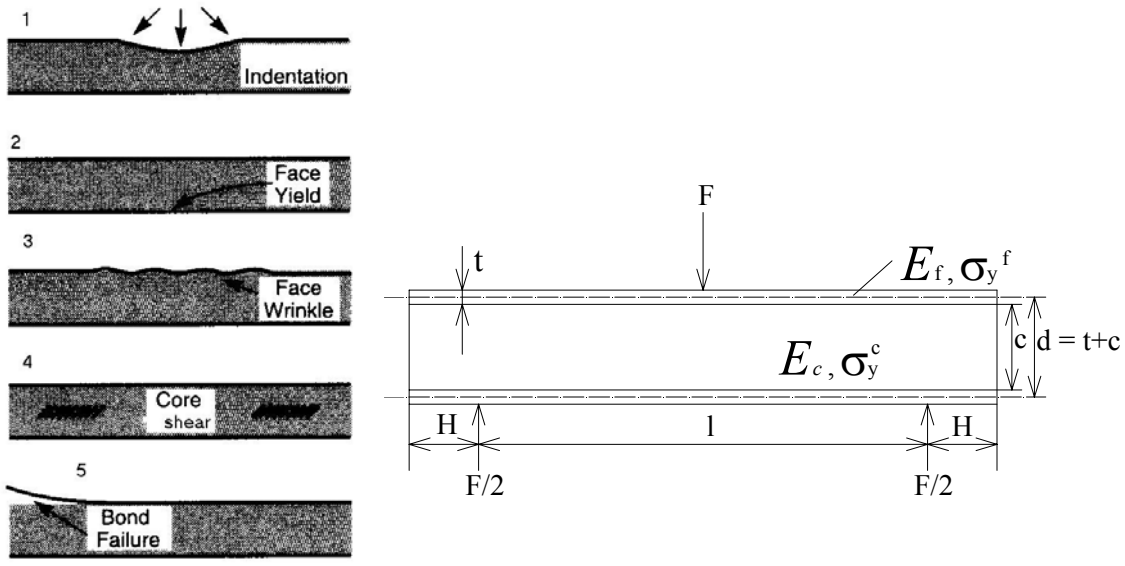

Figure2.9 Failure modes in sandwich beams [9].

Chen et al [12] studied the sandwich beam with Al foam core and Al face sheets under four-point bending and found that it can fail under various failure mechanisms as stated below with accessing the failure loads analytically.

ATTENTION: The Singapore Copyright Act applies to the use of this document. Nanyang Technological University Library

2.6.1.1 Face yield

When the normal stresses in the face sheet reach the yield stress of the face material, yielding of face sheet would begin [12, 62]. Collapse is assumed when the face sheet attains the yield strength of σ_y^f with core yields simultaneously at a stress of σ_y^c. Here 's' is defined as distance between loading indenters and 'l' is distance between supporting indenters.

The load requirement for face yielding for a sandwich having aluminum foam core and aluminum sheet as face sheet under four point bending was studied and derived as given by [12]

$$LF = \left\{ \frac{4 \times (b \times t) \times (c + t) \sigma_y^f}{(l - s)} \right\} + \left\{ \frac{(b \times c^2) \times \sigma_y^c}{(l - s)} \right\} \tag{2.2}$$

2.6.1.2 Core indentation

Failure load was assessed for indentation of sandwich beam having linear elastic bending of the top skins on a rigid –perfectly plastic core [63, 64].

The load requirement for indentation failure mode for a sandwich beam consists of an Al foam core and the top aluminum face sheet under bending has also been analyzed [12]. The load requirements for indentation depend on the indenter geometry and foam density [62]. During indentation of sandwich beam, the foam under the indenter crushes and the face sheet bends to accommodate the foam deformation [12]. In the sandwich beam with aluminum face sheet, indentation involves the formation of plastic hinges in the top sheet adjacent to each indenter with compressive yielding of underlying core. The indentation load required for sandwich beam having metal foam core and metal face sheet of elastic-perfectly plastic material, with a spherical indenter in four-point bending (Figure 2.10) is given by:

$$LF = 4bt\sqrt{\left(\sigma_y^f \times \sigma_y^c\right)} \tag{2.3}$$

ATTENTION: The Singapore Copyright Act applies to the use of this document. Nanyang Technological University Library

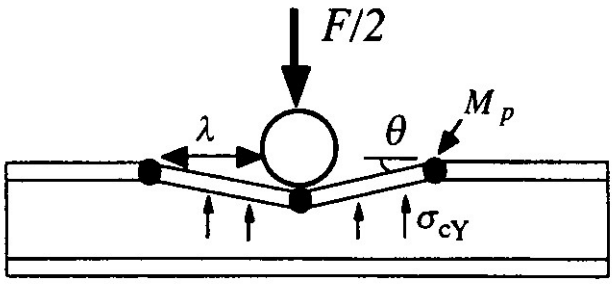

Figure2.10 Indentation failure for a sandwich beam having metal foam core with metallic face sheet under bending [12].

2.6.1.3 Core shear

Shear force is carried by the foam core when a sandwich panel is subjected to transverse shear force [9]. If the required load for shear yielding of sandwich is less than other failure mechanisms then the sandwich beam will fail under core shear mode. Core shear failure mode for a sandwich having aluminum foam core and aluminum sheet as face sheet was investigated [12]. Two modes were found under the category of core shear. In mode A, plastic hinges are formed in the face sheets beneath the inners indenters. While in mode B, plastic hinges are formed in the metal face sheet adjacent to all the rollers. The load requirements for sandwich beam consist of Alporas foam core and aluminum face sheet, under four-point bending (Figure 2.11) are:

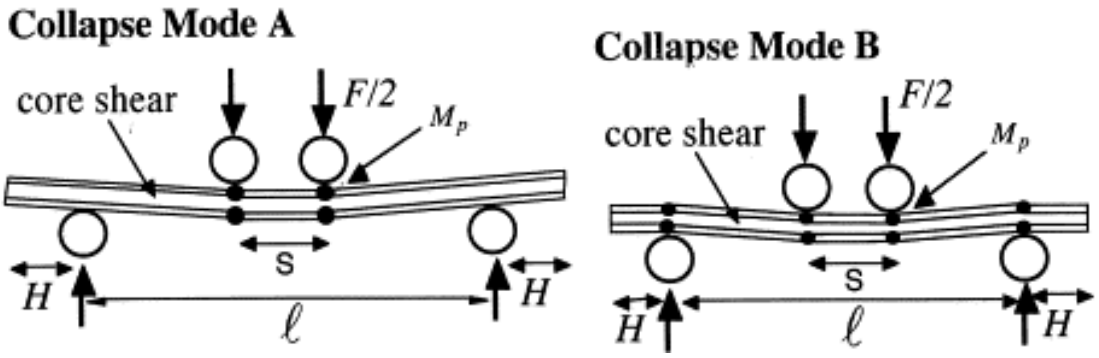

Figure2.11 Competing collapse modes A and B for core shear of a sandwich beam in four-point bending [12].

Mode(A)

$$F_{CSA} = \frac{2bt^2}{(l-s)}\sigma_y^f + 2bc\tau_y^c\left(1+\frac{2H}{(l-s)}\right) \tag{2.4}$$

ATTENTION: The Singapore Copyright Act applies to the use of this document. Nanyang Technological University Library

Mode (B)

$$F_{CSB} = \frac{4bt^2}{(l-s)}\sigma_y^f + 2bc\tau_y^c \tag{2.5}$$

Similarly, equations for the failure loads of different failure modes were developed for sandwich beam, consisting of metal foam and different face sheets [9, 65].

2.6.2 Failure of sandwich comprising Al foam core on plastic foundation under indentation

In various applications such as aerospace, automobile, and building industry, sandwich structures can be subjected to localized loading such as indentation. Performance of those structures under indentation depends on many parameters including the properties of foam core and face sheet. For the safe design of these structures it is necessary to identify the different failure mechanisms with which the structure can fail and the capacity of energy absorption by these structures.

Oliver et al [66] studied the hardness and elastic modulus by indentation to obtain a better understanding of the mechanics governing elastic- plastic contact. They update the implementation of the method for the most accurate measurements of mechanical properties for this type of contacts. The advantages and disadvantages of using different indenters such as spherical, conical, berkovich etc are also explained. Various researchers have also investigated the indentation response of Al foams mainly Alporas [67- 71].

Kadar et al [67] nicely correlated the acoustic emission signals with the indentation response of Alporas and Al-Si foams in terms of deformation mechanisms such as cell wall bending, cell wall buckling and densification of cells beneath the indenter. Olurin et al [68] has investigated the indentation resistance of Alporas foam under flat bottomed circular cylindrical punches and flat plate punches. It was concluded that the indentation pressure strongly depended on indenter size up to a ratio limit (indenter diameter to cell size) of 8. They found crushing of foam underneath the indenter and tearing of foam at the edge of indenter as the failure mechanisms for flat punch. It agrees well with the finding of other researchers [25]. However, Kadar et al [69] found buckling of cell walls in the vicinity of the densified zone in addition to foam crushing. According to them buckling of cells located far away can also occur. They proposed an analytical relationship between the relative density, size of indenter and indentation depth, of which the equation agrees well with FEM

ATTENTION: The Singapore Copyright Act applies to the use of this document. Nanyang Technological University Library

prediction. Kumar et al [70] studied the indentation response of Alporas foam under flat spherical ended indenters and found that deformation is extensively within the zone of plasticity where the cells have collapsed, whereas outside of the zone the material appeared to be in good shape. They compared the effect of both types of indenters and found that after reaching an indentation depth equal to the radius of spherical tip, the response of load-displacement is the same for both indenters. With increasing displacement rate, the load magnitude in the plastic regime as well as energy absorbed increases. Materials properties such as tear energy and shear strength of the foam can be found by conical indentation which is demonstrated by investigation on Alporas Al foam under conical indenters having different cone angles by Rammamurhty et al [71]. They found that for a cone angle of more than 0^0, shearing occurred in addition to the tearing of cells at the periphery with crushing of cells beneath the indenter.

Sandwich structures are sensitive to damage when subjected to localized loading like indentation on strong foundation because of the low strength of the core and the low bending stiffness of the thin face sheets [72]. Various researchers have studied the indentation response of the sandwich structures having a foam core and different type of face sheets [73-79].

Soden [73] derived an analytical solution for failure load of linear elastic beam attached to a crushable foundation. He found a good agreement between this solution and the indentation experiment on sandwich beam with GRP skins and PVC foam cores. Sburlati [74] developed an analytical solution for predicting the force–indentation relationship for clamped or simply supported sandwich beams having foam core under rigid cylindrical and spherical indenters. This solution was developed based on classical sandwich plate theory and a distribution of surface pressures reproducing the contact law of rigid indenters on elastic space.

Zenkert et al [72] proposed an analytical model and investigated that model with FEM and experimental studies on sandwich structures having polymer foam core and composite face sheet. Koissin et al [75] derived the analytical solution for predicting the response of sandwich beams with foam core under indentation in terms of face deflection, crush zone size and contact force. This solution was derived on the principle of minimum work with an

ATTENTION: The Singapore Copyright Act applies to the use of this document. Nanyang Technological University Library

assumption of core crushing followed by elastic-ideally plastic behavior. This solution agreed well with the FEM and experimental investigation.

Shuaeib et al [76] investigated the indentation behavior of the sandwich beam with PVC foam core and glass fiber woven – roving reinforced polyester resin skins. They found linear proportionality relation between the thickness of top skin and indentation load. In addition, with increasing core density, indentation load also increases. Rizov et al [77 and 78] studied the local indentation response of polymeric foams with and without fiber reinforced polymeric composite face sheets both experimentally and numerically. The measured load–displacement response and residual indentation depth compared well with finite element predictions. Rizov [79] developed two dimensional finite element model for elastic plastic non linear response of sandwich composite beams having foam core under local loading. The main aim for this study was to further understand the failure modes caused by static indentation.

Miller [80] used finite element analysis to study the behavior of a sandwich structure with metal foam as core and aluminum as face sheets and proposed a model for initiation load for indentation. Sridhar and Fleck [81] found various failure modes for simply supported sandwich circular plates consisting of metal foam as the core and aluminum face sheets loaded centrally by a flat punch. They found core indentation, core crushing, face sheet punching, and face sheet bending as competing failure modes and the operating failure mechanism depends on the plate geometry, punch radius and material properties.

2.6.3 Failure of sandwich comprising Al foam core under impact

Sandwich structures comprising metal foam core can be used in various applications including defense, aerospace, automobile, and the building industry for various military and civil purposes [7, and 9]. Performance of these structures in the above applications lead to a few investigations such as bullet, blast performance for protective structures, collision in automobile impact, debris impact in aerospace structures etc.

Various Al foams including Alporas and Cymat were investigated under impact by several researchers to understand the failure mechanisms and strain rate sensitivity on various parameters like strength, modulus, plateau stress etc [82-104]. Deshpande and Fleck [82]

ATTENTION: The Singapore Copyright Act applies to the use of this document. Nanyang Technological University Library

have found that the plateau stress and densification strain of Alulight and Duocel Al foam are insensitive to strain rate for high impact velocities (more than 50 mm/sec). While some other researchers found that yield stress show remarkable strain rate sensitivity with enhancement of 50 % in energy absorption capacity of Alporas Al foam in impact loading compare to static loading [83 and 84]. Absorption of impact energy at low and high velocities was investigated by Ramachandra et al [88] for Alporas foam using flat ended and spherical impactors. They found tearing and shearing of the cells at the periphery of the indenter as the failure mechanisms contrast to foam core crushing which is the only mechanism under uniaxial compression. Impact energy absorbed by Al foam was found to be higher under the spherical indenter than the flat end indenter because of the additional mechanism of shearing of cells.

No rate sensitivity was found for Cymat foam under dynamic compression and cell wall fracture was the failure mechanism [89 and 90]. Cymat foam was found to be very anisotropic in nature and their dynamic response depends upon the direction of loading [91-93]. Dynamic compressive flow stress or plateau stress can be increased with the relative density of the foam made with powder metallurgical route but these foams are also found to be strain rate insensitive [94]. It was concluded that the strain rate sensitivity and failure mechanism of Al foams depend upon the composition of Al foam cell wall material [95] but all Al foams can absorb large amount of impact energy.

Various researchers have studied the response of sandwich structures having polymer foam core and composite face sheets to understand the energy absorption capacity and failure mechanism for various applications [95-100]. However, due to temperature limitation associated with polymer foams, researchers are interested to know the response of structures having Al foams with different face sheets under impact loading [101 and 102]. Kretz et al [103] found that the A-pillar of a car made with Al foam core and metallic face sheet is good for energy absorption and the required head injury protection criterion can be achieved with variation of density and microstructure of Al foam. Yu et al [104] investigated dynamic response of sandwich beam having open cell Al foam as core and Al face sheets and compared it with quasi-static loading. The load carrying capacity (for dynamic loading) was found to be higher. Face sheet wrinkling is observed as the failure mechanism in addition to debonding between upper skin and core as well as compression of upper foam with tension of

ATTENTION: The Singapore Copyright Act applies to the use of this document. Nanyang Technological University Library

lower foam core. Gama et al [105] found excellent performance of panels having Al foam and different skins in armors. They found that closed cell Al foams have a good capacity for delaying stress wave propagation and attenuation. They developed one dimensional plain strain finite element analysis which compared with the experiments and found good agreement between two. Hanssen et al [106] investigated the behavior of Al foam panels under blast loading using a ballistic pendulum. They developed an analytical and numerical solution with LS-DYNA for deformation behavior of Al foam panel subjected to a linearly decaying blast loading. They also found that foam panels are good energy absorber and can be very useful as sacrificial layer in blast protection of the structure. Destefanis et al [107] investigated the performance of open cell Al foam as core of sandwich having Al face sheets in bumpers to evaluate their shielding capabilities in manned spacecraft with high impact velocities as 7.0 km/sec. They found that these by layered bumpers have outstanding capabilities to induce multiple shocks to projectile with a strong radial dispersion of the debris cloud. Markaki et al [108] investigated impact response of laminated composites having Al foam and alumina layers at low, intermediate and high velocities. They found that the response of the laminate at low impact velocity is similar to static indentation and the penetration mode changes from plugging to fragmentation in case of low velocity to intermediate one. Villanueva and Cantwell [101] investigated different failure modes and energy absorption capacities of sandwich structures having Alporas Al foam as core and skin as plan composite or fiber metal laminate, under high impact loading, with a nitrogen gas gun. Localized indentation for foam, fiber matrix delamination or longitudinal splitting and fiber fracture of the composite skin were found to be the failure modes. These structures are found to be excellent energy absorbers. These structures were also studied under low velocity impact with buckling and crushing in foam core and fiber fracture in the top face sheet observed as failures causes [102]. Hanssen et al [109] developed numerical simulation model for bird strike with a variation of speed from 140 to 190 m/sec on sandwich panel having Al foam (Hydro) and Al plates, using LS-DYNA. Prediction by this model for local strain, global behavior and local occurrence of failure was agreed well with experimental studies.

2.6.4 Failure of sandwich columns with foam core under end compression

In some engineering applications, sandwich structures are loaded in end compression mode rather than in more common bending conditions. Different failure mechanism were observed such as face sheet micro buckling, shear macro buckling and Euler elastic buckling

ATTENTION: The Singapore Copyright Act applies to the use of this document. Nanyang Technological University Library

depending on the geometrical parameters of sandwich column consisting of PVC foam and glass fiber epoxy face sheet by Fleck and Sridhar [110]. They developed the analytical solution for predicting the failure load for each mechanism and that agreed well with the experimental measurements. Wrinkling in face sheets under compression was studied for a composite column of PVC foam core and unidirectional carbon/epoxy face sheets by Gdoutos et al [111]. Hoff and Mautner's expression for the load resulting in face wrinkling failure was found to be in well agreement with wrinkling failure stress in experimental observation which is defined as the stress at which the strain on the convex side of the panel reaches a maximum value. Vadakke and Carlsson [112] investigated compressive failure mechanism of sandwich panel of PVC foam core with glass and carbon epoxy composite sheets under end compression loading. Buckling of debonded face sheet followed by rapid propagation of debonding was found to be the mechanisms for the sandwich panel having artificial debond between one of face sheet and foam core loaded under end compression. Compression failure of composite face sheet was also observed in panel without any artificial debond between face sheet and foam core. Loads for failure was found to be decreasing with increasing debonding length and decrease in foam density. Post buckling strength was found to be negligible. Core shear failure with negligible face sheet delamination was found to be the failure mechanism for sandwich panel of PVC foam core and orthotropic fiber reinforced plastic face sheets tested for buckling in uni-axial compression by Roberts et al [113].

2.6.5 Performance of Al foams filled structures under end compression

Metal foams have a very good energy absorption capacity when inserted into metal tubes [9]. Hanssen et al [114] studied the crushing of square aluminum extrusions filled with Al foam (Hydro) under quasi-static compression loading. They showed the potential of Al foam as an absorber of a high amount of energy. They also found that foam bonded components have higher amount of specific mass energy absorption than components having foam without bond. Folding mechanism was observed with presence of lobes in the side walls during crushing of non-filled extrusion tubes. An increment in number of lobed was recognized in foam-filled extrusion if it was not ruptured and hence increment in absorption of energy. Design rules have been generated for determining the minimum weight of extrusion based on the results obtained for the square foam filled extrusions. Hanssen et al [115] investigated the potential of numerical simulation of crushing of square Al tubes filled with Al foams with the help of four existing models in LS –DYNA. They found that the fracture of foam is very

ATTENTION: The Singapore Copyright Act applies to the use of this document. Nanyang Technological University Library

local and/or global failure mechanism which has not accounted in these models. Ryes et al [116] have performed numerical analysis for bending of square aluminum filled with Al foam (Hydro) using material models including newly implemented fracture criterion for both extrusion and foam by LS DYNA and compared with experimental investigation. The general behavior, mean and peak loads predicted by numerical simulation were found to be within reasonable accuracy with the experiments.

Hanssen et al [117] also investigated the performance of circular aluminum extrusion filled with Hydro foam under static and dynamic crushing. They observed two distinct failure modes; namely axisymmetric (concertina effect) and non- axisymmetric (diamond effect) in crushing of those extrusions. A shift in buckling mode from diamond to concertina was observed with increment in foam filler density. A model for predicting the crush force was developed for both static and dynamic loading conditions which show the divisions of crush force in three main parts (1) average crush force of non-filled extrusions, (2) uniaxial resistance of foam filler and (3) an interaction effect between foam and wall. Increased resistance was observed for crushing the components under dynamic loading due to inertia effects arising in walls compare to static loading.

A closed form analytical solution was developed by Santosa et al [118] for mean crush force for Al foam filled Al columns from a combination of analytical and numerical solutions. It was found to be in good agreement with experiments. They found that the mean crush force increased with foam compressive resistance and cross-sectional area of the column. Haberling et al [119] observed improvement in energy absorption capacity of stainless steel tubes filled with Al foams with increment in wall thickness but leads to large load fluctuation during buckling with large increment in structural mass. Asvavisithchai et al [120] observed a significant improvement in energy capacity of steel circular tubes filled with Al foam with increment of length of tube, which was due to stabilization of tube wall by the foam which enabled the tube to resist the folding process. The criterion found for change over mechanisms from concertina to diamond for these tubes is length to width ratio of 1.06. It indicated that if the tube was a length to width ratio more than this, then the failure mode would be diamond producing erratic folds.

Little difference was observed in energy absorption capacity of steel tubes filed with Al foams with different type of bonding including in-situ (making foam inside the tube), loose

ATTENTION: The Singapore Copyright Act applies to the use of this document. Nanyang Technological University Library

push fit and adhesive bonded by Asvavisithchai et al [121]. Similar observations in terms of energy absorption capacity was found in compressive testing of push–fit and laser beam welded Al foam filled steel tubes by Haberling et al[119]. More energy was absorbed in square tubes filled with foam with adhesive due to high bonding strength of glue which enable foam/tube interfacial adhesion [122]. Seitzberger et al [123] studied the experimental and simulation of crushing of steel tubes with circular or square cross-section filled with Al foams at quasi-static compression loading. They found an enhancement of the efficiency of energy absorption capacity of metal tubes due to changes in the deformation modes of the tubes. This is because of the interaction between tube and Al foams.

The advantages of foam filling of tubes (any material such as Al, Brass and Ti) in terms of the enhancement of energy absorption are observed not only in the axial direction but also in the transverse direction by Hall et al [124-125] for quasi-static and dynamic loading. However, the percentage increment in specific energy is found be higher in axial loading compare to transverse loading with the highest absorption in Al tube and moderately with brass and Ti tubes.

2.7 Failure mechanisms map

Equations of the collapse load for different failure mechanisms can be derived for the sandwich structure loaded with specific constraints such as three point bending, flat indenter and constant σ_y^f, σ_y^c . These equations have some variables, some of which are related to materials property (E_f, E_c, ρ_c, ρ_f) and some to beam geometry (Normalized face sheet thickness '*tlc'*, normalized core thickness '*c/l'*, normalized beam width '*b/l'* etc) [10] and therefore it is interesting to find out how the failure modes depend on the geometrical parameters. It is quite obvious that for a given design, the dominant failure mechanism is the one that occurs at the lowest load. Transition from one mechanism to another takes place when both mechanisms have about the same failure load. This information can be shown as a diagram or map, known as a failure mechanisms map. This map is the graphical representation of failure loads with respect to design parameters (as axes) having constant material properties. Axes of those maps are design parameters of the structure. Each map is

ATTENTION: The Singapore Copyright Act applies to the use of this document. Nanyang Technological University Library

divided into different fields according to the dominant failure mechanism.

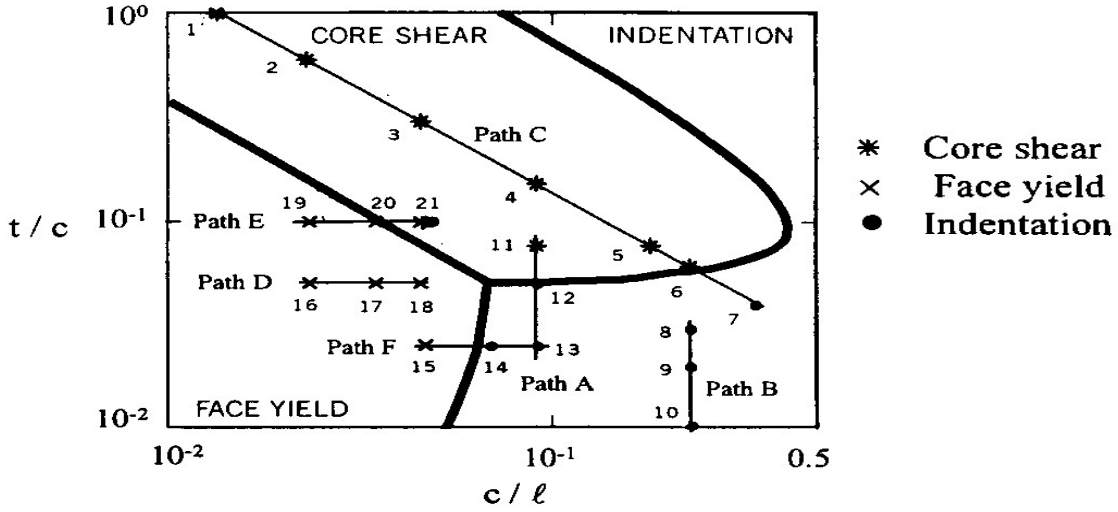

Figure2.12 Failure Mechanism map of sandwich beams subjected to four-point bending [12].

Field boundaries are found by equating the equations for different failure loads. Generally only two non-dimensional design parameters (*c/l, t/c*) are introduced to take into account all the parameters for the structures under bending.

A failure map showing the different failure mechanisms for a sandwich having Al foam as core and Al sheet as face sheet under four point bending was constructed in Figure 2.12 [12]. The map is plotted for collapse load index $\bar{F} = \frac{F}{bl\sigma_y^f}$ on a diagram having axes *c/l* and *t/c*, for selected values of *s/l* and σ_y^c / σ_y^f [12]. These failure maps vary depending on the type of loading (e.g. bending, indentation or end compression) and the type of indenter (e.g. flat or spherical). As certain parameters like indenter size affect the equations for failures, those parameters will influence the regions of failure map [9].

On similar guidelines, the failure mechanism map shown (in terms of normalized face sheet thickness (ratio of face sheet thickness to core thickness),'t/c' and normalized sandwich core thickness (ratio of core thickness to sandwich radius) 'c/R' in Figure 2.13 was generated by Sridhar [126] for simply supported circular sandwich plates of radius R made with metal foam core and cold worked aluminum face sheets loaded under quasi-static indentation. Different failure maps are generated on almost the same guidelines for sandwich structures of

ATTENTION: The Singapore Copyright Act applies to the use of this document. Nanyang Technological University Library

metal foam core or polymer foam with aluminum face sheets under different loading conditions such as three-point bending, four-point bending and indentation [9, 65].

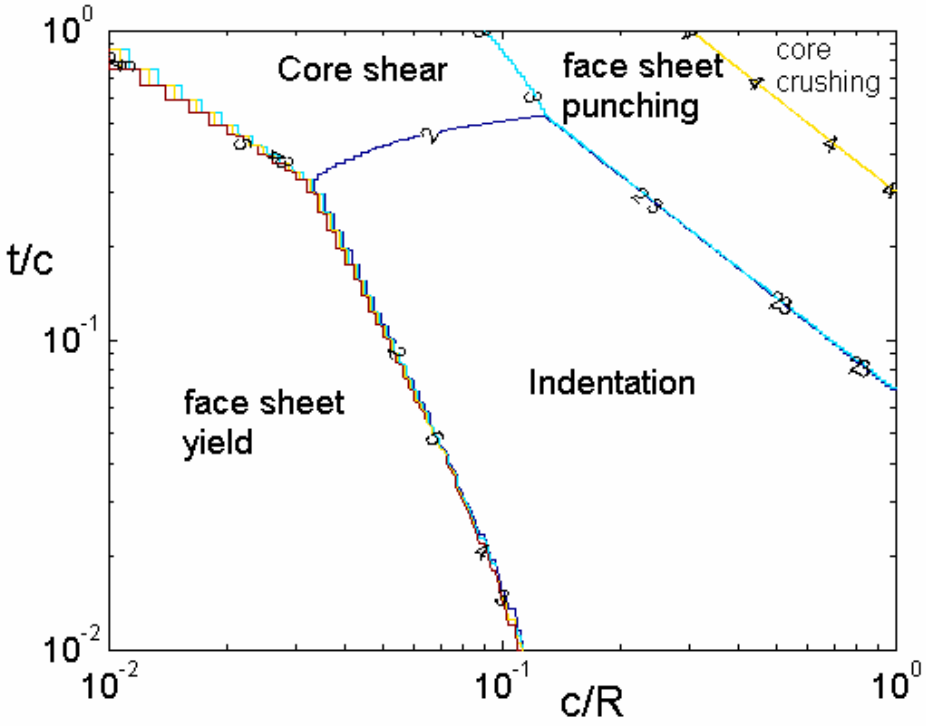

Figure2.13 Failure Mechanism map for simply supported sandwich plate (foam core 'c' and face sheet thickness 't') of radius R loaded by a punch radius 'r' at the centre, with $R/r = 8.0$ and $\sigma_y^c / \sigma_y^f = 0.03$ [126].

2.8 Minimum weight design

It is a task for researchers to minimize the weight of sandwich panels without compromising strength and stiffness. In this way, the cost of structure in terms of total load requirement can be reduced that is the prime requirement of industry. Minimization of weight can be formulated for a structure for required collapse load, stiffness or strength or for all [127-129]. First of all, an equation for the objective function (weight of the structure 'W') was developed, then equations for constraints (such as stiffness, strength etc.), were developed, according to applications. A typical example for minimum weight design for sandwich structure of PVC foam core under bending is shown below [10].

The objective function is:

$$W = 2\rho_f gblt + \rho_c gbl \tag{2.6}$$

In the case of the constraint of certain stiffness δ/P, under bending of the sandwich structure, the constraint equation is:

ATTENTION: The Singapore Copyright Act applies to the use of this document. Nanyang Technological University Library

$$\frac{\delta}{P} = \frac{2l^3}{B_1 E_f t c^2} + \frac{l}{B_2 b c G_c} \tag{2.7}$$

Where 'b', 'c' and 'l' are width, core thickness and length of the structure respectively, g is the Gravitational acceleration, ρ_c is the density of foam core, ρ_f is the density of face sheet, B_1 and B_2 are constants.

The optimum value of core thickness of sandwich structure, c, is obtained by setting dw/dc equal to zero after substituting the value of '*t*' from Equation 2.7 in Equation 2.6. If this value of core thickness is substituted back into the Equation 2.7, then the value of optimized face sheet thickness can be obtained. The minimum weight of the sandwich panel will be obtained for the optimized thickness of face sheet and core.

The graphical method is another way of achieving this. Here, the objective function 'W' is written in terms of free variables (from Equation 2.6)

$$\frac{t}{l} = \frac{W}{2bl^2 \rho_f g} - \frac{\rho_c}{2\rho_f}\left(\frac{c}{l}\right) \tag{2.8}$$

Constraint is also written in terms of free variables (Equation 2.7)

$$\frac{t}{l} = \frac{2B_2 G_c}{B_1 E_f \left(\frac{c}{l}\right)} \left\{ \frac{1}{\left(B_2 \frac{\delta}{P} b G_c \left(\frac{c}{l}\right)\right) - 1} \right\} \tag{2.9}$$

The intersection of these two plots of objective function and constraints with respect to the dimensionless (free variable and length) axes gives the optimum design. A typical example of this type of plot for a sandwich, having polyurethane foam as core and aluminum as a face sheet, is shown in Figure 2.14 (a). The optimization procedure can also be carried out by considering only the face sheet thickness, *t*, and core thickness, *c*, as the free variables. Then, equations for objective function (W) and for constraints, strength and stiffness can be generated. Subsequently, plots of different failure modes like core shear, face yield etc are superimposed on the plots of objective function and constraint functions on the same dimensionless axes. A typical example for polyurethane foam core sandwich with aluminum sheet is shown in Figure 2.14 (b).

ATTENTION: The Singapore Copyright Act applies to the use of this document. Nanyang Technological University Library

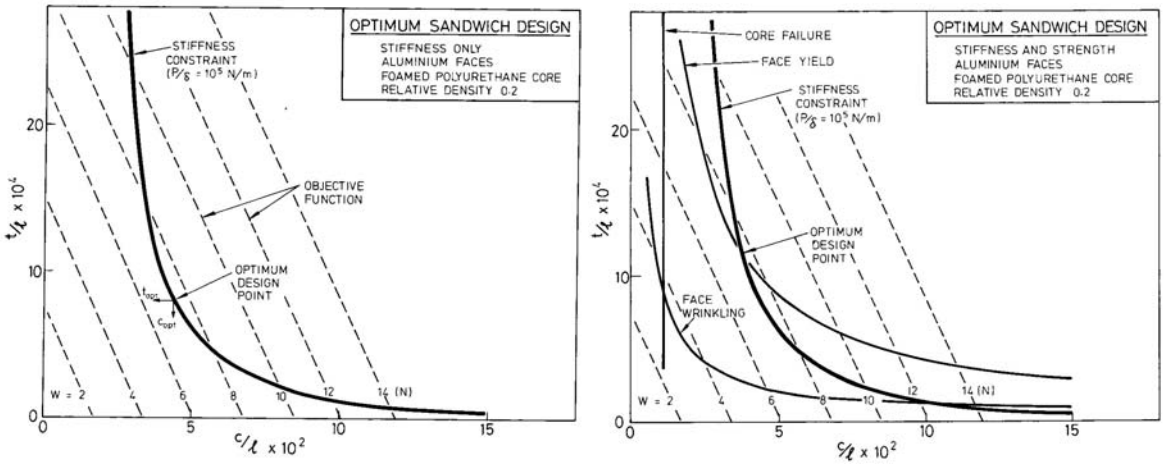

(a) (b)

Figure2.14 Optimum design with graphical method of optimization for sandwich having polyurethane core and aluminum face sheets (a) stiffness constraint only (b) both stiffness and strength constraints [10].

On similar guidelines, minimum weight designing was carried out for sandwich structures with metal foam cores and aluminum face sheets under bending [9, 12].

Minimum mass designing was carried out by Hanssen et al [130] for square aluminum columns filled with Al foams having parameters of foam plateau stress, column wall material characteristics stress, width, thickness and length of column and other constraints. This study showed the significance in saving of mass, length and volume by utilizing foam filler in crash behavior. Design rules have been generated for determining the minimum weight of extrusion based on the results obtained for the square foam filled absorbers by Hanssen et al [114].

Budiansky [128] carried out a detailed analysis for minimum weight of columns having solid square or circular sections with similar metal foam filled tubes, hollow tubes and tubes whose wall are foam core sandwiches. He found that on a weight/strength basis, foam core square and circular tubes are inferior to hollow tubes and on top of that circular tubes are better than square one. Here, he also found that flat compression panels are heavier than hat-stiffened which is heavier than skin-stringer panels in which skins and stiffeners are made with metal foam core sandwiches.

Minimum mass designing was carried out on similar guidelines for sandwich structures having metal foam core with aluminum face sheets under various loading conditions such as

ATTENTION: The Singapore Copyright Act applies to the use of this document. Nanyang Technological University Library

bending, having different geometrical variable such as length, width and thickness of structure with properties of foam core and face sheet under different constraints [9, 10, 131, 132].

2.9 Finite element analysis

The behavior of the material in FEM would give a good indication of its real-life behavior, if the simulation is done correctly. The models in FEM are developed in terms of yield criterion and constitutive laws governing it in its real life. To choose the perfect model for a particular material, it is necessary to adopt the correct behavior of the material, model and the governing equations.

2.9.1 Model for metallic foams

Constitutive laws governing the yield criterion for metallic foams are developed and modified [48, 80,133-136]. As reported behavior of the metallic foams is linear isotropic elastic in the elastic regime as for conventional metals. In the plastic regime, Alporas aluminum foams display isotropic hardening behavior [48].

2.9.1.1 Elastic regime

The generalized Hooke's law is used to calculate the linear elastic strain tensor in the form

$$\varepsilon_i^e = C_{ij}\sigma_j \tag{2.10}$$

where i , j = 1,2,3,…….

and $\varepsilon_i^e, \sigma_j$ are the elastic strain and stress tensor, respectively, while C_{ij} is the compliance matrix. This matrix is characterized by a set of modulli and Poisson's ratio. All the metals and brittle materials show this behavior.

2.9.1.2 Plastic regime

Linear elasticity is limited by the yield criterion. Plastic yielding is the most usual mechanism for "failure" of ductile metals. These mechanisms can be described by rate–dependent incremental plasticity theory. According to this theory, the elastic theory fails at a value where plastic behavior starts.

ATTENTION: The Singapore Copyright Act applies to the use of this document. Nanyang Technological University Library

Yield criterion: It is a law defining the limit of elasticity under any possible combination of stress. The yield function $f(\sigma_{ij})$ is expressed as

$$f(\sigma_{ij}) = const. \tag{2.11}$$

e.g. one yield criterion, knows as Von-Misses Criterion is given below

$$(\sigma_1 - \sigma_2)^2 + (\sigma_2 - \sigma_3)^2 + (\sigma_3 - \sigma_1)^2 = 6k^2 \tag{2.12}$$

where k is a dependent parameter.

Various models have been developed to describe the shape of a yield surface for homogenous metallic foams [137].

2.9.1.2.1 Classical J_2 plasticity:

It is the simplest and most common model to predict plastic deformation in fully dense metal. The yield surface in this model is expressed as

$$f = \sigma_e - Y = 0 \tag{2.13}$$

Where Y is the uni-axial yield strength of the material and σ_e is the Von –Misses effective stress defined by

$$\sigma_e = \sqrt{\frac{3}{2}\left\{(\sigma_1 - \sigma_2)^2 + (\sigma_2 - \sigma_3)^2 + (\sigma_3 - \sigma_1)^2\right\}} \tag{2.14}$$

This yield surface is independent of the mean stress. A material that satisfies the above behavior cannot fail due to the hydrostatic load and is plastically incompressible (ε_{vol}^{P}) when an associated flow rule is assumed. Due to plastic compressibility of metallic foams, J_2 plasticity is not valid for description of plastic deformation of foams under multiaxial loads.

2.9.1.2.2 Crushable foam model:

This model embraces the ability of modeling the foams with different deformation behavior under compression and tension. There are two flavors of the models currently available in ABAQUS/EXPLICIT, based on volumetric and isotropic hardening constitutive models. Both models use a yield surface with an elliptical dependence of deviatoric stress on pressure stress in the meridional plane. The isotropic hardening model was originally developed for

ATTENTION: The Singapore Copyright Act applies to the use of this document. Nanyang Technological University Library

Alporas foam only [48]. It assumes almost symmetric behavior in tension and compression. The evolution of yield surface is governed by an equivalent plastic strain, which has contribution from both the volumetric and deviatoric plastic strains. It is based on the experiments done on Alporas foam [48], where the yield surface is an ellipse centered at the origin in the p-σ_e stress plane. Yield surface is defined as

$$f = \sqrt{\sigma_e^{\,2} + \alpha^2 p^2} - B = 0 \tag{2.15}$$

and

$$B = \sigma_c \sqrt{\left(1 + \left(\frac{\alpha}{3}\right)^2\right)} \tag{2.16}$$

where p is mean stress = -1/3 (σ_{ii})

B represents the size of the (vertical) axis of the yield ellipse; α represent the shape of the yield ellipse.

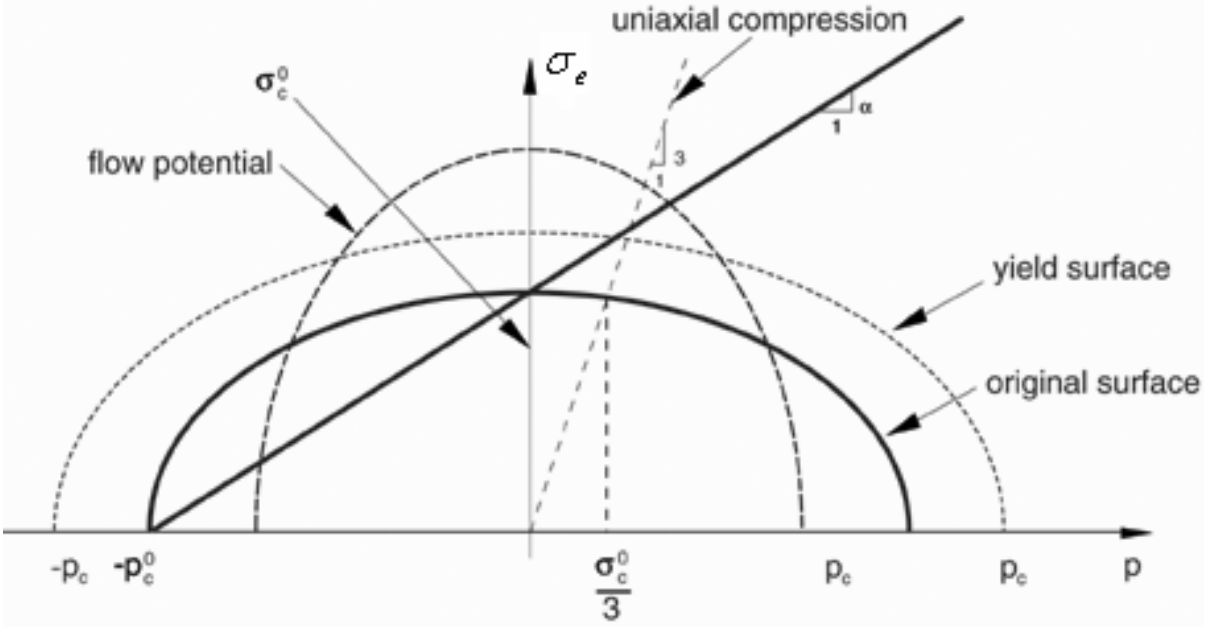

Figure2.15 Yield surface and flow potential for isotropic hardening model [137].

The yield surface is Mises circle in which the deviatoric stress plane and the ellipse in the meridional stress plan as shown in Figure 2.15

The parameter α can be calculated using the initial stress in uniaxial compression, σ_c^0 and the initial yield stress in hydrostatic compression, P_c^0, as

ATTENTION: The Singapore Copyright Act applies to the use of this document. Nanyang Technological University Library

$$\alpha = \frac{3K^{'}}{\sqrt{9 - K^{'2}}} \tag{2.17}$$

$$K^{'} = \frac{\sigma_c^0}{P_c^0} \tag{2.18}$$

Flow potential: The flow potential for the isotropic hardening model is given by

$$FP = \sqrt{\left(q^2 + \beta^2 p^2\right)} \tag{2.19}$$

where β represents the shape of flow potential ellipse on the *p*-*q* plane.

$$\beta = \frac{3}{\sqrt{2}} \sqrt{\frac{1 - 2\upsilon_p}{1 + \upsilon_p}} \tag{2.20}$$

where υ_p is the plastic Poisson's ratio, which is the ratio of the transverse to the longitudinal plastic strain under uniaxial compression.

The plastic strains are defined to be normal to a family of self–similar flow potential parameterized by the value of the potential *G*

$$\varepsilon^{pl} = \dot{\lambda} \frac{\partial FP}{\partial \sigma} \tag{2.21}$$

where $\dot{\lambda}$ is the non-negative plastic flow multiplier

The strain hardening of the foam is described by $\sigma_c = \sigma_c(\varepsilon^{pl})$, where ε^{pl} is the equivalent plastic strain in uniaxial compression under isotropic behavior. So the hardening law defines the value of the yield stress in uniaxial compression as a function of the absolute value of axial plastic strain. Here, uniaxial compression or shear test data is required to define the evolution of the yield surface.

2.9.2 Model for brittle materials

Ceramics and CFRP are both brittle materials with high strength and stiffness. They show only the elastic response in deformation, and is followed by catastrophic failure. In the elastic regime, behavior of these materials is similar to any conventional metal. The elastic behavior of these materials can be explained in the same way as metallic foam (earlier). But elastic

ATTENTION: The Singapore Copyright Act applies to the use of this document. Nanyang Technological University Library

regime represents the behavior of the materials up to 0.2 % strain and not able to explain the failures of those materials. Due to different types of failures in both materials, different failure models are employed, which can be explained as follows.

2.9.2.1 Brittle cracking model for ceramics

Brittle cracking model in ABAQUS/EXPLICIT was found to be the only model for defining the failure of ceramic material [137]. It is developed for the behavior of concrete material. Usually, the tensile strength of the concrete material is one tenth of the compressive strength. Therefore, concrete material fails under tensile mode. Ceramic material follows almost the same kind of behavior. This model offers a way to predict the behavior of the material, where brittle behavior dominates. Therefore the assumption is that the material is linear elastic in compression and failure behavior is dominated by tensile cracks.

This model is based on the brittle aspects of concrete behavior, according to which the micro cracks coalesce to form discrete macro cracks representing regions of highly localized deformation. It almost always involves softening of the material.

Cracking is incorporated in this model in such a way that it does not track down the individual crack but the presence of the cracks enters into constitutive calculations at each material calculation point of FEM, because the crack affect the stress and material stiffness associated with the material calculation points. Once a crack is generated at the material calculation point then the direction of cracking becomes important. This model follows fixed orthogonal cracks model, which is one of the basic cracking direction models. According to this model the crack extension can be aligned normal to the maximum principal tensile stress at the time of crack initiation and other cracks can only form in such a way that the normal of crack surface is orthogonal to the first crack. The maximum number of cracks is limited by the number of direct stress components present at that material calculation point of the FEM A simple Rankine criterion is used to detect the crack initiation. According to this criterion, a crack forms when the maximum principal tensile stress exceeds the tensile strength of the brittle material.

ATTENTION: The Singapore Copyright Act applies to the use of this document. Nanyang Technological University Library

2.9.2.2 Model for CFRP

Engineering Constant material model is found to be only inbuilt model which explains the failure of unidirectional carbon fiber reinforced polymer matrix composite. It was modeled as a homogenous orthotropic material using this model which is sufficient enough to study the macroscopic behavior of the laminate. This model flexible enough to define the angle of fiber reinforcement such as 0^o, 30^o and 90^o etc [138]. The local coordinate system was defined for each sheet of fiber reinforced material to indicate the fiber direction as it will indicate the longitudinal and transverse directions for the sheets which is very important for any orthotropic material. Unidirectional fiber reinforcement was modeled as a layer of laminate layed-up in an unidirectional manner.

2.10 Problem identification

From the literature review it was found that although there is a failure analysis of sandwich beams of traditional materials such as metallic foams core and metallic sheets for designing of safe structures, very little work has been carried out for the structural design of sandwich with hybrid sandwich beams especially with brittle materials as ceramic and carbon fiber reinforced plastics face sheet under bending.

Structures with sandwich columns comprising of PVC foam core and various face sheet under end compression loading were investigated by various researchers to find the possible failure mechanisms under which these beams can fail. However, designing of those columns with metal foam core would be different under end compression.

The review of previous research has taken up to study the indentation behavior of sandwiches of PVC foams with various face sheets. Indentation behavior is also studied for metal foam core alone. There is however, a lack of understanding of the failure mechanisms when various types of face sheets are joined with metal foam blocks, which will be useful for designers to use foams for various structures in real applications.

A thorough search of literature dealing with the sandwiches with Al foam with metallic and composite face sheet under various impact conditions shows the energy absorption potential of these foams. There is however, a lack of comparison of performance of Al foam block

ATTENTION: The Singapore Copyright Act applies to the use of this document. Nanyang Technological University Library

with various face sheets under impact loading which will be useful for designing these foams for automobile or military and civil defense applications.

Energy absorption capability was well proven for these foams in tubes of square or circular cross-section made with different materials from the literature. However, the performance of these foams in rectangular tubes is not explored.

ATTENTION: The Singapore Copyright Act applies to the use of this document. Nanyang Technological University Library

CHAPTER-3

Characterization of materials

3.1 Introduction

Sandwich structure is made of low-density core material, flanked between two strong and stiff face sheets. Aluminum foams have shown a great potential as a core material in sandwich structures [7].The performance of these sandwich structures depends upon various surrounding constraints such as type of loading & boundary conditions and material used as core and face sheets of those sandwiches. For various applications, the constraints and conditions are different, so therefore in the present research work, the performance of sandwich structures consisting of Al foam core with various combinations of face sheets such as aluminum, stainless steel, alumina and CFRP are investigated under various loading conditions such as bending, indentation, impact and end compression to give an over view of these sandwich structures. It is known that the basic characteristics of the materials used in sandwiches plays an important role in the performance of the sandwich constructions. Thus, a detailed morphological & mechanical analysis of various materials used in the construction of sandwich structure is necessary. It is to be noted that the surface characteristics plays a role in mechanical characterization of the foam material [9].

In this chapter, surfaces characterization of Al foams (Alporas and Cymat) using optical and SEM imaging is discussed. An ultrasonic study of Alporas foam was performed to relate the density of the foam with the porosity of the foam. Mechanical characterization including tensile, compressive and shear testing of Al foams are carried out and discussed here. Various materials are used in present research work as face sheets in the sandwich beam with Al foam core to analyze the variation in the performance of those beams with different types of failure. Therefore, the mechanical characterizations of these materials are performed. It was also used as input data for FEM studies to predict the behavior of sandwich beams under various loadings and constraints.

ATTENTION: The Singapore Copyright Act applies to the use of this document. Nanyang Technological University Library

3.2 Surfaces characterization of Al foams

Various surface characterizations of Alporas and Cymat Al foams, with an understanding of the equipment involved and precautions for handling it are discussed here with procedural details. Some as-received features regarding Alporas and Cymat foams are also mentioned briefly.

3.2.1 Chemical composition

Alporas foam was manufactured by GLEICH GmbH MetallPlatten Service, Germany while Cymat foam was manufactured by Alusion, Canada. The chemical composition for Alporas foam is shown in Table-3.1. A typical composition range (vol. %) of Cymat foam is (10-20 % Sic and rest Al alloy) [15].

Table3.1 Chemical composition of Alporas foam

Element	Weight (%)
Ca	1.69
Ti	1.22
Fe	~ 0.04
Mg	~ 0.01
Al	Remaining

3.2.2 Relative density measurement

Relative density is defined as the ratio of the apparent foam density to the density of solid cell wall material. It is an important parameter for foam material because most of the properties of foams scale with relative density. Relative density needs to be measured as accurately as possible. It varies from one location to another in the same block. So, for an accurate assessment of the properties in experiments and input data for FEM modeling, the value of relative density was averaged out at different locations. Thirty two samples of each Alporas and Cymat foams with size of 50 X 50 X 50 mm^3 and 50 X 50 X 40 mm^3 respectively were cut from different locations of the same block of the foam whose density was measured by volume and weights of the foam blocks.

ATTENTION: The Singapore Copyright Act applies to the use of this document. Nanyang Technological University Library

The results for relative density measurement of Alporas and Cymat foam are listed in Table-3.2 and Table-3.3 respectively. The values of mean relative density, found to be 9.5% and 4.7 % for Alporas and Cymat foams respectively, are used in various design calculations.

Table3.2 Relative density of Alporas foam with standard deviation

Relative density	**Value**
Minimum relative density	8.22%
Maximum relative density	11.11%
Mean relative density	9.5%
Standard deviation of relative density	0.887 %

Table3.3 Relative density of Cymat foam with standard deviation

Relative density	**Value**
Minimum relative density	4.1%
Maximum relative density	5.0%
Mean relative density	4.7%
Standard deviation of relative density	0.224 %

3.2.3 Cell size measurement

Cell size plays an important role in designing the dimensions of the specimens for study of mechanical behavior of foam material because of the size ratio factor (specimen size to cell size). This measurement gives an average value of cell size, which is used as a guideline for designing the foam samples. Every dimension of the sample should be higher than the product of a specific integer (defined from size ratio) and average cell size to suppress the size effect. As there is no available software for direct and automatic measurement of cell sizes, different samples were analyzed as follows: A mixture of cold mounting acrylic resin and hot mounting power ‘condufast’ (black in color) was poured on those samples. These samples were kept to dry the mixture for one day. Samples were then grinded on sand paper in such a way that except for the cell walls (white) everything would be black in color. This gives a very good color contrast between the pore and cell walls. Snaps were taken for those faces and analyzed using the Analytical Imaging Station (AIS) software, which can measure the length, area, perimeter etc. It is a multifunctional image analysis software package with which imported images can be analyzed in terms of the surface features. Statistical analysis can also be carried out for the analyzed data with this software. Manual estimation was carried out to address the cell size which is difficult for irregular shaped foam cells. The average of longest distance between cell wall in one cell and perpendicular distance to this

ATTENTION: The Singapore Copyright Act applies to the use of this document. Nanyang Technological University Library

longest distance between cell wall was treated as cell size in the present study. In order to observe the inhomogeneity as well as the shape of the cells, the foams were also analyzed under optical microscope. Around 220 cells of Alporas foam and 180 cells of Cymat foam were analyzed for each block of size 50 x 50 x 50 mm^3 for Aproas foam and 100 x 100 x 40 mm^3 for Cymat foam with statistical analysis such as standard deviation, mean, maximum, and minimum. The results for all the measured samples are shown in Table 3.4 for Alporas foam and Table 3.5 for Cymat foam with the frequency distribution curves for each in Figure 3.1 and Figure 3.2 respectively. This data belong to more than 1700 cells of different samples for Alporas foam and 1500 for Cymat foam. This data agrees with the previously reported results (Miyoshi –2000) for Alporas [18] and product manual for Cymat foam [139].

Table3.4 Cell size measurements for Alporas foam with standard deviation

Cell size	Value
Minimum cell size	0.41 mm
Maximum cell size	10.69 mm
Mean cell size	3.5 mm
Standard deviation of cell size	1.69 mm

Table3.5 Cell size measurements for Cymat foam with standard deviation

Cell size	Value
Minimum cell size	1.61 mm
Maximum cell size	28.76 mm
Mean cell size	13.37 mm
Standard deviation of cell size	5.82 mm

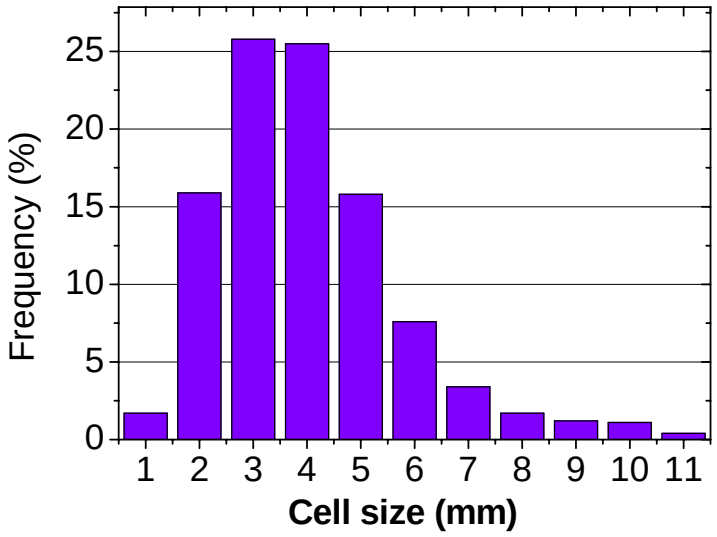

Figure 3.1 Frequency distribution of cell size measurement for Alporas foam.

ATTENTION: The Singapore Copyright Act applies to the use of this document. Nanyang Technological University Library

Figure 3.1 shows that even though the difference between minimum and maximum cell size of Alporas foam is very large but most of the cells fall in the size range of 2-5 mm. The number of cells larger than 7 mm is negligible. The specimen with abnormally big cell can be discarded from specimen lot or the analysis to prevent inconsistency in behavior. Most of the samples follow the same trend with little deviation. Large variation was found in cell measurement of Cymat foam as seen in Figure 3.2, even the standard deviation was found to be as high as 5.82. Most of the cells lie in between 7 to 18mm.

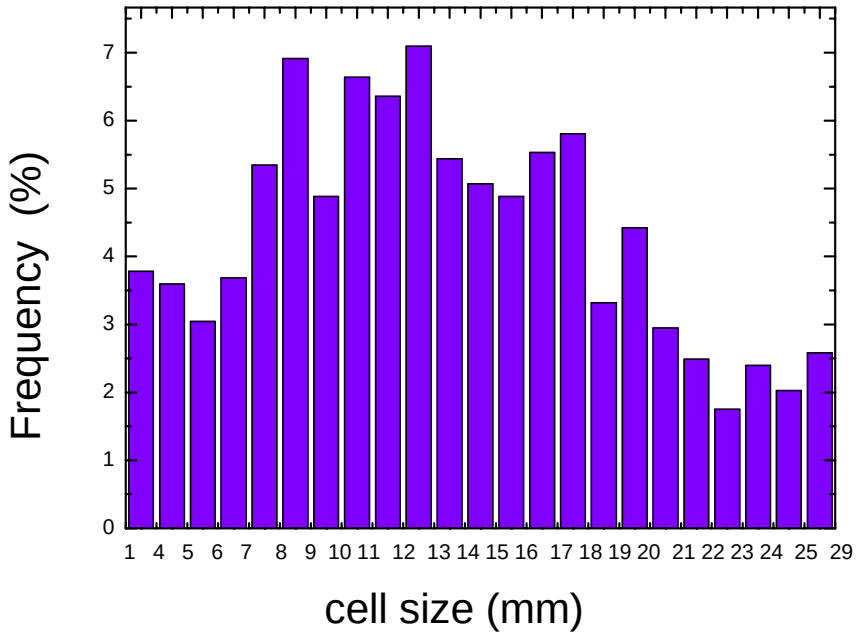

Figure 3.2 Frequency distribution of cell size measurement for Cymat foam

The selection of test specimen geometry for this foam will not be simple as one side dimension should not be small because of criterion of size ratio (greater than a specific number for specimen dimension to cell size) and at the other side it will have limit of lengthy specimen due to size limitation of testing jigs.

3.2.4 Morphology of foam cells

Optical micrographs of Alporas foam cells are depicted in Figure 3.3 (a) and (b). The cross-sections of the cells are not equiaxed. There are Caves (arrow A), wiggles (arrow B), and voids in the cell walls as shown in Figure 3.3 (b). The presence of this type of irregularities was found to be very random across any section. Scanning electron microscope images of

ATTENTION: The Singapore Copyright Act applies to the use of this document. Nanyang Technological University Library

Alporas foam cells are shown in Figure 3.4 (a) and (b). Figure 3.4 (a) shows the wall of typical foam cell, the thickness of the cell wall (arrow C) is from 2μm to 500 μm. SEM of the cavity (arrow D)in foam cells are also shown in Figure 3.4 (b).

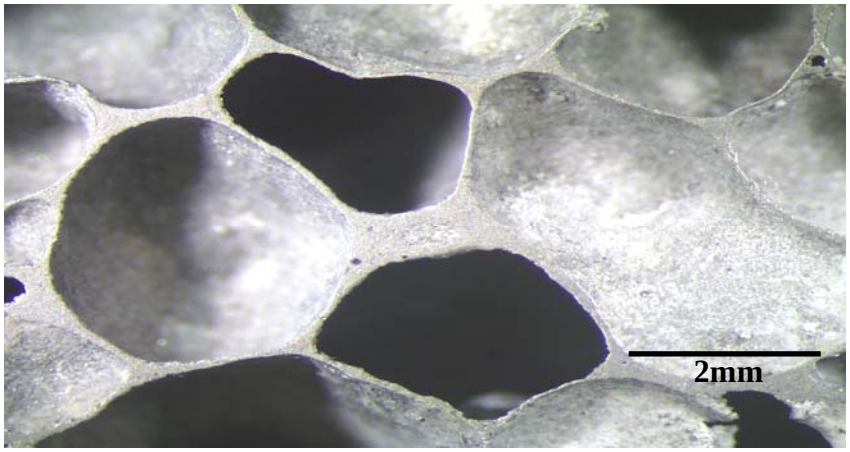

(a)

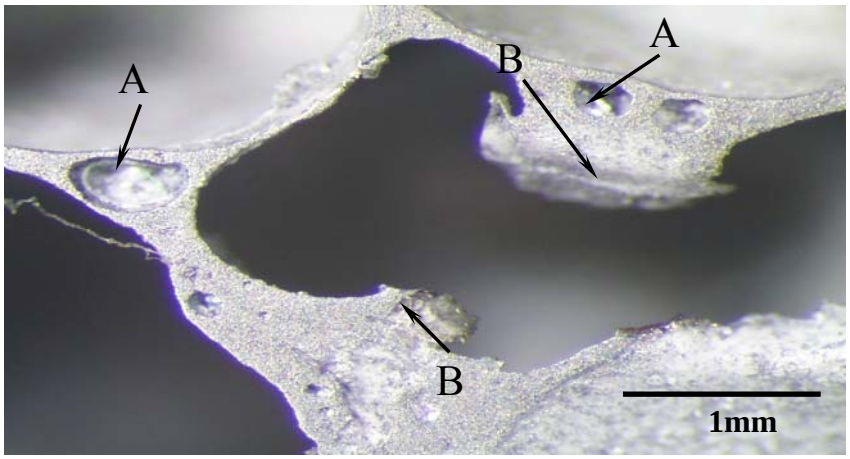

(b)

Figure 3.3 Optical micrographs of Alporas foam (a) random cells (b) cavity between cell walls.

3.2.5 Ultrasonic measurement of Alporas Al foams

NDE (nondestructive evaluation) techniques especially ultrasonic can be more useful to correlate the inhomogeneity of foams with mechanical properties because the output signals from such a test depend to a great extent on the internal morphologies (like pores etc) of the materials. In addition, these tests are capable of providing rapid results without the need to destroy the test samples, thus well suited to manufacturing environment. In this area, NDE

ATTENTION: The Singapore Copyright Act applies to the use of this document. Nanyang Technological University Library

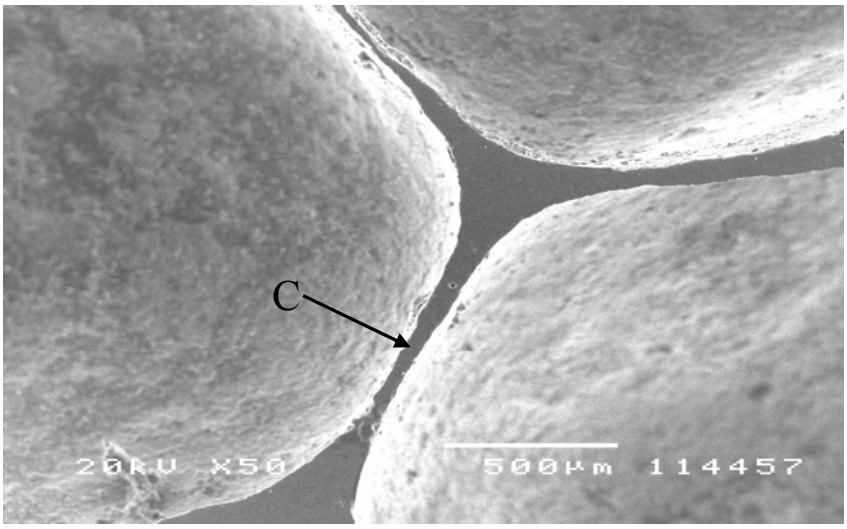

(a)

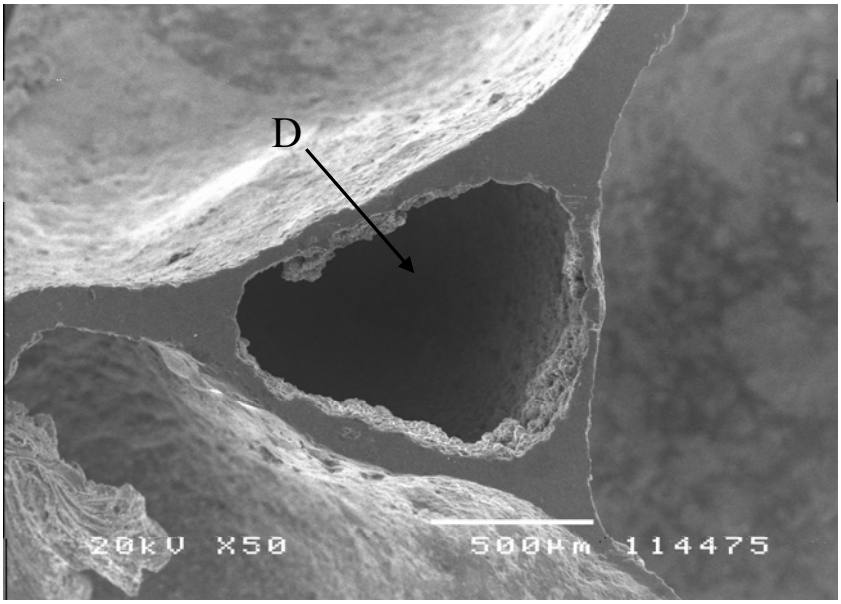

(b)

Figure 3.4 SEM images of Alporas foam (a) showing walls (b) cells showing irregularity

(nondestructive evaluation) has not been utilized to a great extent so it would be quite interesting to know the response of foam when subjected to ultrasonic waves in terms relation of pore structure (in terms of porosity) of metal foam with density of material

In the present research work, ultrasonic evaluation of Alporas Al foam was carried out using Krautkramer USD 15 SX model instrument using pulse echo and through transmission technique. Schematic sketch of an ultrasonic test setup for through transmission technique

ATTENTION: The Singapore Copyright Act applies to the use of this document. Nanyang Technological University Library

employed in this study is shown in Figure 3.5. A large range of frequency of the probes was involved which is varied from 0.5 MHz to 15 MHz.

3.2.5.1 Response with ultrasonic testing

Response of ultrasonic testing of Alporas foam was measured using two techniques as explained below.

3.2.5.1.1 Pulse echo technique:

In this technique, ultrasonic waves are used to send from one probe placing at one end of the specimen and same probe act as the receiving probe. Signals received from the back wall of the sample are analyzed in terms of location of any discontinuity or pores etc, but this investigation is carried out only on one side of surface of the specimen by probe. When this technique was applied to foam specimens of different density with all frequency probes (0.5 MHz to 15 MHz) available, then no signal was received back from wall of the foam specimens. It indicates high attenuation of Alporas foam having lot of uneven pores.

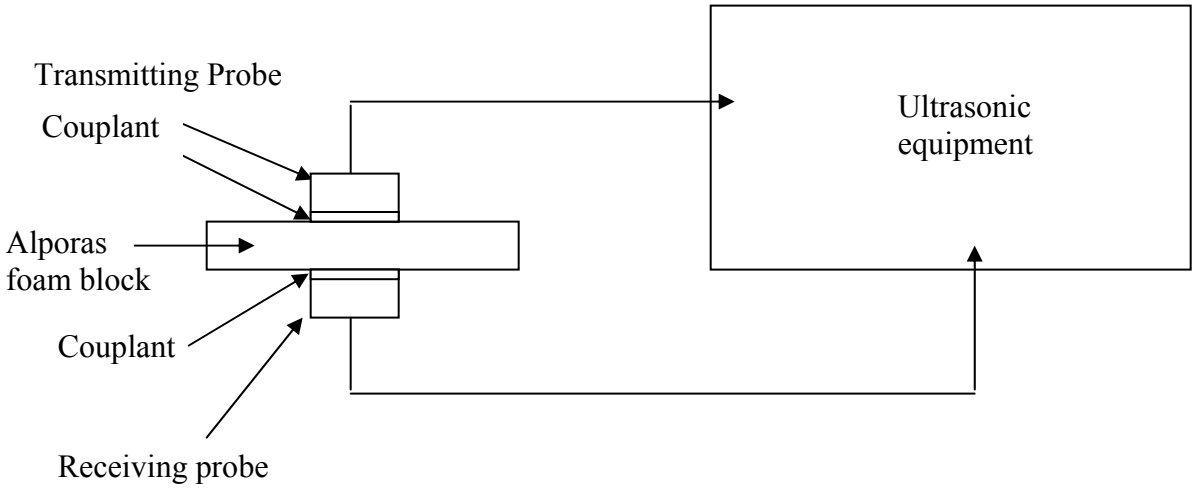

Figure 3.5 Schematic sketch of an ultrasonic test setup for through transmission technique with Alporas foam specimen.

3.2.5.1.2 Through transmission technique:

In this technique, ultrasonic waves are used to send from one sending probe placing at one end of the specimen and other probe placed at the other end of the specimen to receive the signal act as the receiving probe as shown in Figure3.5. Signals received in terms of echo height (which is time traveled by ultrasonic waves through the sample) are analyzed in terms

ATTENTION: The Singapore Copyright Act applies to the use of this document. Nanyang Technological University Library

of location of any discontinuity or pores, etc. Due to the involvement of both sides of the specimen in this technique, the response here will be more promising than pulse echo technique due to the presence of large amount of inhomogeneity (lot of pores) in the Alporas Al foam.

Firstly, the ultrasonic response in terms of echo height was measured for Al block of height around 40mm with all possible combination (sending ad receiving) of frequency probes which include same frequency combination and different frequency combination. In this technique, specimens are needed to be kept in between two probes which are not suitable for measuring the response from probes of different circumference (circumference of some probes are very small in compare to specimen and very difficult to hold the specimen on that probe). The same procedure was repeated for Al foam of different frequency probes. Change in echo height representing the time travel by ultrasonic waves is recorded for Alporas foam specimens in compare to pure Al block.

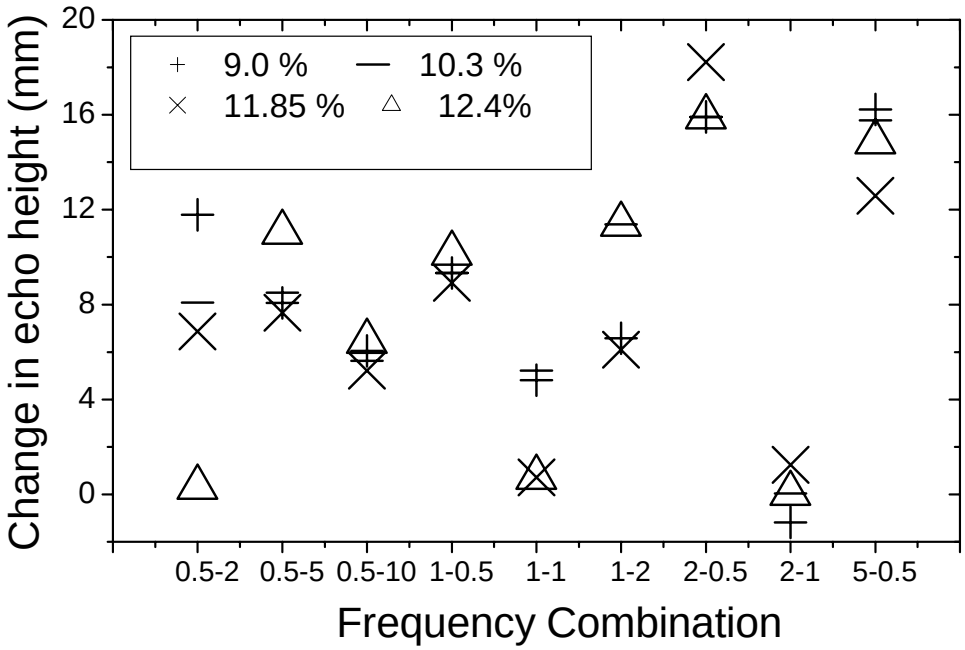

Figure 3.6 Change in echo height for specimens of Alporas foam having different relative density with different combination of probes having different frequencies.

Some important points are drawn to understand the relation between porous structure and density of foam. There is an obvious change in echo height because of the presence of the pore, as ultrasonic wave travel in solid medium. The distance traveled by the ultrasonic wave was found both higher and lower in comparison to pure aluminum depending upon the

ATTENTION: The Singapore Copyright Act applies to the use of this document. Nanyang Technological University Library

structure of the pores for combination of probes. Figure 3.6 shows the reduction or increment in back wall height for various samples having different porosity. The frequency of the probes (transmitting and receiving both) employed for the experiments is shown in x-axis while the level of porosity is indicated by the different symbols in the Figure 3.6. For most of the frequency combinations, it was found that the back wall echo is increased and the reason could be the increment in traveling of ultrasonic wave as the solid surface is present only though the walls of the pores as shown in Figure 3.7 with the possible ways. The proof of having more pores with lesser relative density is clear from Figure 3.6 by showing more distance traveled by the ultrasonic wave for lesser relative density with frequency combination of 0.5 MHz transmitting and 2 MHz receiving probes.

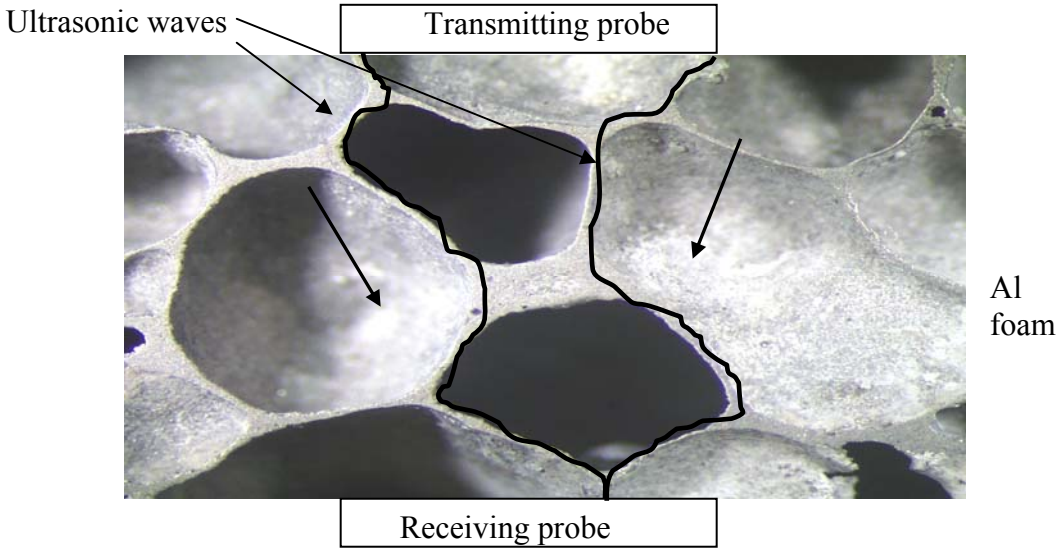

Figure 3.7 Possible paths of ultrasonic waves inside the Al foam specimen.

This relation of more pores with low relative density is not validated for probes of all other frequency combinations which could be due to lack of proper holder for probes (one at the bottom of specimen and other is on the top of the specimen).

3.3 Mechanical characterization of materials

Mechanical testing of foam core and face sheet materials used in sandwiches plays an important role to understand the deformation behavior of that sandwich of foam core and face sheet. Furthermore data of mechanical testing of face sheets are required to input in simulation to predict the behavior of sandwich beam consisting those face sheets.

ATTENTION: The Singapore Copyright Act applies to the use of this document. Nanyang Technological University Library

3.3.1 The mechanical characterization of foams

Mechanical testing is very important both for modeling and understanding of the deformation behavior of foam. Specimens were carefully prepared and designed in such a way that the effect of size becomes negligible (dimension in every direction is greater than five times that of cell). Mechanical testing was done using Instron Testing machine UTM (5567), under displacement control. This machine is used for different tests like tensile, compressive, bending and shear etc. with a proper selection of load cell so that the load to be measured is not less than 1% of the load cell capacity for reliable results. Jigs and fixtures are also selected properly based on the type of testing and dimensions of the specimen. Despite of all the precautions taken, results can have an error of ±0.5% [140].

3.3.1.1 Sample preparation

If the samples are cut by band saw or hand saw they would incur cell wall damage, which might cause measurement of variant properties [9]. Hence, samples were cut by EDM (Electro discharge machine) Robfil 300 to minimize the damage to the cell wall material. Samples were cleaned with acetone and were dried for one day to remove any left out grease or oil inside the samples. They were eventually grinded for 2-4 minutes on SiC paper to remove any unevenness.

3.3.1.2 Tensile testing

To overcome the size effect, tensile specimens with high thickness (20 mm) Alporas foam were chosen for which only screw driven jigs could be used. For good gripping and prevention of crushing of foam in gripping area, aluminum sheets were glued to specimens with an epoxy adhesive. Testing was carried out under displacement control at 0.1 mm/min. specimens were unloaded during testing process to obtain elastic Young's modulus.

Parameters were set for loading and unloading in such a way that the load reaches a certain level of displacement (0.1, 0.2 mm) in first two cycles and then unload it to zero load level. Data were recorded and different curves plotted showing Young's modulus and strength. The tensile set-up is shown in Figure 3.8 along with loading grips.

The stress-strain response is shown in Figure 3.9. Strong hardening behavior was observed before peak stress is reached. This peak stress appears at a relatively low strain of about 2%.

ATTENTION: The Singapore Copyright Act applies to the use of this document. Nanyang Technological University Library

It was observed that fracture starts from large cells and the stress decreases drastically after that. The mean tensile strength was found to be 1.51 MPa while loading and unloading modulus are 0.27 and 0.33 GPa respectively.

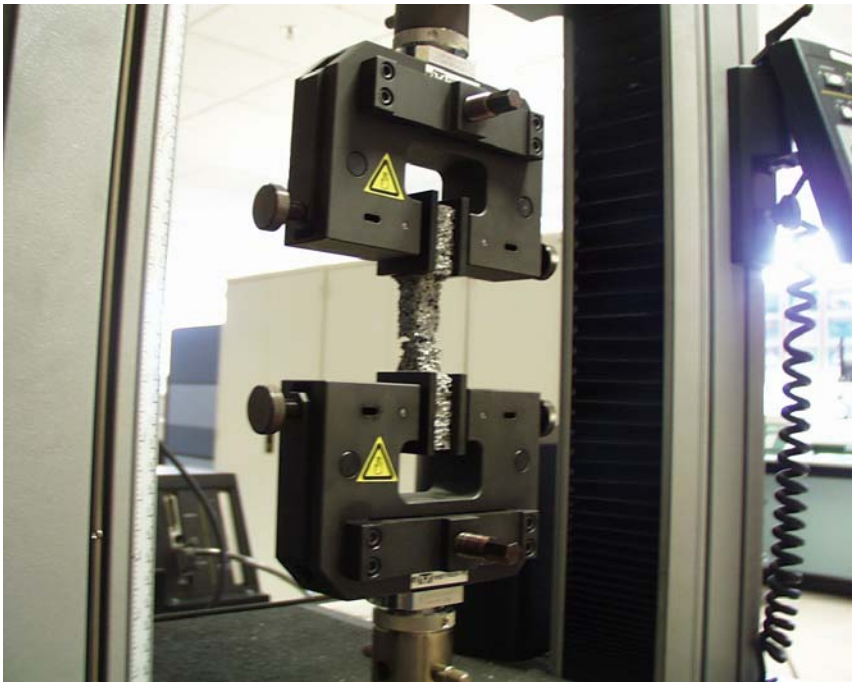

Figure 3.8 A specimen of Alporas foam during tensile testing.

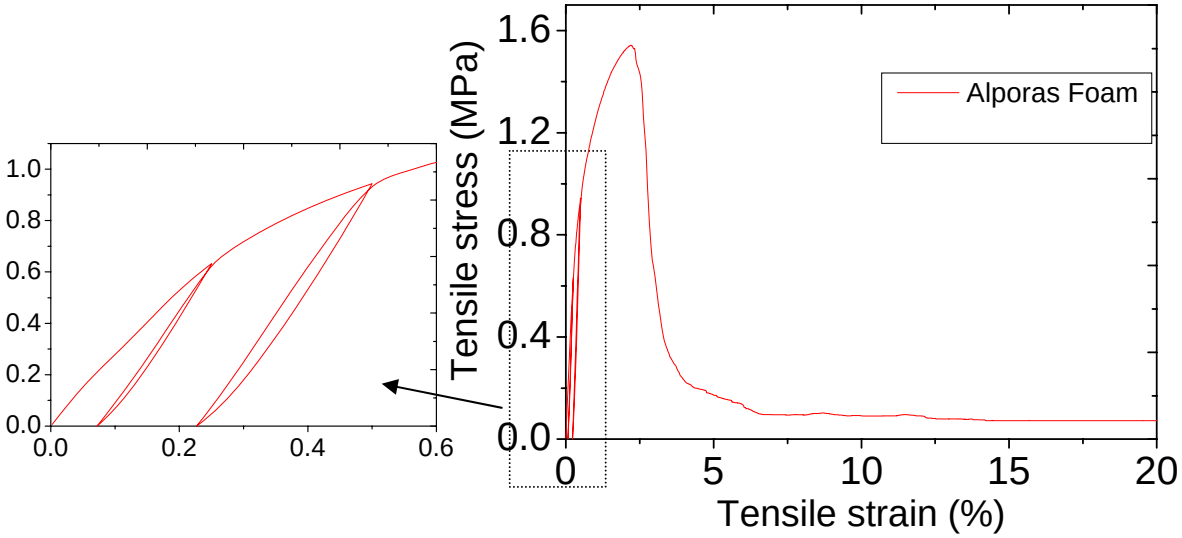

Figure 3.9 Tensile stress strain curve of Alporas foam of relative density of 9.5 % (20mm thick).

ATTENTION: The Singapore Copyright Act applies to the use of this document. Nanyang Technological University Library

3.3.1.3 Uniaxial compression testing

Specimens have cubic dimensions of (50 x 50 x 50 mm^3) for Alporas and (100 x 100 x 40 mm^3) for Cymat foam which satisfies the criterion of size ratio set for metal foam [9]. Lubricating spray (molybdenum sulphide) is applied in between loading platen and the specimen to reduce friction. Compression test profiler was used for compression testing of Alporas foam. Since Cymat is anisotropic in nature, loading was applied in the direction perpendicular to its foaming (skin to skin, if skin is present) which is its thickness direction also [139].

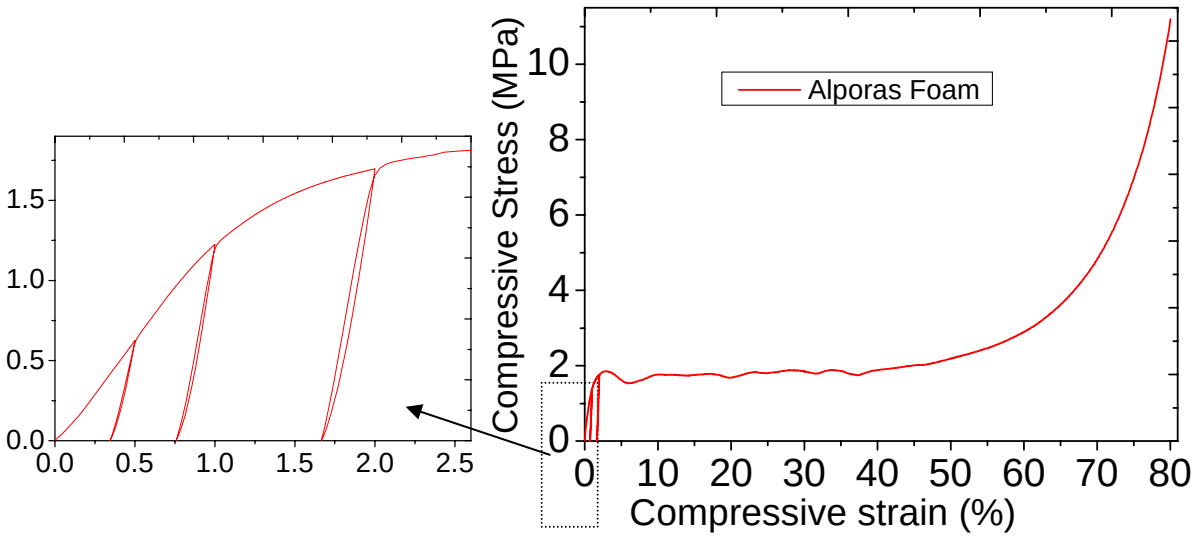

Figure 3. 10 Compressive stress-strain response of Alporas foam of relative density 9.5 % up to 80% strain.

This direction was chosen because loading will be applied to all the sandwiches in this direction as it is easy to make sandwich that way and strength is the lowest in this direction [139]. Loading and unloading profiles were set similar as in the case of tensile profiler. For the first two loading and unloading cycles, low displacement rate was (0.05 mm/min) selected but for the final loading cycle it was 0.1 mm/min. Data for compression testing was collected and different plots were drawn to show the unloading modulus and strength of both the foams.

It was observed that crush bands were formed under compression at certain locations in Alporas foam specimens. It may be due to the presence of weak cells at these locations. Compressive stress-strain response for Alporas foam material is shown in Figure 3.10 up to 80% strain. The stress increases monotonically with strain initially due to elastic bending of

ATTENTION: The Singapore Copyright Act applies to the use of this document. Nanyang Technological University Library

cell walls. Once the plastic stress value is reached, the deformation continues at uniform stress. This plateau region continues up to around 50% of the strain value and after that the stress increases very sharply with no increase in strain due to foam densification. The mean compression strength obtained from testing is 1.85 MPa. The loading and unloading moduli are 0.13 and 0.59 GPa, respectively.

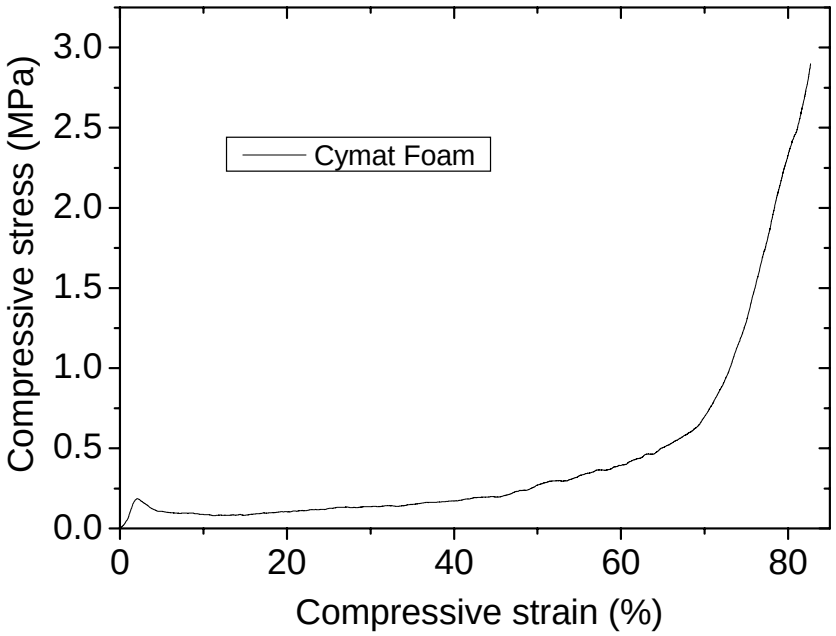

Figure 3. 11 Compressive stress-strain curve of Cymat foam of relative density of 4.7 % up to 80% strain.

A typical compressive stress-strain behavior of Cymat foam is shown in Figure 3.11. The mean value from compression strength was measured to be 0.2 MPa. Cells were crushed in layers for Cymat foam under compression. It may be due to the presence of bigger cells compare to Alporas and cells crush before transferring the load to next cell. Overall stress – strain response is found to be similar as in Alporas foam.

3.3.1.4 Shear testing

Double lap shear testing is the most commonly used method to measure the shear properties of Alporas foam. It is known that the shear behavior of foam material depend upon the ratio of specimen thickness to cell size [9]. For maximum practical possible geometries of sandwich beams, many foam cores are used which could failed under core shear failure of beam. Therefore It is necessary to perform the shear test for all the geometries (thickness is main

ATTENTION: The Singapore Copyright Act applies to the use of this document. Nanyang Technological University Library

constraints as other dimensions usually full fill the criterion set for size ratio) of foam core used in sandwich beam. These thicknesses of the Alporas foam are 3 mm, 8 mm, 20 mm and more than 20 mm (shear properties are uniform for more than 20 mm thick Alporas foam) [25]. The shear stress – strain response of Alporas foam was obtained by conducting double lap shear loading configuration and the specimen preparation closely followed the ASTM STD. C-273 [141]. Note that the double-lap shear configuration produces a more uniform shear stress state in the configuration provided the loading plates are stiff enough to measure the shear stiffness of the foam reliably well [9]. It is found that if the ratio of the cell size (specimen size to cell size) is more than 5 then the response of foam is more uniform. Specimens prepared for shear testing are of the dimension of 100 x 20 x 20 mm^3, 100 x 20 x 8 mm^3 and100 x 20 x 3 mm^3. Sandblasting was carried out for all steel plates for better gripping with Alporas foam blocks. Steel plates after sandblasting are shown in Figure 3.12 (a). These sandblasted steel plates with Alporas foam blocks were washed with acetone and cleaned with a white cotton cloth until they stop turning black after rubbing.

Specimens were prepared by joining steel plate to Alporas foam with Redux–322 adhesive between them. The whole assembly was loaded with the help of tightening holder in one direction and with steel block in another direction. This loaded assembly was kept in oven for curing at 175^0C for 1 hour. Few prepared specimens are shown in Figure 3.12(b).

(a) (b)

Figure 3.12 Specimens preparation for shear testing (a) sandblasted steel plates (b) cured foam specimens (20mm and 8 mm of thickness).

ATTENTION: The Singapore Copyright Act applies to the use of this document. Nanyang Technological University Library

The tensile method was chosen for shear testing and data was recorded. Shear stress-strain data was subsequently calculated from the recorded load and extension data. One specimen undergoing the double lap shear testing is shown in Figure 3.13.

It was found that the fracture starts from big or weak cells and spreads along the loading plane in shear loading. Here, hardening behavior was not pronounced before peak stress as it was in tensile loading. But the stresses decrease drastically similar to the case of tensile loading after peak stress. Shear strength and modulus of Alporas foam was found to be decreased with increasing size ratio (specimen size to cell size) as shown in Figure 3.14. It tallies with the observation of Andrews et al [25].

Figure 3.13 A specimen of Alporas foam undergoing double lap shear testing.

An increased constraint of the cell walls at the boundary was thought be the reason for happening so. This size effect was found to be negligible after increasing size ratio of around 5. In other words, strength value of the specimen with thickness of 20mm or more will not fluctuate with the size ratio. The mean shear strength determined from samples with 20 mm thickness was found to be 1.05 MPa, which is termed as the shear strength of the Alporas foam. Shear stress versus shear strain responses of foam specimens of different thicknesses are shown in Figure 3.14. The difference in shear strength observed for samples of the same category is minimal.

ATTENTION: The Singapore Copyright Act applies to the use of this document. Nanyang Technological University Library

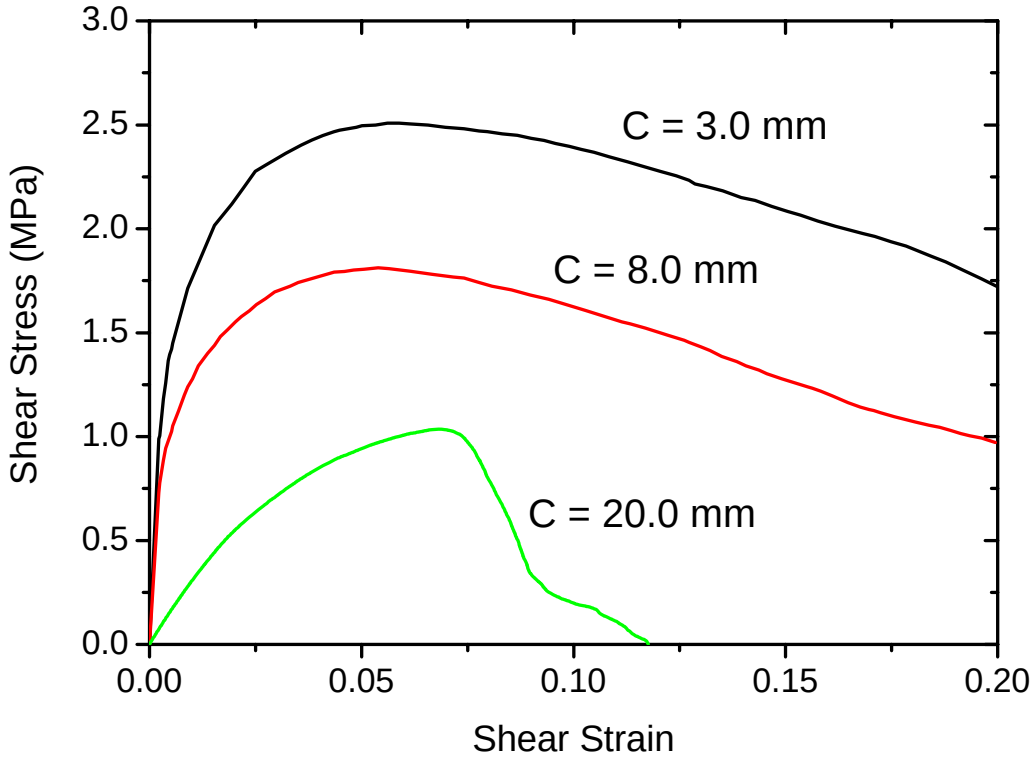

Figure 3.14 Shear stress –strain behavior of Alporas foam of different thicknesses.

3.3.1.5 Bending

Not many researchers have studied the behavior of Alporas foam under bending, so it was not clear whether the bending behavior is dependent upon the foam specimen size as it was found to influence other mechanical testing including tensile, compressive and shear. Three-point and four-point bending experiments are carried out on various Alporas foam specimens in order to know the behavior of foam under bending. These tests also show how bending modulus of Alporas foam depends upon the specimen size.

Various rectangular blocks of Alporas foam specimens (with geometrical details as given in Table-3.6) were cut with EDM. Symbols used in this Table are explained in the Figure 3.17 (a). Both three- point and four-point bend tests were performed under displacement control at a rate of 0.25 mm/ min. Surface displacement analyzer (SDA) was employed for continuous monitoring of deformed geometry. Snapshots of the loaded sandwich beams were taken at every significant change in the foam specimen.

Bending strength and modulus were calculated for these specimens with equations for the beam under bending with appropriate assumptions [142].

ATTENTION: The Singapore Copyright Act applies to the use of this document. Nanyang Technological University Library

Bending strength for foam core under three- point bending and four-point bending are given by:

$$\sigma = \frac{3(LF)L}{2bc^2} \tag{3.1}$$

$$\sigma = \frac{3(LF)(l-s)}{2bc^2} \tag{3.2}$$

Bending modulus for foam core under three- point bending and four-point bending are given by:

$$E = \frac{(F_e)l^3}{4\delta bc^3} \tag{3.3}$$

$$E = \frac{27(F_e)l^3}{128b\delta c^3} \tag{3.4}$$

Where LF is the load for failure, F_e is the load in the elastic limit, δ is the deflection at the mid point of the specimen in length direction while l, L, b, and c are explained in the Figure 3.17(a).

Table3.6 Details of specimens for Alporas foam tested under three and four-point bending with test results

Specimen No.	**c (mm)**	**s (mm)**	**l (mm)**	**H (mm)**	**L (mm)**	**Type of bending**	**Bending strength (MPa)**	**Bending modulus (GPa)**
1	20		85	7.5	100	Three-point	3.76	0.51
2	20		110	10	130	Three-point	2.51	0.73
3	20		203	18.5	240	Three-point	1.91	1.37
4	20		103	9.5	122	Three-point	2.16	1.3
5	30	20	80	15	110	Four-point	3.60	0.46
6	3	25	100	17.5	135	Four-point	1.75	0.80
7	3	20	80	15	110	Four-point	1.60	0.77
8	20	25	100	17.5	135	Four-point	2.06	0.95

ATTENTION: The Singapore Copyright Act applies to the use of this document. Nanyang Technological University Library

Load displacement behavior of almost all the specimens under a similar type of bending (either four-point or three-point) was found to be similar. Typical load-displacement behavior of Alporas foam specimen under three-point and four-point bending is shown in Figure 3.15. Hardening behaviors was observed in almost all the specimens under bending up to peak load similar to shear loading. Decrease in load after this peak was found in all the foam specimens under bending, which is due to higher rate of damage in foam specimens because of loading through the upper indenters. Once the crack is generated then it grows rapidly through the weaker cells.

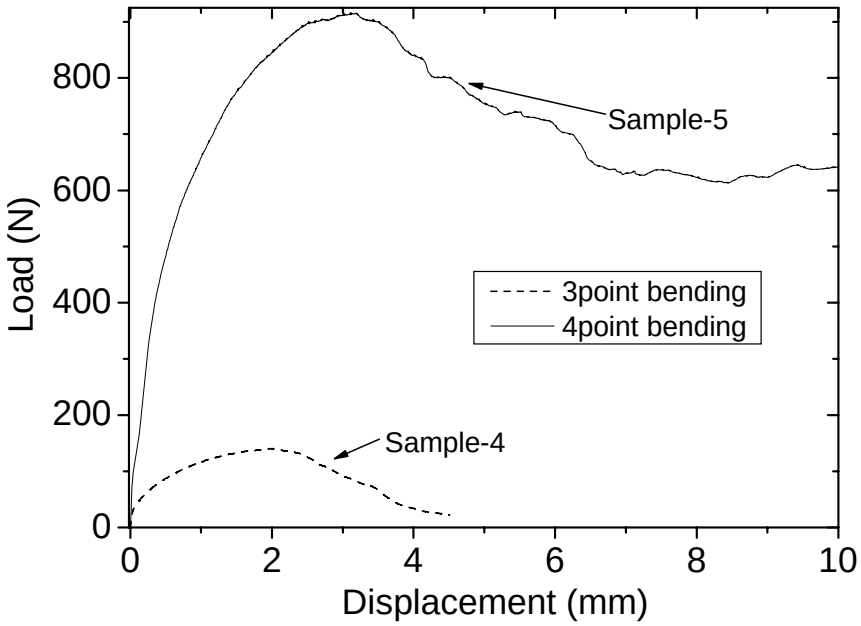

Figure 3.15 Load-displacement behavior of Alporas foam of sample - 4 and sample-5 (Table 3.6) under three-point and four-point bending respectively.

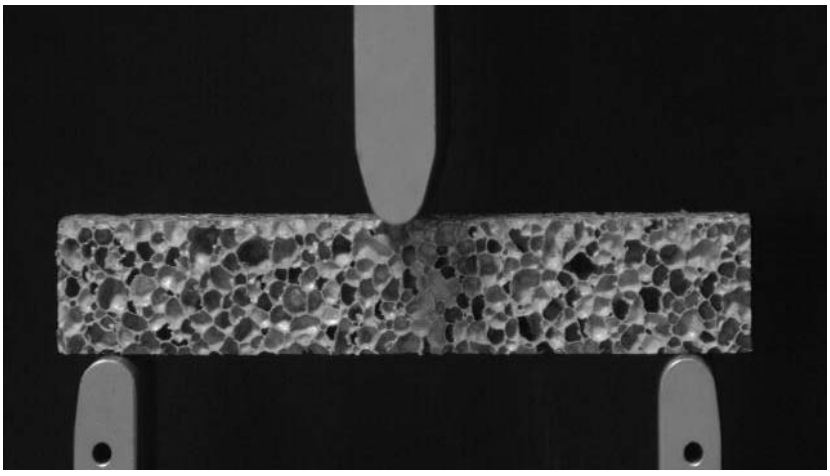

ATTENTION: The Singapore Copyright Act applies to the use of this document. Nanyang Technological University Library

(a)

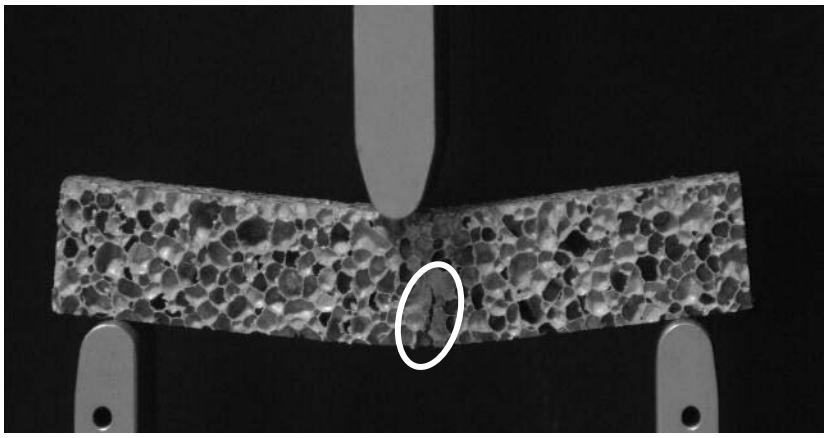

(b)

Figure 3.16 In-Situ picture of the Alporas foam specimens having geometry of sample – 4 (Table3.6) under three-point bending (a) starting of test (b) failure of foam specimen at a displacement of 4.5 mm.

Cracking of Alporas foam under three- point bending was started from middle lower of the foam core as shown in snapshots of sample–4 (Table-3.6) taken at failure seen in Figure 3.16 (b) at a displacement of 4.5 mm compare to initial snapshot of the foam in Figure 3.16 (a).It shows the locations of typical failure, which was observed in almost all the foam tested under three-point bending because of concentrated loading under the supporting indenters.

Cracking of Alporas foam under four- point bending started from middle lower of the foam core as shown in snapshots of sample - 5 (Table-3.6) taken at failure seen in Figure 3.17 (b) at a displacement of 4.5 mm compare to initial snapshot of the foam in Figure 3.17 (a).

The portion of the specimen between the two loading indenters was under constant stress because of four-point bending. The path of the cracking is shown in the Figure 3.17 (b) which is observed in almost all the foam tested under four-point bending.

The modulus and strength of all Alporas foam specimens under three-point and four-point bending are reported in Table3.6. Variation (1.60 to 3.76 MPa) in the bending strength of the foam specimens was observed to be small. The average bending strength of Alporas foam of relative density 9.5 % is found to be 2.58 MPa and 2.25 MPa under three and four-point bending respectively. Average bending modulus is found to be 0.98 GPa and 0.75 GPa under three-point and four-point bending respectively.

ATTENTION: The Singapore Copyright Act applies to the use of this document. Nanyang Technological University Library

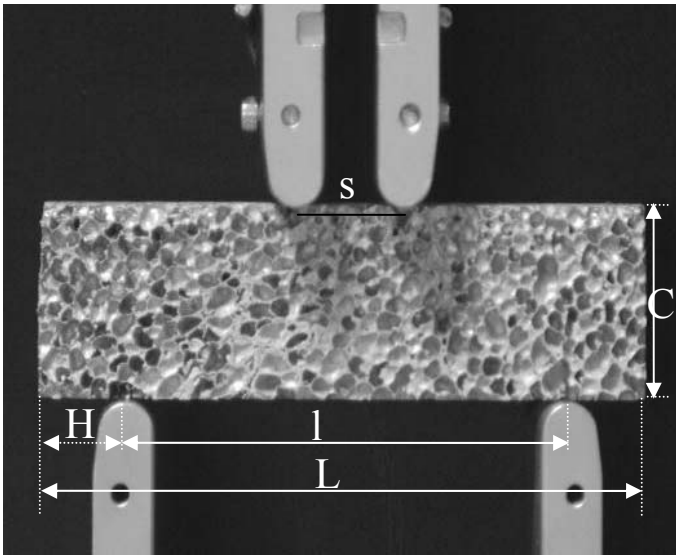

(a)

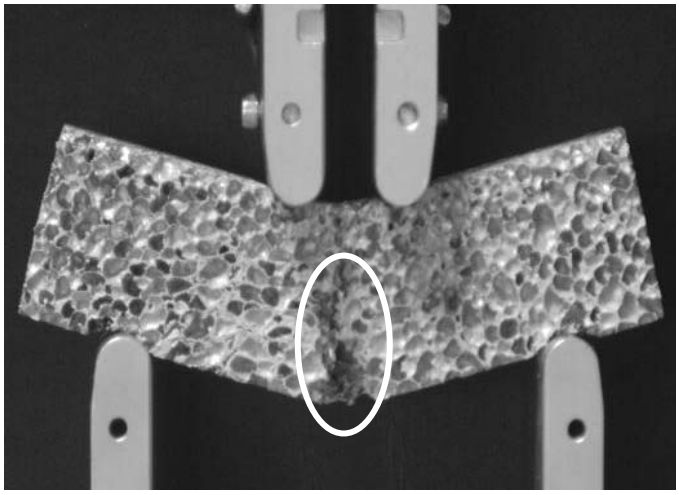

(b)

Figure 3.17 In-Situ picture of the Alporas foam specimens having geometry of sample – 5 (Table3.6) under four-point bending (a) starting of test (b) failure of foam specimen at a displacement of 10 mm.

3.3.2 Mechanical characterization of face sheets

In this project, Al, SS, alumina and CFRP materials are used as face sheet materials of sandwich structures. In this section, the experimentation carried out for these materials and their mechanical characterization is elaborated. Based on the material, uniaxial tensile, compressive and bending tests were carried out using the Instron Testing machine UTM (5567) under displacement control.

ATTENTION: The Singapore Copyright Act applies to the use of this document. Nanyang Technological University Library

3.3.2.1 Mechanical property of Aluminum and Stainless steel face sheet

Here, tensile behavior was reported for both types of sheets.

3.3.2.1.1 Al sheets:

Different types of Al sheets were used in the study of the behavior of sandwiches with Al foam core under various loading conditions which is explained below.

(1) elastic-perfectly plastic (aluminum alloy 1100 half-hard) sheet having thicknesses of 0.5 and 1.0mm was used as face sheet for sandwich structure with both Alporas and Cymat foam core which is investigated for failure analysis under indentation and impact loading.

(2) elastic-perfectly plastic (aluminum alloy 1050 half-hard) sheet having thickness of 0.5 and 3.0 mm was used as face sheet for sandwich column with Alporas foam core which is investigated for failure analysis under end compression loading.

Tensile properties of Al sheets with different thicknesses were measured by conducting uniaxial tensile tests on dog-bone type specimens according to ASTM STD. E8-04 [143]. Tensile stress-strain behavior of Al-1100 and Al-1050 sheets was found to have nearly elastic-perfectly plastic response as shown in Figure 3.18 (a) and (b) respectively. The measured properties of these Al face sheets are listed in Table 3.7.

Table3. 7 Material properties of various metallic sheets of various thicknesses

Material	**Thickness of sheet (mm)**	**Tensile Strength (MPa)**	**Young's Modulus (GPa)**
Al 1100	0.5	134	68
	1.0	121	69
Al 1050	0.5	111.5	67
	3.0	121.4	71
SS-314	0.5	650	191
	1.0	702	190

3.3.2.1.2 Stainless Steel sheets:

Stainless steel (SS) sheets with thicknesses of 0.5 and 1.0mm were used in studying the behavior of sandwiches consisting of Al foam core under indentation and impact loading

ATTENTION: The Singapore Copyright Act applies to the use of this document. Nanyang Technological University Library

conditions. The tensile properties of SS (SS-314) sheets with different thicknesses were measured by conducting uniaxial tensile tests according to ASTM STD. E8-04 [143]. Tensile stress-strain behavior of these sheets was found to be strain hardening as shown in Figure 3.19. The measured properties of these SS face sheets are listed in Table 3.7.

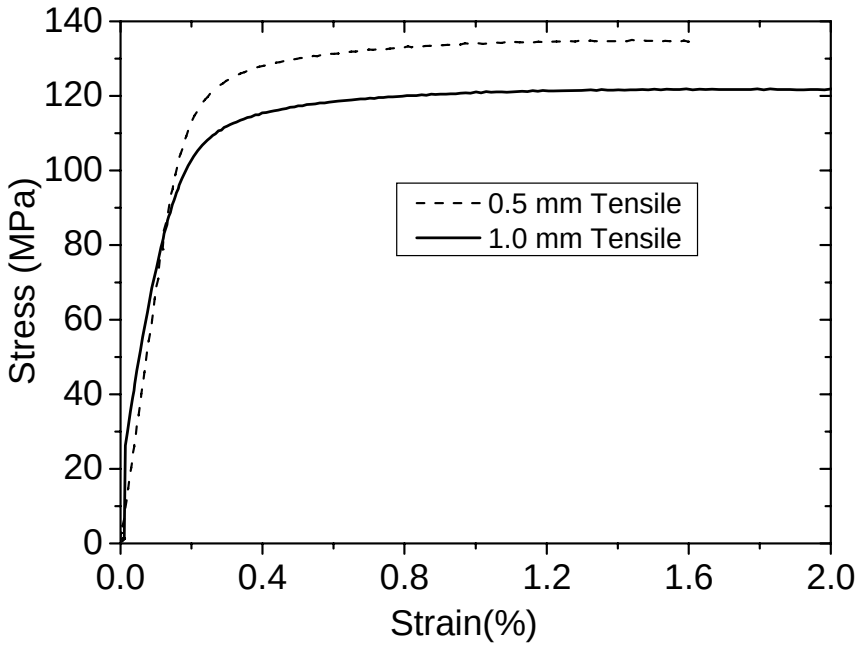

(a)

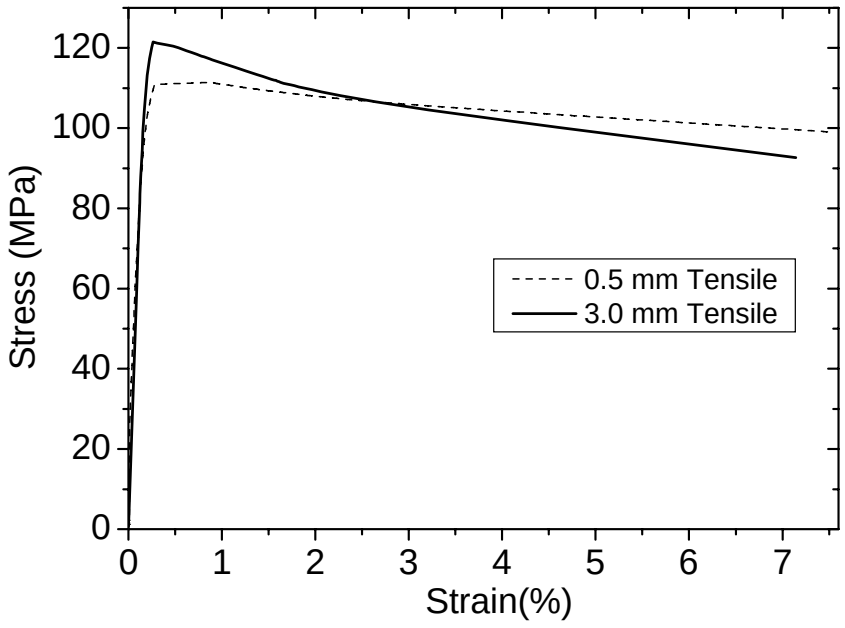

(b)

Figure 3.18 Tensile stress-strain responses of Al sheets showing nearly elastic-perfectly plastic behavior (a) Al-1100 (b) Al-1050.

ATTENTION: The Singapore Copyright Act applies to the use of this document. Nanyang Technological University Library

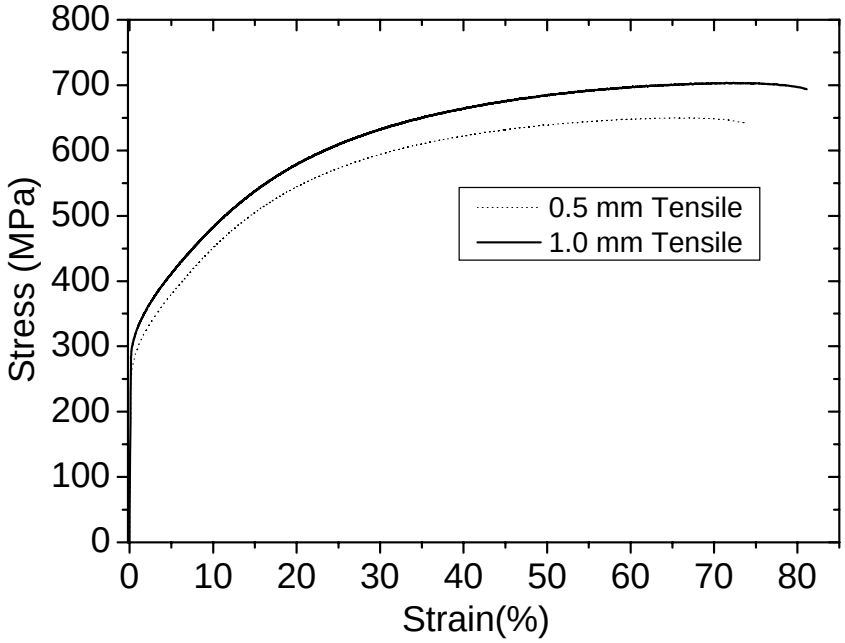

Figure 3.19 Tensile stress-strain response of strain hardened SS sheets (SS-314).

3.3.2.2 Mechanical property of alumina and CFRP face sheet

Here, bending behavior of alumina and various mechanical behavior of CFRP sheets are discussed.

3.3.2.2.1 Alumina sheets:

Alumina (Al_2O_3) supplied by PI-KEM UK, was used as face sheets for the construction of sandwich beams with Alporas foam and investigated for failure analysis under four-point bending. It is well known that the failure strength and modulus of ceramics is strongly influenced by their inherent porosity. Weibull statistics is commonly employed to study the statistical variation in strength with material volume [55, 144].

Uniaxial tension tests on alumina sheets are ruled out due to the premature failure at the grip portion while loading. Herein, bending tests on alumina face sheets of varying thicknesses are carried out using the Instron- 5567 UTM and the average modulus and strength is taken from 3 specimens each. Figure 3.20 shows the average stress-strain response under four-point bend tests for various specimen thicknesses. As the thickness of alumina sheet increases, number of defects and voids present in the sheets increase which is the source of failure for these plates and responsible for bending strength in bending loading. Alumina sheets fail in

ATTENTION: The Singapore Copyright Act applies to the use of this document. Nanyang Technological University Library

tensile mode under bending loading because compression strength of alumina is much higher compare to tensile strength. Poisson's ratio for ceramics sheet from the literature was found to be 0.22 [145]. The measured properties of these alumina face sheets are listed in Table 3.8.

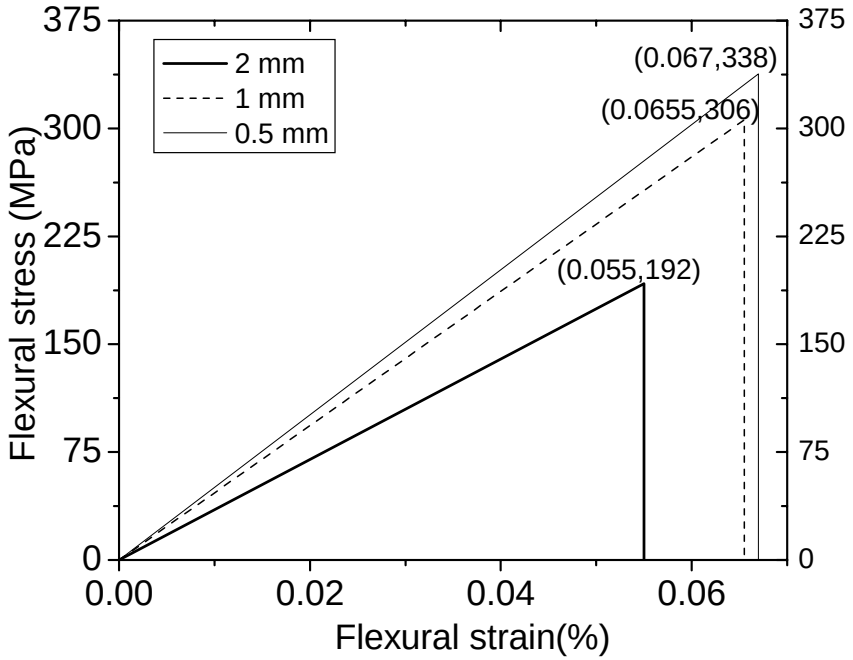

Figure 3.20 Stress-strain responses of alumina face sheets with various thicknesses under four-point bend tests.

Table3.8 Material properties of alumina sheets of various thicknesses

	Alumina sheet		
Property	**2mm thickness**	**1mm thickness**	**0.5 mm thickness**
Density (kg/m^3)	3960	3960	3960
Young's modulus (GPa)	349	467	504
Bending strength (MPa)	192	306	338
Failure strain (%)	0.055	0.0655	0.067

3.3.2.2.2CFRP sheets:

CFRP laminates were made from commercially available carbon fiber epoxy prepregs (Fiberdux-913C-HTA, from Hexcel Composites, UK). To fabricate the composite laminate of a specific thickness, the required number of plies of prepreg (each of size 300 mm x 300 mm and 0.125 mm in thickness) were hand-laid to obtain a unidirectional lay-up and pressed on a hot press at a nominal pressure of 700 kPa and maintained at a temperature of 120 ^{0}C for 1 hour as was recommended by the composite manufacturer.

ATTENTION: The Singapore Copyright Act applies to the use of this document. Nanyang Technological University Library

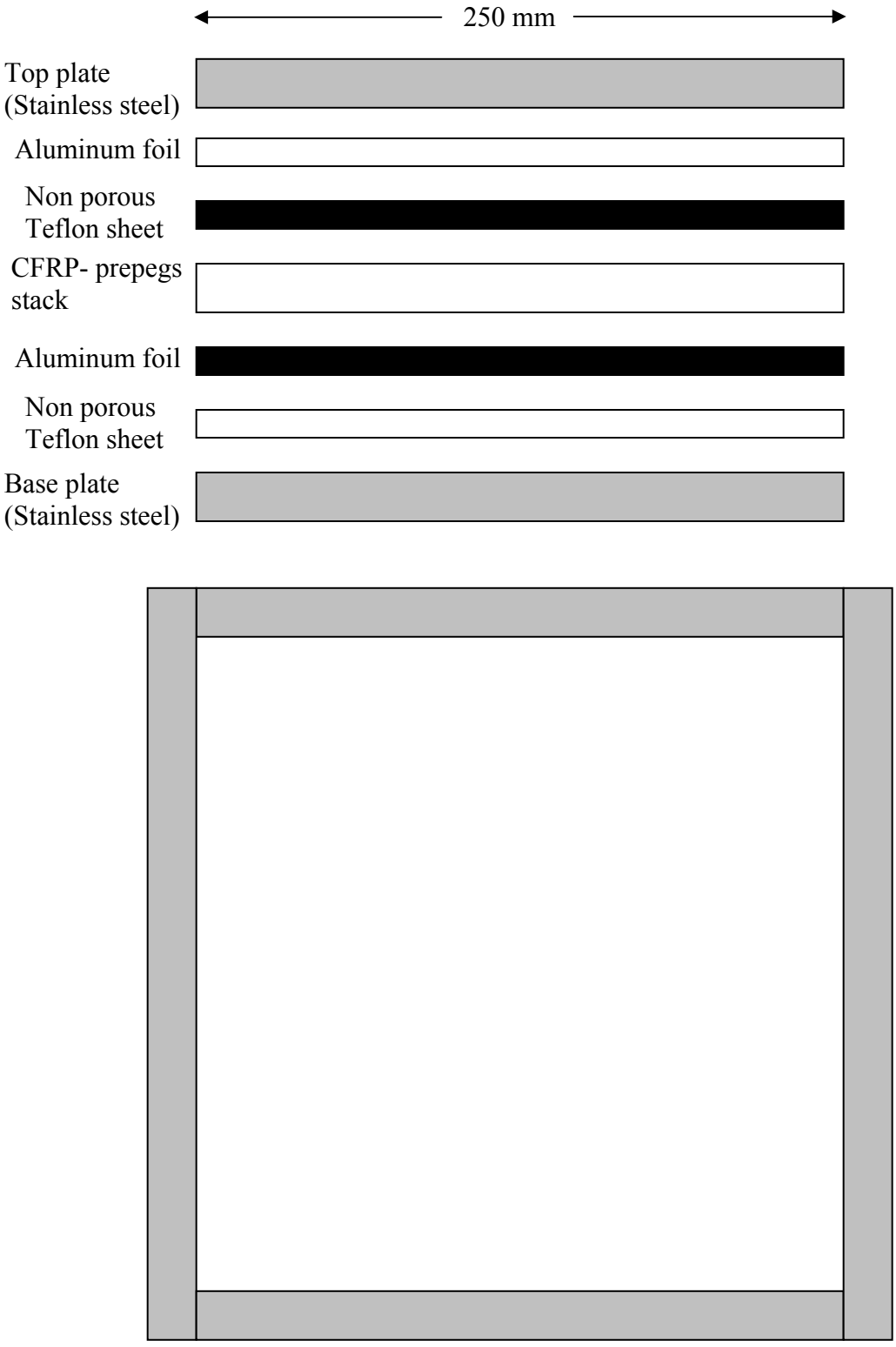

Figure 3.21 Order of arrangement of the prepreg stack with other materials and mould dimensions before commencement of curing process.

ATTENTION: The Singapore Copyright Act applies to the use of this document. Nanyang Technological University Library

The order of stacking of prepregs, teflon sheets, and other molding materials were as shown in Figure 3.21.To prevent laminate warpage and to achieve thermal stress free laminate, the cured laminate was allowed to cool down to room temperature in the hot press machine overnight (around 12 hr). Teflon sheets and Al foils were removed and edges of composite laminate were cut with diamond cutter to remove the uneven portion.

The compression tests were conducted on an Instron universal testing machine fitted with 100 kN load cell using IITRI test fixture [146]. Strain gauge rosettes were mounted in the middle of the specimens and strains in both longitudinal and transverse directions were monitored simultaneously using portable data logger.

Specimens of composite laminates were prepared according to ASTM STD. D3039/D3039M to study the tensile behavior of these laminates [147]. Specimen geometry of the tensile test specimens was prepared according to dimensions of 12.5 mm width, 2 mm thickness and 130 mm gauge length.

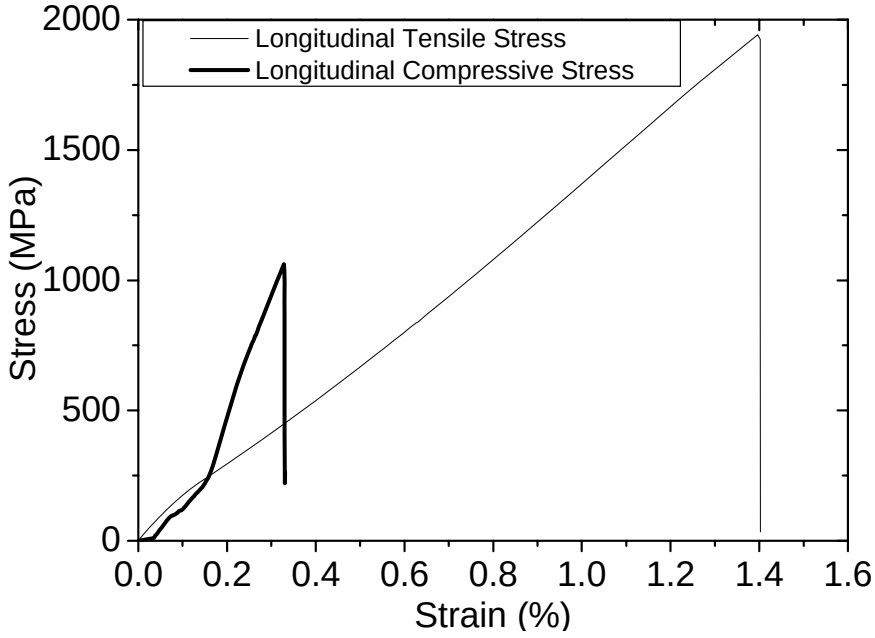

Figure 3.22 Longitudinal tensile and compressive stresses of CFRP laminate [146].

Each specimen was loaded on to a standard 100 kN screw-driven INSTRON-5565 universal testing machine fitted with mechanical wedge grips (which is suitable for flat specimens) at a crosshead speed of 2.5 mm/min [146]. Annealed aluminum end-tabs of 1 mm thickness were bonded to the end of the specimens using a Redux-322 adhesive to enable a smooth transfer of load into the specimen. The mating surfaces of the aluminum end-tabs and composite

ATTENTION: The Singapore Copyright Act applies to the use of this document. Nanyang Technological University Library

adherends were abraded using emery cloth and cleaned chemically with acetone. The use of annealed Al end-tabs enabled the knurled surfaces of the grips to 'bite' firmly into the specimen tabs, thus preventing slippage between the specimen and grips. In addition tabs distribute pressure applied by the grips evenly over the surface of the specimen, thus preventing local damage in the laminate. Load and strain measurements were recorded using a computerized data logging system. Obtained longitudinal stress-strain behavior of these composite laminate are shown in Figure 3.22. Results for composite laminates under compression and tensile loading are summarized in Table 3.9.

Table3.9 Composite laminate material properties under compression and tensile loading.

Property	**Value**
Longitudinal compressive elastic modulus E_{11}^{c}	126 GPa
Transverse compressive elastic modulus E_{22}^{c} and E_{33}^{c}	9.8 GPa
Longitudinal tensile elastic modulus E_{11}^{t}	150GPa
Transverse tensile elastic modulus E_{22}^{t} and E_{33}^{t}	9.5 GPa
Shear moduli G_{12}, G_{23}	1.1 GPa
Shear modulus G_{13}	3.92 GPa
Poisson's ratio υ_{12}, υ_{13}	0.26
Poisson's ratio υ_{23}	0.25
Ultimate longitudinal compressive strength σ_{11}^{c}	1000 MPa
Ultimate transverse compressive strength σ_{22}^{c}	155 MPa
Ultimate longitudinal tensile strength σ_{11}^{t}	1900 MPa
Ultimate transverse tensile strength σ_{22}^{t}	57 MPa
Interlaminar shear strength τ_{13}	100 MPa

ATTENTION: The Singapore Copyright Act applies to the use of this document. Nanyang Technological University Library

Chapter- 4

Sandwich beam with Al foam core and alumina face sheet under four- point bending

4.1 Introduction

It is widely known that metal foams especially, Al foams posses a good combination of properties such as high specific stiffness and strength, recyclable, good corrosion resistance [7, 13, 14]. The performance of these metallic foams can be enhanced by bonding it in between two strong and stiff face sheets to produce a lightweight structure. Under static loading conditions, the face sheets carry the axial load or resist against bending, whereas the core bears the shear stresses [60, 61]. Sandwich beams with minimal weights, desired stiffness and strength can be designed specific to suit various applications. This can be achieved by optimizing different parameters such as materials of core and face sheets or design geometry of beam with the knowledge of operating failure mechanism at the design loads [9, 12, 65].

Traditionally, sandwich structures having metal foam core with metallic face sheet have been studied well in terms of possible failure mechanisms depending upon its geometrical parameters such as thickness of core or face sheet, length of the beam etc. These structures are optimized for minimum weight for various applications having specific strength and stiffness. Recently, Ashby and Brechet [148] envisaged that better design performance may be achieved with 'hybrid' sandwich constructions by employing non-traditional pair of materials. Furthermore, in comparison to metal face sheet, alumina sheet imparts not only greater stiffness but also wear resistance and fire retardation to the sandwich beams structure. Thus, detailed study on sandwich structure constituting aluminum foam core and elastic (alumina or CFRP) face sheets would be carried out under bending for safe designing of these structures in real applications.

In this chapter, bending studies are discussed on beams consisting of alumina (Al_2O_3) face sheets and Alporas (an alloy of Al, Mn and Si) foam core to study the various competing failure modes. Failure mode map is constructed showing all possible failures in terms of non-dimensional geometrical parameters of the beam for a given face sheet to core yield strength

ATTENTION: The Singapore Copyright Act applies to the use of this document. Nanyang Technological University Library

ratio. Numerical simulations were carried out to verify the analytical solutions and compare with the experimental measurements of stiffness and failure load. Minimum weight design for those sandwich beams was also constructed with optimum geometrical parameters of these beams to enhance the load carrying capacity with safe usage in real applications.

4.2 Sandwich beam with Al foam core and alumina face sheet under four – point bending

Here, analytical equations developed for failure loads and stiffness are discussed and compared with numerical simulation and experimental observations for these sandwich beams under four-point bending.

4.2.1 Analytical analysis of sandwich beams under four point bending

Consider a sandwich beam of width *b* and length *L*, comprising of two identical face sheets of thickness *t* and foam core of thickness *c*. The beam is subjected to four point bending load as shown in Figure 4.1: the outer rollers acts as supports and the inner rollers load the specimen. Both the supporting and loading rollers have a diameter of 10 mm. The loading indenters are separated by a distance *s*.

4.2.1.1 Elastic Stiffness

The maximum deflection of the beam is due to both flexural and shear deformations. Noted that shear deformation predominates in the core and hence the approximate expression for the elastic deflection can be expressed as [60].

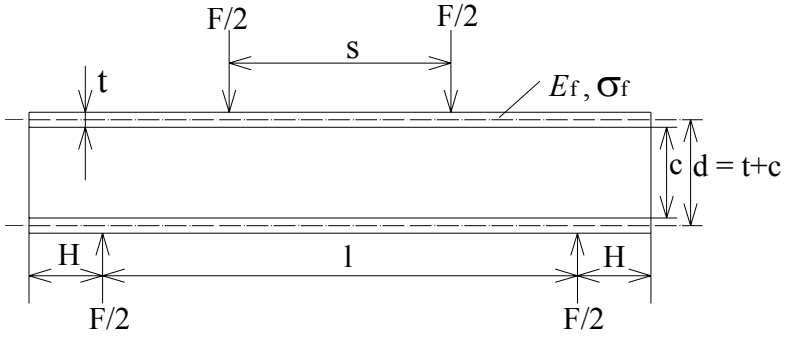

Figure 4.1 Schematic of a sandwich beam under four-point bending showing geometrical and material parameters.

$$\delta = \frac{F(l-s)^2(l+2s)}{48(EI)_{eq}} + \frac{F(l-s)}{4(AG)_{eq}} \tag{4.1}$$

ATTENTION: The Singapore Copyright Act applies to the use of this document. Nanyang Technological University Library

where l is the distance between supporting rollers, F is the total load applied on the beam, s is the inner loading span, $(EI)_{eq}$ and $(AG)_{eq}$ are the equivalent flexural and shear rigidity of the sandwich beam respectively. The equivalent flexural rigidity is given by

$$(EI)_{eq} = \frac{E_f btd^2}{2} + \frac{E_f bt^3}{6} + \frac{E_c bc^3}{12} \approx \frac{E_f btd^2}{2} \tag{4.2}$$

and the equivalent shear rigidity $(AG)_{eq}$ is given by

$$(AG)_{eq} = \frac{bd^2}{c} G_c \approx bcG_c \tag{4.3}$$

where G_c is core shear modulus and the spacing $d = c + t$ of the mid plane of the face sheets. E_f and E_c are the Young's moduli of the face sheet and foam core materials, respectively.

4.2.1.2. Estimation of failure loads

Total of three possible mutually competing modes are identified analytically and experimentally for the sandwich beams: the face sheet is assumed to fail by tensile fracture in a linear elastic manner and the foam core as a rigid-perfectly plastic material. As the adhesive used (between foam core and face sheets) has a higher shear strength compared to shear strength of foam core, bond failure mechanism was rule out. Face sheet under compression wrinkles when the normal stress reaches the elastic instability stress [60].

4.2.1.2.1. Face sheet cracking:

Alumina ceramic face sheet is brittle and its tensile strength is approximately 10 to 15 % of compressive strength [144]. Therefore, tensile strength of the ceramic material was considered to be the failure strength for the face sheets of the sandwich beams. It is known that for a sandwich beam under four-point bending, the upper face sheet is under compression while the lower face sheet is in tension and hence, the failure initiates in the bottom face sheet. It was assumed that the face sheet will start cracking when the lower face sheet of the sandwich beam reaches tensile failure strength of σ_y^f. The failure load for face sheet cracking is calculated by equating the moments within the sandwich beam (summation of the moments due to elastic brittle face sheet and rigid-plastic foam core) to the external bending moment applied to sandwich beam.

Moment due to face sheet is given by

ATTENTION: The Singapore Copyright Act applies to the use of this document. Nanyang Technological University Library

$$\frac{M_f}{I_{eff}} = \frac{\sigma_y^f}{(t+\frac{c}{2})} \tag{4.4}$$

where the effective second moment of area (I_{eff}) having considered the tensile failure of the lower face sheet is given by

$$I_{eff.} = \frac{bt^3}{12} + \frac{bt(c+t)^2}{4} \tag{4.5}$$

External applied bending moment to sandwich beam is given by

$$M_{\max} = \frac{F(l-s)}{4} \tag{4.6}$$

Now, equating the internally resisting moment (moment due to foam core and face sheet) to the maximum externally applied bending moment we obtain,

$$\frac{F}{2}\frac{(l-s)}{2} = \frac{\left\{\left(\frac{bt^3}{12}\right)+\left(\frac{bt(c+t)^2}{4}\right)\right\}\sigma_y^f}{\left(t+\frac{c}{2}\right)} + \left\{\sigma_y^c \frac{bc^2}{4}\right\} \tag{4.7}$$

$$F = \frac{4\left\{\left(\frac{bt^3}{12}\right)+\left(\frac{bt(c+t)^2}{4}\right)\right\}\sigma_y^f}{\left(t+\frac{c}{2}\right)(l-s)} + \left\{\sigma_y^c \frac{bc^2}{(l-s)}\right\} \tag{4.8}$$

Ceramics in general have much higher failure strength due to stiff covalent bonds when compared to foam core and hence,

Load for failure for face sheet cracking

$$F_{FSC} = \frac{2\left\{bt^3 + \left(3bt(c+t)^2\right)\right\}\sigma_y^f}{3(2t+c)(l-s)} \tag{4.9}$$

4.2.1.2.2 Core indentation:

The applied transverse load F induces a uniform bending moment $M = F(l-s)/4$ between the loading rollers and it is assumed that the upper face sheet is subjected to a compressive force of $P = M/(c+t)$ while the lower face sheet experiences a tensile force of equal magnitude. Indentation failure appears when foam core is compressed beneath the upper indenters within a region of 2λ in a rigid-ideally plastic manner, so that the transverse load on the sandwich face from the core is $q = b\sigma_y^c$ as shown in Figure 4.2. Recently, Steeves and

ATTENTION: The Singapore Copyright Act applies to the use of this document. Nanyang Technological University Library

Fleck [149] have analyzed the indentation failure as an elastic beam on a plastically deforming foundation and following expression to initiate indentation failure in the foam core was obtained on the similar guidelines.

$$F_{CI} = bt\left(\frac{\pi^2(t+c)E_f\left(\sigma_y^c\right)^2}{3(l-s)}\right)^{1/3} \tag{4.10}$$

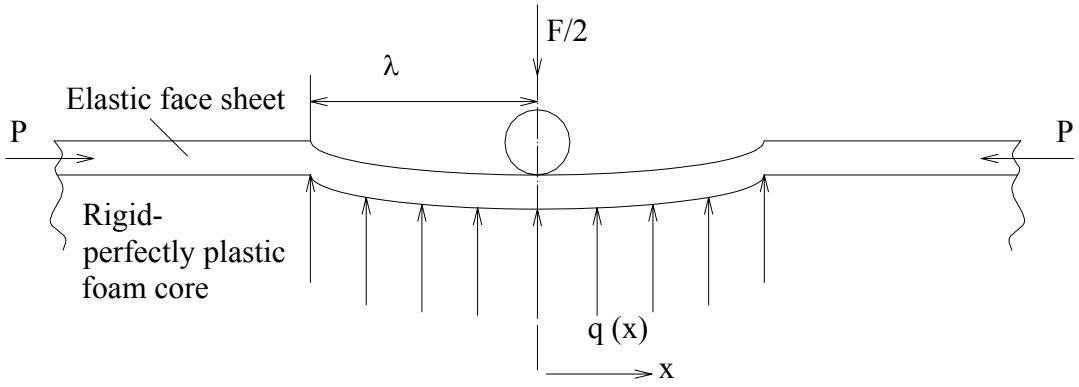

Figure 4. 2 Indentation zone beneath loading indenter.

4.2.1.2.3. Core shear:

The compliant core in the sandwich construction carries the shear load under bending. When the transverse shear stress exceeds the core shear strength, the sandwich beam fails in the shear mode. Two competing shear failure mechanisms are identified depending upon the beam overhang length [12]. Figure 4.3 shows these two possible failure mechanisms termed Mode-A and Mode-B. Failure load F_{cs} was calculated by equating the external work done by the sandwich beam to the internal work done by face sheets and core.

In collapse mode-A, the face sheets on the right hand side of the sandwich panel rotate through an angle θ whereas the left side rotate through -θ. Hence, the foam core shears by an angle 2θ. At the same time of the core shear it is assumed that the bottom face sheet is subjected to tensile fracture.

External work done by the applied forces is,

$$W_E = \frac{F}{2}\frac{(l-s)}{2}2\theta \tag{4.11}$$

Internal work done by the face sheet

ATTENTION: The Singapore Copyright Act applies to the use of this document. Nanyang Technological University Library

$$W_{if} = 4M_f\theta \tag{4.12}$$

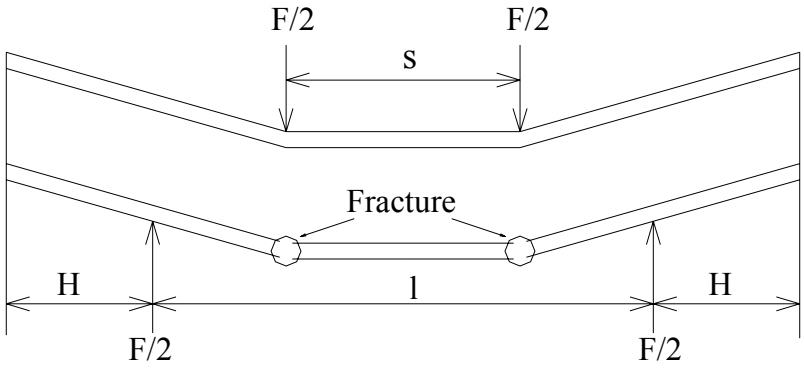

(a) Mode-A

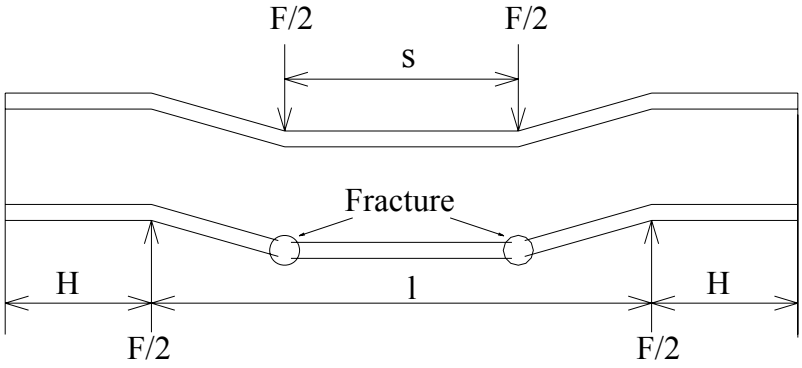

(b) Mode-B

Figure 4. 3 Two competing shear failure modes of sandwich beams (a) Mode-A (b) Mode-B.

Internal work done by the core

$$W_{ic} = \left[bc\tau_c^y(2H + l - s)\theta\right] \tag{4.13}$$

where τ_y^c is the shear strength of the foam core and $M_f = \frac{bt^2}{6}\sigma_y^f$ is the working bending moment in the face sheet to initiate brittle fracture. Equating the external work done by the force F to the internal work done, Mode-A core shear failure load can be expressed as

$$\frac{F}{2}\frac{(l-s)}{2}2\theta = \left[bc\tau_y^c(2H + l - s)\theta\right] + \left[\frac{4}{6}bt^2\sigma_y^f\theta\right] \tag{4.14}$$

$$F_{CSA} = \frac{\left[2bc\tau_y^c(2H + l - s)\right]}{(l-s)} + \frac{4\left[bt^2\sigma_y^f\right]}{3(l-s)} \tag{4.15}$$

In core shear Mode-B, it was assumed that there is no deformation in the core beyond the overhang length as shown in Figure 4.3(b). Similar to core shear Mode-A,

ATTENTION: The Singapore Copyright Act applies to the use of this document. Nanyang Technological University Library

Here, internal work done by the face sheet

$$W_{if} = 8M_f\theta \tag{4.16}$$

Internal work done by the core

$$W_{ic} = \left[bc\tau_c^y(l-s)\theta\right] \tag{4.17}$$

Failure load for core shear Mode-B was calculated by equating the work done and is expressed as

$$\frac{F}{2}\frac{(l-s)}{2}2\theta = \left[bc\tau_y^c(l-s)\theta\right] + \frac{4\left[bt^2\sigma_y^f\theta\right]}{3} \tag{4.18}$$

$$F_{CSB} = \left[2bc\tau_y^c\right] + \frac{\left[8bt^2\sigma_y^f\right]}{3(l-s)} \tag{4.19}$$

The overhang length H decides the transition from Mode-A to Mode-B. By equating the two failure loads, the critical overhang length was estimated as

$$H = \frac{t^2}{3c}\frac{\sigma_y^f}{\tau_y^c} \tag{4.20}$$

If the overhang length is more than the aforementioned value, the sandwich beam fails under Mode-B and vice versa.

The prediction of load for failure under face sheet wrinkling category contain terms such as Young's modulus of face sheet which is very high in value for alumina face sheet [12, 60] . So, load for failure would be very high for wrinkling as compare to other failures which suppress the possibility for this failure to occur. This is the reason that the analytical solution for wrinkling was not developed and discussed here.

4.2.2 Experimental procedure of testing of sandwich beams under four point bending

Details of the mechanical characterization of the materials (Alporas foam core and Alumina face sheet of various dimensions) involved in the sandwich beams under four point bending are explained in the chapter 3.

In order to identify all the possible failure modes, the maximum number of practically possible geometries of the sandwich beams were tested with alumina face sheets of different thicknesses. In the present work, alumina face sheet of thickness of 0.5 mm, 1.0 mm and 2.0

ATTENTION: The Singapore Copyright Act applies to the use of this document. Nanyang Technological University Library

mm and Alporas core of 9.5% relative density with varying thickness are employed to fabricate the beams. Details of the beam geometries are listed in Table 4.1.

Sandwich beams of 25 mm width were prepared by bonding alumina face sheets to Alporas foam core using Redux–322 adhesive*. Foam core specimens of required geometry were cut from a panel of 300 mm x 300 mm x 50 mm by electron discharge machining (EDM), to minimize cell wall damage. The foam blocks and alumina plates were degreased and cleaned with acetone using white cotton cloth. Foam specimens were then adhered to alumina plates using Redux – 322 epoxy adhesive on a nylon carrier mesh. The sandwich beams were air cured in an oven at 175^0C for 1 hour under a nominal contact pressure of 0.1MPa as explained in Chapter 3. The supplier's data sheet stated that the shear strength of Redux adhesive is about 20 MPa, which is much higher than that of the foam shear strength. Hence, the bond interface failure is not expected.

All the tests were conducted under displacement control by setting a cross-head displacement of 1.0 mm/min. A surface displacement analyzer (SDA) was employed for continuous monitoring of deformed geometry. Snapshots of the loaded sandwich beams were taken when there is a significant change in the beam geometry.

Table4.1 Geometry of sandwich beams under four point bending (all dimensions are in mm)

Specimen (geometry)	**Core thickness, *c***	**Face thickness, *t***	**Outer roller span, l**	**Inner roller span, *s***	**Overhang length, *H***	**Failure mode**
1	3	2.0	80	20	15.0	FSC
2	3	1.0	100	25	17.5	FSC
3	3	0.5	100	25	17.5	FSC
4	20	0.5	100	25	17.5	CI
5	50	0.5	100	25	17.5	CI
6	20	1.0	100	25	17.5	CS
7	30	2.0	80	20	15.0	CS
8	50	2.0	80	20	15.0	CS

Where FSC- Face sheet cracking, CI- Core indentation, CS- Core shear

4.2.3 Finite element modeling

In this section, finite element simulation of sandwich beam with Al foam core with alumina (brittle) face sheet under four-point bending is discussed. All the test geometries were simulated numerically using ABAQUS® commercial finite element program. The main

* supplied by Hexel Composites, Australia

ATTENTION: The Singapore Copyright Act applies to the use of this document. Nanyang Technological University Library

objective of this numerical simulation model was to verify the experimental results in terms of load prediction for failure and the investigation of failure zones in the sandwich beam. All the tested sandwich beam geometries were numerically analyzed in the present study. The alumina face sheet is assumed to be perfectly bonded to the core, eliminating the delamination failure mode.

4.2.3.1 Material constitutive modeling

In the elastic region, Alporas foam can simply be modeled as isotropic homogenous materials, which require the knowledge of only two parameters (viz. Young's modulus and Poisson's ratio). In plastic region, it is modeled as crushable foam with isotropic hardening behavior. Alumina face sheet is modeled as an elastic material with brittle cracking (failure criterion) model. ABAQUS has both foam constitutive and brittle cracking failure models inbuilt in it.

4.2.3.2 FE modeling of sandwich beam

Distinct failure modes namely face sheet cracking; core indentation and core shear were observed in sandwich beams under four point bending. The detail dimension of the tested and modeled sandwich beam is listed in Table-4.1. Owing to the similar modeling for all the beams modeling of only one beam is described in Appendix A-1.

4.2.4. Comparison of analytical, simulated and experimental results

Constructed failure mechanism map is an overview of the different failure mechanism that take place for these sandwich beams under four point bending depending on various geometrical parameters. A total of three competing failure modes namely core shear, core indentation and face sheet cracking were identified under four point bending of sandwich beams consisting of alumina face sheet and Alporas foam core.

In the following paragraphs, the load-displacement responses in experiments are compared with numerical simulations and analytical predictions. In addition, the elastic stiffness of the beam and failure load values are compared with the analytical formulae.

ATTENTION: The Singapore Copyright Act applies to the use of this document. Nanyang Technological University Library

4.2.4.1 Failure mechanisms map for sandwich beam under four point bending

For a given sandwich beam geometry and material system the dominating failure mode is one which requires the lowest load to fail among all possible modes. A failure mechanism map is drawn in Figure 4.4 in terms of non-dimensional parameters $\bar{c} = c/l$ and $\bar{t} = t/c$ based on the analytical formulae presented in section 4.2.1. It shows an overview of all possible failure modes of the selected geometry of sandwich beams in the region of each failure mode. In the present investigation, due to the limited quantity of materials available in standard geometries, experimented beam geometries are carefully chosen to identify all the competing failure mechanisms.

The failure load given by equations (4.9), (4.10) and (4.19) contains fracture stress of face sheet and core shear strength, and both of these are functions of their respective thicknesses. Therefore, the boundaries corresponding to different failure modes depend upon the thickness of face sheet and its influence is as shown in both the Figures 4.4(a) and 4.4(b) with marking of different lines for different thickness of face sheet. The effect of core thickness is represented by the shrinkage of core shear failure region in the failure mechanism map of Figure 4.4(a) (3 mm thick core) as compared to Figure 4.4(b) (20 mm core thickness).

This is due to the increment in load requirement to fail under core shear as the core thickness increases (discussed in Chapter 3). For all the geometries selected, the beam overhang length *(H)* was larger than the critical value given by equation (4.20). Hence, core shear Mode-B was observed in the reported experiments and only this mode was plotted in the failure map in core shear category.

4.2.4.2 Face sheet cracking

The load versus displacement curve for sandwich beam geometry - 2 (Table-4.1), failed experimentally by face sheet cracking, was compared with analytical calculations and simulation results as shown in Figure 4.5. It is a typical example of the geometries failed by face sheet cracking. Load increases monotonically with displacement in a linear manner and drops suddenly, indicating the catastrophic failure, when the lower face sheet cracked under tensile fracture.

ATTENTION: The Singapore Copyright Act applies to the use of this document. Nanyang Technological University Library

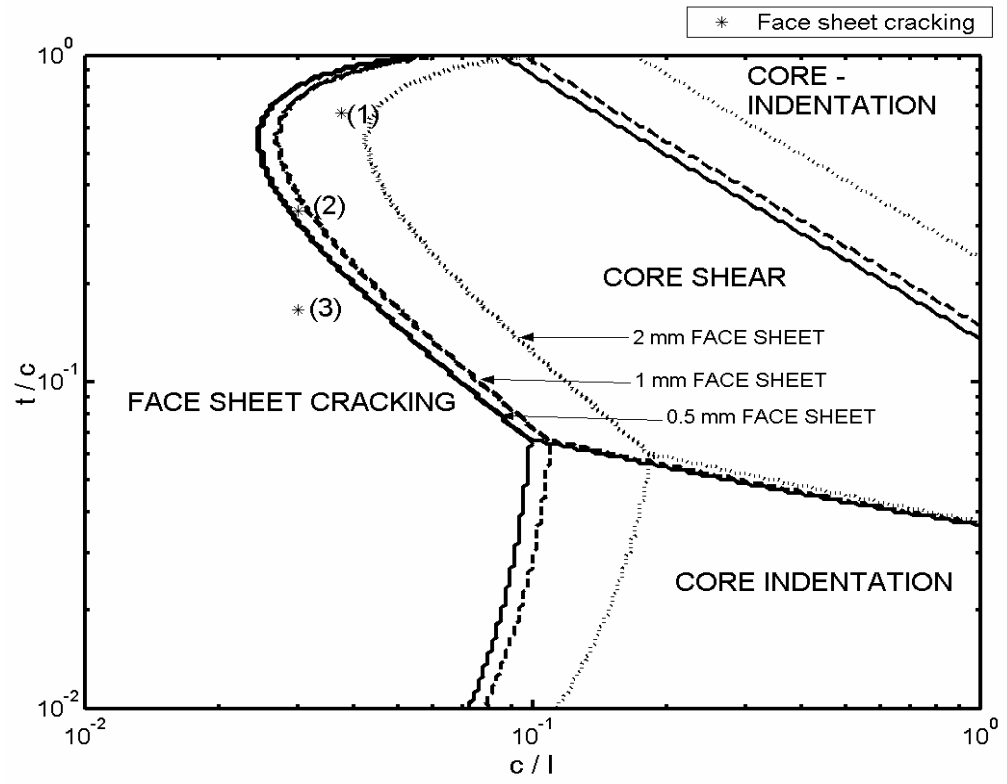

(a)

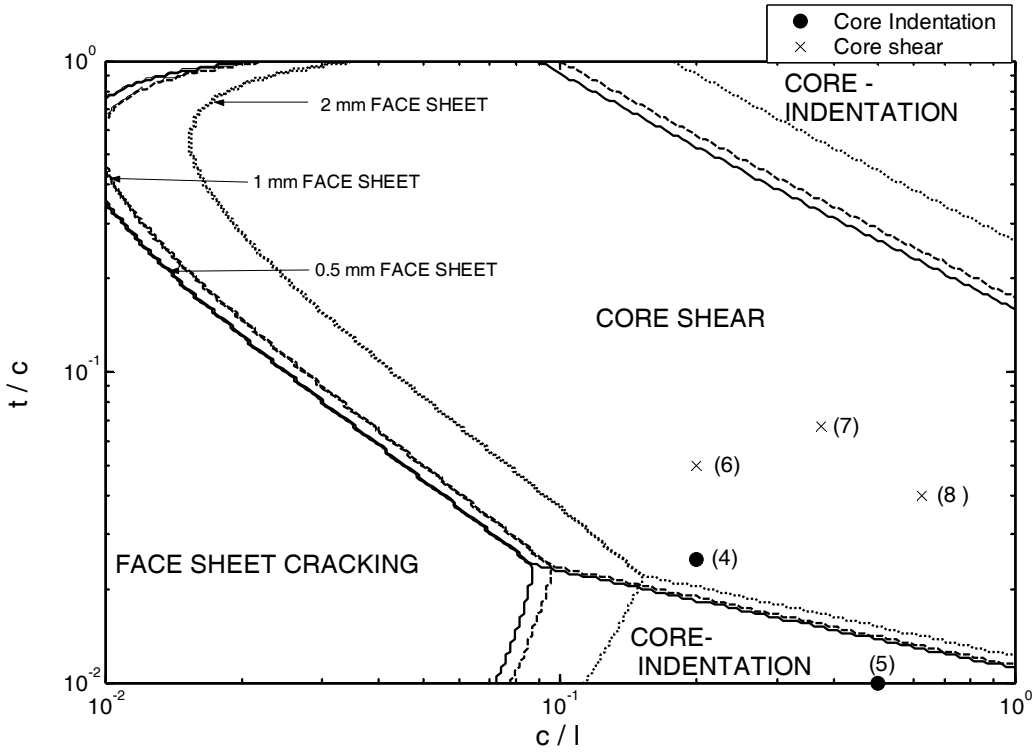

(b)

Figure 4. 4 Failure mechanisms map for sandwich beam having foam core thickness (a) 3 mm and (b) greater than or equal to 20 mm (In both case effect of alumina face sheet thickness is shown on map for a fixed of 0.25).

ATTENTION: The Singapore Copyright Act applies to the use of this document. Nanyang Technological University Library

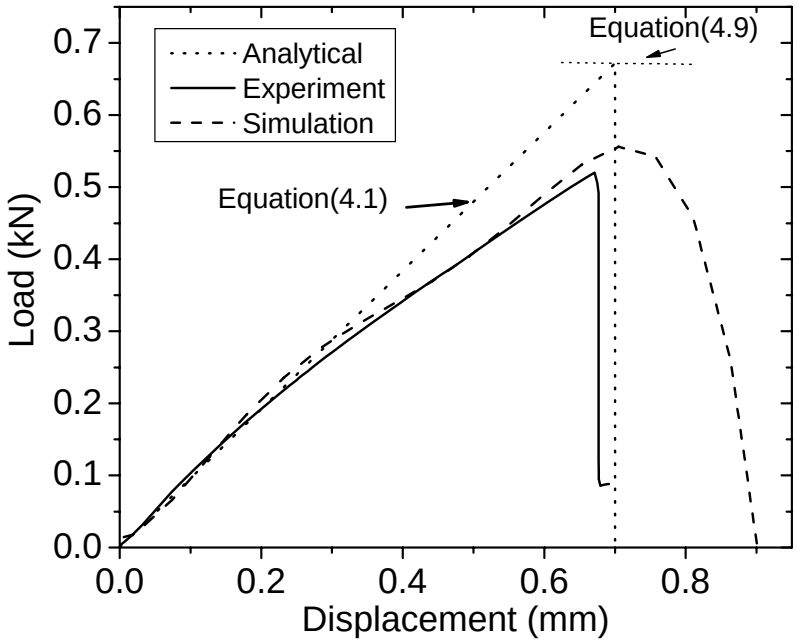

Figure 4. 5 Load and displacement curves derived from analytical, experimental and numerical analysis for the sandwich beam having geometry no-2 (Table-4.1) which failed under face sheet cracking.

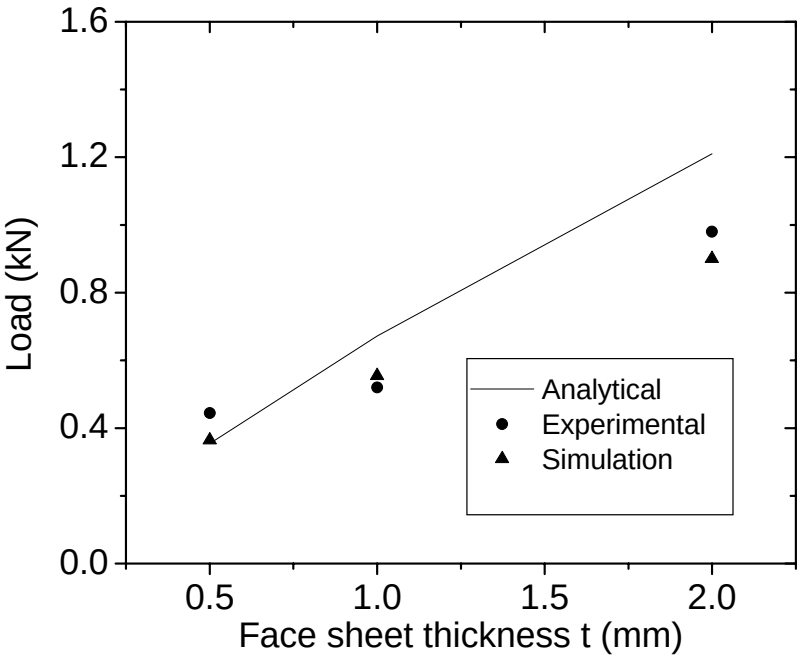

Figure 4. 6 Effect of face sheet thickness t on the face sheet cracking failure for sandwich beams having geometries (1, 2, 3) Table-4.1.

The deflection for failure was very low because of a very high Young's modulus of alumina face sheet. This failure mode was dominant when the span length *(l)* was large and face sheet

ATTENTION: The Singapore Copyright Act applies to the use of this document. Nanyang Technological University Library

thickness, *t*, was small with respect to core thickness, *c*. It agrees with the findings on the sandwich beam made with aluminum foam core and ductile aluminum face sheets [12].

Analytical equation 4.9 for face sheet cracking failure suggests that the face sheet cracking load increases with the thickness of the face sheets. Figure 4.6 shows the effect of face sheet thickness on the failure load for the three different tested geometries of sandwich beam. There is a good agreement between the experimentally measured failure load values with numerical and analytical predictions.

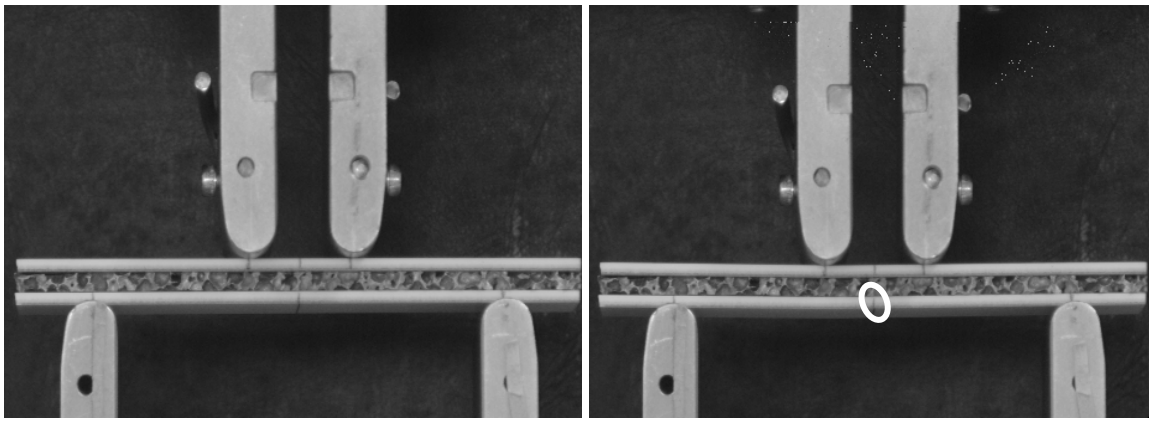

(a) *(b)*

Figure 4. 7 In-Situ picture of the sandwich beam specimens expected to fail by face sheet cracking (geometry – 1) (a) starting of test (b) failure of test at a displacement of 0.4 mm.

Cracking of lower face sheet was observed in snapshots of geometry - 1 (Table-4.1) taken at failure as shown in Figures 4.7 (b) at a displacement of 0.4 mm compared to the initial snapshot of the beam in Figure 4.7 (a). It shows typical failure which was observed in almost all the sheets failed under this mode. The normal stress contours obtained from the numerical simulation confirmed that the cracks were initiated in the lower face sheet (see Figure 4.8(a)). It was confirmed that the maximum principal tensile stress in the lower face sheet exceeded the failure limit and at this stage the shear stresses in the core and the compressive stresses in the top face sheet are within their design limits.

ATTENTION: The Singapore Copyright Act applies to the use of this document. Nanyang Technological University Library

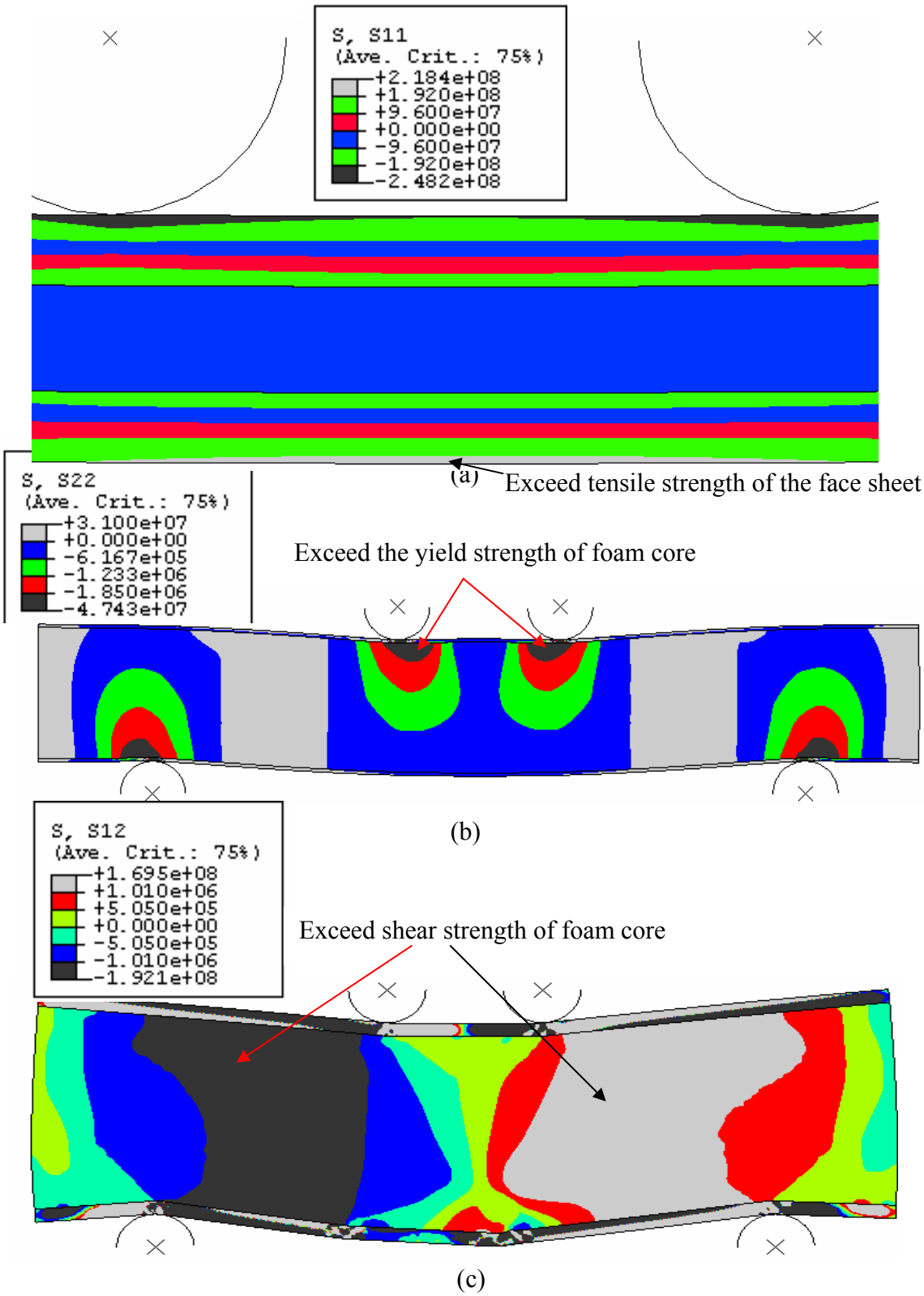

Figure 4. 8 Stress contours (in Pa) in the sandwich beam at the failure. (a) Normal tensile stress (S11) contours showing face sheet cracking at the lower middle portion of the face sheet of the sandwich beam (geometry -1), (b) Through thickness compressive stress (S22) contours showing core indentation underneath the upper indenters (geometry-4), and (c)

ATTENTION: The Singapore Copyright Act applies to the use of this document. Nanyang Technological University Library

Shear stress (S13) contours showing shear failure in the middle portion of the foam core within the loading and supporting indenter (geometry -7).

4.2.4.3 Core indentation

Core indentation failure mode was experimentally observed for smaller values of t/c and large values of c/l. The failure map indicates that the beam having equal dimensions of length, face sheet thickness and core thickness will also fail under this category, which is not a practically feasible design (as shown in Figure 4.4 (a)).

Two geometries were tested to check the validity of analytical and numerical simulations. The load – displacement observations are shown in Figure 4.9(a-b). It is clear from the figure that the loads for indentation drop after initiation of indentation, which correspond to the reduction in cross sectional area. Minor wiggles in the load-displacement curve were found due to the cracking of the face sheet near the rollers, which is highlighted in Figure 4.9. Here, prediction for failure loads by analytical solution (4.10) was found to be in agreement with the simulation and experiments.

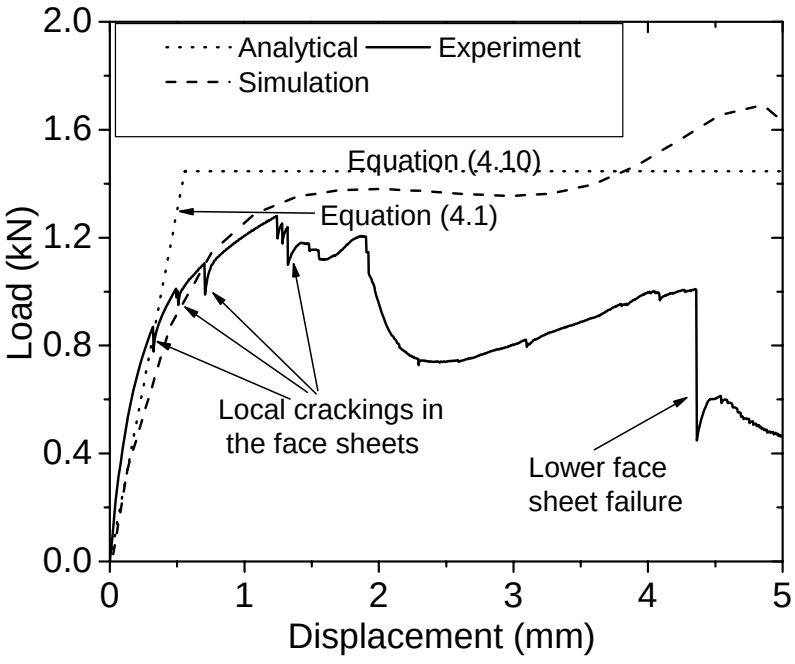

(a)

ATTENTION: The Singapore Copyright Act applies to the use of this document. Nanyang Technological University Library

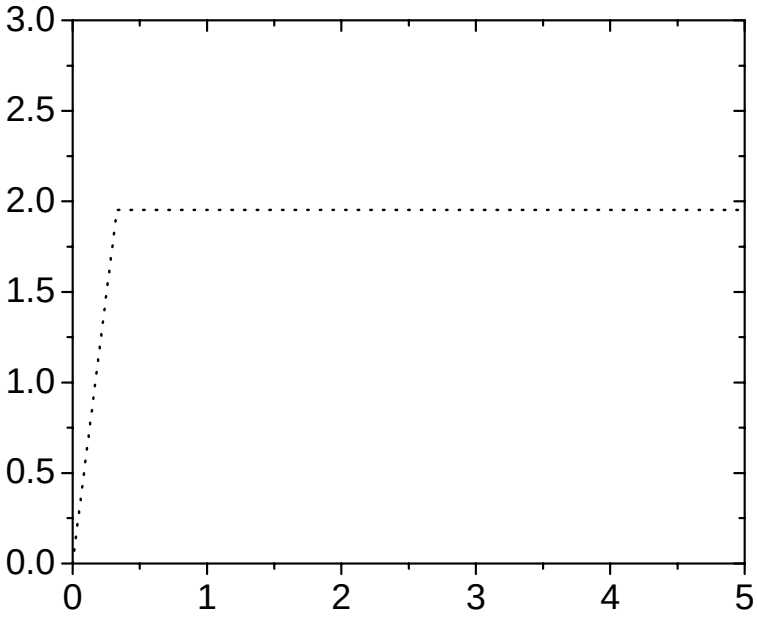

ATTENTION: The Singapore Copyright Act applies to the use of this document. Nanyang Technological University Library

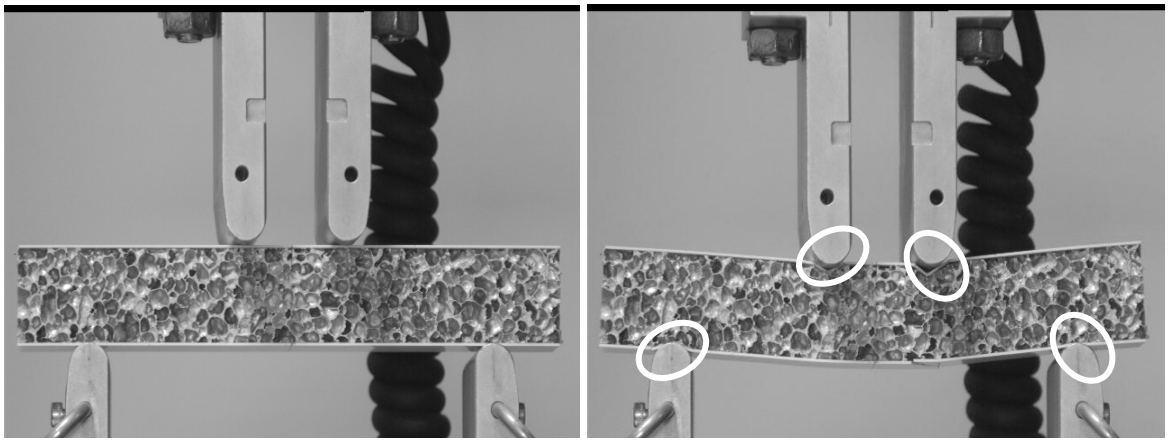

(a) *(b)*

Figure 4. 10 In-situ picture of the sandwich beam specimens expected to fail by core indentation (geometry – 4) (a) starting of test (b) failure of test at a displacement of 5 mm.

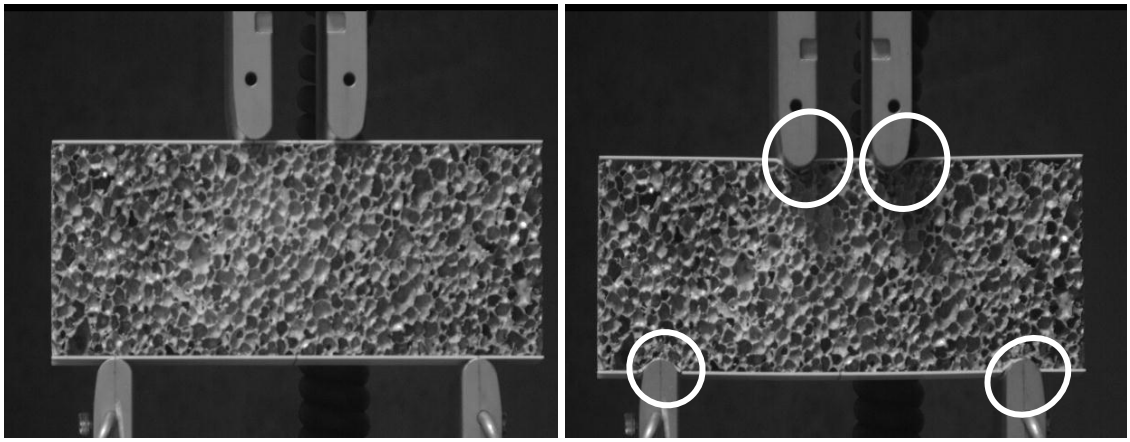

(a) *(b)*

Figure 4. 11 In-situ picture of the sandwich beam specimens expected to fail by core indentation (geometry –5) (a) starting of test (b) failure of test at a displacement of 5 mm.

4.2.4.4 Core shear

The load versus displacement responses of beams failed in core shear are shown in Figure 4.12 (a-c) and the response is compared with numerical and analytical predictions. For each beam, the overhang length was chosen to be more than the critical value so that the failure would appear in core shear mode-B. The serration responses in the experiment near the peak load represent local contact failure of face sheet underneath the indenters.

Failure load measurements for core shear agreed well with the simulation for all the geometries tested, but deviated from the analytical equation (4.19) by maximum of 20% (especially for geometry 8). However, the stiffness predicted by equation (4.1) was found to be in good agreement with the simulated and experimentally measured values.

ATTENTION: The Singapore Copyright Act applies to the use of this document. Nanyang Technological University Library

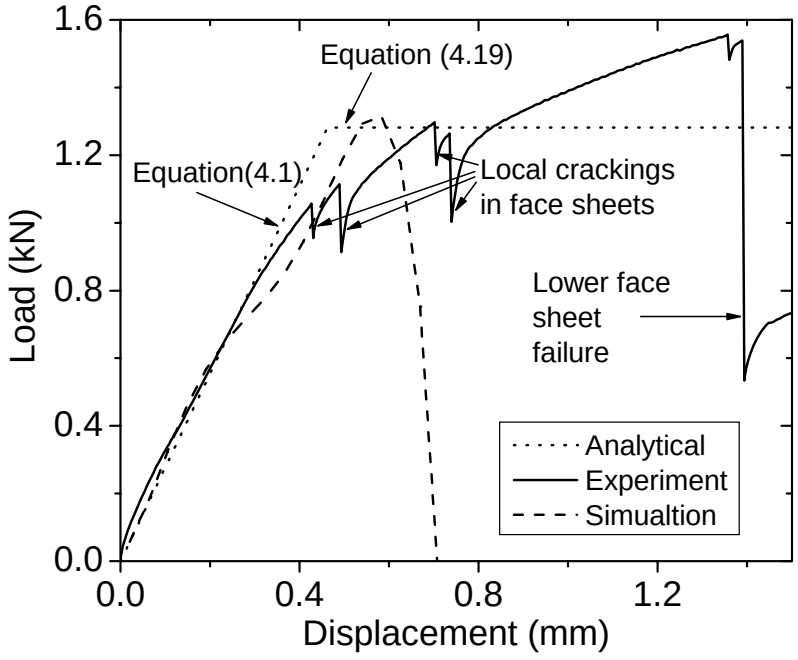

(a)

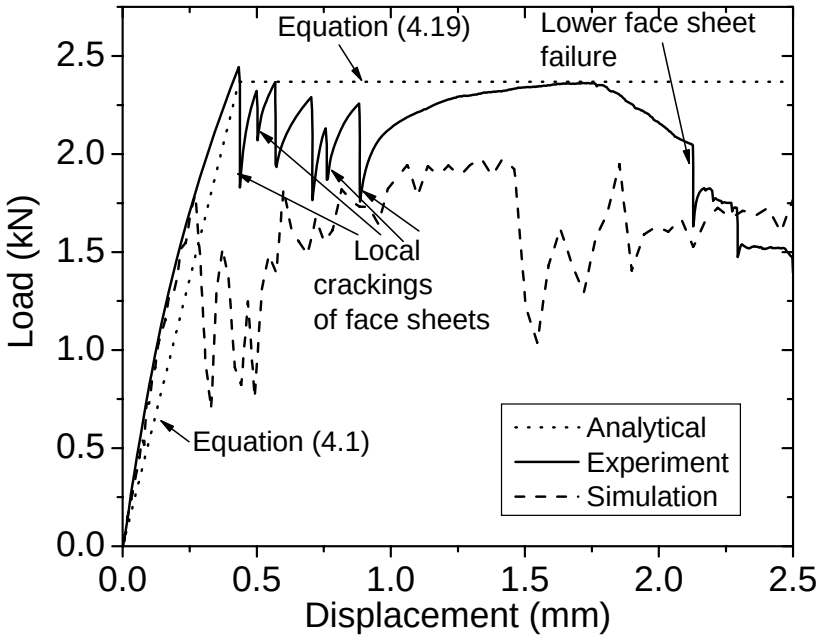

(b)

ATTENTION: The Singapore Copyright Act applies to the use of this document. Nanyang Technological University Library

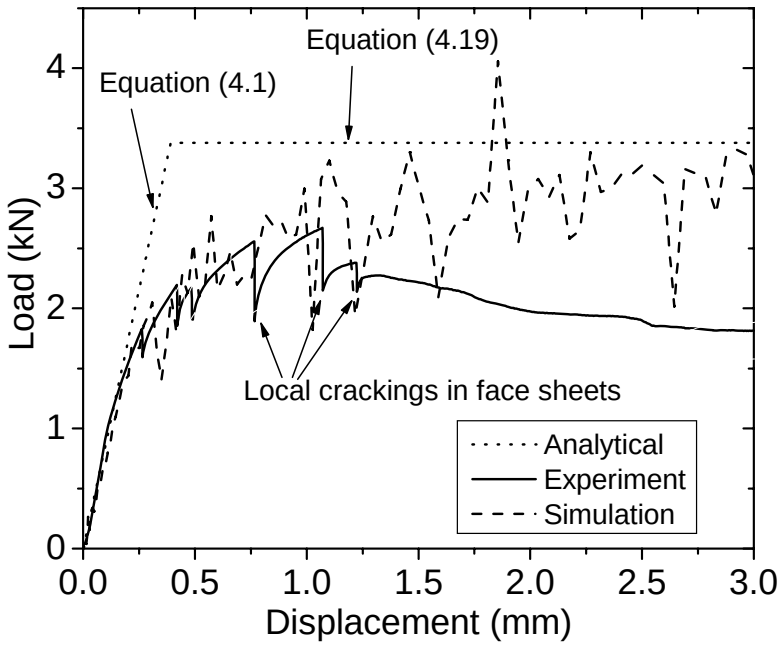

(c)

Figure 4. 12 Load versus displacement responses under core shear as derived from analytical, experiments and numerical analysis for (a) geometry - 6, (b) geometry – 7, and (c) geometry - 8.

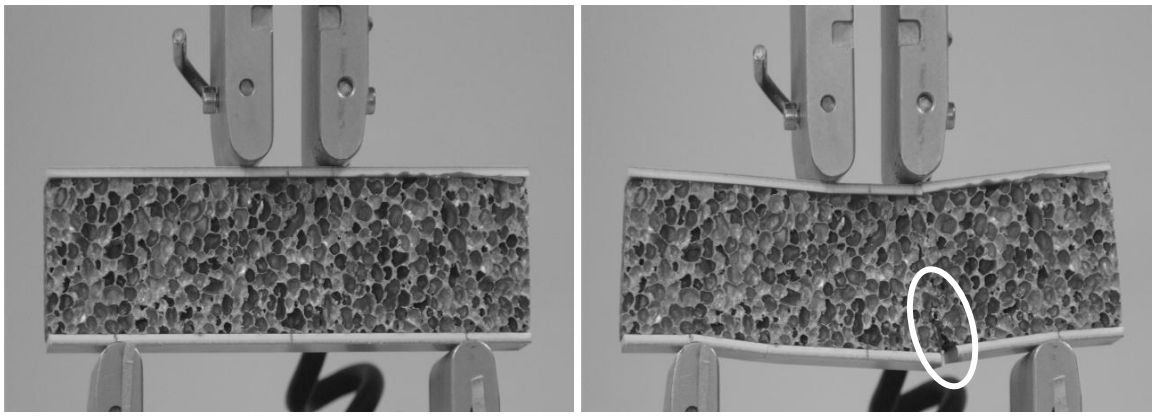

(a) *(b)*

Figure 4. 13 In-situ picture of the sandwich beam specimens expected to fail by core shear mode-B (geometry – 7) (a) starting of test (b) failure of test at a displacement of 2.5 mm.

The snapshot in Figure 4.13(b) clearly reveals mode B shear failure in the sandwich beam (geometry - 7) compare to the initial condition Figure 4.13 (a). Shearing of the core occurs between upper loading indenter and lower supporting indenters and is confirmed from FE simulations (see Figure 4.8(c)); within this domain shear stress contours exceed the core

ATTENTION: The Singapore Copyright Act applies to the use of this document. Nanyang Technological University Library

shear strength. Cracking of lower face sheet was observed with further loading as the tensile stress exceeded the rupture strength of the face sheet in the lower region.

Local cracking was found in many sandwich beams, in the region near to upper indenters because the local stress exceeds the tensile strength of face sheet. Contact failure was not accounted as a failure mode because even after exceeding this limit, the beam was able to take further load.

4.2.5 Minimum weight design

Optimization in structure design having the minimum weight and other objective functions such as cost with some constraints like strength or stiffness of structure plays an important role in the real applications because of the enhancement of load carrying capacity of those structures. The minimum weight and failure mode of the sandwich beam has to be found out for a given load carrying capacity. Non-dimensional terms such as face sheet thickness $\bar{t}$, core thickness $\bar{c}$ and inner span $\bar{s}$ are defined as follows:

$$\bar{c} \equiv \frac{c}{l} \quad , \bar{t} \equiv \frac{t}{c} \text{ and } \bar{s} \equiv \frac{s}{l} \tag{4.21}$$

The ratio of strength of the core to face sheet and density ratio (ρ_c and ρ_f are the densities of core and face sheet respectively) are defined as

$$\bar{\sigma} \equiv \frac{\sigma_y^c}{\sigma_y^f} \text{ and } \bar{\rho} \equiv \frac{\rho_c}{\rho_f} \tag{4.22}$$

Non-dimensional mass index of the sandwich beam is defined in terms of mass (M) of the sandwich beam by

$$\bar{M} \equiv \frac{M}{bl^2\rho_f} = \frac{2btl\rho_f + bcl\rho_c}{bl^2\rho_f} = 2\frac{t}{c}\frac{c}{l} + \frac{c}{l}\frac{\rho_c}{\rho_f} = 2\bar{t}\bar{c} + \bar{c}\bar{\rho} \tag{4.23}$$

Appropriate structural load index $\bar{F}$ is

$$\bar{F} \equiv \frac{F}{bl\sigma_y^f} \tag{4.24}$$

The dependence of geometrical parameters and foam density upon structural load index is determined for each failure mode as follows:

ATTENTION: The Singapore Copyright Act applies to the use of this document. Nanyang Technological University Library

Now, the failure loads for face sheet cracking, core indentation and Mode-B core shear can be expressed in non-dimensional form (structural load index) as:

$$\overline{F}_{FSC} = \left[\frac{2\left(\bar{c}\right)^2\left(\bar{t}\right)^3 + 6\left(\bar{c}\right)^2\bar{t}\left(1+\bar{t}\right)^2}{3\left(1+2\bar{t}\right)\left(1-\bar{s}\right)}\right] + \left[\frac{\left(\bar{c}\right)^2\bar{\sigma}}{\left(1-\bar{s}\right)}\right] \tag{4.25}$$

$$\overline{F}_{CI} = \left(\frac{\pi^2\left(\bar{c}\right)^4\left(\bar{t}\right)^3\left(1+\bar{t}\right)\left(\bar{\sigma}\right)^2}{3\left(1-\bar{s}\right)}\frac{\left(E_f\right)}{\left(\sigma_y^f\right)}\right)^{1/3} \tag{4.26}$$

$$\overline{F}_{CSB} = \left[2\bar{c}\bar{\sigma}\frac{\tau_y^c}{\sigma_y^c}\right] + \left[\frac{8\left(\bar{c}\right)^2\left(\bar{t}\right)^2}{3\left(1-\bar{s}\right)}\right] \tag{4.27}$$

Optimum weight design can be defined with selection of beam geometry which minimizes the mass index $\overline{M}$ for a particular structural load index $\overline{F}$. Contours of $\overline{M}$ and $\overline{F}$ are shown in Figure 4.14 (failure mechanism map for sandwich beam having Alporas foam core and 2 mm thick alumina face sheet) having $\bar{\sigma} = 0.0096$, $\bar{\rho}$ = 0.06 and $\bar{s}$ = 0.25. Both these contours are increasing towards the leading diagonal of map with increasing $\bar{t}$ and $\bar{c}$.

An analytical expression for the minimum mass index of the sandwich beam can be found out for each failure mode by following few steps:

(i) Solve failure load expression for either $\bar{c}$ or $\bar{t}$ in terms of other parameters such as $\bar{t}$ or $\bar{c}$ and $\overline{F}$ respectively.

(ii) Replace the value of that solved $\bar{c}$ or $\bar{t}$ in mass index $\overline{M}$ (equation 4.23)

(iii) Solve $\frac{\partial\overline{M}}{\partial\bar{c}} = 0$ or $\frac{\partial\overline{M}}{\partial\bar{t}} = 0$ (for maximum and minimum) and get the optimum value of $\bar{c}$ or $\bar{t}$.

(iv) Obtain the optimum value of other parameter ($\bar{t}$ or $\bar{c}$) by replacing the optimum value of $\bar{c}$ or $\bar{t}$ in failure load equation.

(v) Obtain the analytical minimum mass index by putting those optimum parameters ($\bar{c}$ and $\bar{t}$) into mass index $\overline{M}$ (equation 4.23).

By following the same steps explained above, minimum mass index expression was obtained for each failure mode with optimum parameters ($\bar{c}$ and $\bar{t}$).

ATTENTION: The Singapore Copyright Act applies to the use of this document. Nanyang Technological University Library

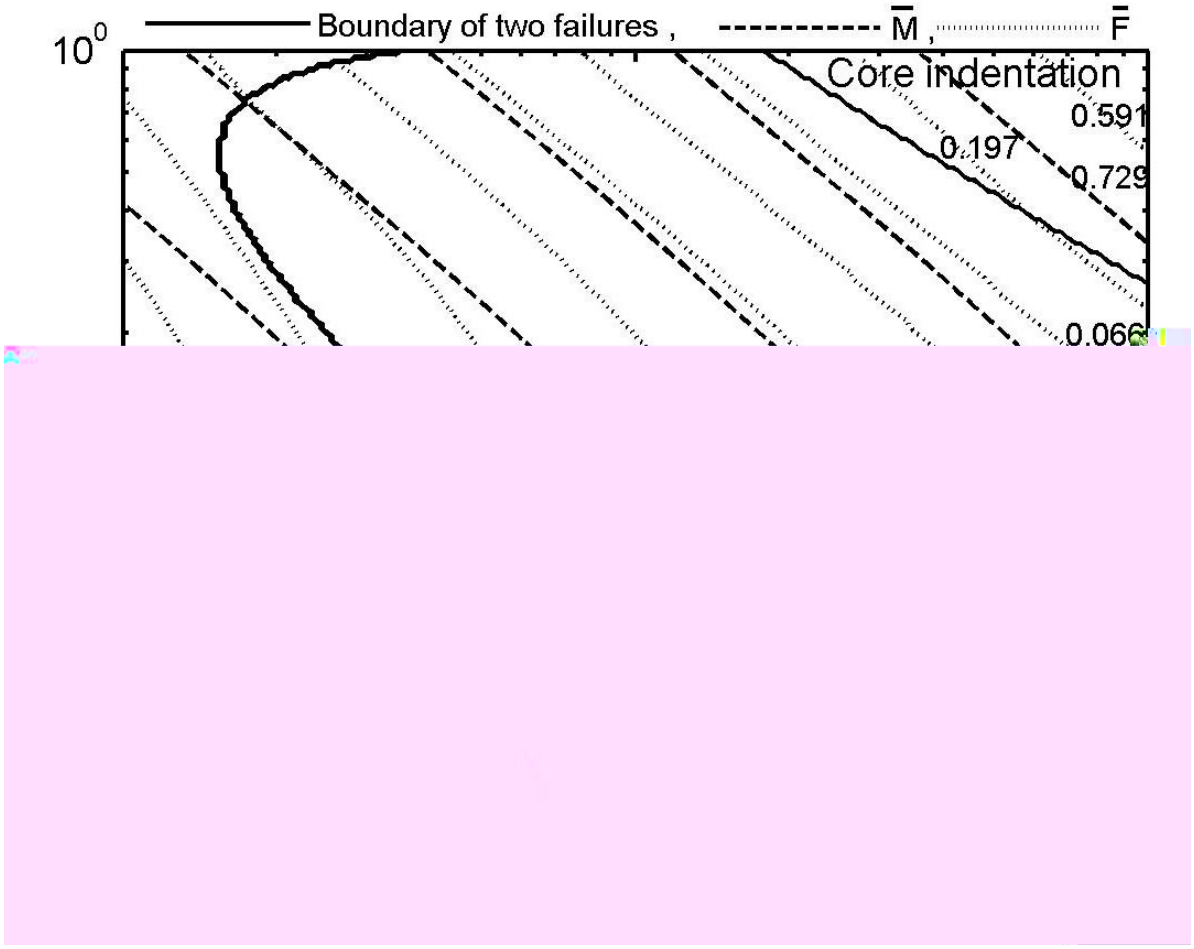

Figure 4. 14 Contours of the dimensionless mass index and structural load index in collapse mechanism map of sandwich beam of Alporas foam core with alumina face sheet of 2mm thickness having , $\bar{\rho}$ =0.06 and $\bar{s}$ = 0.25.

Minimum mass index expression for face sheet cracking, core indentation, core shear mode-B, face sheet cracking-core indentation, core indentation-core shear mode-B, and face sheet cracking –core shear mode-B is given as:

$$\left(\bar{M}_{\min}\right)_{FSC} = 0.406131\sqrt{\bar{F}} \tag{4.28}$$

$$\left(\bar{M}_{\min}\right)_{CI} = 1.55476\left(\bar{F}\right)^{3/4} \tag{4.29}$$

$$\left(\bar{M}_{\min}\right)_{CSB} = \left(95.05\bar{F} - 0.708\right)\left(0.064646 + \frac{0.17}{\sqrt{32122.5\left(\bar{F}\right)^2 - 478.57\bar{F} + 1.78}}\right) \tag{4.30}$$

ATTENTION: The Singapore Copyright Act applies to the use of this document. Nanyang Technological University Library

$$\left(\overline{M}_{\min}\right)_{FSC-CI} = 2.00184\left(\overline{F}\right)^{3/4} \tag{4.31}$$

$$\left(\overline{M}_{\min}\right)_{CI-CSB} = \left(1.369\sqrt{F + 0.000627}\right) + 0.0343 \tag{4.32}$$

$$\left(\overline{M}_{\min}\right)_{FSC-CSB} = \left(2.566\sqrt{F + 0.015}\right) - 0.0314 \tag{4.33}$$

The minimum weight design is found by calculating the minimum mass index $\overline{M}_{\min}$ necessary to suppress all possible failures for a given structural load index $\overline{F}$. Therefore, the dominant mechanism or combination of mechanisms (at the boundary of two failures), is the one having the largest value of $\overline{M}_{\min}$ at each value of $\overline{F}$. So for getting a clear picture of the minimum weight design, the largest $\overline{M}_{\min}$ for each value of $\overline{F}$ is plotted for each failure mode and the combination of modes, which is shown by Figure 4.15 (a). This minimum weight design map is valid only for $\overline{\sigma} = 0.0096$, $\overline{\rho}$ = 0.06 and $\overline{s}$ = 0.25 and for alumina face sheet of 2mm thickness.

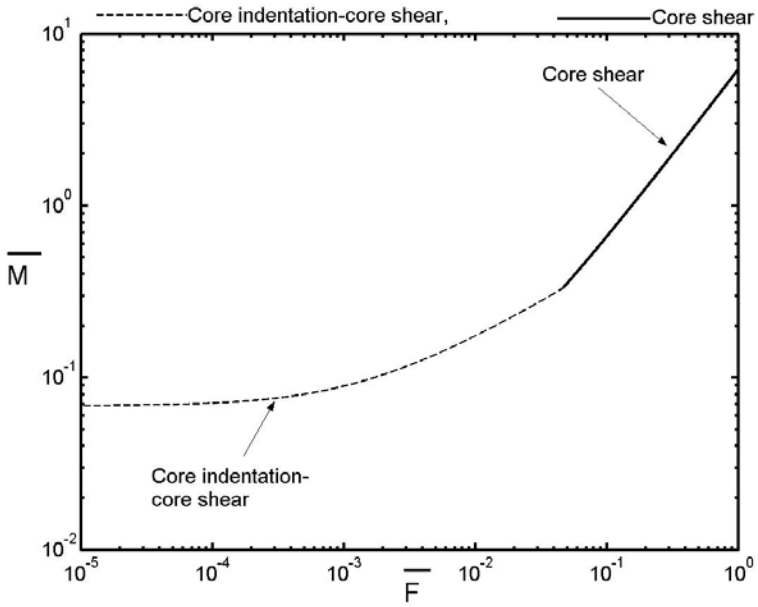

(a)

ATTENTION: The Singapore Copyright Act applies to the use of this document. Nanyang Technological University Library

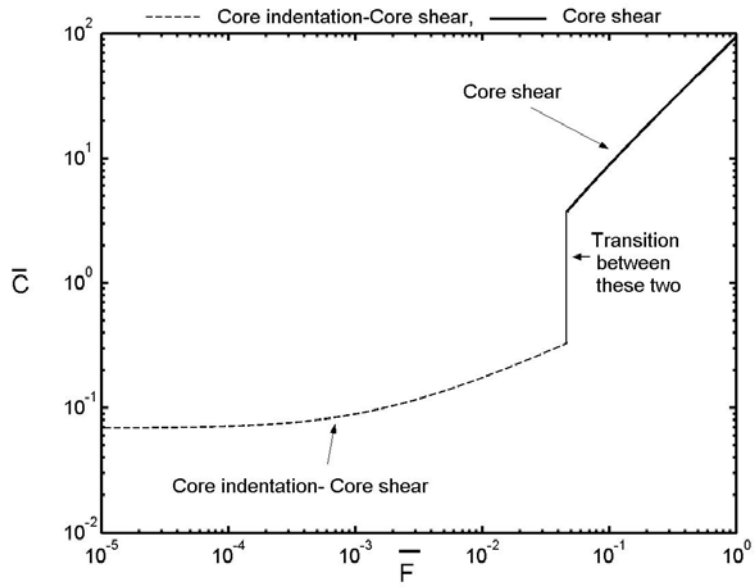

(b)

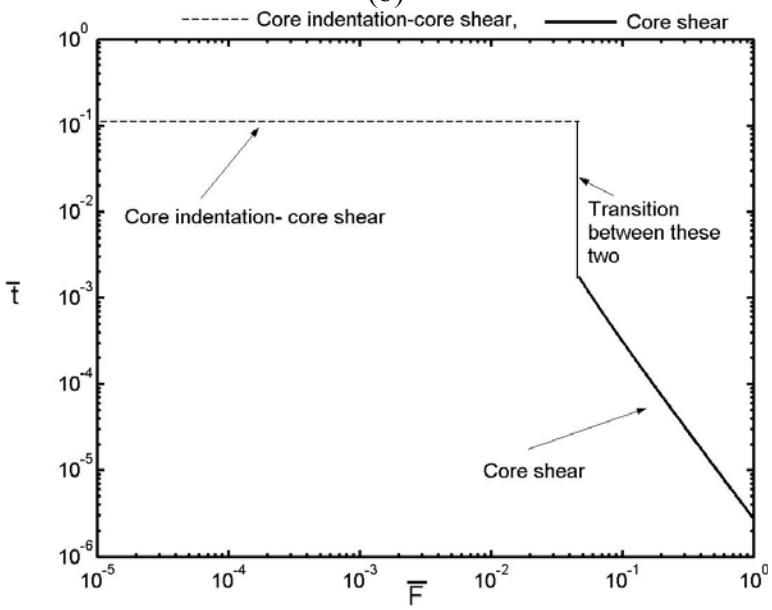

(c)

Figure 4. 15 Minimum weight design of sandwich beam with Alporas foam core and 2 mm thick alumina face sheet with optimum geometrical parameters having $\bar{\sigma} = 0.0096$, $\bar{\rho} = 0.06$ and $\bar{s} = 0.25$ (a) Variation of minimum mass index $\bar{M}$ with structural load index $\bar{F}$ considering for all failure modes (b) Variation of $\bar{c}$ with structural load index $\bar{F}$ for minimum weight design of sandwich beam (c) Variation of $\bar{t}$ with structural load index $\bar{F}$ for minimum weight design of sandwich beam.

The trend of minimum weight design was found to be in the increasing order with structural load index due to square root term of $\bar{F}$ for core shear failure mode. If these parameters are

ATTENTION: The Singapore Copyright Act applies to the use of this document. Nanyang Technological University Library

changed then the values of the map will be changed too however the general layout will remain the same. It was observed from the Figure 4.15 (a) that the local minimum mass design is achieved at boundary between the core indentation and core shear for lower values of $\overline{F}$ and with in core shear domain for higher values of $\overline{F}$ with constant values of $\overline{\sigma} = 0.0096$, $\overline{\rho} = 0.06$ and $\bar{s} = 0.25$. The associated optimum geometrical parameters ($\bar{c}$ and $\bar{t}$) are also plotted with structural load index as shown in Figure 4.15 (b) and (c). The trend of $\bar{c}$ was found to be always in the increasing order with structural load index while $\bar{t}$ was found to be in the decreasing order with structural load index in core shear failure boundary region. Similarly the minimum weight design can be constructed for sandwich beam having Alporas foam core with various thickness of alumina face sheet.

ATTENTION: The Singapore Copyright Act applies to the use of this document. Nanyang Technological University Library

Chapter- 5

Sandwich beam with Al foam core and CFRP face sheet under three- point bending

5.1 Introduction

Weight saving without compromising structural integrity, is of prime importance in various applications such as automobile, aircraft, building and defense [7]. Metallic foams can play a vital role in these areas, especially with their usage as core material in various sandwich structures [7]. The performance of carbon fiber reinforced polymer (CFRP) composite material is excellent, especially its specific strength and stiffness. Therefore sandwich structures with metal foam core with CFRP face sheet would be very useful in those applications. It is necessary to evaluate the performance of these structures in various loading conditions such as bending and impact as it will help to understand the usage of the structure safely in real applications. Minimum weight design with optimized geometrical parameters of these structures is very much required to utilize the maximum load carrying capacity of the structure.

In this chapter, bending studies were conducted and discussed on beams consisting of CFRP face sheets and Alporas (an alloy of Al, Mn and Si) foam core to find various competing failure modes. For the identified failure modes, the analytical expressions for the failure load are provided. A failure mode map is constructed showing all possible failures in terms of non-dimensional geometrical parameters of the beam, for a given strength ratio of face sheet to core yield strength. Finite element simulations were carried out to verify the analytical solutions and to compare with the experimental measurements of stiffness and failure load.

5.2 Sandwich beam with Al foam core and CFRP face sheet under three – point bending

Here, analytical equations developed for failure loads and stiffness are discussed and compared with numerical simulation and experimental observations for these sandwich beams under three-point bending.

ATTENTION: The Singapore Copyright Act applies to the use of this document. Nanyang Technological University Library

5.2.1 Analytical analysis of sandwich beams under three- point bending

Consider a sandwich beam of width *b* and length *l*, comprising of two identical face sheets of thickness, *t* and foam core of thickness, *c*. The beam is subjected to three- point bending load as shown in Figure 1: the outer rollers of 10mm act as support while the central inner roller loads the specimen.

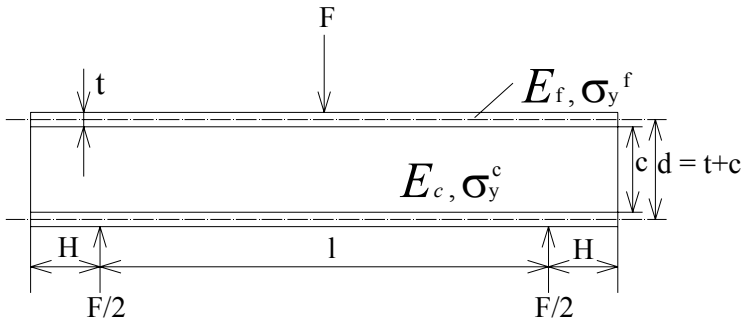

Figure 5. 1 Schematic of a sandwich beam under three-point bending showing geometrical and material parameters.

5.2.1.1 Elastic Stiffness

The maximum elastic deflection of the sandwich beam, which occurs at the centre of the beam under three – point bending can be expressed as [60]

$$\delta = \frac{Fl^3}{48(EI)_{eq}} + \frac{Fl}{4(AG)_{eq}} \tag{5.1}$$

where *l* is the distance between supporting rollers and *F* is the central load applied on the beam.

5.2.1.2. Estimation of Failure loads

The analytical formulae for the different failure modes are developed and discussed in the following paragraphs. A total of three possible competing failure modes, namely face sheet cracking, core indentation and core shear were identified for the sandwich beams. The upper face sheet was assumed to fail by compressive fracture in a linear elastic manner because of the characteristics of CFRP material and the foam core as a rigid-perfectly plastic material.

5.2.1.2.1. Face sheet cracking:

CFRP sheet used for the face sheet of the sandwich beam is brittle and possesses a lower compressive strength than the tensile strength; by about 50% as shown in Table 3.9 (in

ATTENTION: The Singapore Copyright Act applies to the use of this document. Nanyang Technological University Library

general it varies from 30 to 60%) [150]. Therefore, the compressive strength of the CFRP was considered to be the failure strength for the upper face sheets of the sandwich beams. The failure load for face sheet cracking is calculated by equating the moments within the sandwich beam (summation of the moments due to elastic brittle face sheet and rigid-plastic foam core) to the external bending moment applied to the sandwich beam.

Moment due to face sheet is

$$M_f = \frac{I_{eff} \times \sigma_y^f}{(t+\frac{c}{2})} = \frac{\{(\frac{b \times t^3}{12}) + (\frac{b \times t \times (c+t)^2}{4})\} \times \sigma_y^f}{(t+\frac{c}{2})} \tag{5.2}$$

where the moment of inertia I_{eff} has included the compressive failure of the upper face sheet. Now, equating the internally resisting moment to the maximum externally applied bending moment,

$$M_{\max} = \frac{Fl}{4} = \frac{\{(\frac{b \times t^3}{12}) + (\frac{b \times t \times (c+t)^2}{4})\}\sigma_y^f}{(t+\frac{c}{2})} + \left\{\sigma_y^c \frac{bc^2}{4}\right\} \tag{5.3}$$

So, load for failure for face sheet cracking is given by

$$F_{FSC} = \frac{4\{(\frac{b \times t^3}{12}) + (\frac{b \times t \times (c+t)^2}{4})\}\sigma_y^f}{(t+\frac{c}{2})l} + \left\{\sigma_y^c \frac{bc^2}{l}\right\} \tag{5.4}$$

5.2.1.2.2 Core indentation:

It is assumed that indentation failure appears when foam core is compressed beneath the upper indenter in a rigid-ideally plastic manner. Similar to the sandwich beam analysis with alumina face sheet under four point bending, the expression for the initiation of indentation failure in the foam core in sandwich beam with CFRP face sheet under three point loading is given by

$$F_{CI} = bt\left(\frac{\pi^2 (t+c) E_f \left(\sigma_y^c\right)^2}{3l}\right)^{1/3} \tag{5.5}$$

5.2.1.2.3. Core shear:

When the transverse shear stress in foam core exceeds the shear strength, the sandwich beam fails in shear mode. Two competing shear failure mechanisms are identified similar to sandwich with alumina sheet under bending as explained in Chapter 4. Figure 5.2 shows one

ATTENTION: The Singapore Copyright Act applies to the use of this document. Nanyang Technological University Library

possible failure mechanism termed Mode-A. Failure load F_{CSA} for core shear Mode A was calculated on similar lines to sandwich as in the Chapter 4 and can be expressed as

$$F_{CSA} = \frac{\left[2bc\tau_y^c(2H+l)\right]}{l} + \frac{2\left[bt^2\sigma_y^f\right]}{3l} \tag{5.6}$$

Similar to core shear Mode-A, failure load for core shear Mode-B (as shown in Chapter 4) was calculated and is expressed as

$$F_{CSB} = \left(2bc\tau_y^c\right) + \frac{\left(2bt^2\sigma_y^f\right)}{l} \tag{5.7}$$

The overhang length H decides the transition from Mode-A to Mode-B. By equating the two failure loads, the critical overhang length was estimated as

$$H = \frac{t^2}{3c}\frac{\sigma_y^f}{\tau_y^c} \tag{5.8}$$

If the overhang length is more than the aforementioned value, sandwich beam fails under Mode-B, and vice-versa.

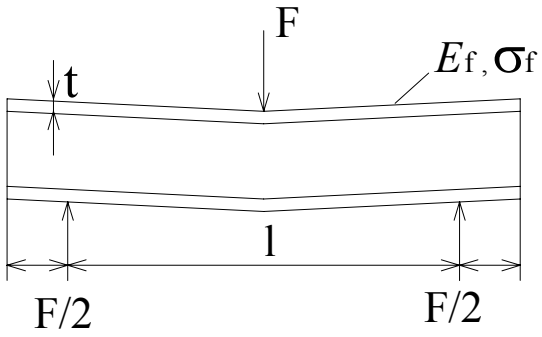

Figure 5. 2 Sandwich in core shear failure under Mode-A.

CFRP face sheet has a very high Young's modulus similar to alumina face sheet which gives very high load for failure under wrinkling compare to other failure mechanisms. This is the reason that analytical solution for wrinkling was not developed and discussed here.

5.2.2 Experimental procedure of sandwich beams under three- point bending

5.2.2.1 Materials

Unidirectional carbon fiber reinforced polymer and Alporas foam are used in this experimental study. The mechanical behavior of the materials is already being described in Chapter 3.

ATTENTION: The Singapore Copyright Act applies to the use of this document. Nanyang Technological University Library

5.2.2.2 Sandwich beam

In order to identify all the possible failure modes, the maximum possible geometries of the sandwich beams were tested with different thicknesses of unidirectional CFRP face sheets. The full details of the tested beam geometries are listed in Table 5.1. Sandwich beams of 25 mm width were prepared by bonding CFRP face sheets to Alporas foam core using Redux–322 adhesive*. The CFRP sheets are sandblasted for better bonding between the sheets and the foam core as was explained in Chapter 3. All the three–point bending tests with sandwich beams were conducted under displacement control with a cross-head displacement of 1.0 mm/min. Surface displacement analyzer (SDA) was employed for continuous monitoring of the deformed geometry. Snapshots of the loaded sandwich beams were taken at every significant change in the beam geometry.

5.2.3 Finite element modeling

All the test geometries were simulated numerically using ABAQUS commercial finite element program. The carbon fiber reinforced polymer composite laminate face sheet is assumed to be perfectly bonded to the core, eliminating the delamination failure mode. The foam core is completely constrained by the face sheets and behaves in approximately a plane-strain manner. The face sheets are much wider than their thickness and hence, a plane-strain analysis on the sandwich beams is justified. Four nodded bilinear plane strain quadrilateral elements with reduced integration (CPE4R) have been used to discretize the assembly. For improved accuracy, fine mesh was incorporated in the regions of high stress or strain gradient, such as the region underneath central roller. Load was applied in terms of displacement through the one upper loading indenter while two supporting lower indenters are constrained completely. The loading and supporting rollers are modeled as rigid-bodies. A contact algorithm within ABAQUS models frictionless contact between the rollers and the sandwich beams. The constitutive law for Alporas foam core is described earlier in Chapter 4. Unidirectional carbon fiber reinforced polymer matrix composite was modeled as homogenous orthotropic material with the “engineering constant” material model which is sufficient enough to study the macroscopic behavior of the laminate. This model gives us the flexibility to define the angle of fiber reinforcement such as 0^o, 30^o, 90^o, etc [139]. The local

* supplied by Hexel Composites, Australia

ATTENTION: The Singapore Copyright Act applies to the use of this document. Nanyang Technological University Library

coordinate system was defined for each sheet of fiber reinforced material to indicate the fiber direction as it will represent the longitudinal and transverse directions for the sheets which is very important for any orthotropic material. Unidirectional fiber reinforcement was modeled as a layer of laminate lay-up in one direction. The symmetric stiffness matrix is calculated from the data of the measured properties for the laminates as listed in Chapter 3.

Simulation of all the beams tested confirms that the stresses in these sheets were reaches the strength limit of sheets only when the failure mode is face sheet cracking and then failure was accounted at the iteration when stress in the face sheet spread through the thickness immediately beneath the loading roller, as consider by Steeves and Fleck [151].

5.2.4 Failure mechanisms map for sandwich beam under three- point bending

The dominant failure mode is the one which requires the lowest load to fail among all possible failure modes for a given sandwich beam geometry. A failure mechanism map in terms of non-dimensional geometrical parameters ($\bar{c} = c/l$ and $\bar{t} = t/c$) based on analytical formulae presented earlier, is shown in Figure 5.3.

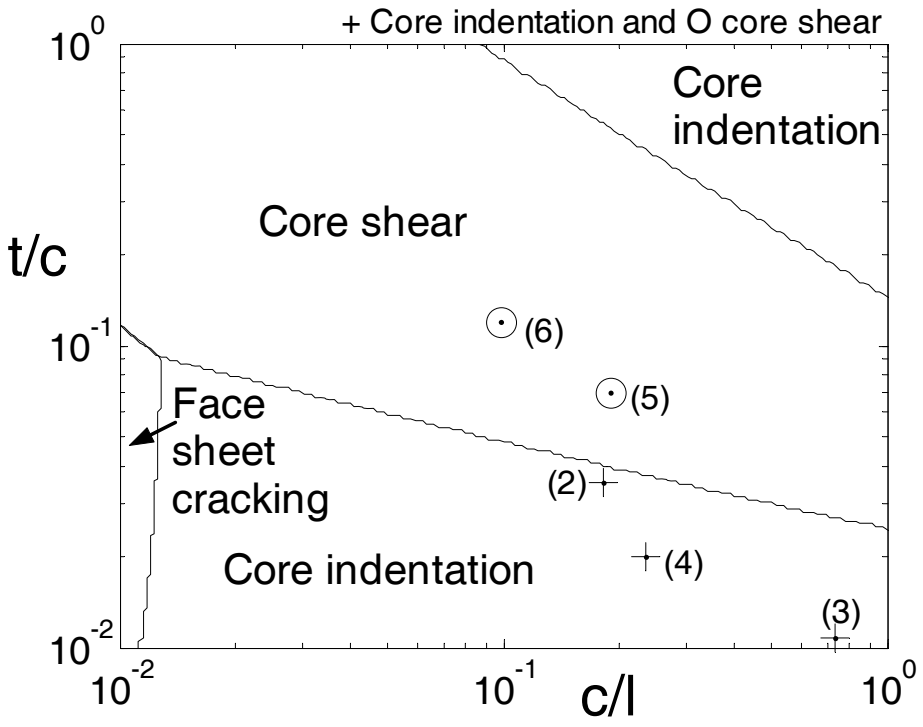

(a)

ATTENTION: The Singapore Copyright Act applies to the use of this document. Nanyang Technological University Library

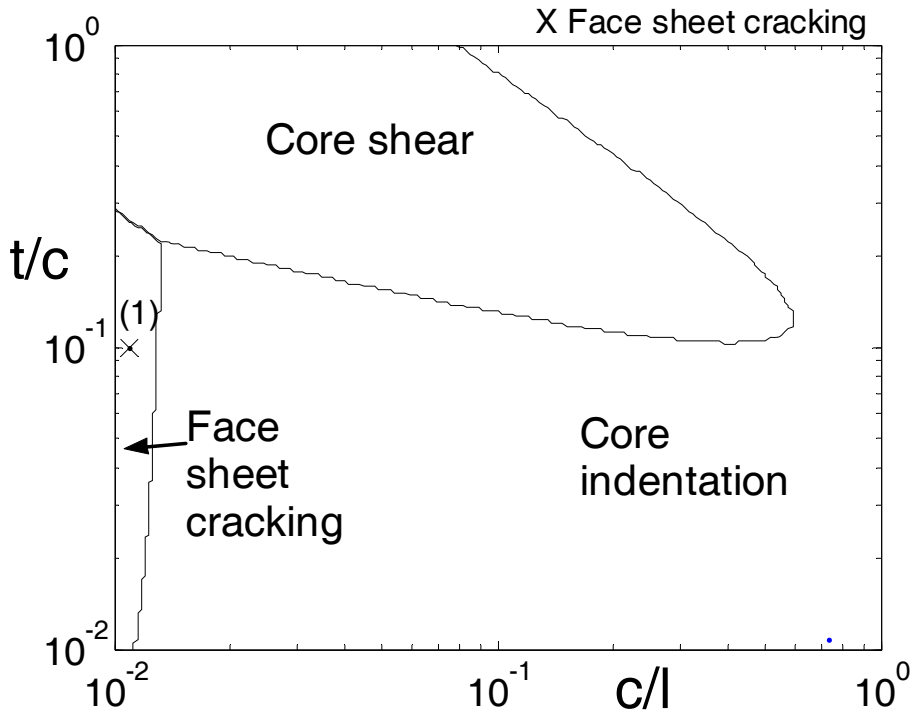

(b)

Figure 5. 3 Failure mechanisms map for sandwich beam having foam core and unidirectional carbon fiber reinforced polymer composite face sheet for a fixed H/l = 0.09 showing the three possible failure modes (a) 20 mm thick foam core (b) 3 mm thick foam core.

It shows an overview of all possible failure modes with the locations of the selected geometry of sandwich beams. The boundary of the failure modes is drawn by equating analytical equations for failure loads presented earlier. The failure load given by equations (5.4), (5.5) and (5.6), contains compressive and shear strength of the foam which depend on the thickness of core if it is below 20 mm. As the size ratio (specimen size to cell size) effect on the shear strength become negligible after exceeding this size ratio of 6 for this density Alporas foam as shown in Chapter 3.

This effect of core thickness on the failure regions is represented by the shrinkage of the domain of core shear failure in the failure mechanism map of Figure 5.3(a) (20 mm thick core) as compared to Figure 5.3(b) (3 mm core thickness, as shear strength of the foam is increased so the domain for core shear is less). For all the geometries selected, the beam overhang length *(H)* was less than the critical value as calculated by Equation 5.8. Hence, core shear Mode-A was observed in experiments and only this mode was indicated in failure map in core shear category.

ATTENTION: The Singapore Copyright Act applies to the use of this document. Nanyang Technological University Library

5.2.5 Comparison of analytical, numerical results with experimental observations

A total of three competing failure modes; namely face sheet cracking, core shear and core indentation was identified under three point bending of the sandwich beams. Local cracking or contact failure was not observed as it was found in sandwich beams with alumina face sheets because of lower tensile strength of the alumina sheets as compared to that of the carbon fiber reinforced sheets. As the adhesive used (between foam core and face sheets) has a higher shear strength compared to shear strength of foam core, bond failure mechanism was not observed.

In the following paragraphs, the experimentally measured load-displacement responses are compared with numerical simulations and analytical predictions. In addition, the elastic stiffness of the beam and failure load value is compared with the analytical formulae. An overview of analytical, simulation and experiential studies of sandwich beam with Alporas foam core and CFRP face sheet is given in Table 5.1 with full geometrical details of the sandwich beam specimens.

Table5.1 Geometry of sandwich beams under three-point bending (all dimensions are in mm)

Specimen	***c* (mm)**	***t* (mm)**	***l* (mm)**	***H* (mm)**	**Failure mode**	**Observed failure load (kN)**	**Analytical failure load (kN)**	**FEM Computed load (kN)**
1	3	0.3	254	23	*FSC*	0.21	0.19	0.16
2	20	0.7	110	10	*CI*	1.18	1.13	1.13
3	60	0.65	82	7	*CI*	1.73	1.67	1.70
4	20	0.4	85	7.5	*CI*	0.73	0.71	0.77
5	20	1.4	103	9.5	*CS*	1.54	1.52	1.99
6	20	2.4	203	18.5	*CS*	1.65	1.68	1.9

Where *c*- Core thickness, *t*- Face sheet thickness, *l*- Supporting roller span, *H*- Overhang length, *CI*- Core indentation ,*CS*- Core shear and *FSC* – Face sheet cracking.

5.2.5.1 Face sheet cracking

The load versus displacement curve for sandwich beam geometry - 1 (Table 5.1), failed experimentally by face sheet cracking was compared with analytical calculations as shown in Figure 5.4. Load increases monotonically with displacement in a linear elastic manner and drops suddenly indicating catastrophic failure, when the upper face sheet cracked under compressive fracture. This failure mode was dominant when the span length, *l,* was very

ATTENTION: The Singapore Copyright Act applies to the use of this document. Nanyang Technological University Library

large and face sheet thickness, *t*, was small with respect to core thickness, *c*. This result is similar to the findings on the sandwich beam made with aluminum foam core and alumina face sheets as explained in Chapter 4. There is good agreement between the experimentally measured failure load values with analytical predictions but there is little deviation from the numerical simulation results.

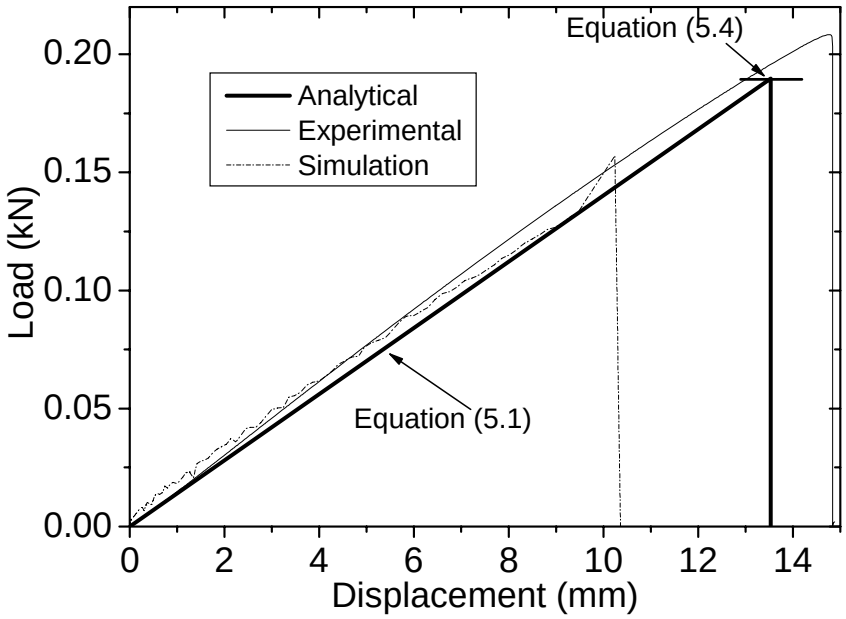

Figure 5. 4 Load and displacement curves derived from analytical, experimental and numerical analysis for the sandwich beam having geometry no-1 (Table-5.1) which failed under face sheet cracking.

The reason of this deviation could be the poor mesh refinement in high strain area because of the geometrical considerations of this beam (length to thickness ratio for CFRP face sheet was 0.001). Cracking of top face sheet at the centre was observed in snapshots of geometry - 1 (Table-5.1) taken at failure load of 0.21 kN as shown in Figure 5.5. It shows the location of typical failure, which was observed in almost all the specimens with the same dimensions that failed under this mode. Due to the practical constraints of fabricating long thin CFRP face sheets and constraints on the maximum allowable span length on the test system, more tests were not conducted to probe this failure mechanism.

The normal stress contours obtained from the numerical simulation confirmed that the failure was initiated in the upper face sheet (see Figure 5.6). It was confirmed that the normal stresses in the upper face sheet below the loading indenter exceeded the failure limit of the

ATTENTION: The Singapore Copyright Act applies to the use of this document. Nanyang Technological University Library

material and at this stage the shear and compressive stresses in the core were within their design limits.

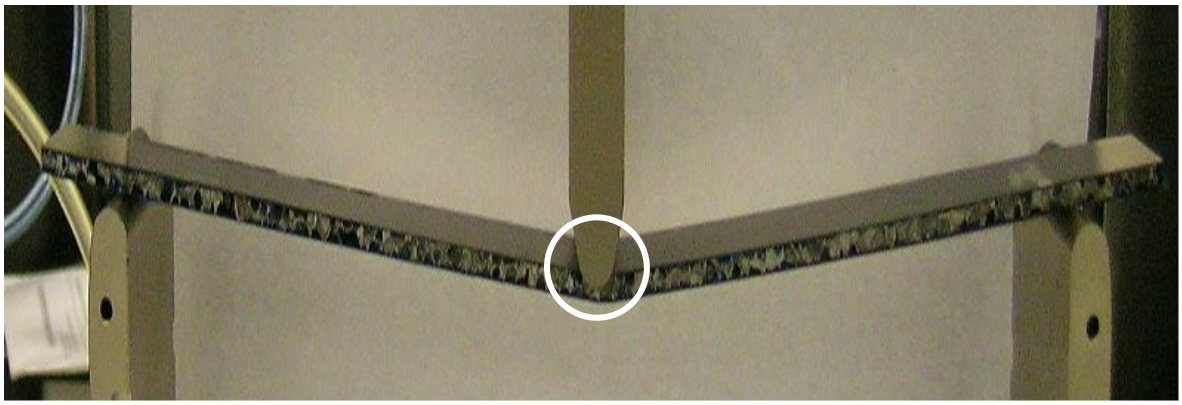

Figure 5. 5 In-Situ picture of the sandwich beam specimen failed by face sheet cracking (geometry – 1) at a displacement of 14.8mm.

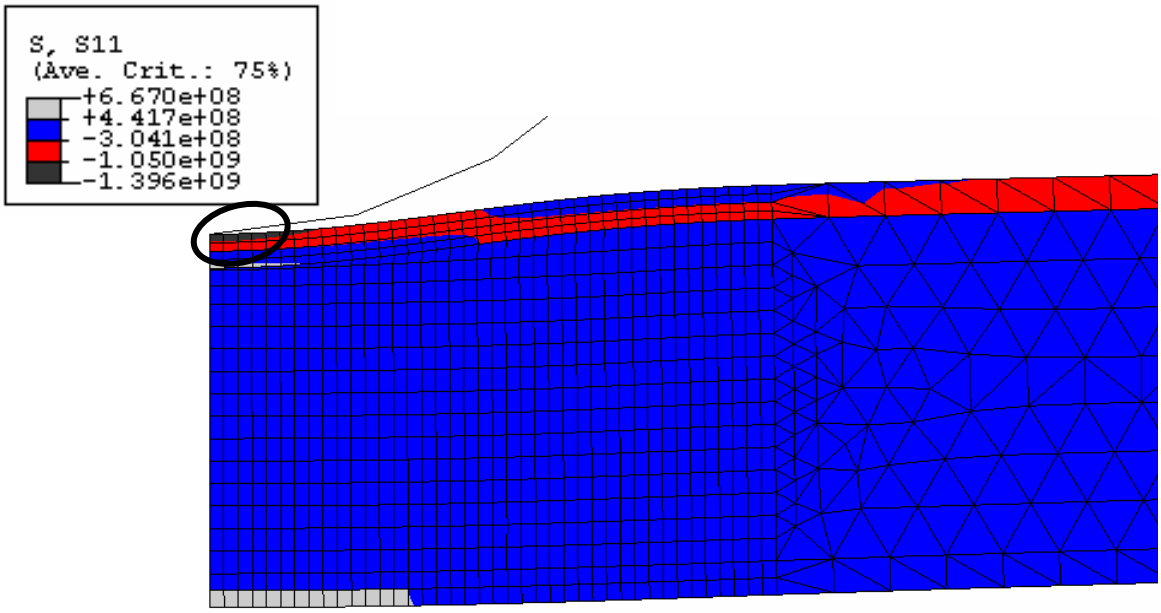

Figure 5. 6 Stresses S11 (in Pa) contours in half sandwich beam showing face sheet cracking in area of face sheet below upper indenter (geometry -1) at a displacement of 10.3 mm.

5.2.5.2 Core indentation

It is to be seen from the failure mechanism map in Figure 5.3 (a) and (b) that core indentation is the dominant mode for (i) Zone I: small value of *t*/*c* across a wide range of *c*/*l* values (ii) Zone II: for very high value of both *t*/*c* and *c*/*l* (i.e. right hand upper most portion of the map). Unfortunately, practical constraints limit the fabrication of thick face sheets; hence, three geometries were tested in Zone I to verify the core indentation failure mechanism (see

ATTENTION: The Singapore Copyright Act applies to the use of this document. Nanyang Technological University Library

Table 5.1). The load – displacement observations from analytical, numerical simulation and experimental measurements are shown graphically in Figure 5.7 for the sandwich beam (specimen- 4 Table 5.1). It is to be noted that once localized indentation occurs in the core, the failure load remains almost constant with progressive indentation amount. Sandwich beams with other geometries failed under core indentation failure mode (specimen 2 and 3 Table 5.1) have similar load-displacement response.

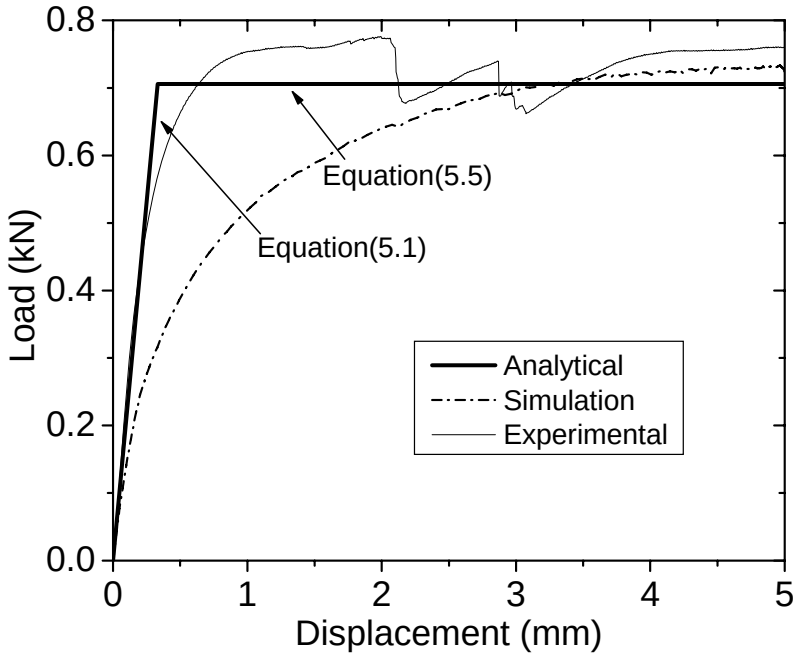

Figure 5. 7 Comparison of load and displacement curve for analytical, simulation and experimental observations for sandwich beam having geometry-4 (Table-5.1) failed under core indentation.

The experimental load also remains almost constant after the peak as shown in the Figure 5.7 which could be attributed to the ease in crushing of foam beneath the indenters for these geometries rather than cracking of high strength face sheet and shearing of foam core. From this specimen, prediction for failure loads by analytical solution (5.5) was found to be in good agreement with the simulation and experiments. The stiffness of the sandwich beams predicted by Equation (5.1) was also found to be in good agreement with the simulation and experimentally measured values. The deflection for failure was very low because of very high Young's modulus of CFRP face sheet.

Indentation of the foam is predicted by simulation as a stress contour in the zone that exceeds the compressive strength of foam as shown in Figure 5.8 with slight indentation at the

ATTENTION: The Singapore Copyright Act applies to the use of this document. Nanyang Technological University Library

supporting indenters. Crushing of the foam in numerical simulation was verified experimentally (as seen in Figure 5.9) except for the indentations above the supporting rollers by virtue of the magnitude.

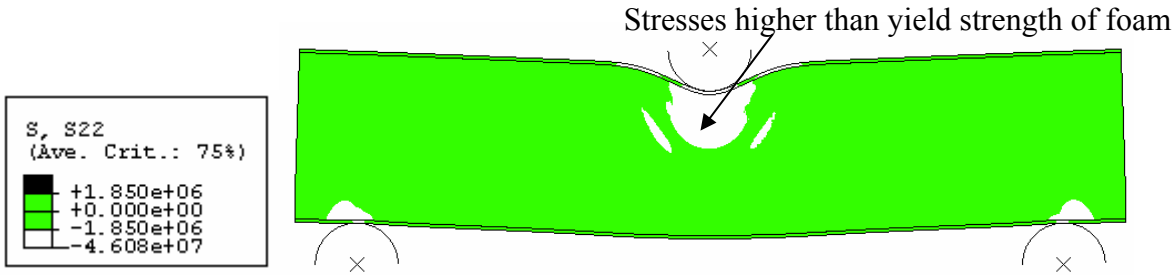

Figure 5. 8 Compressive stress (S22 in Pa) contours in sandwich beam showing core indentation failure underneath the upper indenter (geometry-4) at a displacement of 5 mm.

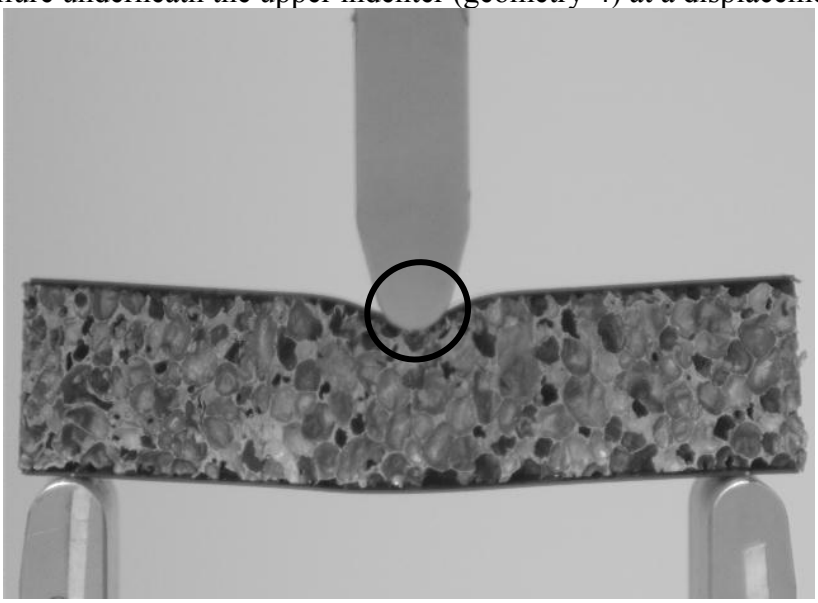

Figure 5. 9 In-situ picture of the sandwich beam specimens failed by core indentation (geometry – 4) at a displacement of 5mm.

5.2.5.3 Core shear

A comparison of the predicted load versus displacement response by the analytical and numerical simulation with experimental observations for the beam of geometry-6, which failed in core shear, is shown in Figure 5.10, and is carried out with experimental observations. Specimens with two geometries (5 and 6 in Table 5.1) probe this failure mechanism. The overhang length for the geometries selected for core shear mode was set to be lesser than the critical value so that shearing of foam core occurs only in Mode-A(as explained by equation 5.8). For the consistency in the experimental study, ratio of overhang

ATTENTION: The Singapore Copyright Act applies to the use of this document. Nanyang Technological University Library

length to supporting span length (*H/l*) on the failures was kept constant for all the geometries tested.

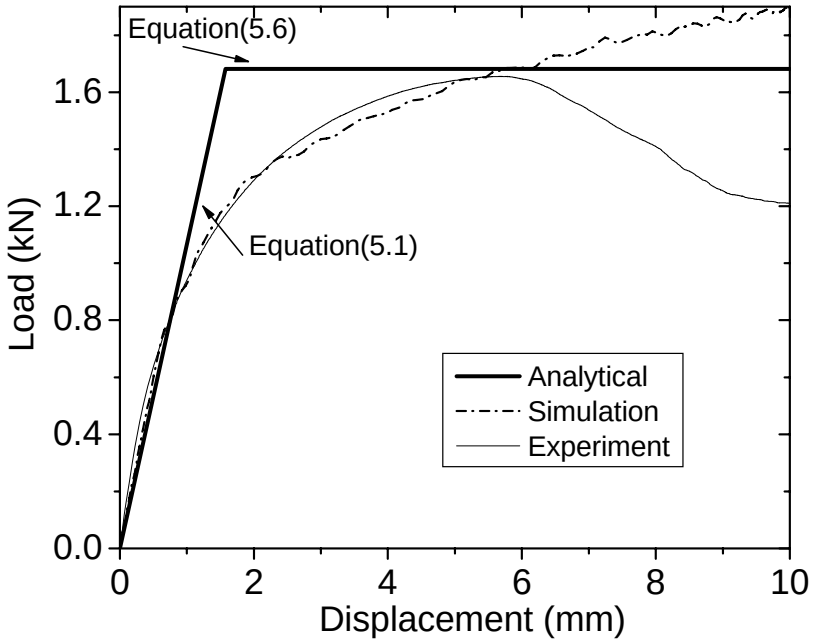

Figure 5. 10 Load versus displacement responses under core shear as derived from analytical, experiments and numerical analysis for sandwich beam geometry -6, Table-5.1 at a displacement of 10mm.

The prediction of load for failure by analytical analysis (5.6) agreed well with the experimental observations and numerical simulation responses. The prediction for stiffness by equation (5.1) was also found to be in good agreement with the numerical simulation and experimentally measured values.

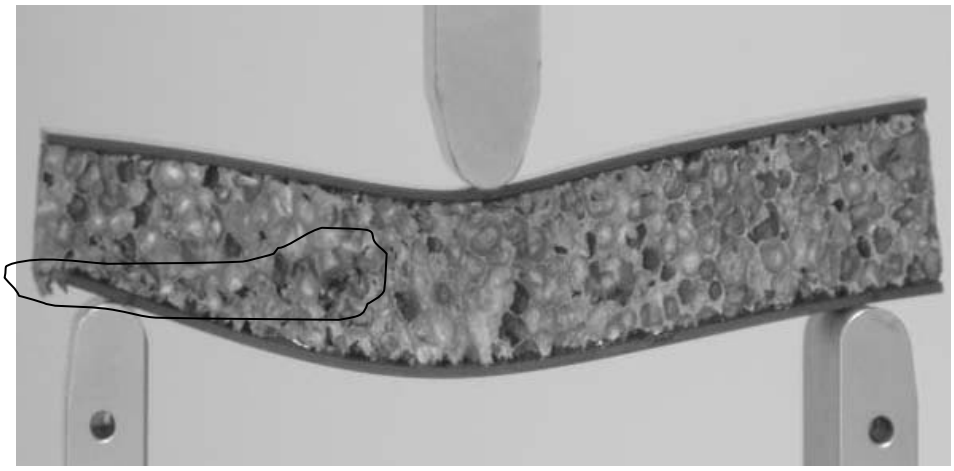

Figure 5. 11 In-situ picture of the sandwich beam specimens failed by core Shear Mode-A (geometry – 6) at a displacement of 10mm.

ATTENTION: The Singapore Copyright Act applies to the use of this document. Nanyang Technological University Library

The snapshot of the tested sandwich beam (specimen – 6, Table 5.1) shown in Figure 5.11 reveals clearly the presence of core shear failure Mode-A. Shearing of the foam core was found to occur between side most foam core and upper loading indenter in the experiment and the location can be confirmed from FE simulations, as can be seen in Figure 5.12: within this domain the shear stresses exceed the core shear strength.

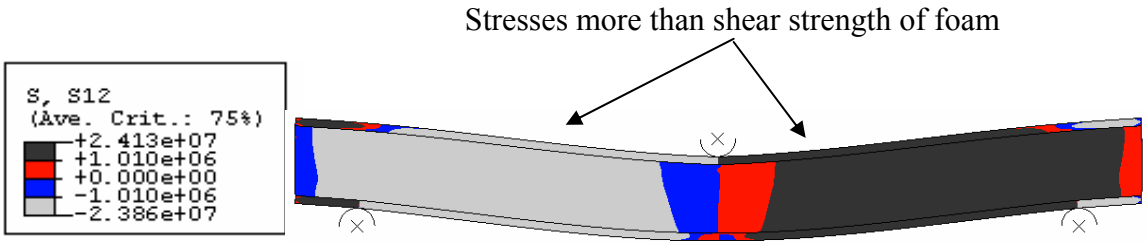

Figure 5. 12 Shear stress (S12 in Pa) contours in sandwich beam showing core shear mode-A failure in the area from lower indenter to upper indenter (geometry-6) at a displacement of 10 mm.

Local cracking of the CFRP sheet was absent in all sandwich beams due to high tensile strength of laminates as it was found in many sandwich beams with alumina sheets in the region near indenters.

5.2.6 Minimum weight design

Optimization in designing of the structure having the minimum weight and other objective functions such as cost with constraints like strength or stiffness of structure plays an important role in the real applications. The minimum weight of the sandwich beam has to be found out for a given load carrying. Non-dimensional terms such as face sheet thickness $\bar{t}$, core thickness $\bar{c}$, ratio of strength of core to face sheet $\bar{\sigma}$ and density ratio $\bar{\rho}$ defined in Chapter 4 are stated below:

$$\bar{c} \equiv \frac{c}{l} \quad ,\bar{t} \equiv \frac{t}{c}, \bar{\sigma} \equiv \frac{\sigma_y^c}{\sigma_y^f} \quad \text{and} \quad \bar{\rho} \equiv \frac{\rho_c}{\rho_f} \tag{5.9}$$

Non-dimensional mass index ($\bar{M}$) and structural load index $\bar{F}$ of the sandwich beam are given by

$$\bar{M} \equiv 2\bar{t}\bar{c} + \bar{c}\bar{\rho} \quad \text{and} \quad \bar{F} \equiv \frac{F}{bl\sigma_y^f} \tag{5.10}$$

ATTENTION: The Singapore Copyright Act applies to the use of this document. Nanyang Technological University Library

Now, the failure loads for face sheet cracking, core indentation and Mode-B core shear can be expressed in non-dimensional form (structural load index) as:

$$\overline{F}_{FSC} = \left[\frac{2\left\{\left(\bar{c}\right)^2\left(\bar{t}\right)^3\right)+3\left(\left(\bar{c}\right)^2\bar{t}\left(1+\bar{t}\right)^2\right)\right\}}{3\left(1+2\bar{t}\right)}\right]+\left[\left(\bar{c}\right)^2\overline{\sigma}\right] \tag{5.11}$$

$$\overline{F}_{CI} = \left(\frac{\pi^2\left(\bar{c}\right)^4\left(\bar{t}\right)^3\left(1+\bar{t}\right)\overline{\sigma}^2}{3}\frac{\left(E_f\right)}{\left(\sigma_y^f\right)}\right)^{1/3} \tag{5.12}$$

$$\overline{F}_{CSA} = \left[\frac{26}{11}\bar{c}\overline{\sigma}\frac{\tau_y^c}{\sigma_y^c}\right]+\left[\frac{2}{3}\left(\bar{c}\right)^2\left(\bar{t}\right)^2\right] \tag{5.13}$$

Optimum weight design can be defined with the selection of beam geometry which minimizes mass index $\overline{M}$ for a particular structural load index $\overline{F}$. Contours of $\overline{M}$ and $\overline{F}$ with collapse mechanism map for sandwich beam having Alporas foam core and CFRP face sheet having $\overline{\sigma} = 0.0018$ and $\overline{\rho}$=0.208 are shown in Figure 5.13.

Both these contours are increasing towards the leading diagonal of map with increasing $\bar{t}$ and $\bar{c}$. Analytical expression for the minimum mass index of the sandwich beam can found out for each failure mode by few steps, explained in Chapter 4. By following the same steps, minimum mass index expression was obtained for each failure mode with optimum parameters ($\bar{c}$ and $\bar{t}$).

The minimum mass index expression for face sheet cracking, core indentation, core shear mode-A, face sheet cracking-core indentation, core indentation-core shear mode-A, and face sheet cracking-core shear mode-A is shown below.

$$\left(\overline{M}_{\min}\right)_{FSC} = 0.895352\sqrt{\overline{F}} \approx 0.9\sqrt{\overline{F}} \tag{5.14}$$

$$\left(\overline{M}_{\min}\right)_{CI} = 9.73\left(\overline{F}\right)^{3/4} \tag{5.15}$$

$$\left(\overline{M}_{\min}\right)_{CSA} = \left(439.83\overline{F}-0.0787\right)\left(0.208+\frac{0.000075}{\left(\overline{F}+0.00018\right)}\right) \tag{5.16}$$

ATTENTION: The Singapore Copyright Act applies to the use of this document. Nanyang Technological University Library

$$\left(\overline{M}_{\min}\right)_{FSC-CI} = 11.66\left(\overline{F}\right)^{3/4} \tag{5.17}$$

$$\left(\overline{M}_{\min}\right)_{CI-CSA} = \left(2.93\sqrt{F + \left(6.77\times10^{-6}\right)}\right) - 0.0076 \tag{5.18}$$

$$\left(\overline{M}_{\min}\right)_{FSC-CSA} = \left(4.83\sqrt{F + 0.00017}\right) - 0.063 \tag{5.19}$$

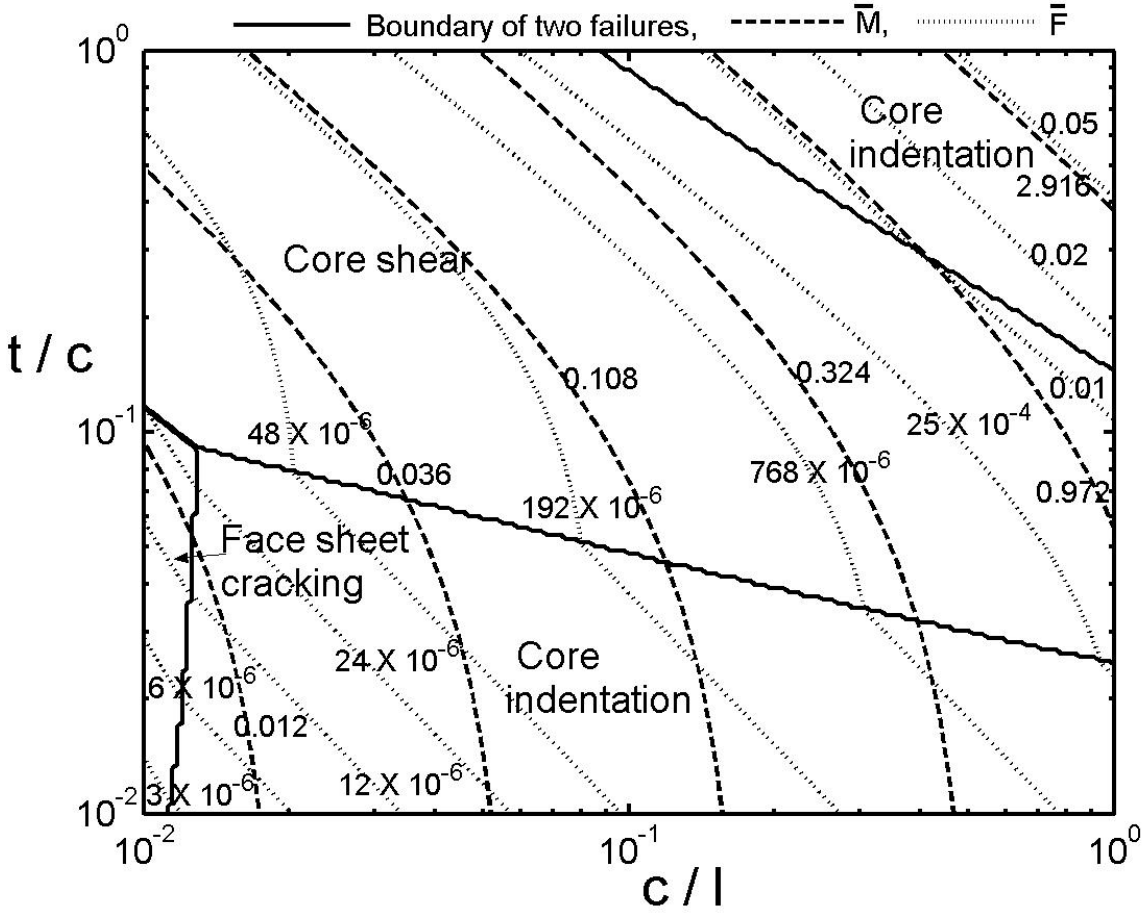

Figure 5. 13 Contours of the dimensionless mass index $\overline{M}$ and structural load index $\overline{F}$ in collapse mechanism map of sandwich beam of Alporas foam core with CFRP face sheet having $\overline{\sigma} = 0.0018$ and $\overline{\rho}$=0.208.

However, these solutions have certain limit of validation depending on the values of $\overline{c}$ and $\overline{t}$ (positive values of $\overline{c}$ make the existence of this $\overline{M}_{\min}$ solution). For example, $\overline{M}_{\min}$ solutions for core shear start in existence for higher value of $\overline{F}$ ($\overline{F} \geq 1.789\times10^{-4}$). The minimum weight design is found by calculating the minimum mass index $\overline{M}_{\min}$ necessary to

ATTENTION: The Singapore Copyright Act applies to the use of this document. Nanyang Technological University Library

suppress all possible failures for a given structural load index $\overline{F}$. So, the dominant mechanism is the one with the largest value of $\overline{M}_{\min}$ at each value of $\overline{F}$. To obtain a clear picture of the minimum weight design, the largest $\overline{M}_{\min}$ for each value of $\overline{F}$ is plotted for each failure mode and combination of modes, which is shown in Figure 5.14 (a).

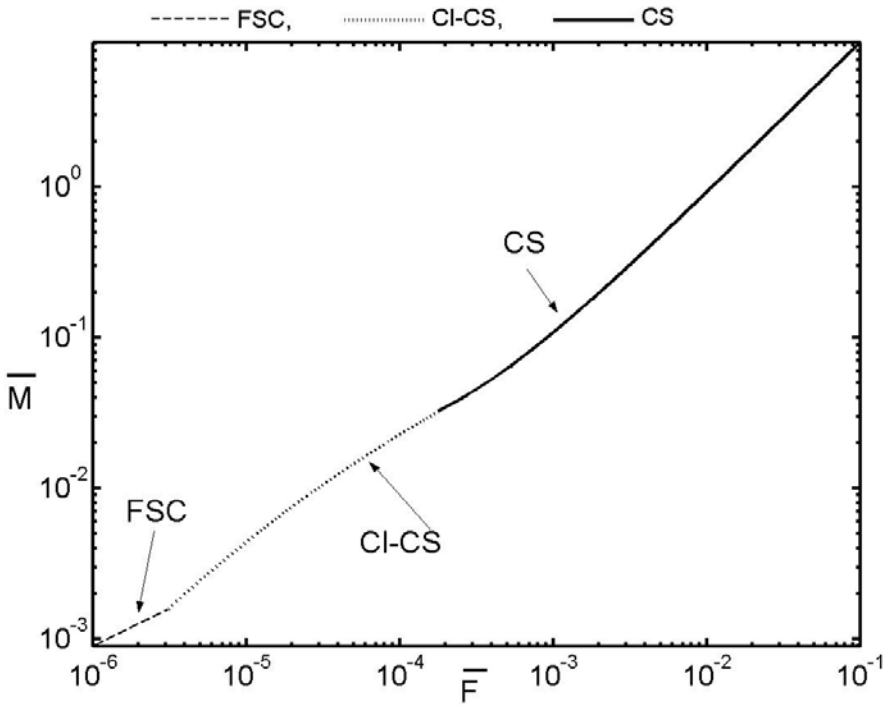

(a)

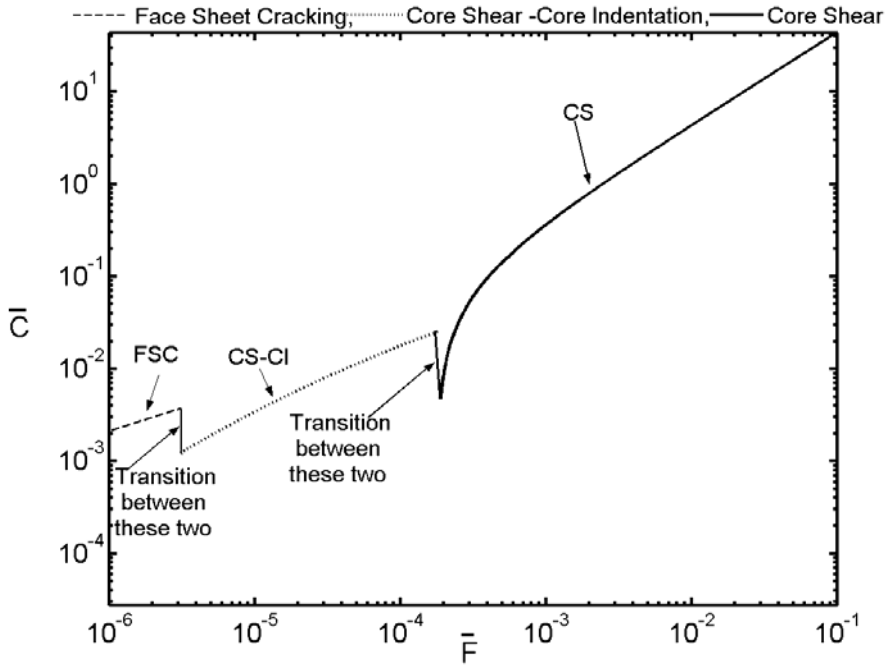

(b)

ATTENTION: The Singapore Copyright Act applies to the use of this document. Nanyang Technological University Library

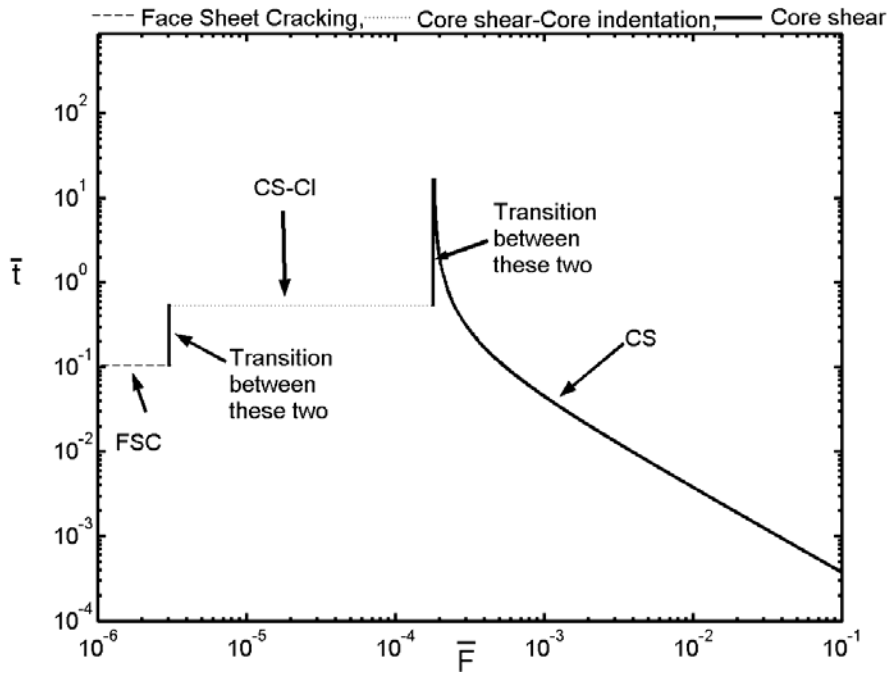

(c)

Figure 5. 14 Minimum weight design of sandwich beam with Alporas foam core and CFRP face sheet with optimum geometrical parameters having $\bar{\sigma} = 0.002$ and $\bar{\rho}$=0.208 (a) Variation of minimum mass index $\bar{M}$ with structural load index $\bar{F}$ considering for all failure modes (b) Variation of $\bar{c}$ with structural load index $\bar{F}$ for minimum weight design of sandwich beam (c) Variation of $\bar{t}$ with structural load index $\bar{F}$ for minimum weight design of sandwich beam.

This minimum weight design map is valid only for $\bar{\sigma} = 0.0018$ and $\bar{\rho}$=0.208. It was observed from Figure 5.14 (a) that the minimum mass design is achieved within the domain of face sheet cracking for lower values of $\bar{F}$ and with in core shear domain for higher values of $\bar{F}$. For intermediate values of $\bar{F}$, the minimum weight design is achieved at boundary between the core indentation and core shear with constant values of $\bar{\sigma} = 0.002$ and $\bar{\rho}$=0.208. The trend of the minimum weight design was found to be in an increasing order with structural load index.

If these constant parameters are changed then the values of the map will be changed, but the trend would remain the same. The associated optimum geometrical parameters ($\bar{c}$ and $\bar{t}$) are also plotted with structural load index as shown in Figure 5.14 (b) and (c). There is no general trend found for it but it depends upon the failure mechanism regime in which it falls. Trend of $\bar{c}$ was found to increase with the structural load index with in the same failure

ATTENTION: The Singapore Copyright Act applies to the use of this document. Nanyang Technological University Library

regime. Trend of $\bar{t}$ was found to be constant with structural load index depending up on the failure regime with few discrepancies which arises due denominator term of $\overline{F}$ in optimum $\bar{t}$ expression for core shear failure mode.

ATTENTION: The Singapore Copyright Act applies to the use of this document. Nanyang Technological University Library

Chapter-6

Indentation response of Al foams with different face sheets

6.1 Introduction

Sandwich panels comprising metallic foam, especially Al foam cores are very efficient in terms of their performance with low weight under various loading conditions such as bending and compression [9]. Most of the previous studies on sandwich structures comprising metal foam cores by various researchers focused on damage mechanisms and models for collapse mechanisms under various loading conditions [25, 68, 70, 71]. However, these structures are sensitive to damage, when subjected to localized loading like indentation due to the low strength of the core and low bending stiffness of the thin face sheets [72].

Sridhar and Fleck [81] have established various failure modes for simply supported circular sandwich plates consisting of metal foam as the core and aluminum face sheets loaded centrally by a flat punch. They found core indentation, core crushing, face sheet punching and face sheet bending as the competing failure modes and these operating failure mechanisms depends on the plate geometry, punch radius and material properties.

The performance of these sandwiches will be varied, if different face sheets such as aluminum, stainless steel, carbon fiber reinforced polymer (CFRP) matrix composite and alumina sheets are used. It will be interesting to know the performance and competing failure mechanisms under which these sandwiches can fail, when subject to indentation loading for example, in case of an accidental drop of heavy tools onto the panels.

Therefore, in the present work, indentation studies are carried out on Al alloy foams namely; Alporas and Cymat blocks bonded to face sheets of different constitutive response under indentation loading with flat and spherical punches. Face sheet materials representing elastic, elastic-perfectly plastic and elastic strain hardening plastic behavior are chosen. The scope of the experimental investigation is further limited due to a finite size of specimens.

Suppose a foam block of square cross-section of side, b, thickness, c, with upper face sheet thickness, t, is subjected to indentation loading with the indenter of diameter $2r$ and the block is resting on a rigid base as shown in Figure 6.1(a). When this metal foam block with face

ATTENTION: The Singapore Copyright Act applies to the use of this document. Nanyang Technological University Library

sheet is loaded by a flat punch at the center, it can fail in various failure modes namely core indentation, core crushing, face sheet punching and face sheet bending as illustrated in Figure 6.1(b) to (e). Under core indentation, the foam core directly beneath the indenter crushes and a plastic zone is also developed at same location and this zone also extends beyond the edges of the indenter, by some radius λ, bending the face sheet to accommodate the foam deformation. A schematic diagram for this type of failure is shown in Figure 6.1 (b). In core crushing failure, the foam core crushes uniaxially due to the movement of the face sheet beneath the indenter. A schematic diagram for this type of failure is shown in Figure 6.1 (c).

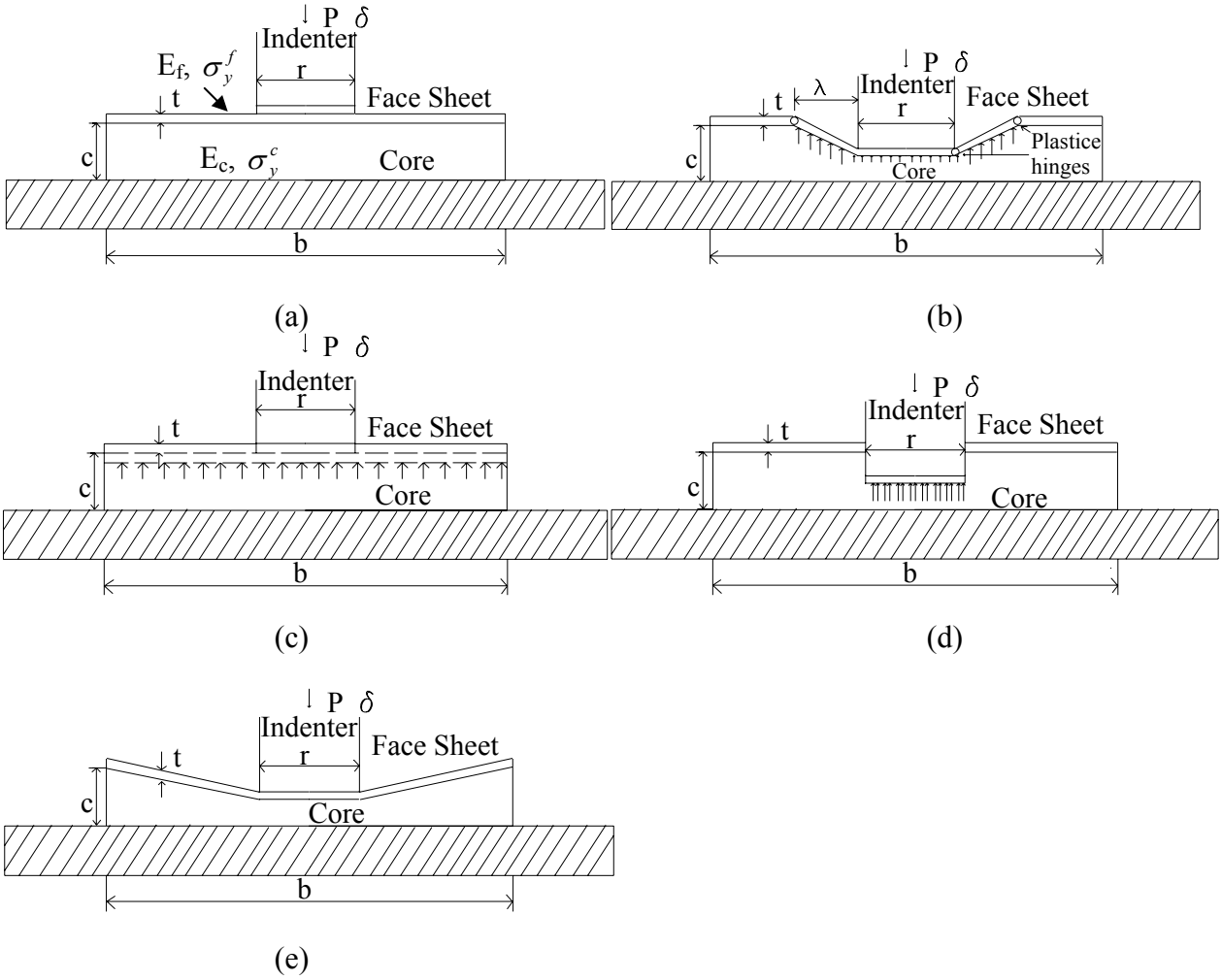

Figure6.1 Failure modes for sandwich beam under indentation loading (a) sandwich of metal foam core under indentation, (b) indentation failure mode, (c) core crushing failure mode, (d) face sheet punching, and (e) face sheet bending.

Under face sheet punching failure mode, the rigid indenter punches through the face sheet around the sharp circumferential edge of the indenter, while crushing the foam core beneath it. A schematic diagram for this type of failure is shown in Figure 6.1(d). In face sheet

ATTENTION: The Singapore Copyright Act applies to the use of this document. Nanyang Technological University Library

bending failure, the face sheet starts to bend when the indentation increases. A schematic diagram for this type of failure is shown in Figure 6.1(e).

6.2. Sandwich structure with Al foam with and without different face sheets under static indentation

6.2.1 Materials for foam core and face sheets

The materials involved in those blocks are Alporas and Cymat foam core and the face sheets are sheets made with Al 1100, Stainless steel (SS-314), Alumina and CFRP. Their mechanical properties with surface characterization are explained in Chapter 3. Materials involved in blocks with experimental protocol adopted for the indentation of foam blocks with and without face sheets is described in the following paragraphs**.** Important findings with different failure mechanism with damaged zones of foam core and face sheets are also explained.

6.2.2 Test specimen preparation and experimentation

In the present investigation, Alporas foam of side 70mm and 25mm thickness were bonded to four types of face sheets as mentioned above. Bonding process of these blocks is described in Chapter 4 using Redux 322 epoxy adhesive. The specimens are indented at the center using a flat punch of 25 mm diameter and also with a spherical punch of 25 mm diameter. Ratio of different sizes depending upon the cell size, indenter diameter, specimen dimension and indentation depth affect the load displacement response in indentation loading [9]. So precautions were taken in choosing these parameters in this study to overcome these size effects. It is to be noted that the ratio of indenter diameter (25mm) to cell size (3.0 mm) exceeds 8 and according to Olurin et al [68] and Andrews et al [25] no significant effects of cell size on indentation pressure will be noticed. The edge effect becomes negligible, if the gap between the two indentations in the same specimen is more than one indenter diameter and the distance from indentation to free edge is also more than or equal to one indenter [25, 76]. In the current study, the distance from free edge to indenter was kept around one indenter diameter (22.5mm), so that the edge effect would be negligible on the load-displacement response. According to Kumar et al [70], if the indentation depth exceeds half of the specimen thickness, then the indentation response is affected by the stiffness of the

ATTENTION: The Singapore Copyright Act applies to the use of this document. Nanyang Technological University Library

rigid support. In the present experiments, indentation depth was kept constant at 8mm which is one third of the specimen thickness (25mm).

All the indentation experiments were conducted under displacement control with a cross-head movement of 0.5 mm/min and up to 8.0 mm indentation depth. Indented specimens were sectioned by electron discharge machining (EDM) for observing the damage zone using Surface Displacement Analyser (SDA). However, due to the non-conduciveness of the adhesive, EDM failed to machine the specimen at the sites under which the foam was crushed and adhesive was present. So these sites were cut later by bench saw at low speed (around 0.5 mm/min.).

6.2.3 Results and discussion

Face sheet bending, face sheet cracking, core indentation, interfacial adhesive failure between the core and face sheet were recognized as active failure mechanisms for aluminum foam (Alporas) blocks with different face sheets under spherical and flat indenters. The behavior of these blocks is discussed in detail along with the analysis of the damage zone.

6.2.3.1 Indentation response with flat indenter

The load – displacement response of Alporas foam with and without various face sheets of 0.5 mm thickness under a flat indenter is shown in Figure 6.2 (a) and 6.2(b) for elastic plastic face sheets and for elastic face sheets respectively. Here, initial peak load was observed for Alporas foam without any face sheet followed by a long plateau. . This curve is similar to that of Alporas foam's response under uniaxial compressive loading as shown in Chapter 3.

The first peak load represents the start of foam cells collapsing beneath the indenter and tearing of the cells at the periphery of the indenter. Similar observations were reported by Olurin et al [68] and Kumar et al [70]. Up to this peak, indentation was very low but the resistance from the foam was high which is due to combination of collapsing and tearing. The indentation failure load can be represented in terms of punch radius r and uniaxial compressive strength of the foam σ_c^y as $\pi\left(r^2\sigma_y^c + 2r\Pi\right)$, where Π is the tearing energy of the foam [68]. The computed indentation peak load (considering these two failure mechanisms)

ATTENTION: The Singapore Copyright Act applies to the use of this document. Nanyang Technological University Library

of 1.65 kN with tearing energy of 9.0 N/mm for 9.5% relative density Alporas foam agrees well with the present experimental measurements.

Load initially increases linearly with the extent of indentation in the case of Alporas foam block with elastic-perfectly plastic aluminum face sheets and the slope is representation of the structure's stiffness. After the initial failure, at which the face sheet starts yielding, the load remains constant with indentation.

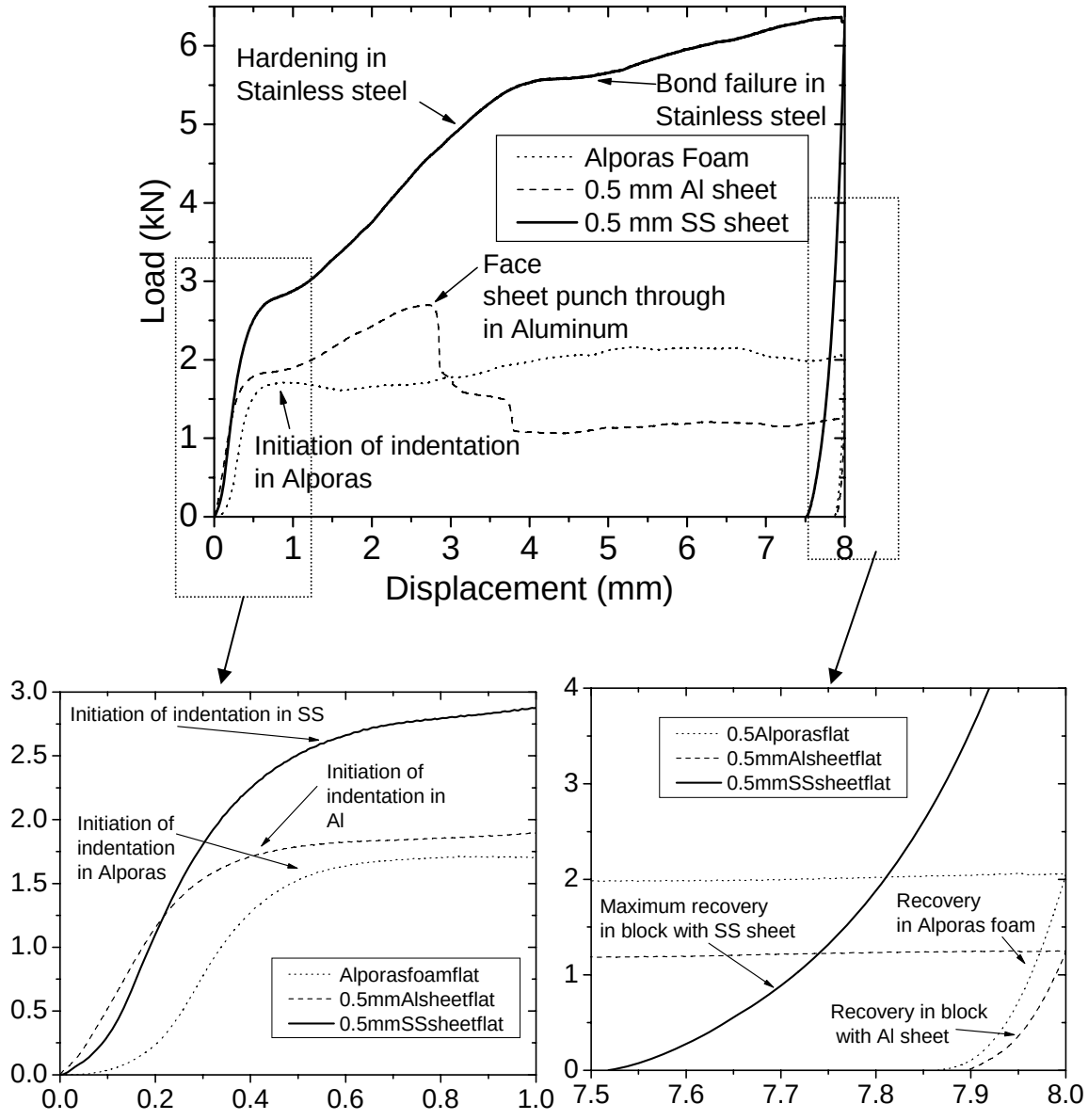

(a)

ATTENTION: The Singapore Copyright Act applies to the use of this document. Nanyang Technological University Library

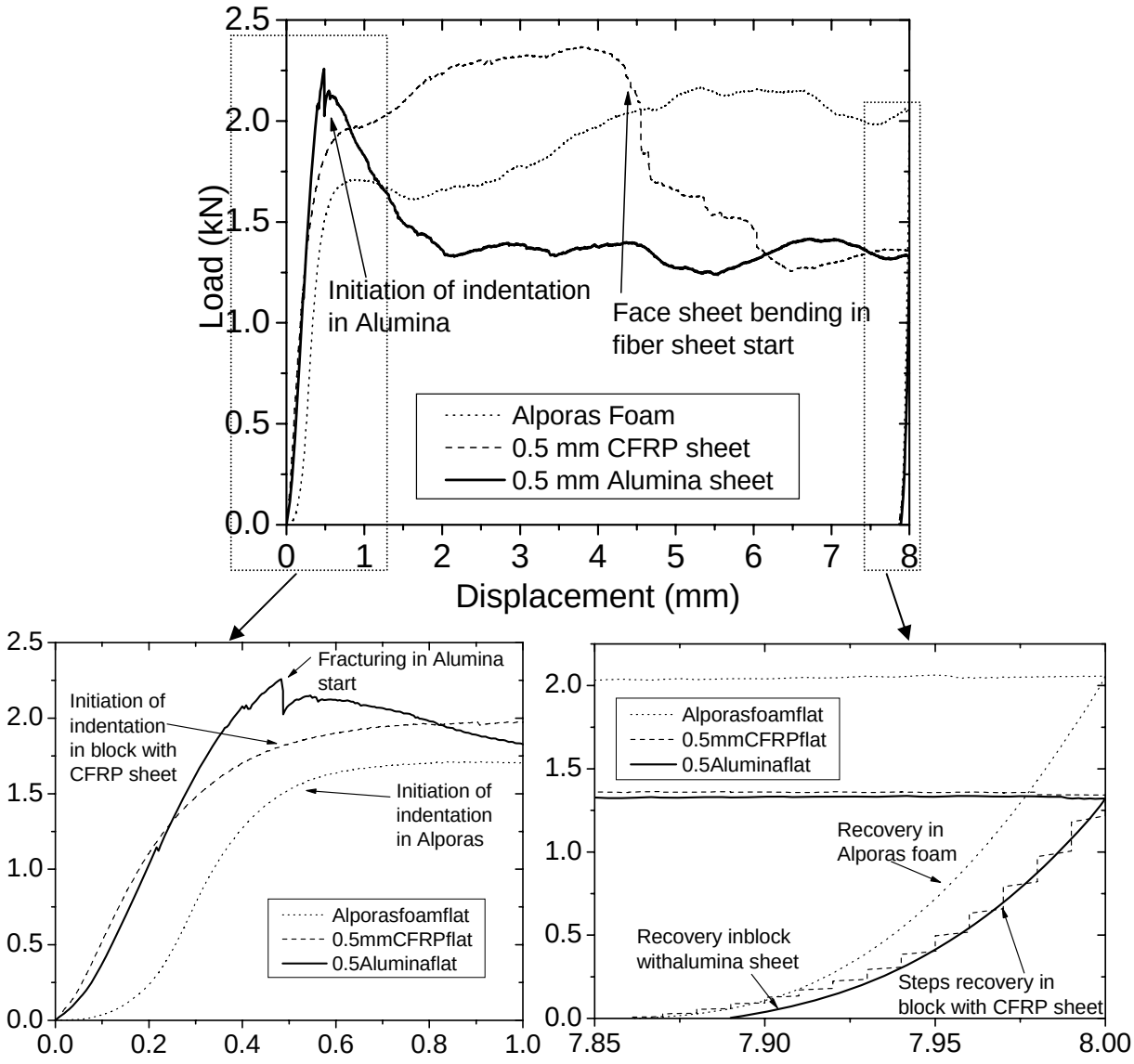

(b)

Figure6.2 Comparison of experimental indentation behavior of Alporas foam with different face sheets with thickness of 0.5 mm under flat indenter (a) blocks with foam and elastic plastic face sheets (b) blocks with foam and elastic face sheets.

With further loading, the face sheet bends as depicted in Figure 6.1e and there is a strong hardening response due to the stretching and bending of the face sheet. After reaching the peak load, the indenter punches through the face sheet and the core beneath it, leading to the sudden drop in the load due to reduction in the stiffness.

The load – displacement response of Alporas foam with and without various face sheets of 1.0 mm thickness under a flat indenter is shown in Figure 6.3 (a) and (b) for elastic plastic

ATTENTION: The Singapore Copyright Act applies to the use of this document. Nanyang Technological University Library

face sheets and elastic face sheets, respectively. In general, the response of blocks with 1mm thick face sheet was found to be similar, with the blocks having 0.5 mm thick face sheets. The difference is that the magnitude of the load required for the same indentation depth in blocks with 1 mm thick face sheet is higher than in blocks with 0.5 mm thickness. For the block with both types of Al sheets, the failure mode is face sheet bending rather than localized core indentation. In the case of stainless steel face sheets, initial failure is triggered by the face sheet bending and there is a strong hardening behavior due to the membrane stretching and bending effect. With further indentation, the bond between the face sheet and core failed by detachment of the SS face sheet from the adhesive.

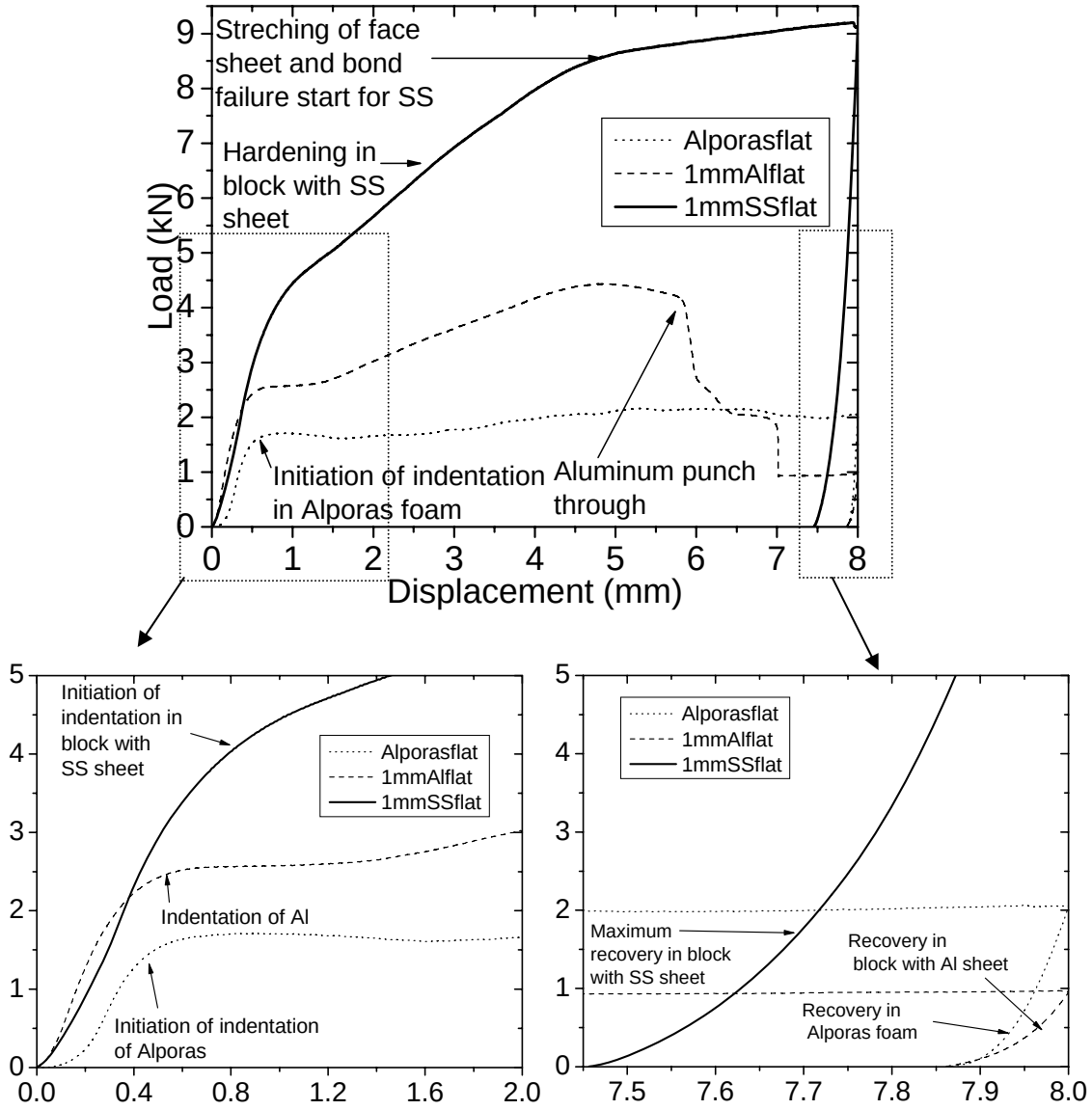

(a)

ATTENTION: The Singapore Copyright Act applies to the use of this document. Nanyang Technological University Library

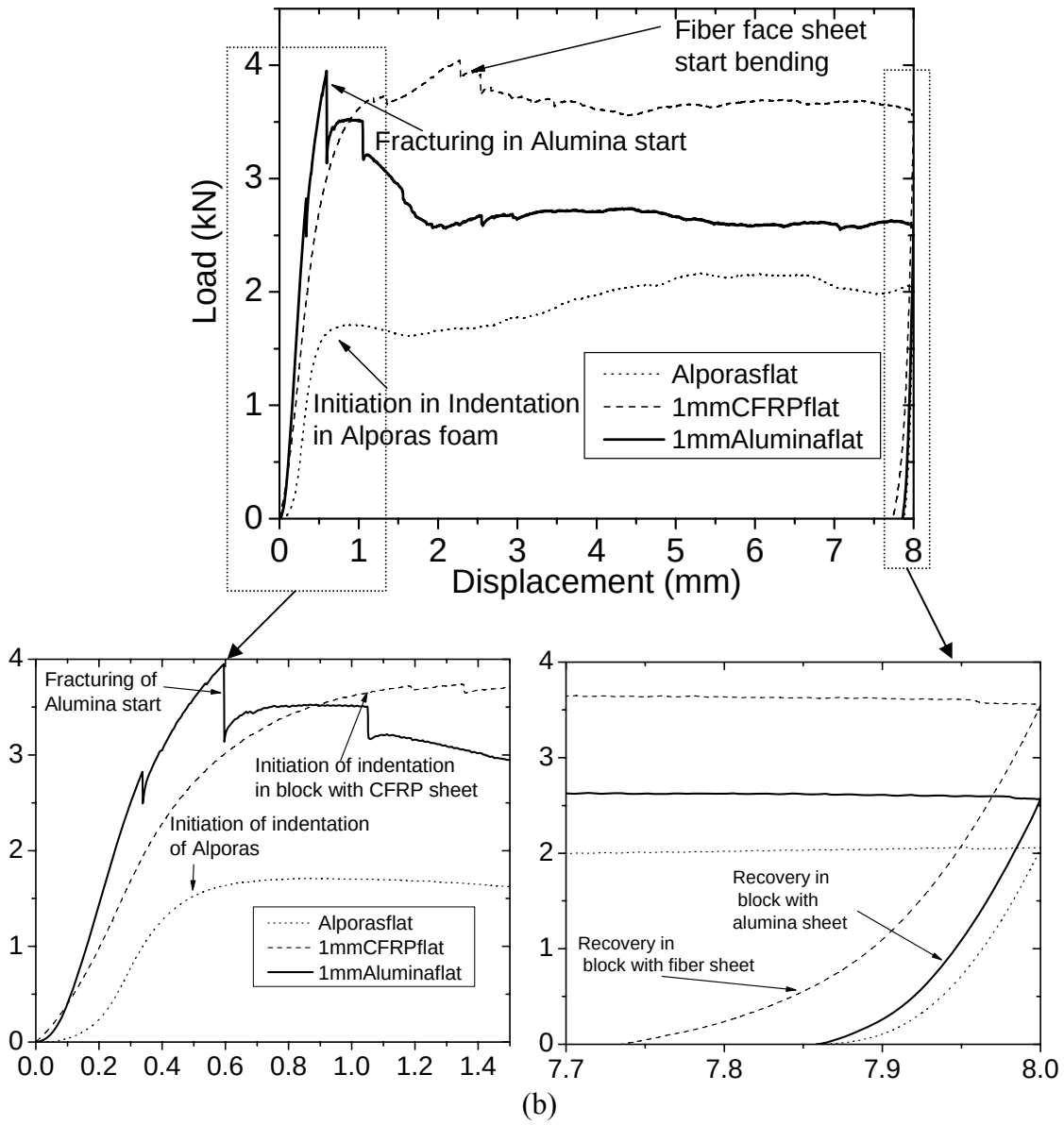

Figure6.3 Comparison of experimental indentation behavior of Alporas foam with different face sheets with thickness of 1mm under flat indenter (a) blocks with foam and elastic plastic face sheets (b) blocks with foam and elastic face sheets.

This failure was initiated at the outer corners of the block and hardening rate was reduced. Face sheet punch through was not observed for the tested geometries. In general, the response of specimens with 1 mm thick face sheet was found similar to the specimens with 0.5 mm thick face sheets. However, the amount of load required for the same indentation depth in blocks with 1 mm thick face sheet is higher than in blocks with 0.5 mm thickness because of higher membrane resistance. Moreover, material strain hardening effect was found to be more pronounced in 1mm thick sheet compare to 0.5 mm thick specimen (see

ATTENTION: The Singapore Copyright Act applies to the use of this document. Nanyang Technological University Library

Chapter 3). Elastic recovery was observed to be the maximum for the specimen with 0.5 mm thick face sheet as 0.5mm, while specimen with 1.0mm face sheet it was 0.55mm.

The indentation response of the specimen blocks with alumina face sheet shows linear elastic behavior up to the peak load and then cracking of alumina would occur around the circumference of the punch due to high stress concentration. This behavior shows that the load for indentation includes the resistance from the foam to collapse beneath the indenter and the load required to fracture alumina along punch circumference. The specimen block with 0.5 mm thick alumina was punched through at the onset of failure and continued with the crushing of the foam beneath the indenter. In the case of specimen blocks with 1.0 mm thick alumina face sheet, cracking occurred gradually and the punch-through happened in the later stages of indentation.

Face sheet bending was observed to be the failure initiation mechanism for specimen blocks with CFRP face sheet. At the beginning of the test, the load increased linearly with indentation and after the initiation of failure due to face sheet bending, the load-displacement response deviates from non-linearity. Face sheet bending was found to be the initial failure mechanism in these blocks due to the appearance of bending curvature in the fiber direction within the zone of the punch diameter. Punching of face sheet also occurred in latter stages of displacement in these blocks as shown by a sudden drop in load during load-displacement response, indicating it as additional failure mechanism.

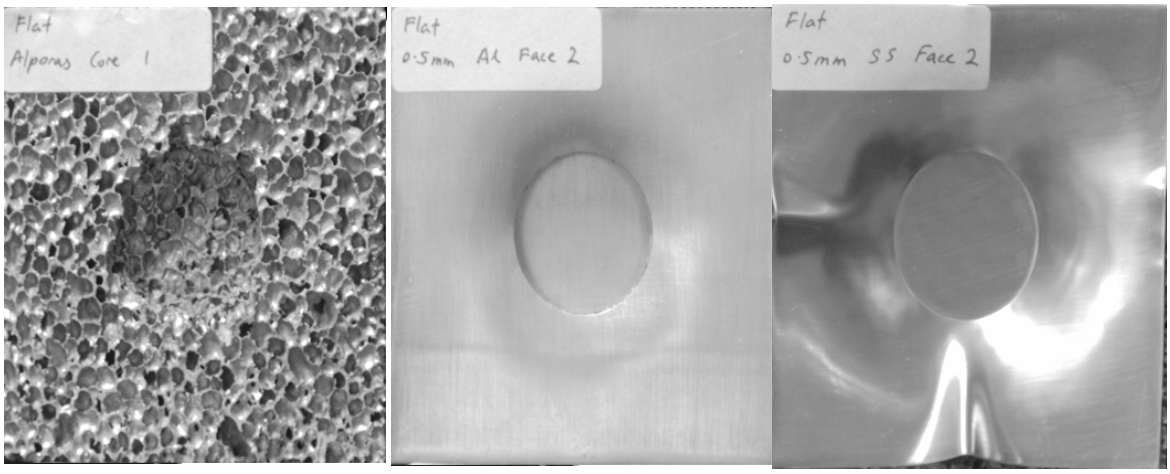

(a) (b) (c)

ATTENTION: The Singapore Copyright Act applies to the use of this document. Nanyang Technological University Library

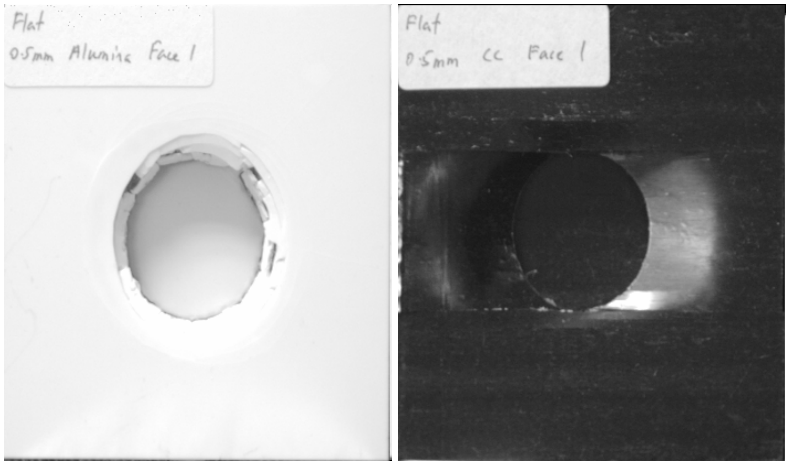

(d) (e)

Figure6.4 Top view of the indented specimens with 0.5 mm thick face sheet under flat indenter (a) Alporas alone, (b) Al face sheet, (c) SS face sheet, (d) Alumina face sheet, and (e) CFRP face sheet.

Clear punch-through was noticed in the face sheets with 0.5 mm thick carbon fiber reinforced plastic laminates, whereas in 1.0 mm thick face sheets only bending of the face sheets occurred. These results correlate the findings of Soden who observed similar behavior of sandwich beams with PVC foam core and GFRP face sheets [76]. Upon unloading, maximum elastic recovery was noticed in the foam blocks with SS face sheets and minimum with alumina face sheets.

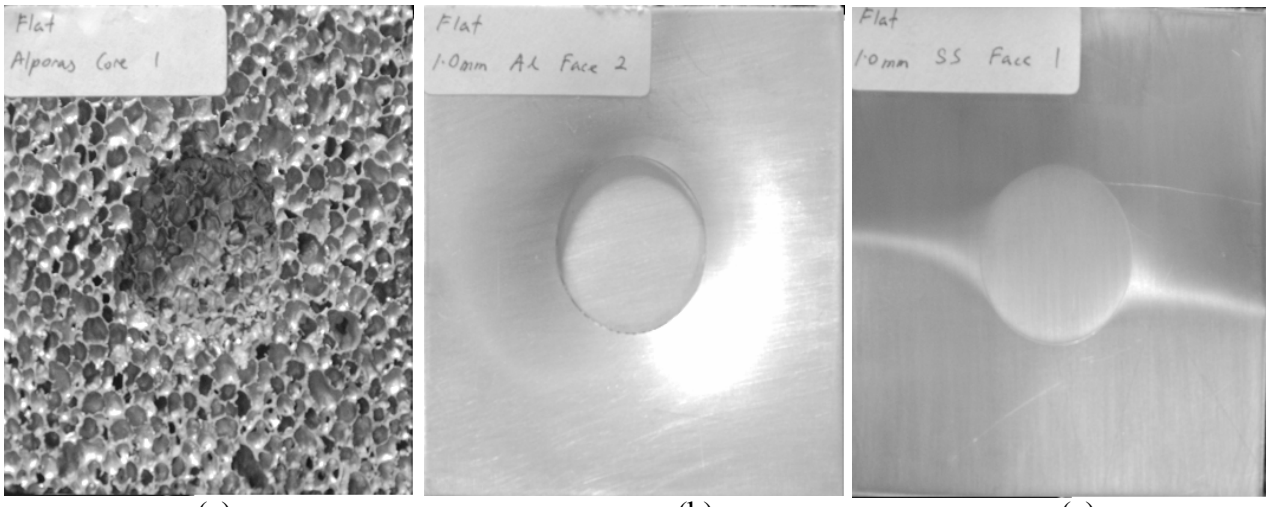

(a) (b) (c)

ATTENTION: The Singapore Copyright Act applies to the use of this document. Nanyang Technological University Library

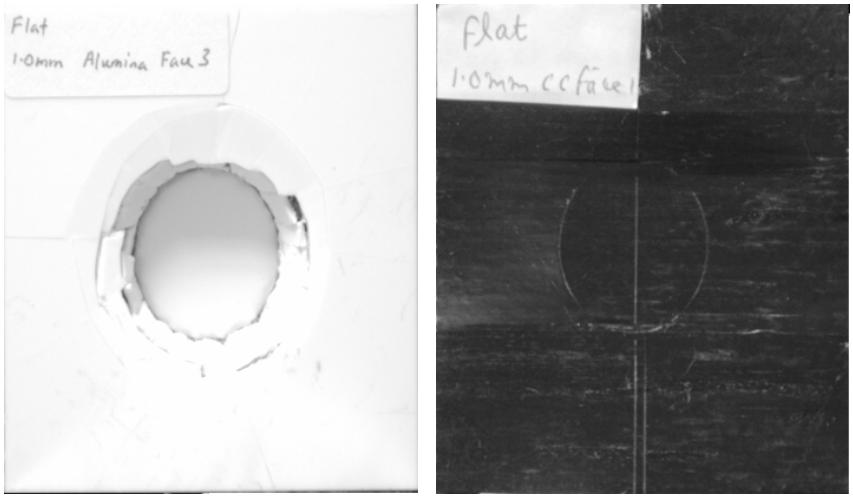

(d) (e)

Figure6.5 Top view of the indented specimens with 1.0 mm thick face sheet under flat indenter (a) Alporas alone, (b) Al face sheet, (c) SS face sheet, (d) Alumina face sheet , and (e) CFRP face sheet.

The top view of the indented blocks with different face sheets of thickness of 0.5 mm and 1.0 mm, under flat indenter are shown in Figure 6.4 and 6.5 respectively. For the considered test geometries the failure mechanism varied from foam indentation to face sheet bending or face sheet crushing depending upon the face sheet type. The amount of core damage is more severe for blocks with 0.5 mm thick face sheet compare to 1.0 mm thick specimens. Debonding is found to be more in specimens with 0.5mm thick SS face sheet (Figure 6.4 (c)), than specimens with 1.0mm sheet (Figure 6.5 (c)). Similarly, bending of face sheet is also more evident in specimens with 0.5 mm thick CFRP sheet as shown in Figure 6.4 (e) than specimens with 1.0 mm thickness (Figure 6.5 (e)).

6.2.3.2. Indentation response with spherical indenter

The load – displacement response of Alporas foam with and without various face sheets of 0.5 mm thickness under a spherical indenter is shown in Figure 6.6 (a) and (b) for elastic-plastic face sheets and for elastic face sheets respectively. Here, the load increases continuously with indentation, without any initial failure in foam block and without any face sheet under indentation. The reason for this hardening behavior is due to the gradual increase in contact area between the indenter and test block, which is representation of geometric hardening. In fact, the indentation depth has not reached the full radius of the indenter (as in

ATTENTION: The Singapore Copyright Act applies to the use of this document. Nanyang Technological University Library

the study by Kumar et al. [70]) and therefore, different behavior was observed by Kumar et al [70] in the latter stages.

The load increases linearly with indentation depth initially in response to the stiffness of the structure with foam core and metallic face sheets. But the initial elastic response is very shallow. The failure mode in this case is due to local indentation beneath the spherical punch. The face sheet material has to stretch to accommodate to the punch profile. The hardening is due to both the bending and stretching of the face sheet.

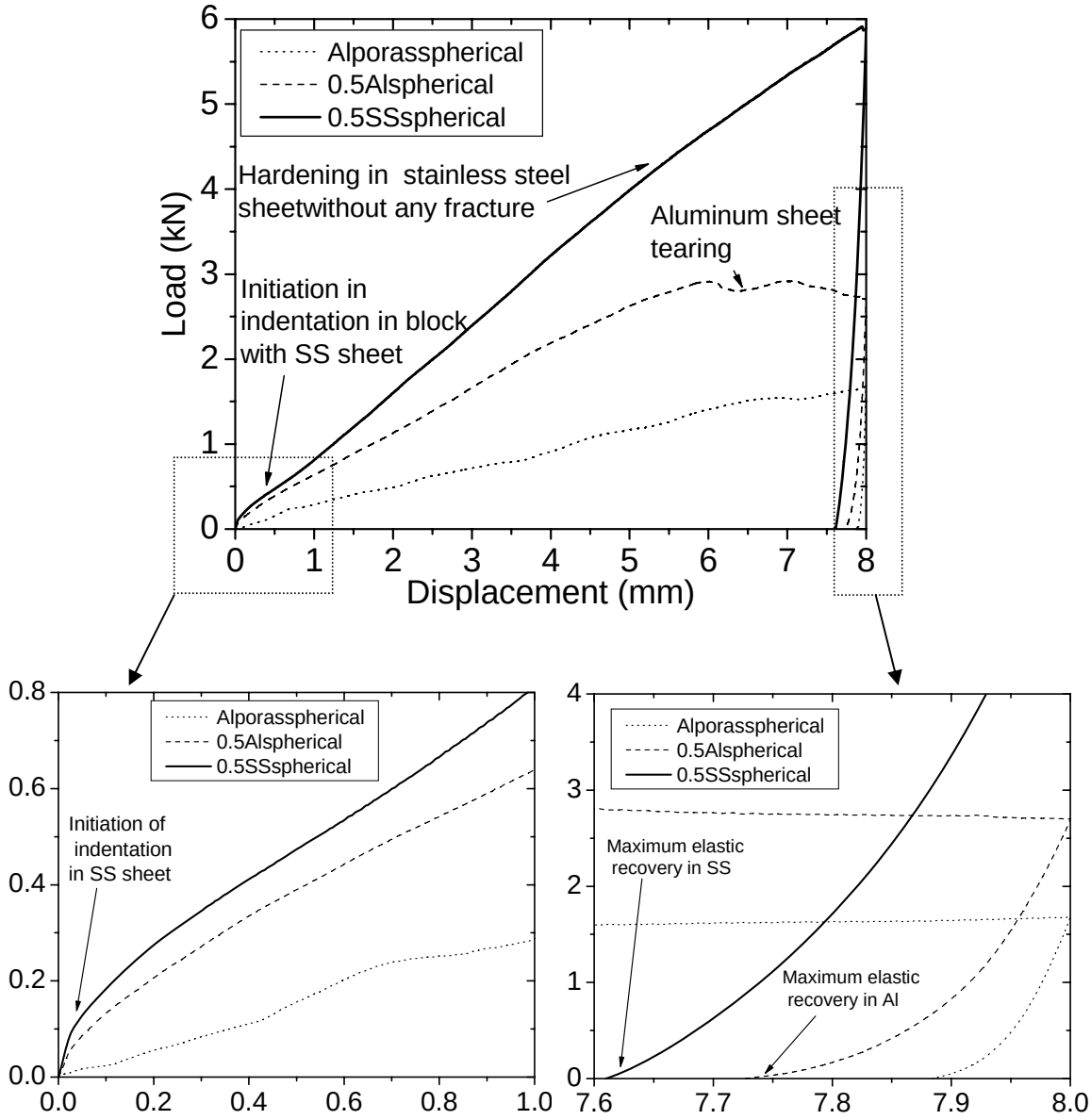

(a)

ATTENTION: The Singapore Copyright Act applies to the use of this document. Nanyang Technological University Library

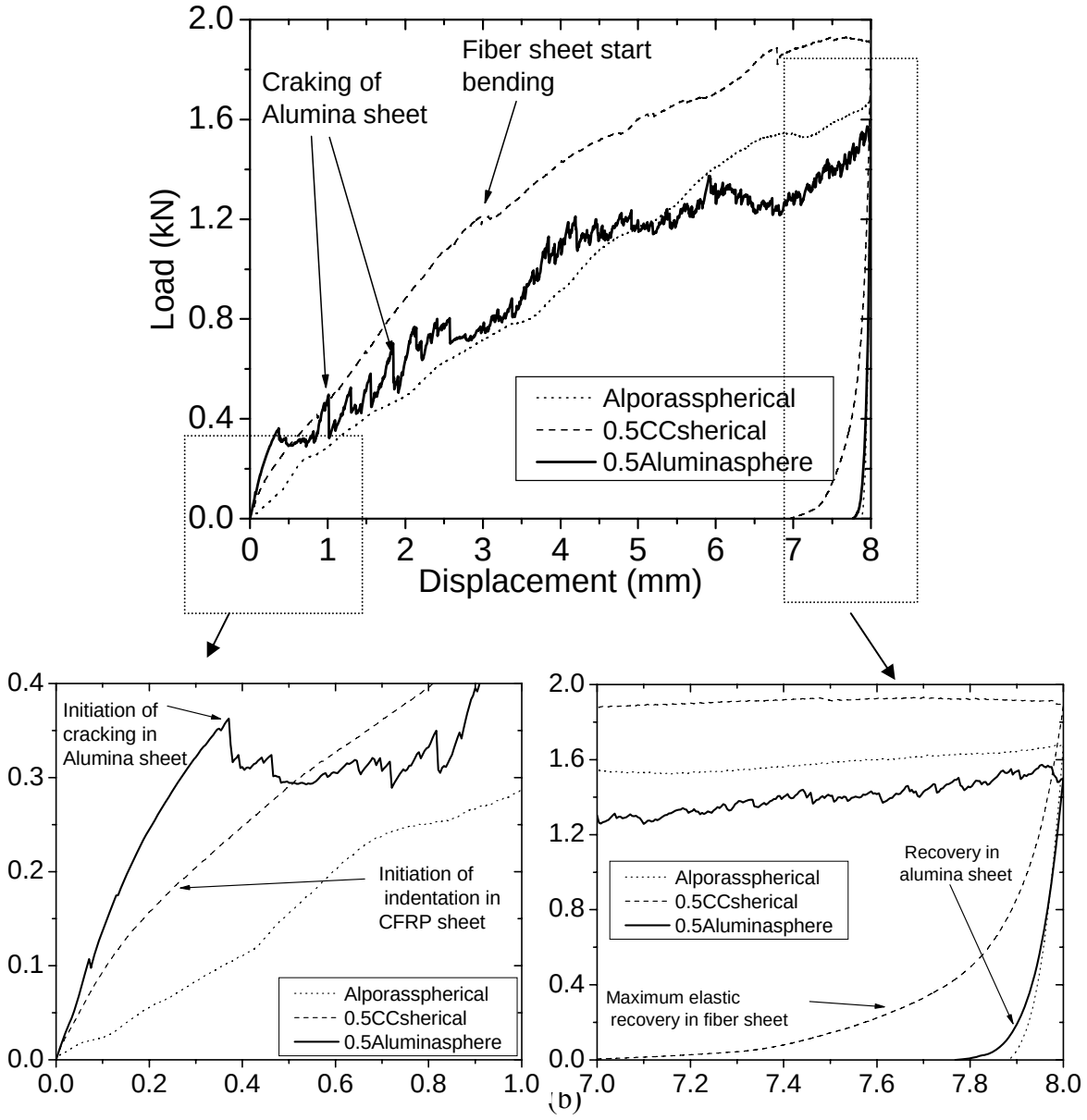

Figure6.6 Comparison of experimental indentation behavior of Alporas foam with different face sheets with thickness of 0.5mm under spherical indenter (a) blocks with foam and elastic plastic face sheets (b) blocks with foam and elastic face sheets.

Tearing of the face sheet was found in blocks with 0.5 mm Al sheet at around 6-7 mm indentation depth. The load–displacement response of Alporas foam with and without various face sheets of 1.0 mm thickness under a spherical indenter is shown in Figure 6.7 (a) and (b) for elastic plastic face sheets and elastic face sheets respectively. In general, the response of these blocks was found to be similar with the blocks with 0.5 mm thick face sheets. However, the amount of load required for the same indentation depth in blocks with 1 mm thick face sheet is higher than in blocks with 0.5 mm thickness.

ATTENTION: The Singapore Copyright Act applies to the use of this document. Nanyang Technological University Library

The rate of hardening increases with increase of thickness of the face sheet in blocks with Al and SS sheets, which is due to higher strength of the sheet with more thickness. Rate of hardening also increases with strain-hardening exponent which is observed from a comparison between blocks with Al and SS sheet of the same thickness. No visible tearing of the face sheets was observed beneath the punch for all the specimens with metallic sheets, except in the case the of Al face sheets with 0.5 mm thickness.

The indentation response of the foam block with alumina face sheets shows localized cracking of alumina at the periphery of contact, due to the generation of high tensile stresses which is a clear localized indentation failure.

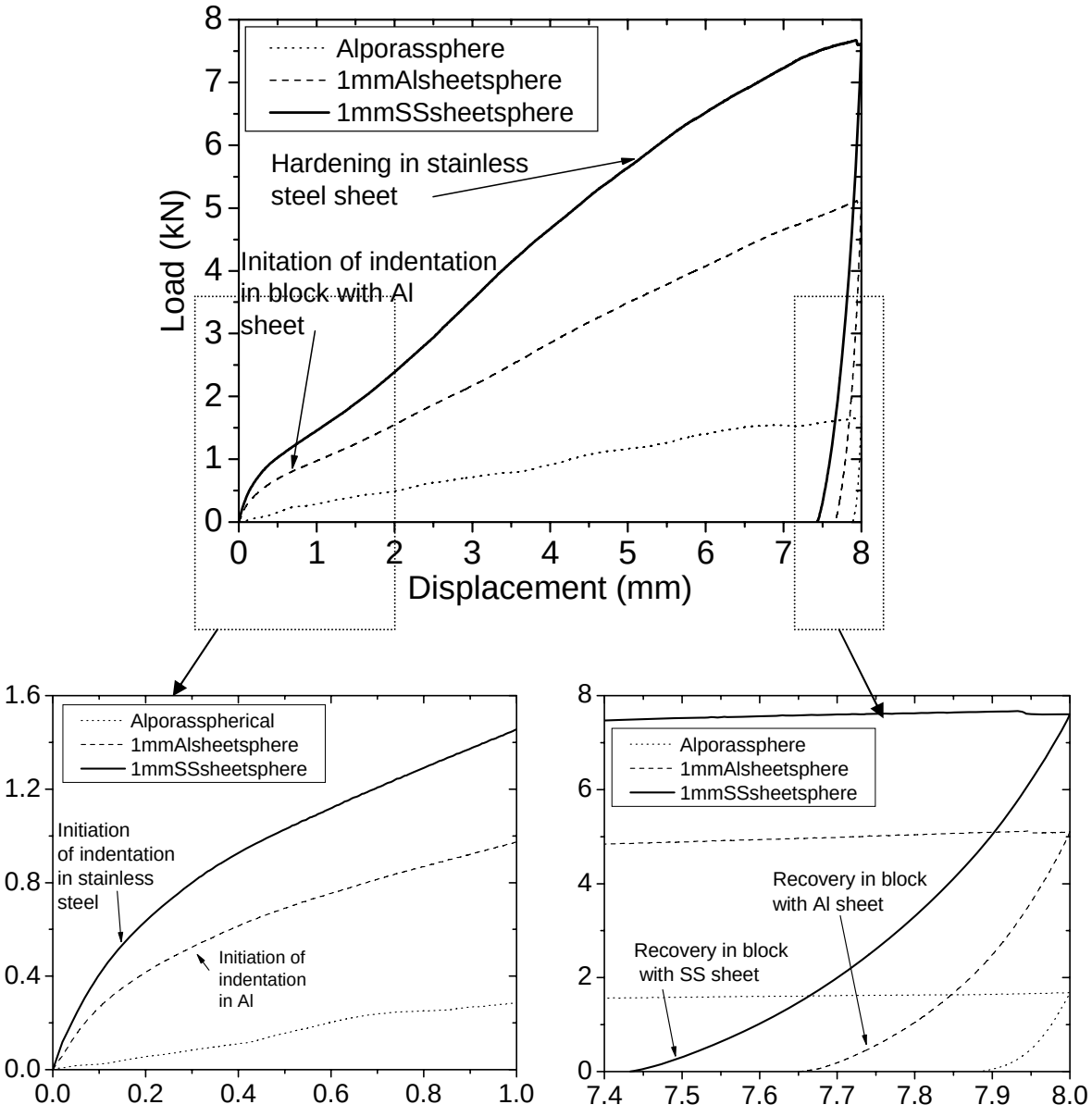

(a)

ATTENTION: The Singapore Copyright Act applies to the use of this document. Nanyang Technological University Library

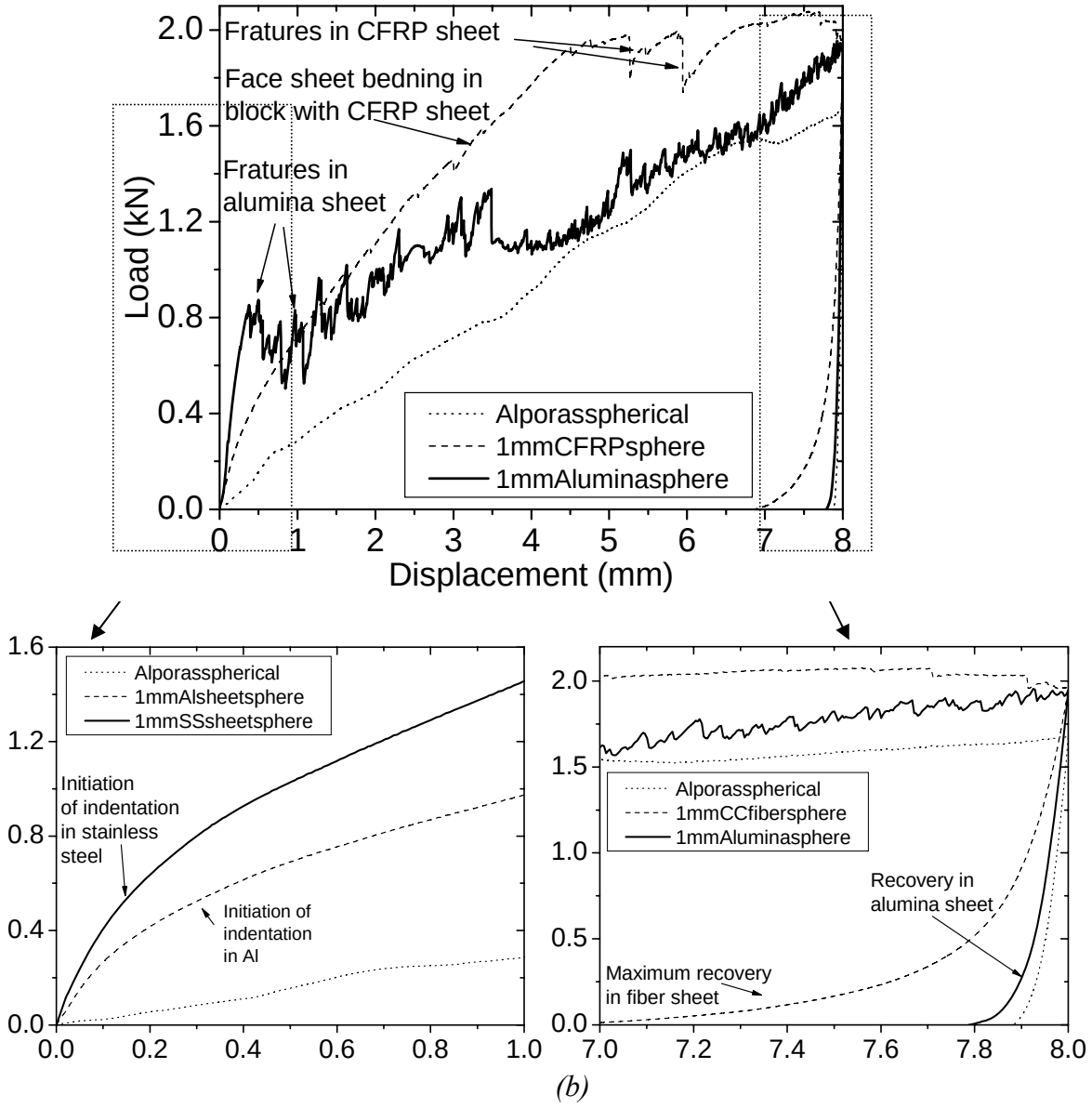

Figure6.7 Comparison of experimental indentation behavior of Alporas foam with different face sheets with thickness of 1.0 mm under spherical indenter (a) blocks with foam and elastic plastic face sheets (b) blocks with foam and elastic face sheets.

When compressive stresses are applied on these blocks during indentation loading, then resistive shear forces are applied by the foam core at the periphery of the indenter and because of which tensile stresses are generated in the face sheets at the periphery of alumina sheet. The crushing of alumina was due to very high shear stresses at the edge of the indenter.

The resistance to indentation was found to be more (almost double) in the specimen with thicker alumina which is due to higher compression strength of the thicker sheet. At larger

ATTENTION: The Singapore Copyright Act applies to the use of this document. Nanyang Technological University Library

indentation depths, much difference was not found between the responses of the stand-alone foam and that of the foam with Al_20_3 face sheet.

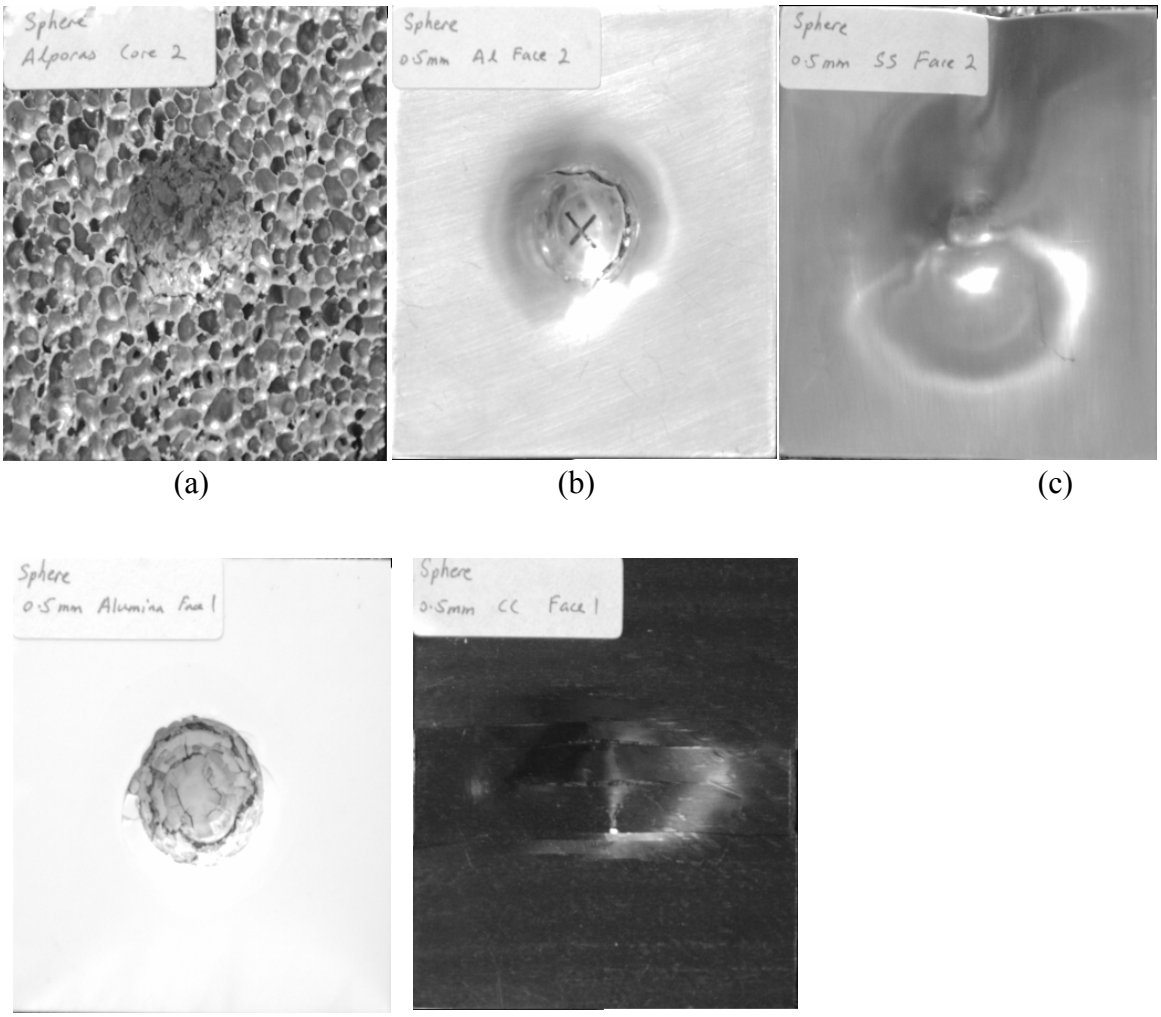

Figure6.8 Top view of the indented specimens having 0.5 mm thick face sheet under spherical indenter (a) Alporas alone, (b) Al face sheet, (c) SS face sheet, (d) Alumina face sheet, and (e) CFRP face sheet.

Few cracks transverse to the fiber direction were found in the face sheet during indentation of the sample block with carbon fiber reinforced plastic (CFRP) face sheet. The occurrence of these cracks is due to the low transverse strength of these laminates as compared to the longitudinal strength. Face sheet bending was observed to be dominant failure mechanism for this type of sample block. In addition, maximum elastic displacement recovery is observed after indentation among all the specimens due to high elastic stiffness of CFRP: displacement

ATTENTION: The Singapore Copyright Act applies to the use of this document. Nanyang Technological University Library

recovery of around 1 mm was found in the sample block with 1.0 mm thick face sheet. The recovery for 0.5 mm thick face sheet block was found to be less.

The top view of the indented blocks with different face sheets of thicknesses of 0.5 mm and 1.0 mm, under spherical indenter are shown in Figure 6.8 and 6.9 respectively. For the considered test geometries the final failure mechanism varied from foam indentation to face sheet bending or face sheet cracking depending upon the face sheet type.

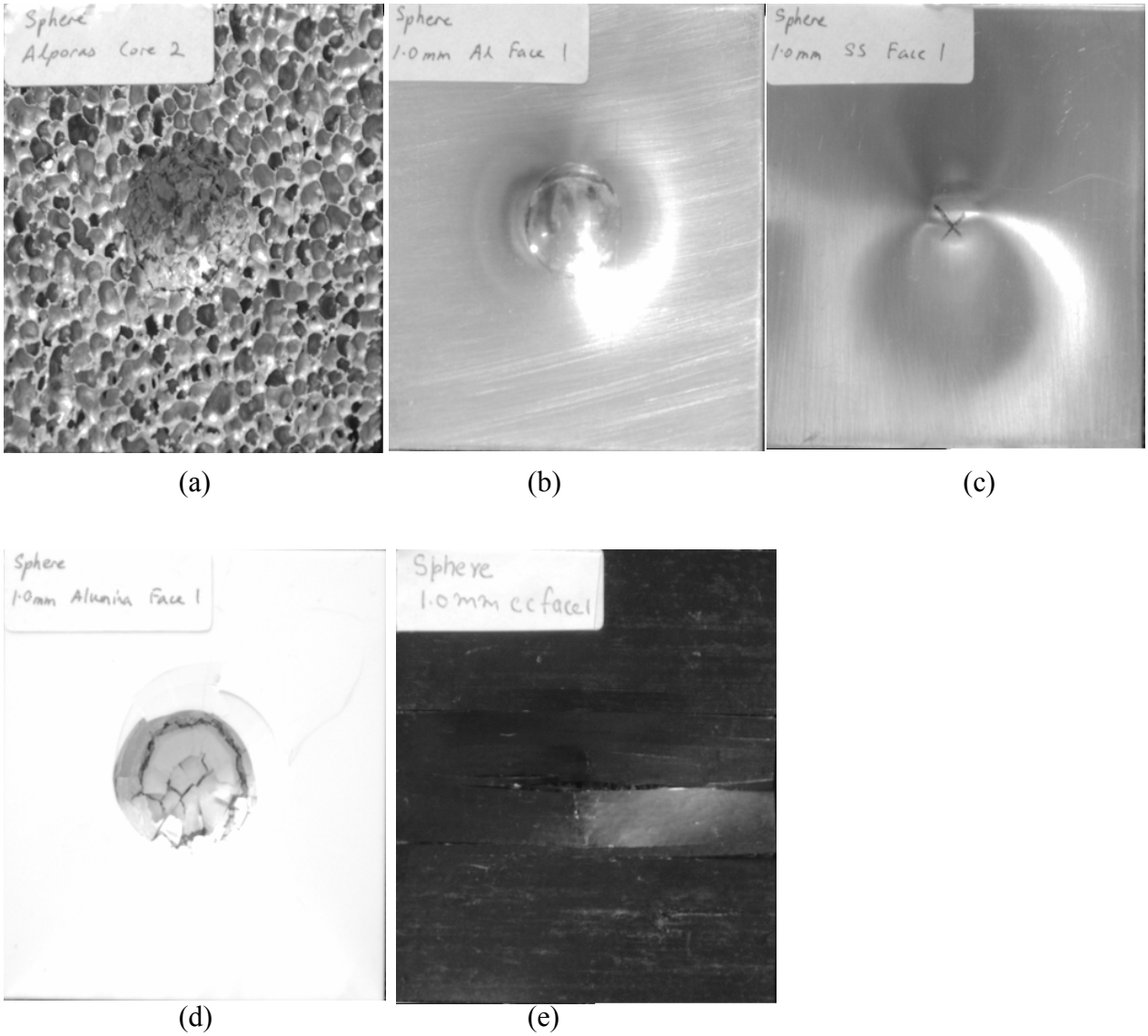

Figure6.9 Top view of the indented specimens having 1.0 mm thick face sheet under spherical indenter (a) Alporas alone, (b) Al face sheet, (c) SS face sheet, (d) Alumina face sheet, and (e) CFRP face sheet.

ATTENTION: The Singapore Copyright Act applies to the use of this document. Nanyang Technological University Library

However, localized core indentation along with face sheet failure seems to be the dominant failure mechanism. The amount of damage is found to be more in the blocks with 0.5 mm thick face sheet as compared to blocks with 1.0 mm thick sheet. Here, face sheet tearing is more visible in specimens with 0.5 mm thick Al sheet in Figure 6.8 (b) than specimen with 1.0 mm sheet as shown in Figure 6.9 (b). Similarly, the amount of debonding is clearly more substantial in specimen with 0.5mm thick SS face sheet in Figure 6.8 (c) than specimen with 1.0mm thickness as shown in Figure 6.9 (c).

However, if different size ratios (indenter diameter to cell size, distance between indentation to free edge with indenter size and indentation depth to thickness of specimen) would have chosen which do not satisfied the size rule then the load-displacement response would be different with different failure mechanisms compare to observed in the present study. For example, if the distance between indentation to free edge would be less than one indenter diameter then less resistance would have been applied by foam cells and there would be a downfall in the slope of load-displacement curve. Similarly, if the indentation depth would have been increased more than 13 mm then load and displacement response would be very steep in later stages of experiments for almost all the blocks.

6.2.3.3 Morphological aspects of damaged zones

The cross-sectional views of the foam blocks after indentation with flat and spherical punches are shown in Figure 6.10 and 6.11 with a uniform magnification factor and are discussed briefly in the following section.

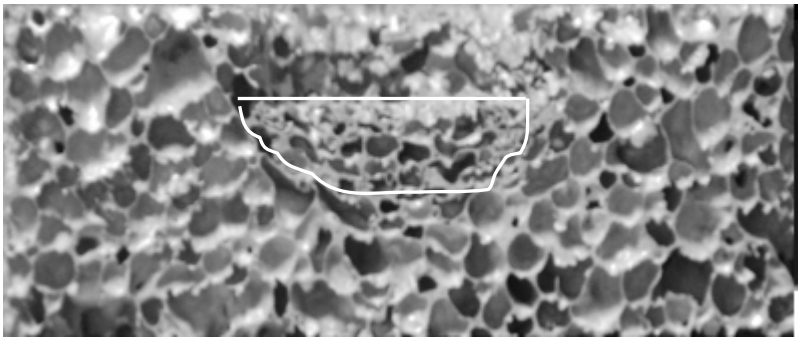

(a)

ATTENTION: The Singapore Copyright Act applies to the use of this document. Nanyang Technological University Library

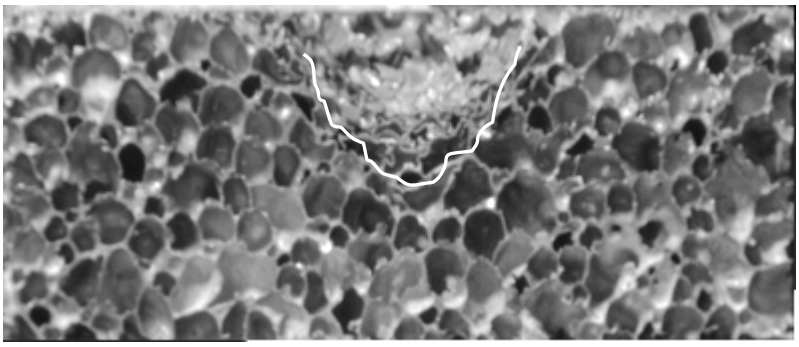

(b)

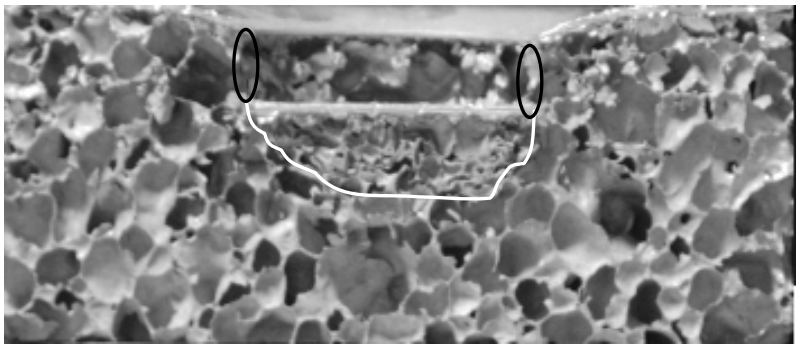

(c)

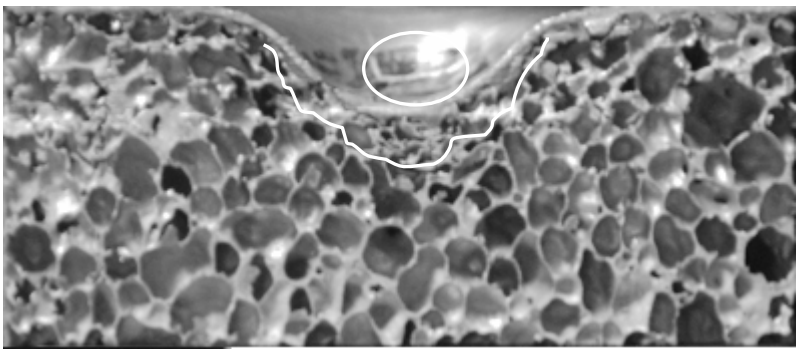

(d)

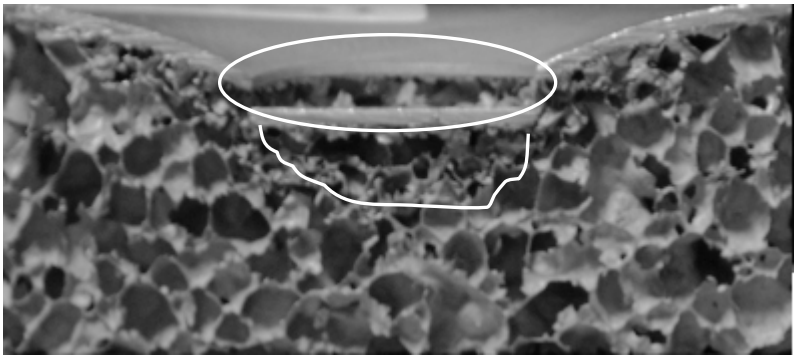

(e)

ATTENTION: The Singapore Copyright Act applies to the use of this document. Nanyang Technological University Library

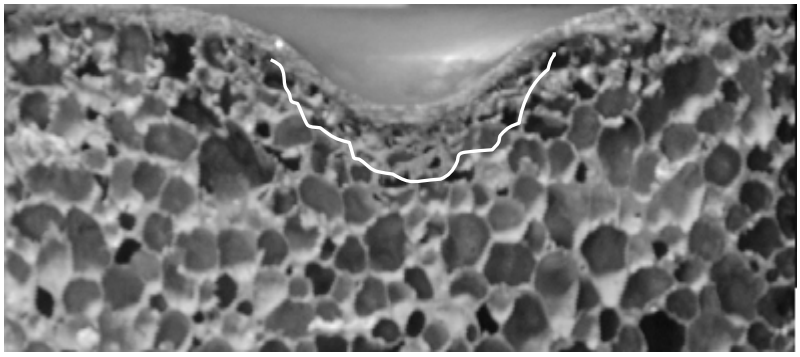

(f)

Figure6.10 Cross-sectional view of the indented foam blocks with Al face sheets under indentation (a) Alporas with flat indenter (b) Alporas with spherical indenter (c) foam block with Al sheet of 0.5mm thickness under flat indenter (d) foam block with Al sheet of 0.5mm thickness with spherical indenter (e) foam block with Al sheet of 1.0 mm thickness under flat indenter (f) foam block with Al sheet of 1.0 mm thickness with spherical indenter.

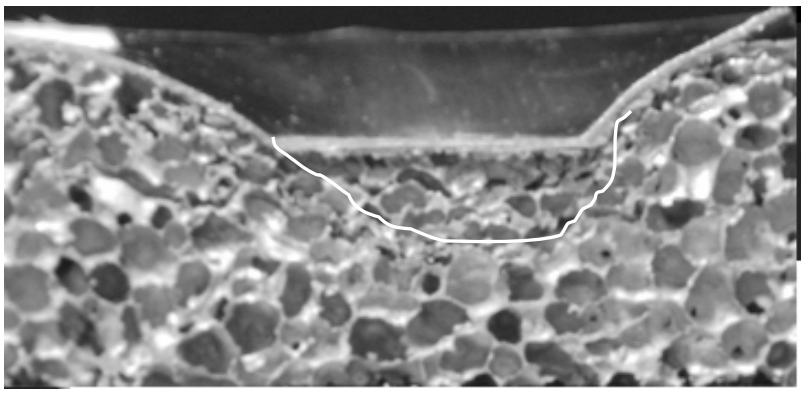

(a)

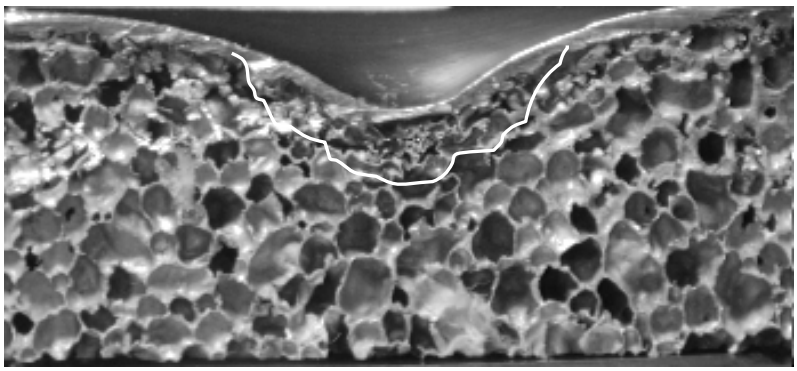

(b)

ATTENTION: The Singapore Copyright Act applies to the use of this document. Nanyang Technological University Library

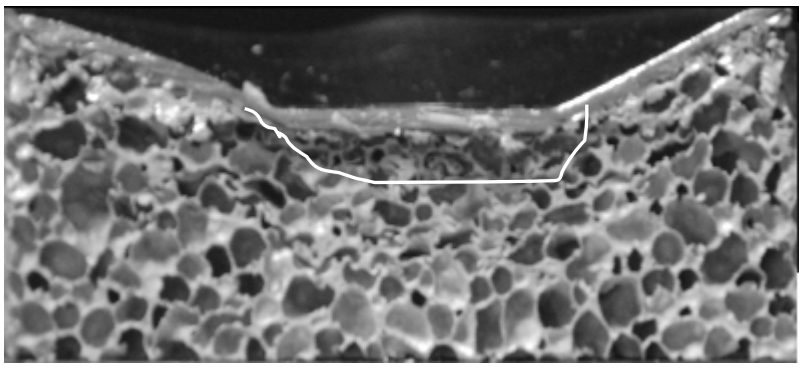

(c)

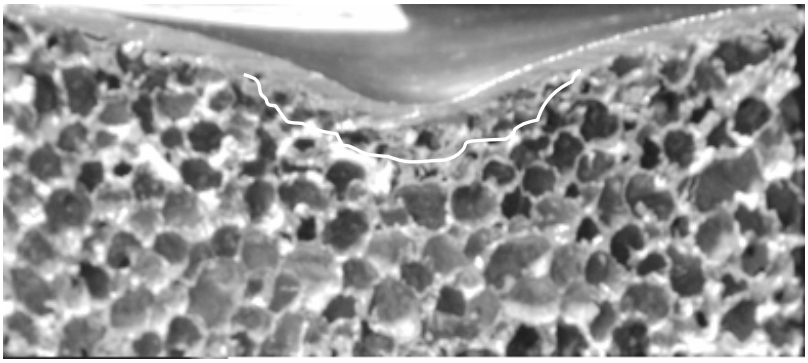

(d)

Figure6.11 Cross-sectional view of the indented foam blocks with SS face sheets under indentation (a) foam block with SS sheet of 0.5mm with flat indenter (b) foam block with SS sheet of 0.5mm thickness with spherical indenter (c) foam block with SS sheet of 1.0 mm with flat indenter (d) foam block with SS sheet of 1.0 mm thickness with spherical indenter.

The cross-sectional macroscopic views of the indented Alporas blocks with flat and spherical indenters are shown in Figure 6.10 (a) and (b) respectively. The foam cells were crushed locally underneath the indenter and it was more severe in the case of flat punch than that of spherical punch for the same indentation displacement. This is due to the fact that the area of contact increases gradually with indentation depth for the spherical punch and remains constant at 491 mm^2 for the flat punch.

Figure 6.10 (c) reveals the indentation behavior of foam cells with flat indenter having Al face sheet of 0.5 mm thickness. The area in which the cells were collapsed was marked in the Figure. The damage zone was predominantly underneath the flat punch and the face sheet punch through was observed (see the elliptical mark). Here, foam cell collapsing in foam core underneath the indenter with face sheet punching in face sheet was observed in the block indented with flat punch. Localized cell wall collapsing with foam cells cracking was observed when foam blocks with 0.5 mm thick Al face sheets were indented by a spherical

ATTENTION: The Singapore Copyright Act applies to the use of this document. Nanyang Technological University Library

punch (see Figure 6.10 (d)). Tearing of the face sheet was also observed at a stage, when there was sudden drop in load in the load displacement curve of Figure 6.6 (a).

Figure 6.10 (e) and (f) show the cross-sectional macroscopic views of the indented blocks with 1.0 mm thick Al face sheets using flat and spherical indenters respectively. The damage zones in block with 1 mm thick Al face sheet are found to be almost similar as to the specimen with 0.5 mm thick Al face sheet under the flat indenter. However, the amount of severity in terms of foam cell collapsing and tearing is less significant. There was no tearing of 1.0mm thick Al face sheet with spherical indenter due to its high strength. Face sheet bending and punch though are the failure mechanisms for all the blocks with 1.0 mm thick Al sheet when indented by the flat punch. Localized indentation beneath the indenter is the failure mode when indented by spherical punch.

Figure 6.11 (a) and (b) reveals the indentation behavior of foam cells of specimens with SS face sheet of 0.5 mm thickness with flat and spherical indenters respectively. The area in which the cells were collapsed was marked in the figure. There is neither punch through nor tearing of the face sheet with either flat indenter or the spherical indenter in SS sheet because of its high strength. Face sheet bending is the failure mechanism for all the blocks with SS sheets when indented by the flat punch. Localized indentation beneath the indenter is the failure mode when indented by the spherical punch.

The cross-sectional macroscopic views of the indented blocks with 1.0 mm thick SS face sheets using flat and spherical indenters are shown in Figure 6.11 (c) and (d) respectively. The damage zones in block with 1.0mm thick SS face sheet are found to be almost similar as in the block with 0.5mm thick SS face sheet under flat punch. However, severity is less in terms of foam cell collapsing and tearing of cells. Failure mechanisms are also found to be similar to those blocks with 0.5mm thick SS face sheet under flat and spherical indenters.

ATTENTION: The Singapore Copyright Act applies to the use of this document. Nanyang Technological University Library

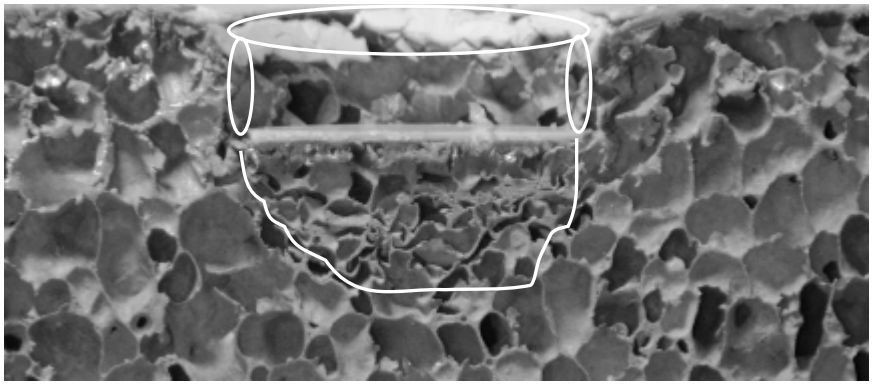

(a)

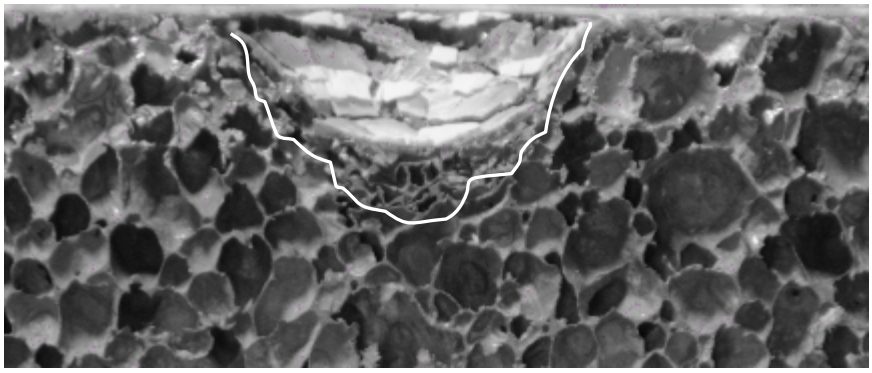

(b)

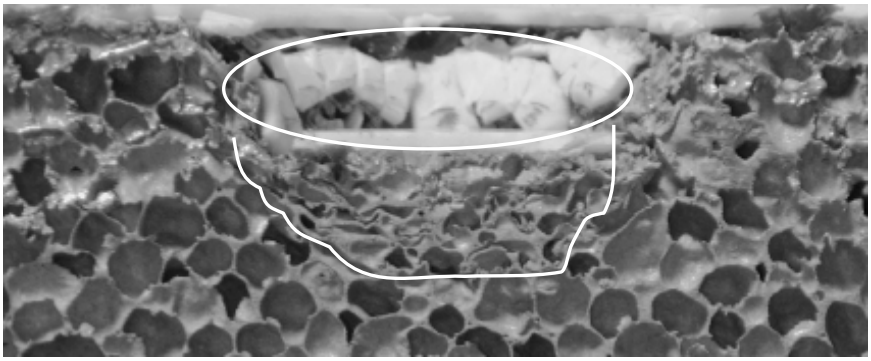

(c)

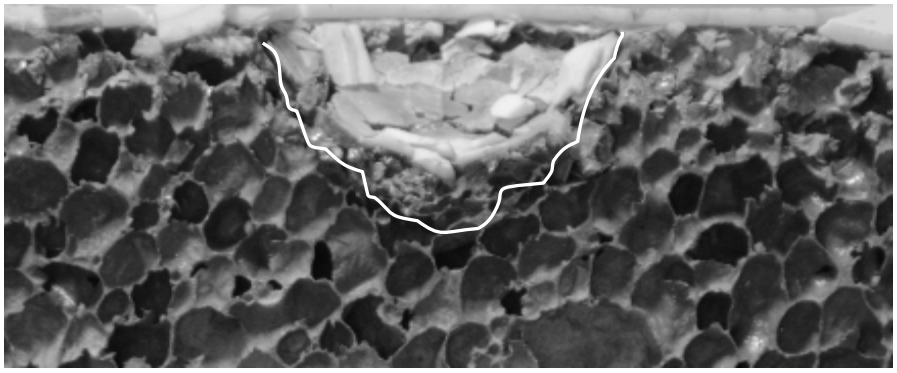

(d)

ATTENTION: The Singapore Copyright Act applies to the use of this document. Nanyang Technological University Library

Figure6.12 Cross-sectional view of the indented foam blocks with alumina face sheets under indentation (a) foam block with alumina sheet of 0.5mm with flat indenter (b) foam block with alumina sheet of 0.5mm thickness with spherical indenter (c) foam block with alumina sheet of 1.0 mm with flat indenter (d) foam block with alumina sheet of 1.0 mm thickness with spherical indenter

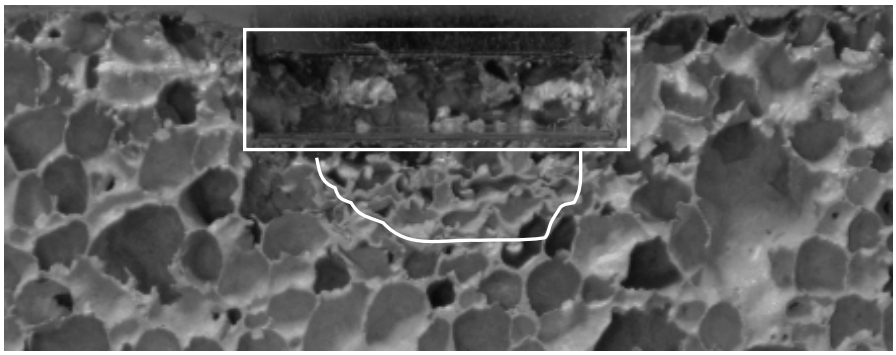

(a)

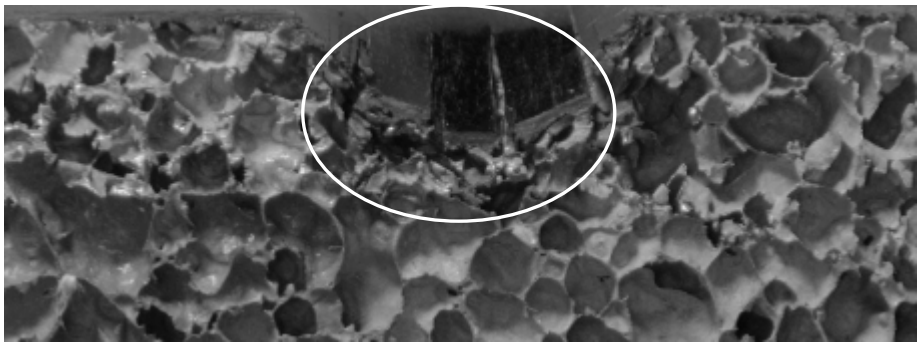

(b)

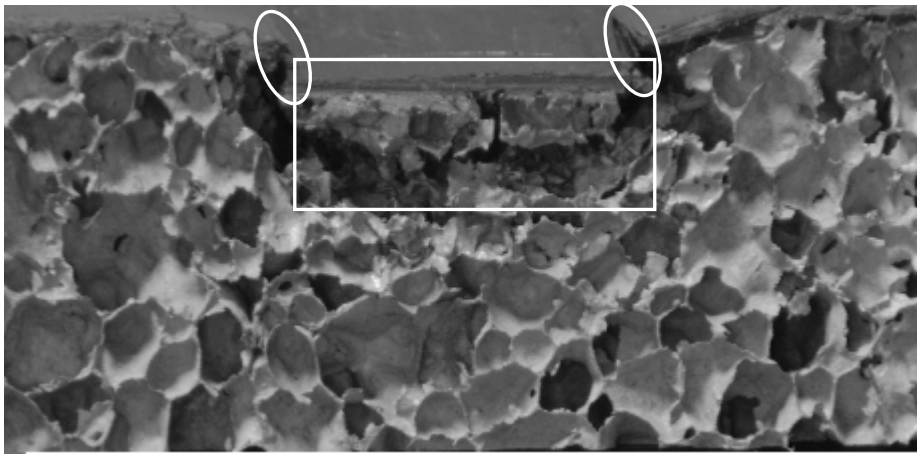

(c)

ATTENTION: The Singapore Copyright Act applies to the use of this document. Nanyang Technological University Library

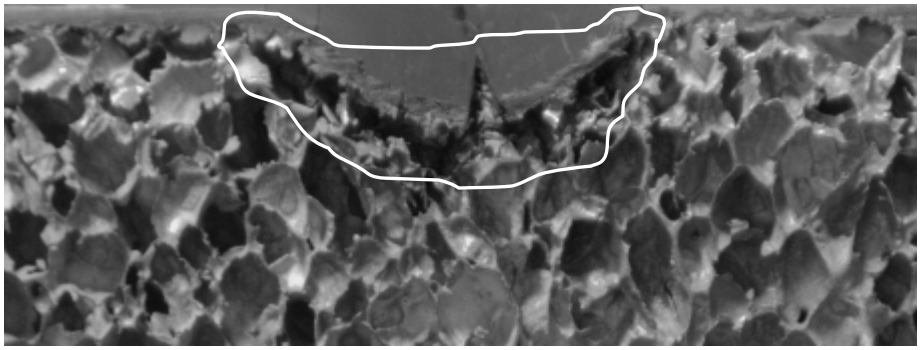

(d)

Figure6.13 Cross-sectional view of the indented foam blocks with CFRP face sheets under indentation (a) foam block with CFRP sheet of 0.5mm with flat indenter (b) foam block with CFRP sheet of 0.5mm thickness with spherical indenter (c) foam block with CFRP sheet of 1.0 mm with flat indenter (d) foam block with CFRP sheet of 1.0 mm thickness with spherical indenter.

The cross-sectional macroscopic views of the indented blocks with 0.5 mm thick alumina face sheets using flat and spherical indenters are shown in Figures 6.12 (a) and (b) respectively. Punch through of the face sheet is shown in the figure with flat indenter due to alumina's low tensile strength along the indenter periphery with collapsing of foam cells beneath the punch. Localized indentation beneath the indenter with crushing of alumina sheet is found to be the failure mode when indented by spherical punch.

Figure 6.12 (c) and (d) reveal the indentation behavior of foam cells having alumina face sheets of 1.0 mm thickness with flat and spherical indenters respectively. In both blocks, damage zones are found to be almost similar to those blocks with 0.5mm thick alumina face sheet. Again, the amount of severity in terms of indentation in foam and crushing or cracking of face sheet in blocks with 1.0mm thick face sheet was lesser than in blocks with 0.5 mm thick face sheet. Clear cracking of alumina face sheet was seen in terms of the separation between the area beneath the indenter and near the edge in block with 0.5 mm thick face sheet, while this was absent in block with 1.0 mm thick alumina face sheet. This is possible due to the high cracking strength of thick face sheet.

Figure 6.13 (a) and (b) show the macroscopic views of the indented blocks with 0.5 mm thick CFRP sheets using flat and spherical indenters respectively. The bending curvature in face sheet is marked by a square zone as shown in Figure 6.13 (a) which indicates the initial failure mechanism to be face sheet bending with flat indenter. Punch through of the sheet was also seen to be another failure of the block in the latter stages of indentation. Transverse

ATTENTION: The Singapore Copyright Act applies to the use of this document. Nanyang Technological University Library

cracking is observed in the CFRP sheet with spherical punches coupled with bending of the sheets, which indicate that the initial failure mechanism is face sheet bending with final failure mechanism of face sheet cracking.

Figure 6.13 (c) reveals the indentation behavior of foam cells with flat indenter with a CFRP face sheet of 1.0 mm thickness. The area in which the cells were collapsed was marked in the figure. The damage zone was predominant underneath the flat punch, but the face sheet was not punch through unlike the block with 0.5mm thick CFRP sheet. Here, face sheet bending was the only failure mechanism observed with some transverse cracks. Damage in the block under spherical punch as shown in Figure 6.13 (d) was found to be similar to that of the block with a 0.5 mm thick CFRP face sheet, but less number of transverse cracks were found in block with 1.0 mm thick face sheet.

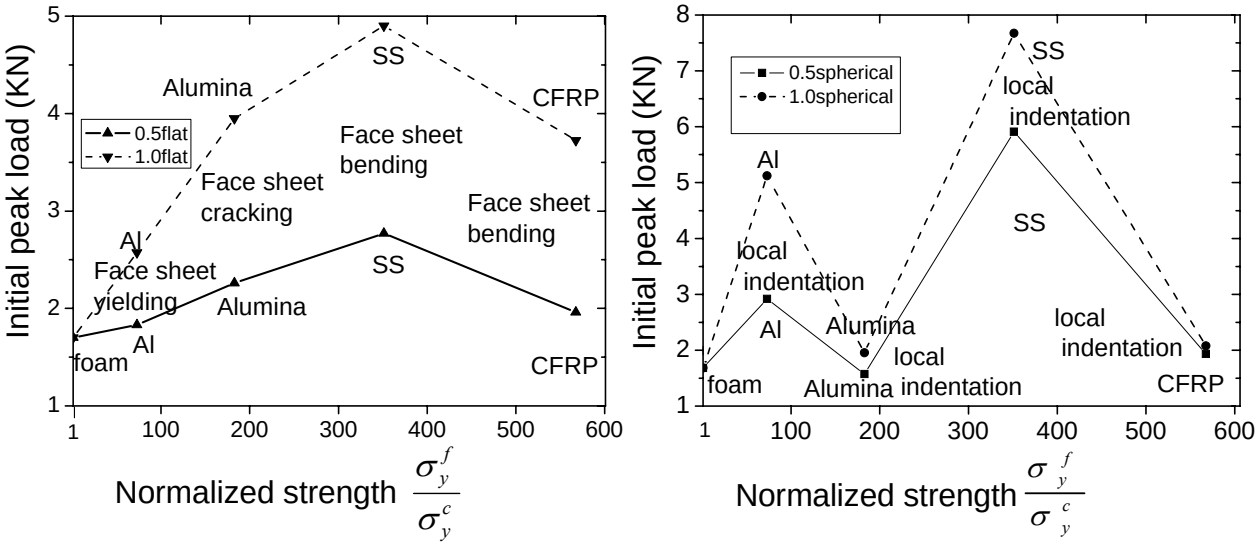

(a) (b)

Figure6.14 Comparison of initial peak for indentation versus strength ratio of face sheet to core (a) for flat indenter, and (b) using spherical indenter.

An overview of the mechanisms for failure initiation and its correlation with different face sheet materials is shown in Figure 6.14 for both flat punch and spherical punch indentation. For the geometry and materials system considered here, the failure initiation mechanism for flat punch depends upon the face sheet constitutive behavior and strength. The trend was only negligibly affected by the thickness effect. With increasing face sheet thickness, the normalized failure load increases. In the case of spherical punch indentation, the brittle face

ATTENTION: The Singapore Copyright Act applies to the use of this document. Nanyang Technological University Library

sheet does not enhance indentation initiation failure load: only the ductile aluminum and SS are useful for energy absorption.

6.2.3.4 Energy absorption

A comparison of energy absorbed by blocks with different face sheets with flat and spherical indenters are shown in Figure 6.15 (a) and (b), respectively. Energy absorption was estimated by measuring the area under the load-displacement curve. Energy absorbed by blocks with flat indentation is found to be more than those by spherical indentation due to more deformation in foam core. With increasing thickness of the face sheet, the amount of absorbed energy is also increased because of the increased material volume. Trend in energy absorption by the blocks with different face sheet materials was found to be similar for both types of indenters. Under the flat indenter, energy absorption for the blocks without any face sheet and with elastic face sheet of 0.5 mm thickness is almost the same. It may be due to the cracking of those face sheets that appears in the early stage of indentation.

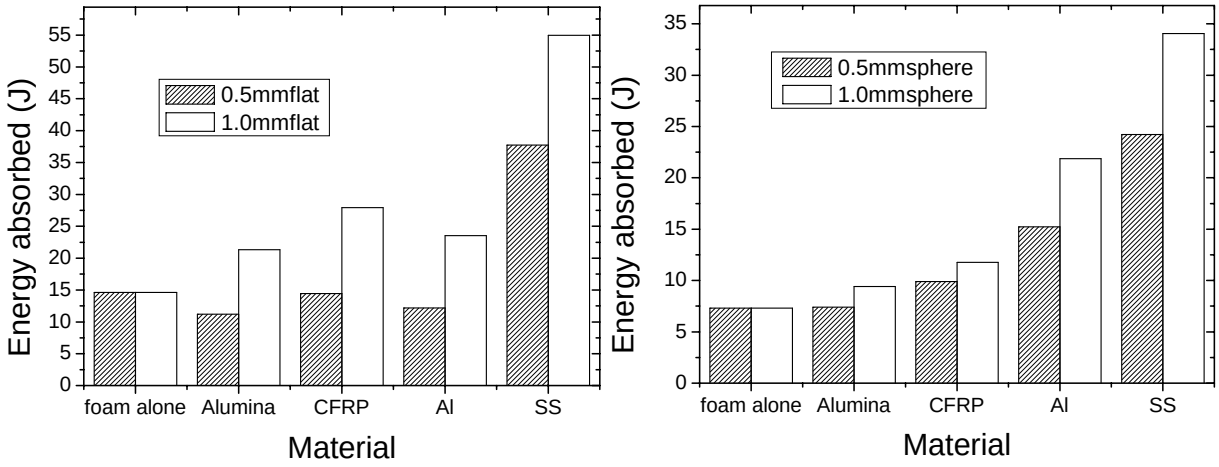

(a) (b)

Figure6.15 Energy absorption by blocks with various face sheets (a) under flat indenter (b) under spherical indenter.

The energy absorbed by foam block with face sheet and with spherical indenter was found to be more than without the face sheet. Maximum energy was absorbed by foam block with elastic plastic sheet and furthermore, the foam block with elastic perfectly plastic sheet absorbed more energy than the elastic face sheet. This trend is missing in flat indentation due to lower absorption of energy by Al sheets due to face sheet punch through.

ATTENTION: The Singapore Copyright Act applies to the use of this document. Nanyang Technological University Library

Chapter -7

Impact response of structures with Al foam and different face sheets

7.1 Introduction

The performance of Al foams is enhanced when one uses it as a core material in a sandwich, with strong and stiff face sheets. This is due to the light-weight and high strength of the resultant sandwich structure. These structures can be used in various applications including automobile, aerospace, building industry for both military and civil purposes. The performance of those structures in the above applications lead to few investigations such as in bullet, blast performance for protective structures, collision in automobile structures, debris impact in aerospace structures. Various researchers have investigated the performance of Al foam under impact loading as explained in Chapter 2.

However, the performance of structures consisting of Al foam core will be different under impact loading if those are attached with different face sheets like Al, SS, and CFRP. This is due to the different contributing behavior of different sheets. Therefore, the selection of face sheet in metal foam cored structure construction depends upon the required property such as impact performance with specific weight for the best use in the real applications. The performance of those sandwiches should be evaluated in other loading conditions such as static indentation for safe usage in real life. In this chapter impact studies carried out on Al alloy foam (namely Alporas and Cymat) blocks bonded to different type of face sheets including Al, SS, CFRP sheets under impact velocity of 6.7 m/sec. with hemi-spherical tool steel punch are discussed. The impact velocity was chosen to be 6.7 m/sec., which is the guideline for assessing the damage in roll over crash in head-on impact of automobiles. This study will clearly evaluate the usage of such structures in safety performance if it is used in automobile parts. At the same time, it shows a good comparison of the performance of structures with different face sheet under low velocity impact and the important findings are compared with quasi static indentation loading to enhance the usage of such structures in various applications. Face sheet materials representing elastic, elastic perfectly plastic and elastic-plastic behavior are chosen. In the following, the materials and experimental

ATTENTION: The Singapore Copyright Act applies to the use of this document. Nanyang Technological University Library

procedures adopted are discussed first and followed by the impact response along with energy absorption capabilities in the results and discussion section.

7.2. Structure with Al foam with and without different face sheets under impact

The experimental protocol adopted for the low velocity impact of foam blocks with and without face sheets is described here**.** Important findings with different failure mechanisms with damaged zones of foam core and face sheets are also explained.

7.2.1 Materials for foam core and face sheets

The materials involved in those blocks are Alporas and Cymat foam core and various sheets including Al 1100, Stainless steel and CFRP. Their mechanical properties with surface characterization are briefly explained in chapter 3.

7.2.2 Test specimen preparation and experimentation

In the present investigation, Alporas foam of cross-section of 100mm X 100mm with different thicknesses 20, 30 and 40 mm were bonded to three types of face sheets such as Al 1100, SS 316, and CFRP sheets of thickness 0.5mm, as described in Chapter-4 using Redux 322 epoxy adhesive. Similarly, Cymat foam of cross-section of 100mm X 100mm X 40mm were bonded to similar types of sheets as mention above but the thicknesses were 0.5 mm and 1.0 mm. Loading was applied on Cymat foams and its structure with various face sheets along thickness (along 40mm direction) direction as explained in Chapter 3. Weight drop impact tests were carried out on foam blocks alone and with various face sheets using Instron DynaTup 8250 impact testing machine. These tests were carried out using a hemispherical steel tup of 13 mm diameter with a rebound brake to avoid multiple impacts, which implies that the impacted area cover around 14 cells in one layer of Alporas foam. Hence the measured response can be considered as the average response of the foam.

A schematic diagram of Dyna Tup 8250 machine is shown in Figure 7.1 with cross sectional view of the clamped specimen. The air pressure in the pneumatic pump placed behind the machine was adjusted to keep the impact velocity constant at 6.7 m/sec which is much greater than the free falling speed limit of this machine.

ATTENTION: The Singapore Copyright Act applies to the use of this document. Nanyang Technological University Library

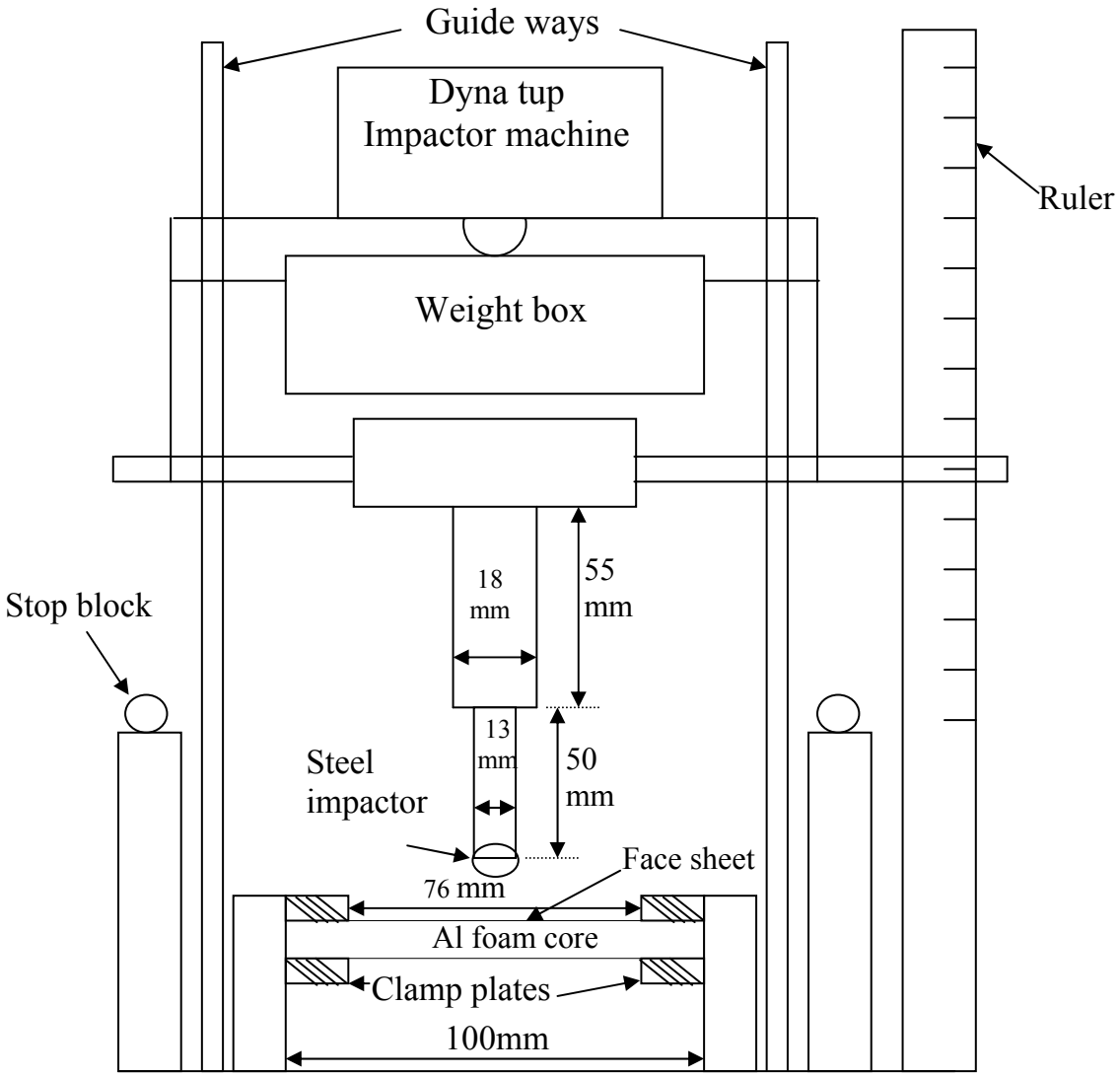

Figure7.1 A schematic view of the Instron Dynatup 8250 testing machine with cross sectional view of clamped block specimen.

Impact velocity of 6.7 m/sec ensure the absorption energy of more than 20J as it is the requirement of initiation of failure for Alporas foams with Glass fiber reinforced polymer [102]. An impactor of 2.65 kg weight would fall on the specimen along two smooth guided columns through the center hole of the clamp plate of 76 mm diameter. The response of the impact test is recorded and collected from the data acquisition system in terms of load, time, energy, velocity and displacement. This thickness of Alporas foam (equal to or more than 20 mm) and impact velocity of 6.7 m/sec. ensures the depth of penetration more than 5 cell layers and the behavior can be considered as the representation of the foam. But due to inadequate thickness of foam specimens, the effect of back support could not prevented on

ATTENTION: The Singapore Copyright Act applies to the use of this document. Nanyang Technological University Library

the impact response [88]. As the objective of this study is to assess the comparative performance of foams with different face sheets, all the precautions and parameters can not be satisfied due to large variation in the strength of the face sheets used which affects the foam crushing, punching etc. To prevent the possible edge effect on the response from foam, the distance from impact zone to clamped edge of the foam specimen is kept more than two diameter of the impactor as the same precaution was practised under quasi-static indentation studies [25, 68].

Pictures of the specimens after impact were taken and subsequently those specimens are sectioned by an electron discharge machining (EDM) to observe the damage zone using a surface displacement analyser (SDA). Due to the non-conduciveness of adhesive, EDM failed to machine the specimen at sites where foam was crushed and adhesive was present so those sites were cut later by bench saw at low speeds. A typical Al foam block of 30 mm thickness, which is punched through by the impactor is shown in Figure 7.2. This picture gives a clear idea about the impact loading of these blocks.

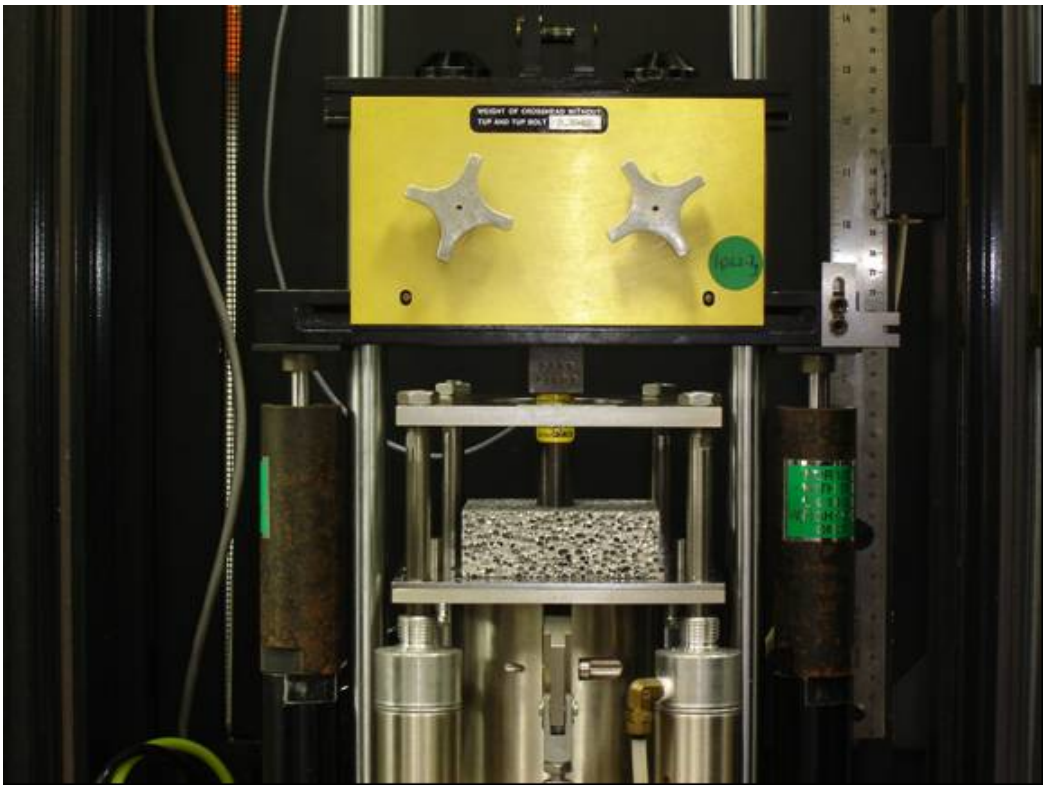

Figure7.2 Punch through Al foam block of 30 mm thickness by impactor.

ATTENTION: The Singapore Copyright Act applies to the use of this document. Nanyang Technological University Library

Alporas specimens with stainless steel face sheets were not punch through during the impact test due to high strength of these sheets. However, Alporas specimens with other face sheets were punch through. Specimens with Cymat foam having various face sheets were not punch through due to crumbling of foam core. In the next section, the behavior of those blocks with both the foam cores is discussed in detail along with the analysis of damage zones.

7.2.3 Results and discussion

7.2.3.1 Impact response of Alporas foam

The load–impactor penetration depth response of Alporas foam of different thicknesses under a weight drop impact loading is shown in Figure 7.3. The impactor penetration depth is equivalent to the displacement moved by the foam block up to the stage of full penetration. Initially the load increases with displacement linearly up to an initial peak load which represents the resistance of foam cells to penetration. This initial peak was not found in the specimens impacted by spherical punch under quasi- static indentation loading.

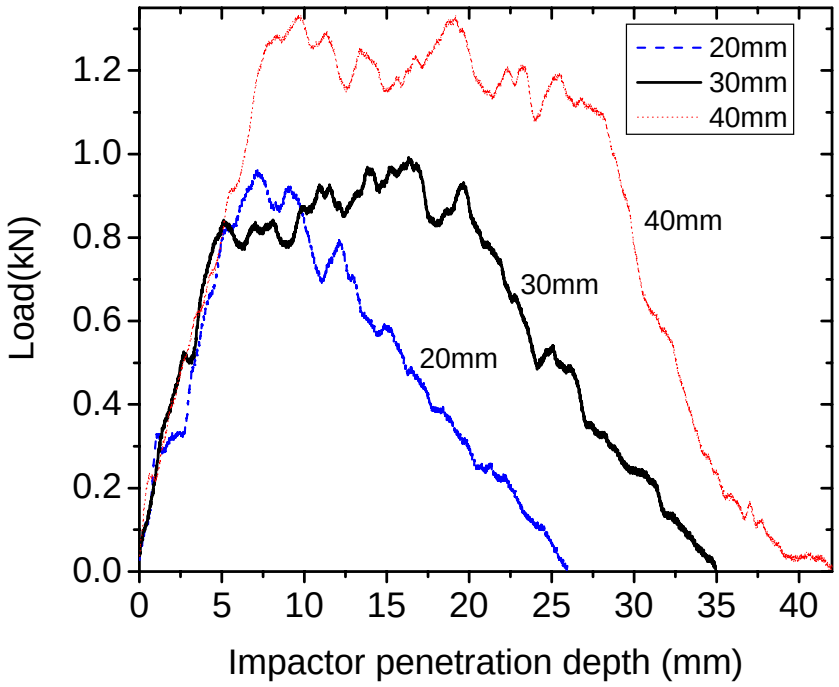

Figure7.3 Comparison of load-impactor penetration depth behavior of Alporas foam with different thicknesses under impact loading.

Long plateaus of load for around 20-25 mm displacement was observed after initial peak load in 30 and 40 mm thick foam specimens, which represent good energy absorption capacity of these foams in dynamic studies.

ATTENTION: The Singapore Copyright Act applies to the use of this document. Nanyang Technological University Library

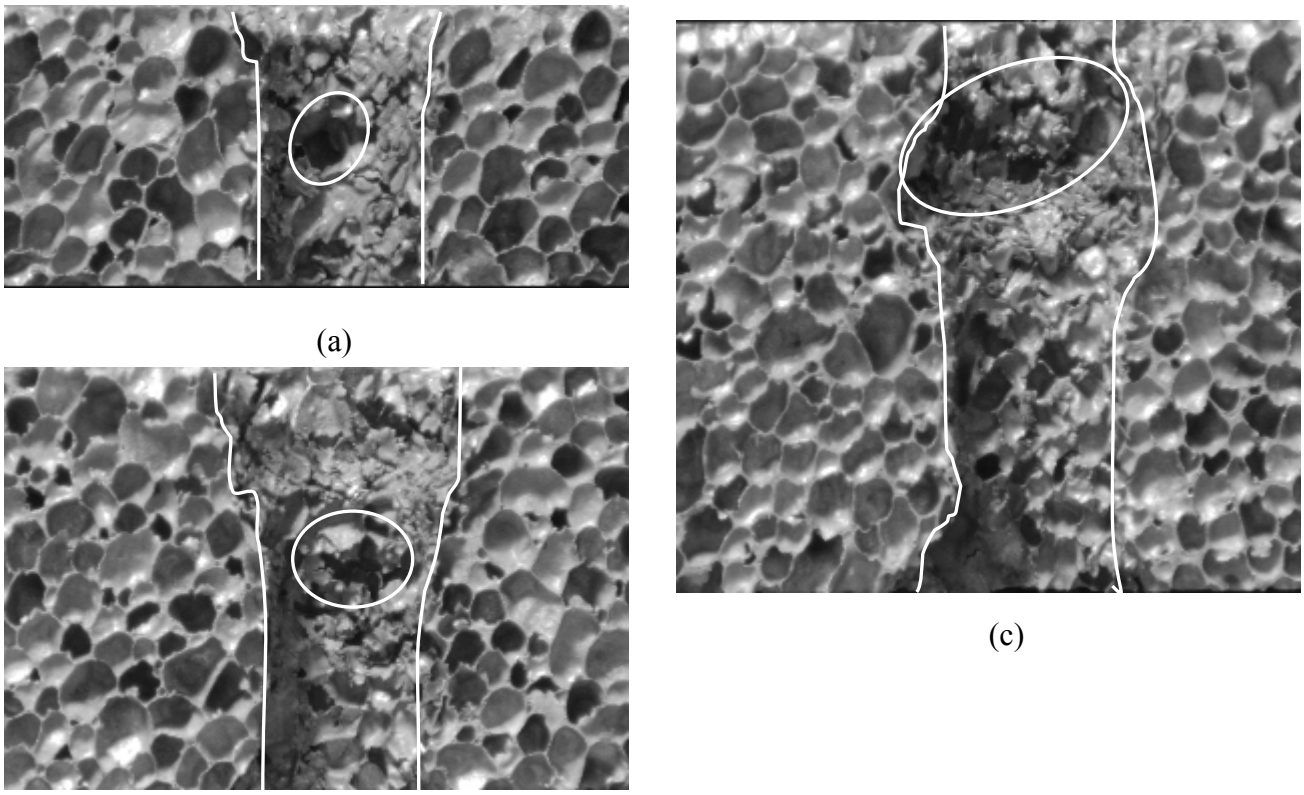

(a)

(b)

(c)

Figure7.4 Cross-sectional view of the impacted Alporas foam block with various thicknesses (a) 20mm, (b) 30mm, and (c) 40mm.

This long plateau in load was absent in Alporas foam when impacted with velocity of 3.7 m/sec. using spherical impactor study done by Ramchandra [88].There, the load was increased till the impactor come into rest after giving its all kinetic energy to Alporas foam. Comparing both studies, it is implied that the loading rate and ratio of impactor size to cell size influence very much the load-displacement response.

The response of load displacement up to the long plateau is found to be similar to the foam's response under uniaxial compressive loading as was shown in Chapter 3, but the value of the load at the plateau was higher in impact loading. This indicates that resistance to impact imparts from crushing of cells beneath the impactor while tearing of cells at the periphery of impactor is another factor which enhance the resistance of the material as shown in Figure 7.4 (Cross-sectional view of the impacted specimens). Deformed zone was not found in these cross-sectional views as it is reported by Ramchancdra et al [88] because all the Alporas foam specimens were punch through in the present study.

ATTENTION: The Singapore Copyright Act applies to the use of this document. Nanyang Technological University Library

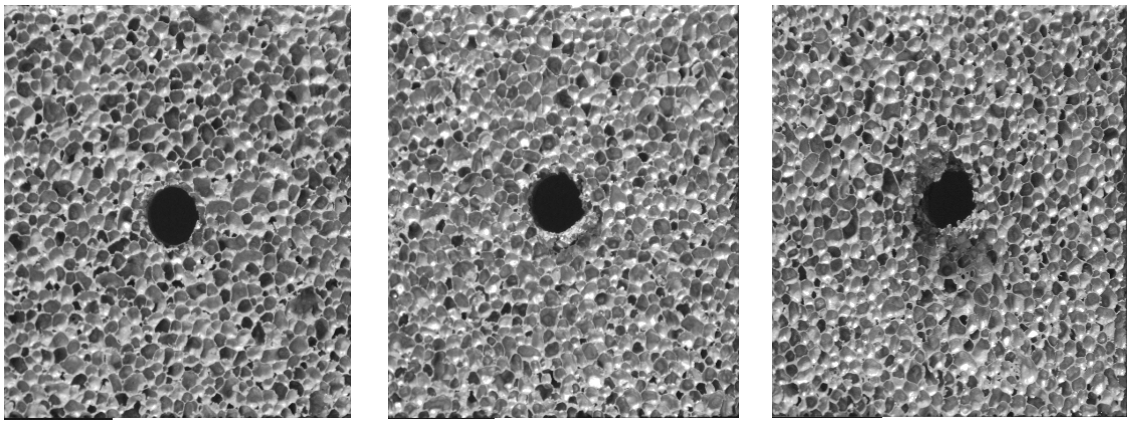

(a) (b) (c)

Figure7.5 Bottom views of the impacted Alporas foam specimens without face sheet having different thicknesses (a) 20mm, (b) 30mm, and (c) 40mm.

However, this plateau was absent for 20 mm thick specimen which indicate the presence of some threshold thickness of the foam which can resist enough the penetration or slowing the penetration process. The passage of the impactor can be seen clearly with the two guided marked lines. The severely damaged zones are marked by elliptical circles. Visible damage area like sitting of some impactor in middle of 30 and 40 mm thick foam specimen occurs due to hitting of the second cylindrical rod of the impactor as shown in Figure 7.1 (as cylindrical rod above than steel impactor one). It is made after crossing that zone by first cylinder of height 50mm. Actually, this damage is not included in this study because the displacement up to 50mm was considered.

Stiffness which is the representation of the material property was found to be the same for all the specimens. All the specimens were punch-through as shown in Figure 7.5 (bottom view of the impacted specimens). It is the reason for the absence of densified zone of cells beneath the impactor in Figure 7.4 which was present in response of Alporas foam under quasi- static indentation loading as shown in Chapter 6. It is clear from Figure 7.5 that as the thickness of the foam increases the resistance of foam increases which can be seen from the penetration of the foam specimen as tearing of foam material and the ligaments bent outwards at the circumference of the hole made by impactor.

ATTENTION: The Singapore Copyright Act applies to the use of this document. Nanyang Technological University Library

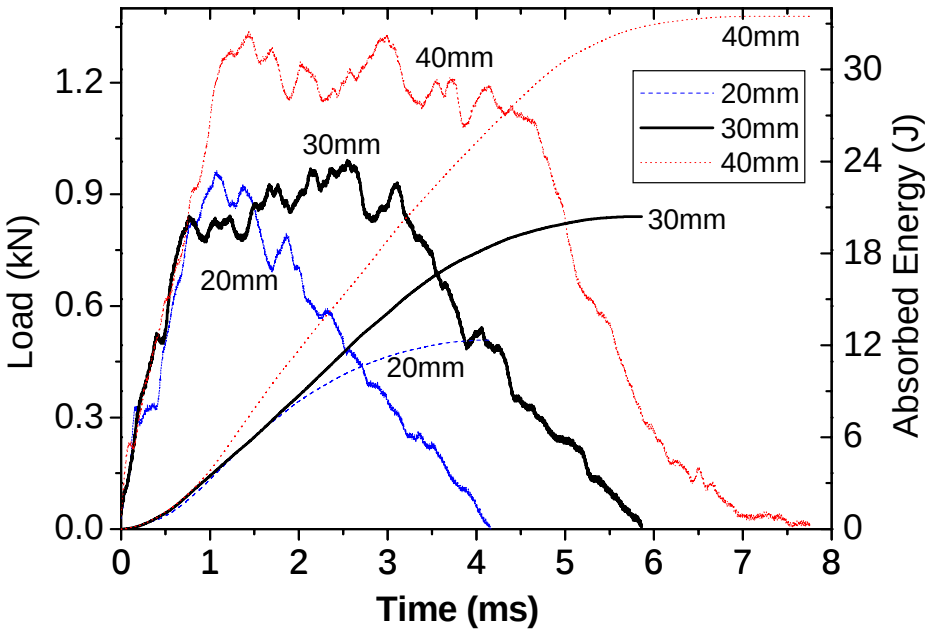

Figure7.6 Absorbed energy and load as a function of time for impact of Alporas foam alone with various thicknesses.

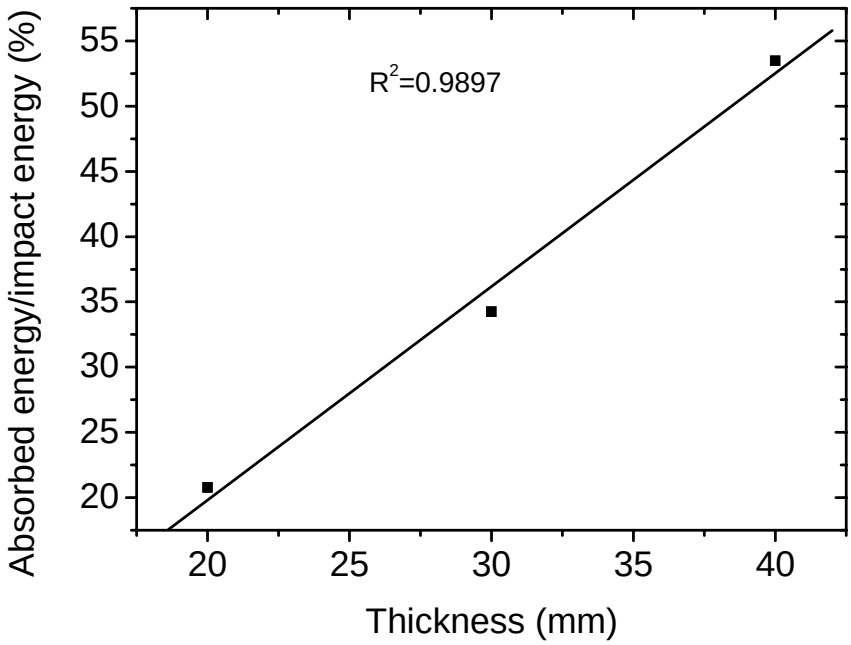

Figure7.7 Normalized absorbed energy vs. thicknesses of Alporas foam under impact loading.

Figure 7.6 shows the absorbed energy and load as function of time of impact for Alporas foam with different thicknesses such as 20mm, 30mm and 40 mm. A linear proportionality relationship was found between the time and distance traveled by the impactor wherever the load-time curve appeared exactly the same as the load-displacement curve.

ATTENTION: The Singapore Copyright Act applies to the use of this document. Nanyang Technological University Library

Absorption of energy by Alporas foam is found to be linear with time initially but the rate of absorption of energy increases tremendously as the time increases. This increment occurs due to absorption of energy by crushed foam cells beneath the impactor. However, it becomes almost flat when the impactor penetrated through the thickness of the foam. Energy absorbing nature of these Al foams is proved by increment in absorption of impact energy with increased foam thickness. Absorbed energy was normalized with impact energy and plotted with thickness of foam as shown in Figure 7.7. The trend between normalized impact energy and foam thickness was found to be linear. This proves that thicker foam can absorbed more energy as expected. The trend line shows that the 70 mm thick Alporas foam block will be able to absorbed 100 % impact energy.

The energy absorbed per unit displaced volume was calculated and found to be 3.87MJ/m^3, 4.95 MJ/m^3 and 6.30 MJ/m^3 for Alporas foam having 20 mm, 30 mm and 40 mm thickness respectively. For above calculations, all punch through Alporas foam specimens were considered. Energy absorbed per unit displaced volume for one Alporas foam specimen tested (not punch through) for lower impact speed of 3.81 m/sec was found to be 3.62 MJ/m^3, which agrees with the chart provided by Ramachandra et al [88] (~3.6 MJ/m^3 for 3.8 m/sec.) for Alporas foam under different impact velocities.

7.2.3.2 Impact response of Cymat foam

The load–impactor penetration depth response of Cymat foam of 40 mm thickness under weight drop impact loading is shown in Figure 7.8. Initially the load increases significantly with a small amount of displacement in an almost linear manner up to an initial peak load which represents the resistance from the first layer of foam cells to penetration. This initial peak was also present with a flat punch under quasi-static indentation loading also similar to the foam's response under uniaxial compression loading. The value of this peak load is found to be the largest for uniaxial loading while it is the smallest under quasi-static indentation loading. This indicates that tearing of the cells at the periphery of impactor is the only energy absorption mechanism under impact loading due to the small ratio of impactor size to cell sizes (~1), while under uniaxial loading, bending of the foam cell walls beneath the loading platen provide an additional resistance.

ATTENTION: The Singapore Copyright Act applies to the use of this document. Nanyang Technological University Library

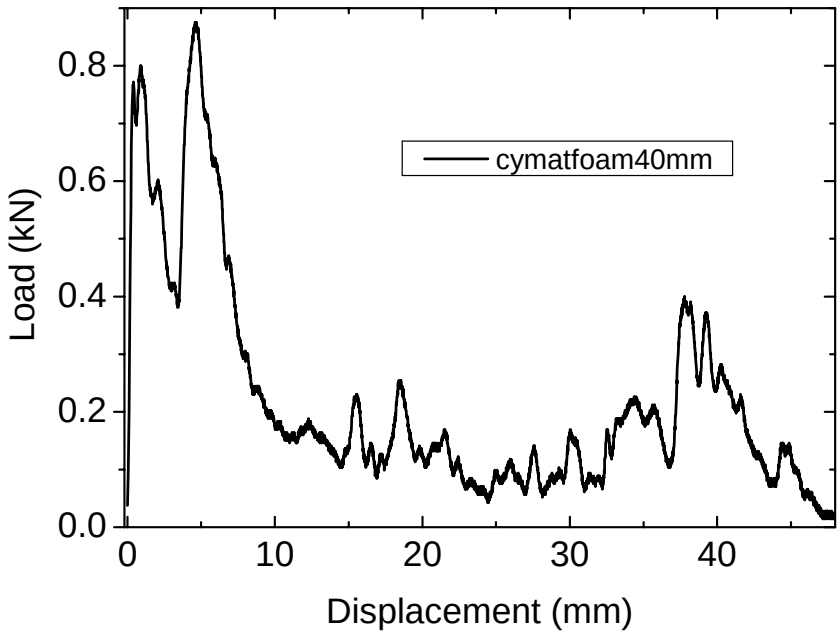

Figure7.8 Comparison of load-impactor penetration depth behavior of Cymat foam with thickness of 40mm under impact loading.

The slope of the load curve was found to be the largest under impact loading compared to two other loading conditions, which is due to the highly localized deformation in the foam cells. There is no plateau observed under impact loading as it was under uniaxial compressive loading because of the highly localized deformation.

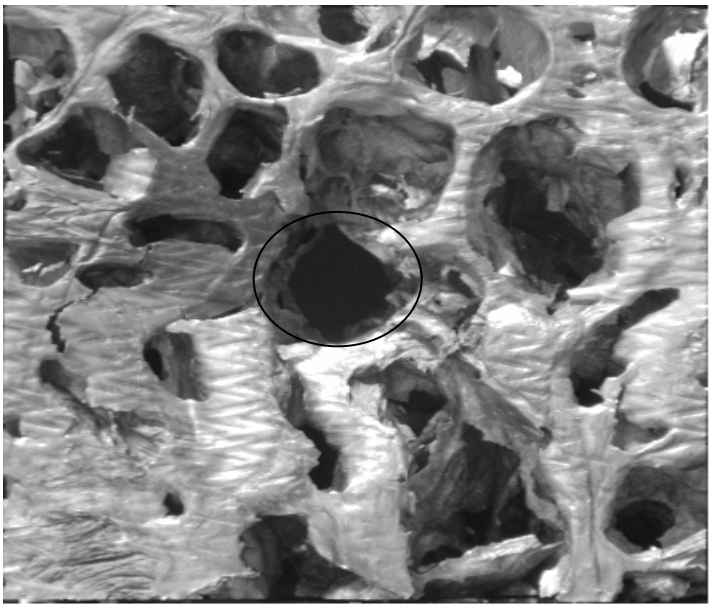

Figure7.9 Bottom view of the impacted Cymat foam specimen with a thickness of 40mm.

Resistance to penetration was found to decrease drastically after the peak load due to the small ratio of impactor size to cell size as observed in Figure 7.9 (bottom view of the

ATTENTION: The Singapore Copyright Act applies to the use of this document. Nanyang Technological University Library

impacted Cymat foam which is punch through by the impactor). Small increments in load response after the peak load are due to resistance offered by smaller cells along the path of the impactor.

This load displacement response can be roughly divided into three phases; firstly as the resistance to penetration (up to peak), secondly, crushing phase and thirdly densification phase which is observed for different set of parameters (impact velocity, direction of loading, density, and cell size) for Cymat foam as study done by Tan et al [93]. But the factors such as dynamic strength, plateau strength are very much dependent on above said parameters for Cymat foam [93].

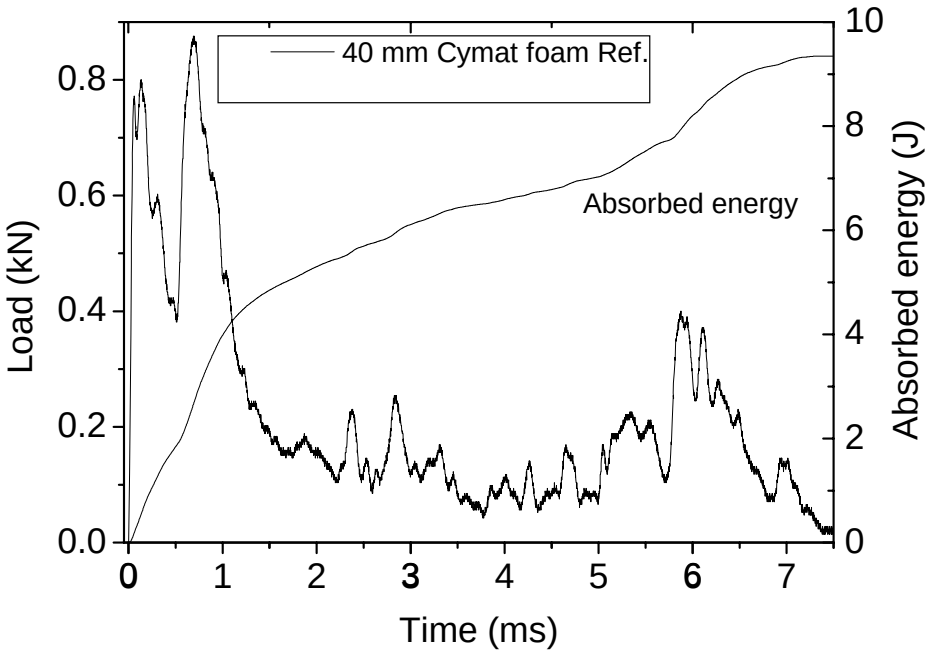

Figure7.10 Absorbed energy and load as a function of time for impact of Cymat foam alone with thickness of 40 mm.

Figure 7.10 shows the absorbed energy and load as function of time of impact for Cymat foam with thickness of 40 mm. The nature of load-time response of Cymat foam is also similar to load-displacement which proves that the time and distance traveled by the impactor is linearly proportional to each other. Absorption of energy by Cymat foam is found to be in a linear manner for a short period of time but the rate of energy absorption decreases when the impactor penetrated through many foam cells. This trend is found to be almost opposite to the Alporas foam because of the lower size ratio (impactor size to cell size) with Cymat foam. Alporas is found to have better energy absorbing capacity compare to Cymat foam which crumbles after impact due to its brittle nature.

ATTENTION: The Singapore Copyright Act applies to the use of this document. Nanyang Technological University Library

7.2.3.3 Impact response of Alporas foam with different face sheets

The load–impactor penetration depth responses of Alporas foam of 30 mm thickness with and without various face sheet of thickness 0.5 mm under a weight drop impact loading are shown in Figure 7.11.

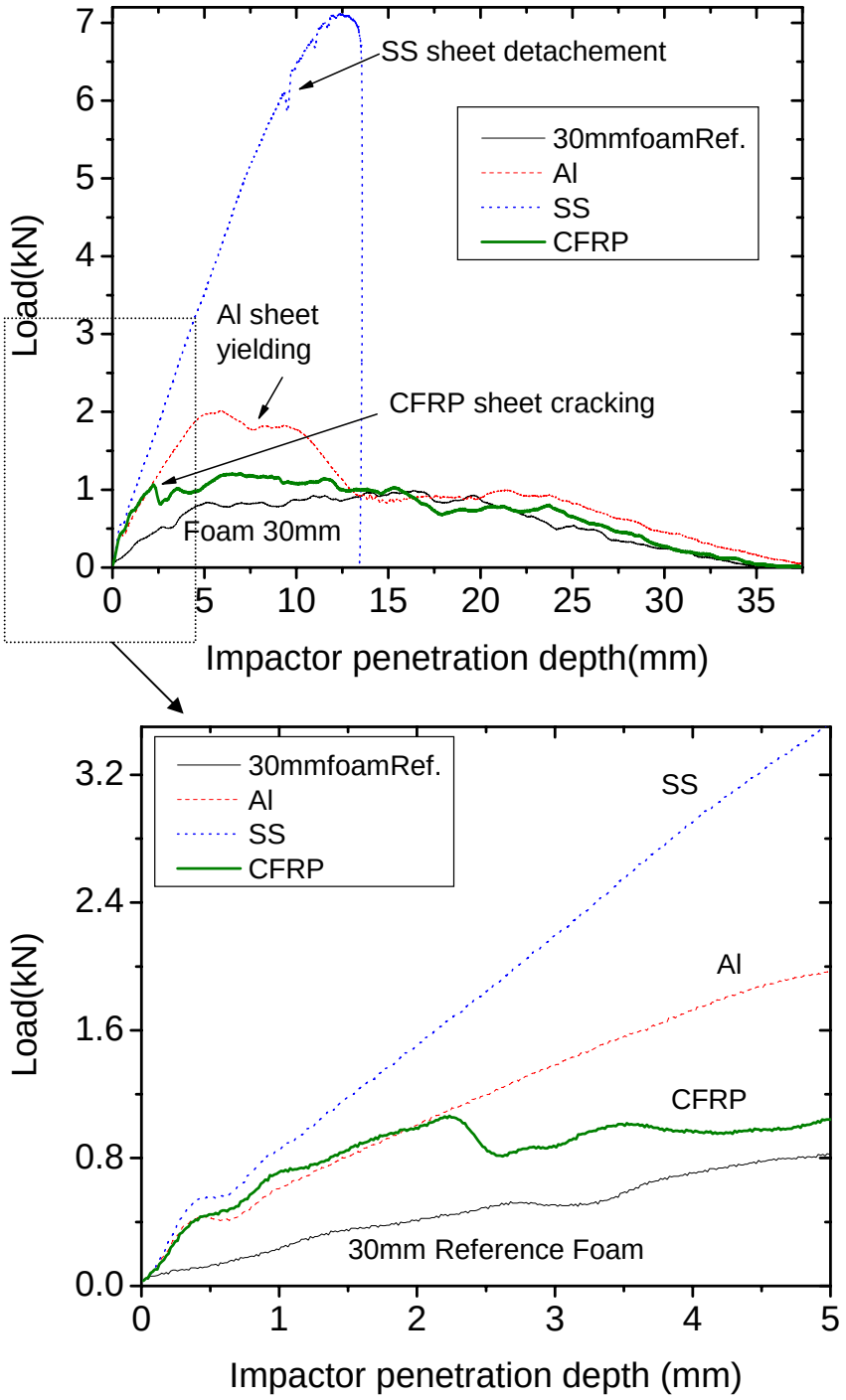

Figure7.11 Comparison of load-impactor penetration depth behavior of 30 mm thick Alporas foam with different face sheets of 0.5 mm thickness under impact loading.

ATTENTION: The Singapore Copyright Act applies to the use of this document. Nanyang Technological University Library

The load was increased almost linearly with displacement up to an initial peak for all the blocks with different face sheet under impact loading which represents the resistance of foam cells to penetration beneath the impactor with bending and stretching of face sheet at the periphery of impactor as shown in Figure 7.12 (cross-sectional views of the impacted specimens with uniform magnification). The stiffness of all the specimens was found to be different which indicates the dominant behavior of the face sheet. Load initially increases linearly with displacement in the case of Alporas foam block with elastic-perfectly plastic Al face sheets and the slope is representative of the structure's stiffness. There is a strong hardening response due to stretching of the face sheet, which is one contributing factor in stiffness.

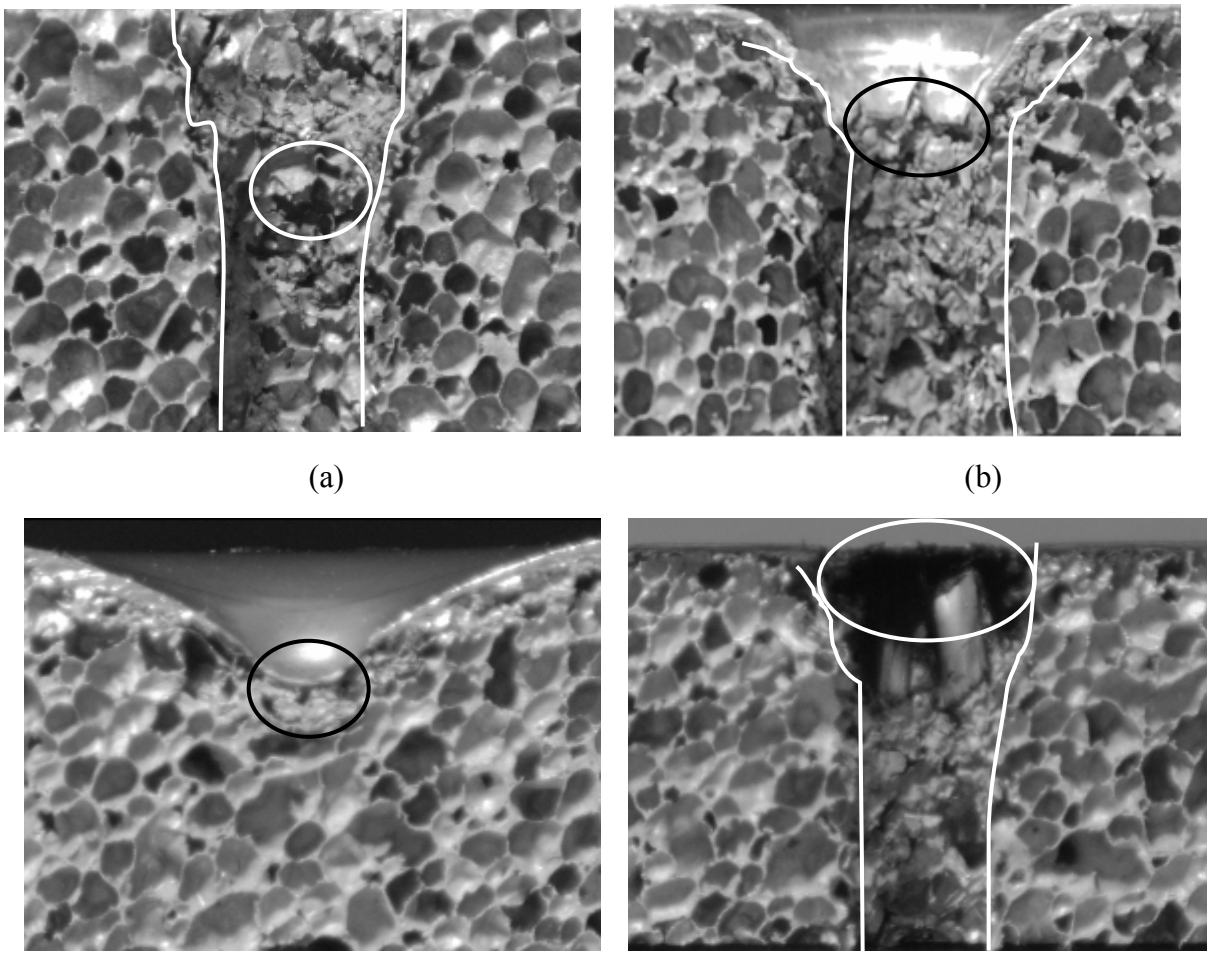

(a) (b)

(c) (d)

Figure7.12 Cross-sectional views of the impacted 30mm thick Alporas foam blocks with different face sheet of thickness 0.5 mm (a) foam alone, (b) Al sheet, and (c) SS sheet and (d) CFRP sheet.

ATTENTION: The Singapore Copyright Act applies to the use of this document. Nanyang Technological University Library

This response continues up to an initial peak and after this, failure occurs due to face sheet yielding and the load decrease along with the displacement of the impactor. The decrease in load continue up to punch through of the face sheet and after that only the foam cells is left to resist the penetration which is similar to the response of Alporas foam block. Face sheet yielding and punch through can be seen clearly in Figure 7.12 (b).

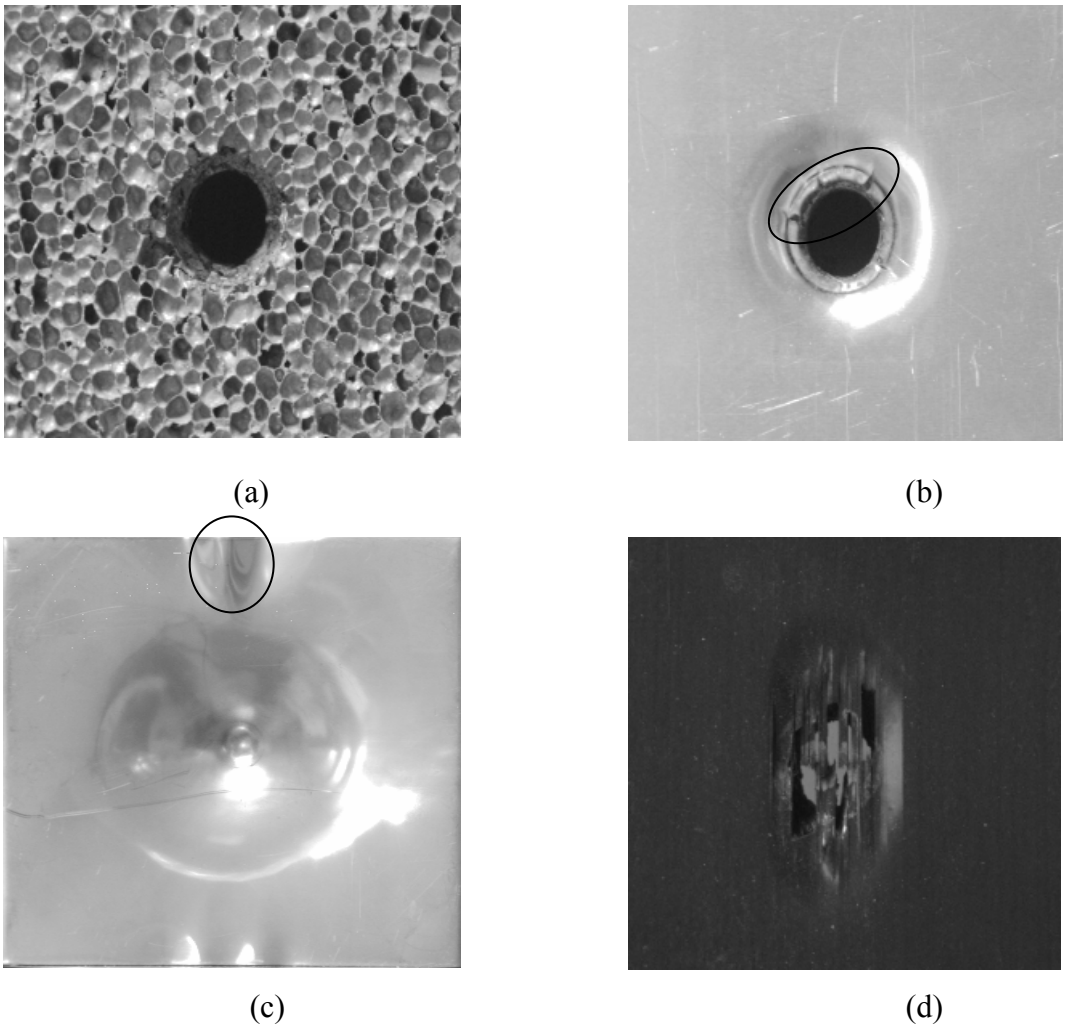

Figure7.13 Top views of the impacted 30 mm thick Alporas foam specimens with different face sheet of 0.5 mm thickness (a) foam alone, (b) Al sheet, and (c) SS sheet and (d) CFRP sheet.

In the case of stainless steel face sheets, an initial failure is triggered by the face sheet bending and there is a strong hardening behavior due to membrane stretching and bending effect. The face sheet material has to stretch to accommodate the punch profile.

ATTENTION: The Singapore Copyright Act applies to the use of this document. Nanyang Technological University Library

The rate of hardening in the case of SS face sheet is observed to be much higher than that of the Al face sheet due to power-law strain hardening in SS. Further loading revealed a slight detachment of the SS sheet from the Alporas foam as shown at the top side of the impacted block in Figure 7.13 (c), which is marked by a sudden drop in load shown in Figure 7.11. This behavior is similar to that of quasi-static indentation with spherical and flat punches as discussed in Chapter 6. All the specimens were penetrated except the block with stainless steel face sheet due to its high strength as shown in Figure 7.13 (top view of the impacted specimens). Important findings in the impacted specimens are marked.

Firstly, wrinkling of the upper skin, secondly, debonding between upper skin and foam core and finally breakage of lower skin were found as failure mechanisms occurred under dynamic three-point bending for sandwich of open-cell Al foam with elastic–perfectly plastic Al face sheets with two lower supports by Yu et al. [104].

Resistance to movement in terms of the load was found to be very steep in case of wrinkling with lower skin failure in latter stages of movement compare to response from punching of CFRP sheets in the present study. It implies that not only the boundary conditions but also the cell structures of the foam play an important role under dynamic loading response.

Load-displacement response of blocks with CFRP face sheet was found to be almost linear but because of the high stiffness of CFRP sheets, they were stiffer than blocks with Al sheets. After few transverse cracks appeared in the face sheet during impact of the foam block, the load deceases with displacement due to reduction in stiffness. In CFRP sheets, delamination between fiber and matrix is observed in cross-sectional view of these blocks (as shown in Figure 7.12 (d) with fiber breakage. Subsequently, the response of load-displacement is similar to the foam block. The occurrence of these cracks is due to the low transverse strength of these laminates as compare to the longitudinal strength. Face sheet punching was observed to be the final failure mechanism for this type of sample block, with face sheet bending as initial failure mechanism as reflected by top and cross-sectional view of this block (Figure 7.12 (d) and 7.13 (d)). These Alporas blocks were found to have more localized damage because of the high strain rate than blocks under quasi-static indentation as shown in Chapter 6. This study shows that 25 Joule impact was sufficient for cracking of unidirectional $[0^0/0^0/0^0/0^0]$ CFRP sheets and punching of Alporas foam core. While G.Reyes et al [102] showed that 20 Joule impact is enough for the localized crushing of 10mm foam core and

ATTENTION: The Singapore Copyright Act applies to the use of this document. Nanyang Technological University Library

permanent deformation of skins of GFRP sheets with $0^0/90^0/0^0/90^0$ or woven lay-up for sandwich of Alporas foam with GFRP sheets. For this type of sandwiches, 37 Joule impact was shown to be sufficient for fiber-matrix delamination and fiber breakage in top skin of cross-ply GFRP with localized crushing of foam core and some shear deformation in the region just ahead of the crushed cells [101].

The response of the load-time for blocks with 30mm thick Alporas foam core with different face sheets as shown in Figure 7.14 is similar to load-displacement response which indicates the linearity between displacement and time.

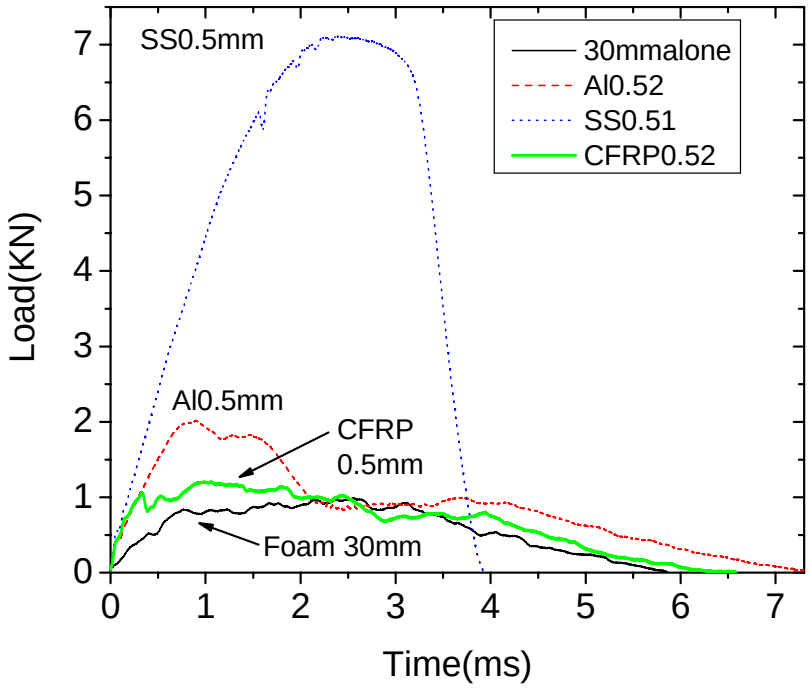

Figure7.14 Load-time for impact of Alporas foam of 30 mm thickness with out and with different face sheet under impact loading.

Figure 7.15 shows the energy absorbed as a function of time of impact for Alporas foam block with various face sheet of 0.5 mm thickness. Trend of absorption of energy by blocks was found to be similar for various face sheets except for the block with SS sheets. Block with SS face sheet absorbed almost 100 % of impacted energy due to high strength the face sheet.

ATTENTION: The Singapore Copyright Act applies to the use of this document. Nanyang Technological University Library

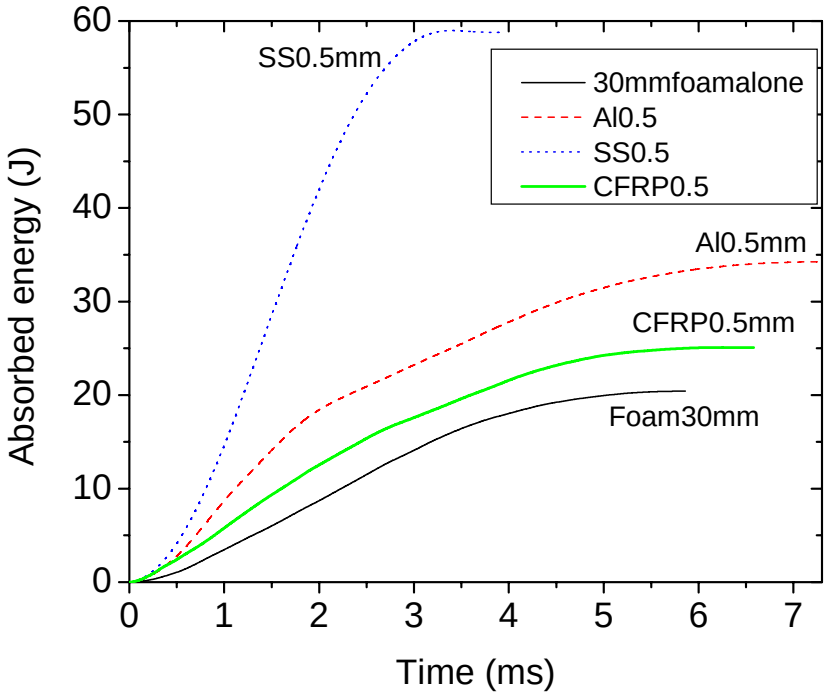

Figure7.15 Absorbed energy and load as a function of time for impact of Alporas foam of 30 mm thickness with out and with different face sheet under impact loading.

The load–impactor penetration depth response of Alporas foam of 40mm thickness with different face sheet under a weight drop impact loading is shown in Figure 7.16. The trend is found to be almost similar to the blocks 30 mm thickness except for a few differences, such as increase in resistance to penetration or load for specimen with similar face sheet with less displacement traveled by the impactor. This "hardening" effect is due to increase in face sheet stretching and bending as a result of a thicker face sheet.

Top views of the impacted blocks of 40 mm thickness are similar to 30 mm thick blocks, however cross-sectional views of impacted blocks with 40mm thick foam make the failure mechanism clearer than blocks with 30 mm as shown in Figure 7.17. For example bending of face sheet is seen more clearly as an initial failure mechanism in the Alporas foam block of 40mm thickness shown in Figure 7.17 (d) having CFRP face sheet than blocks with 30mm thickness.

ATTENTION: The Singapore Copyright Act applies to the use of this document. Nanyang Technological University Library

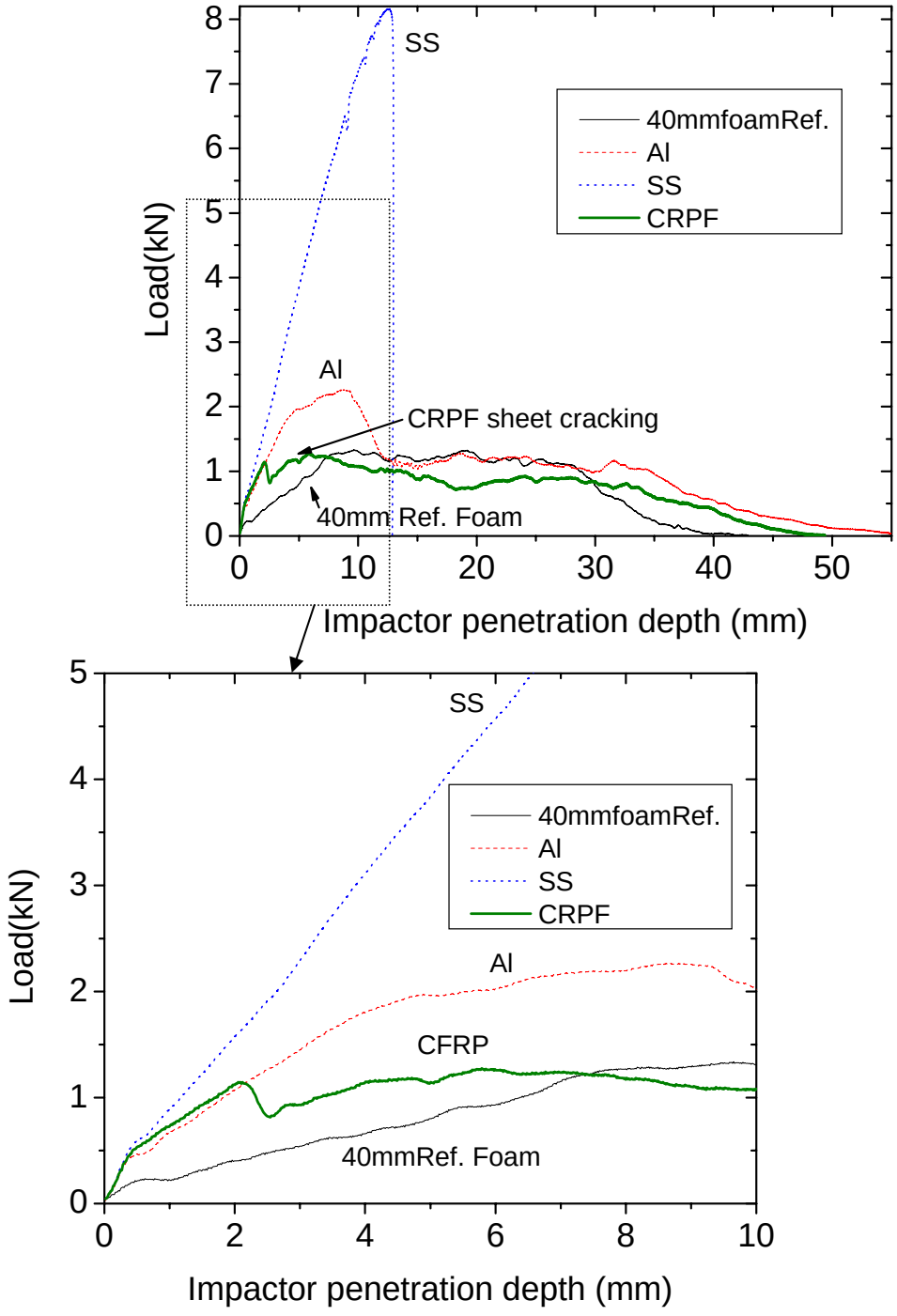

Figure7.16 Comparison of load- impactor penetration depth behavior of Alporas foam of 40 mm thickness with different face sheets of 0.5 mm thickness under impact loading.

ATTENTION: The Singapore Copyright Act applies to the use of this document. Nanyang Technological University Library

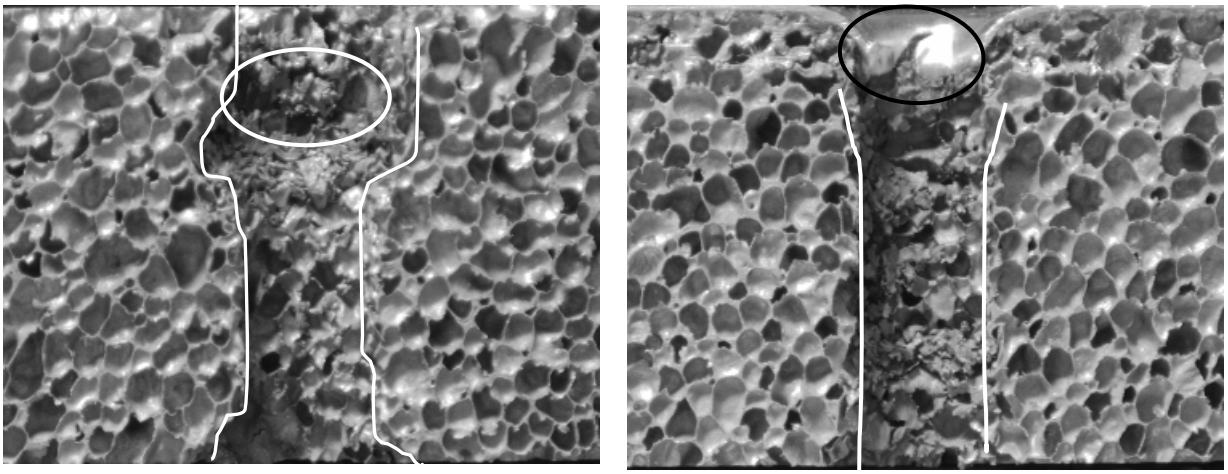

(a) (b)

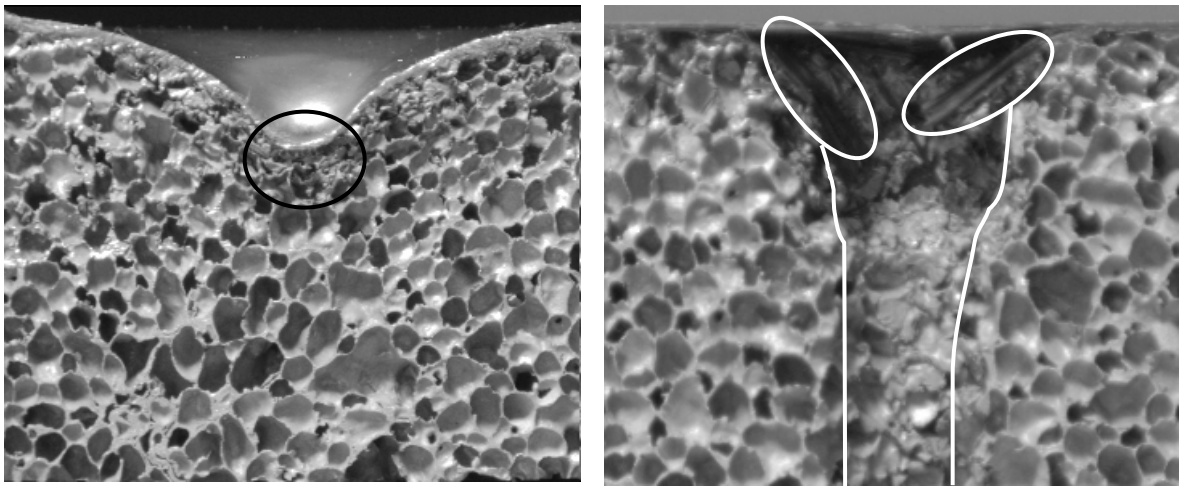

(c) (d)

Figure7.17 Cross-sectional views of the impacted Alporas foam blocks with 40mm thickness with out and with different face sheet of thickness 0.5 mm (a) without face sheet, (b) Al sheet, (c) SS sheet and (d) CFRP sheet.

Absorbed energy was normalized with impact energy for specimens with 40mm thick Alporas foam core and plotted as shown in Figure 7.18 and compared with the blocks with 30 mm thick foam core.

The trend of normalized absorbed energy with impact energy was found to be similar in both type of specimens but the amount of absorption is higher for blocks with 40 mm thickness because of higher resistance by more foam cells. Almost all the impact energy was absorbed by block with SS and an indent mark was left on the face sheet similar to the one under spherical punch under static indentation as shown in Chapter 6. Blocks with CFRP face sheets performed little better in energy absorption as compared to blocks without sheets.

ATTENTION: The Singapore Copyright Act applies to the use of this document. Nanyang Technological University Library

Unidirectional lamina preparation for CFRP sheets is the reason for such performance. Blocks with multidirectional lamina CFRP sheet will show the better performance for the same type of structures.

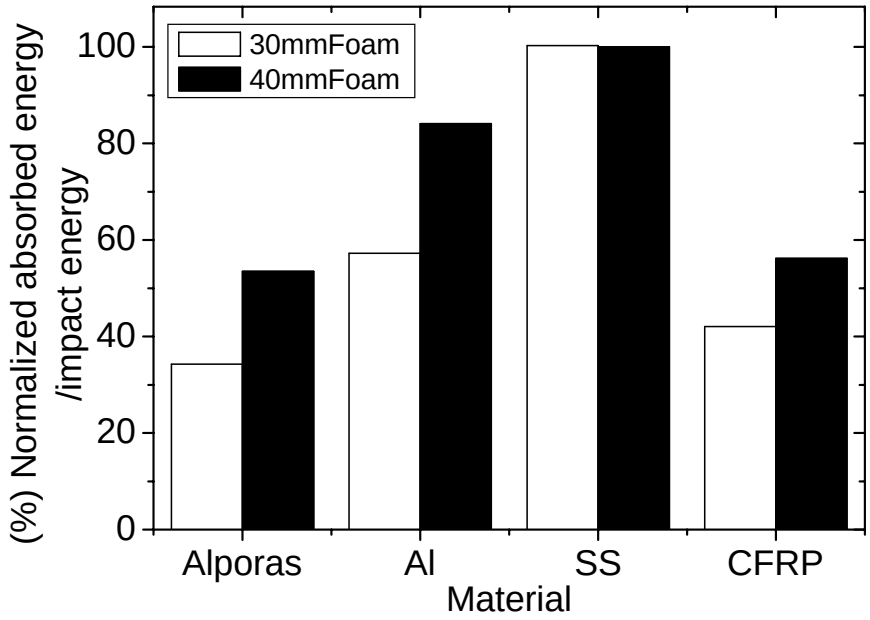

Figure7.18 Normalized absorbed energy vs. blocks of Alporas foam having thicknesses of 30 and 40 mm without and with different face sheet of 0.5mm thickness under impact loading.

7.2.3.4 Impact response of Cymat foam with different face sheets

The load–impactor penetration depth response of Cymat foam of 40mm thickness with and without various face sheet of thickness 0.5mm under a weight drop impact loading is shown in Figure 7.19.

Load was increased in a zigzag manner with displacement up to an initial peak for all the blocks with different face sheets under impact loading. It represents the resistance of foam cells of first layer to penetration beneath the impactor with more stretching of face sheet due to membrane effect and crumbling of foam cells beneath the impactor. It was found that the stiffness of the foam block with stainless steel face sheet is lesser than the foam block without. It resulted from the variation in cell distribution in Cymat foam. There is a strong hardening response due to stretching of the metallic face sheet to accommodate the punch profile. The load–impactor penetration depth response of Cymat foam of 40mm thickness with various face sheet of 1.0mm thickness under a weight drop impact loading is shown in

ATTENTION: The Singapore Copyright Act applies to the use of this document. Nanyang Technological University Library

Figure 7.20. It shows the comparison between response of block with 0.5 mm thick face sheet and with 1.0 mm thick face sheet.

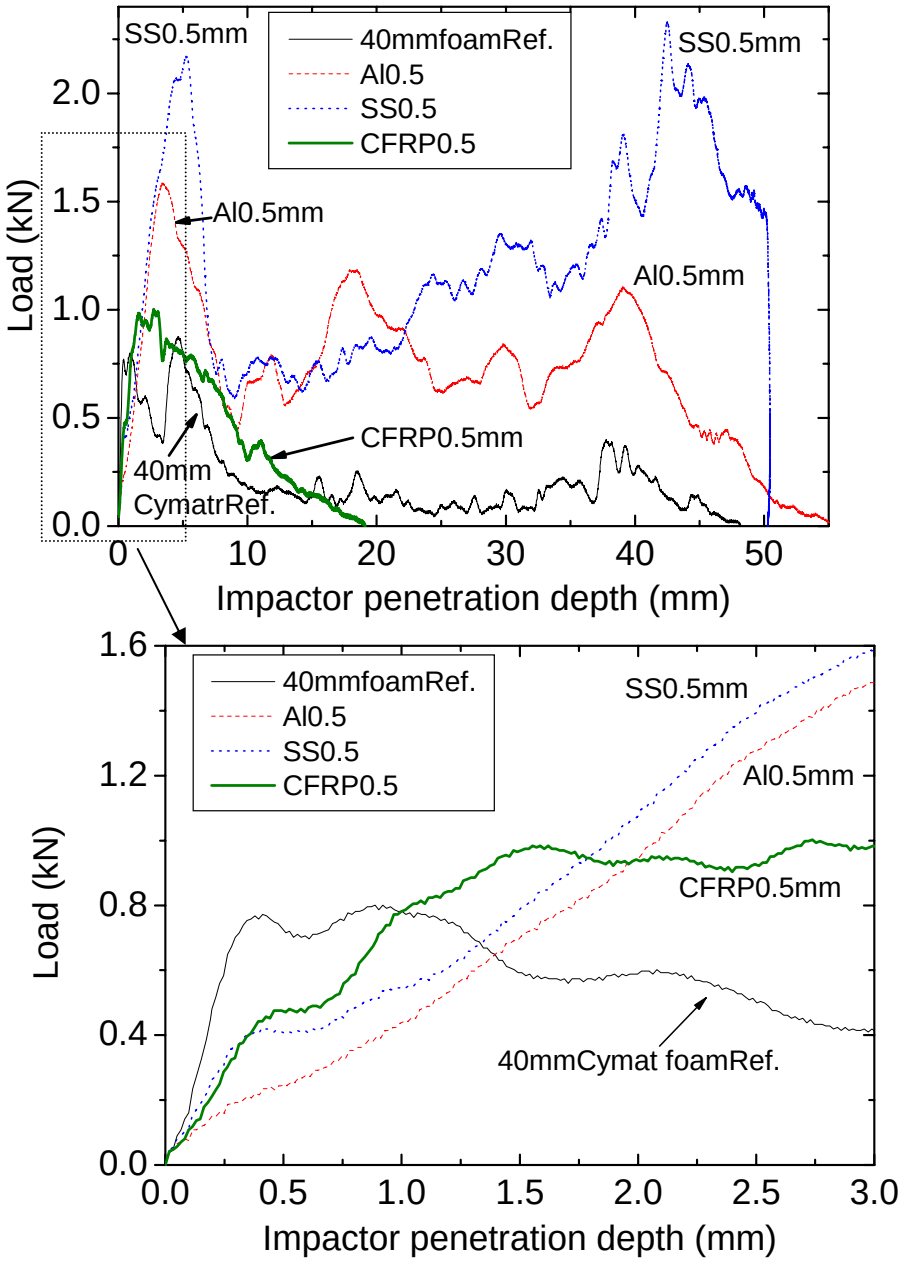

Figure7.19 Comparison of load- impactor penetration depth behavior of Cymat foam of 40 mm thickness with different face sheets of 0.5 mm thickness under impact loading.

Cymat foam block with elastic-perfectly plastic aluminum face sheets of 0.5 mm thickness failed due to face sheet punching. This phenomenon was absent in foam block with 1.0 mm Al sheet due to its high strength. Face sheet bending also takes place due to crumbling of brittle Cymat foam to accommodate the punch profile in both the blocks. Hills and valleys were found in the load–displacement response here because of simultaneously happening of

ATTENTION: The Singapore Copyright Act applies to the use of this document. Nanyang Technological University Library

foam crumbling and face sheet bending, which are clearly observed in Figure 7.21 (c) and 7.21 (d) (top view of impacted specimens).

Resistance to impact in terms of load was found to be the maximum in block with 1.0 mm thick Al face sheet among all the blocks because of large variation of foam cells, more bending of face sheet and crumbling of foam core as shown in Figure 7.21 (d). Important findings in the impacted specimens are marked as shown in Figure 7.21.

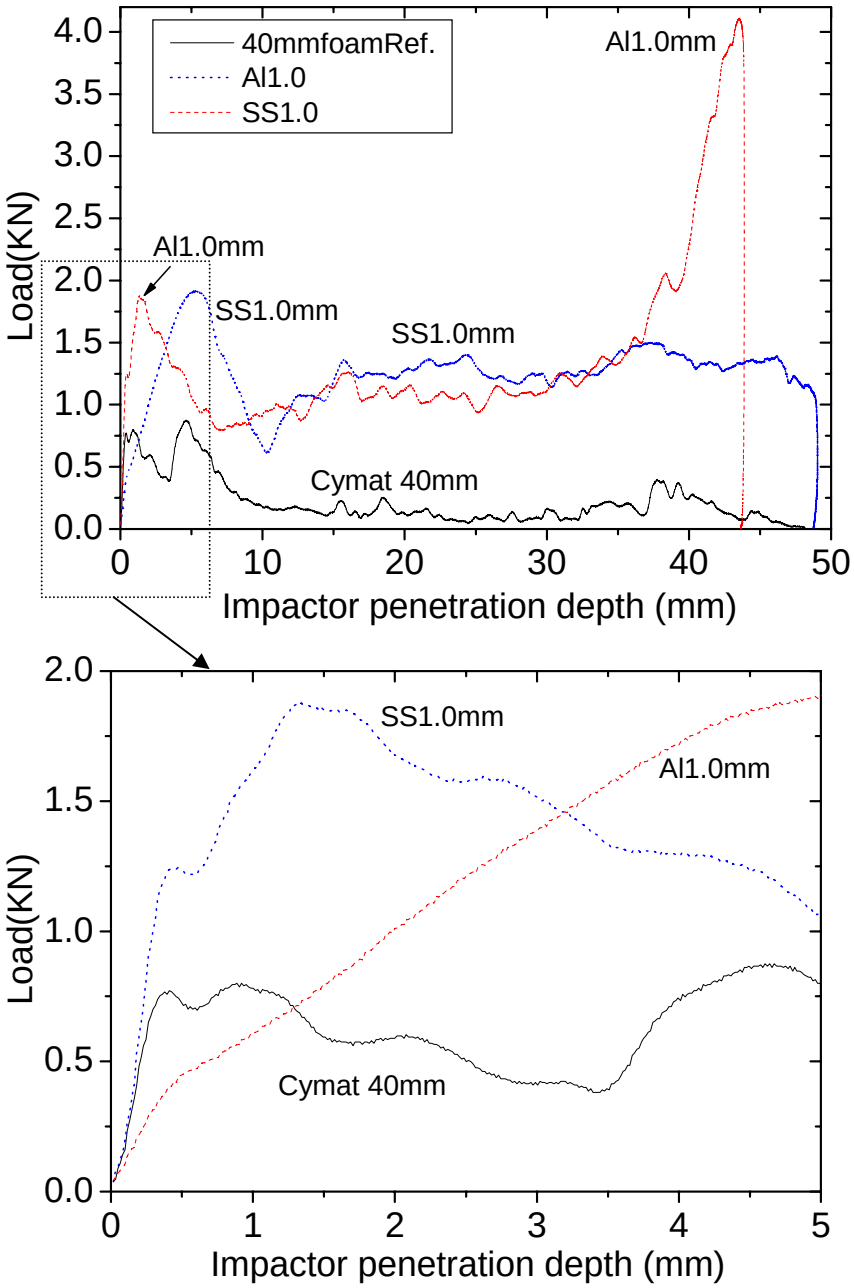

Figure7.20 Comparison of load- impactor penetration depth behavior of Cymat foam of 40 mm thickness with different face sheets of 1.0 mm thickness under impact loading.

ATTENTION: The Singapore Copyright Act applies to the use of this document. Nanyang Technological University Library

In the case of stainless steel face sheets, the initial failure is triggered by the face sheet bending and there is a strong hardening behavior due to face sheet stretching and bending. The face sheet material has to stretch to accommodate the punch profile.

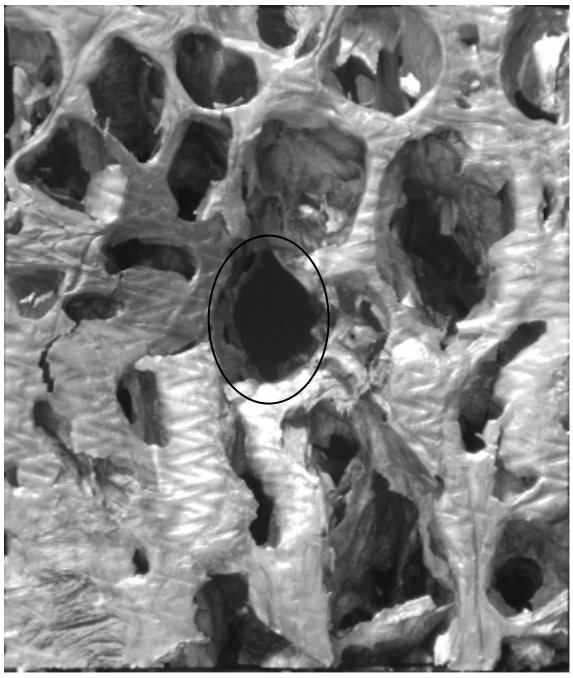

(a)

(b)

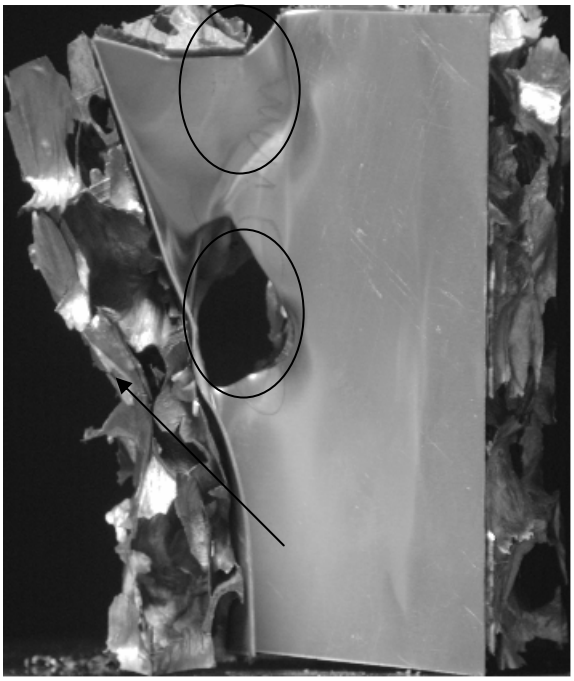

(c)

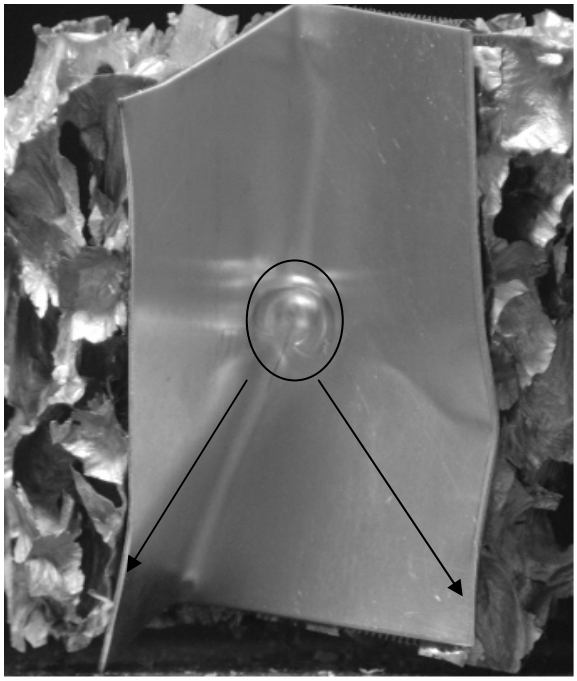

(d)

ATTENTION: The Singapore Copyright Act applies to the use of this document. Nanyang Technological University Library

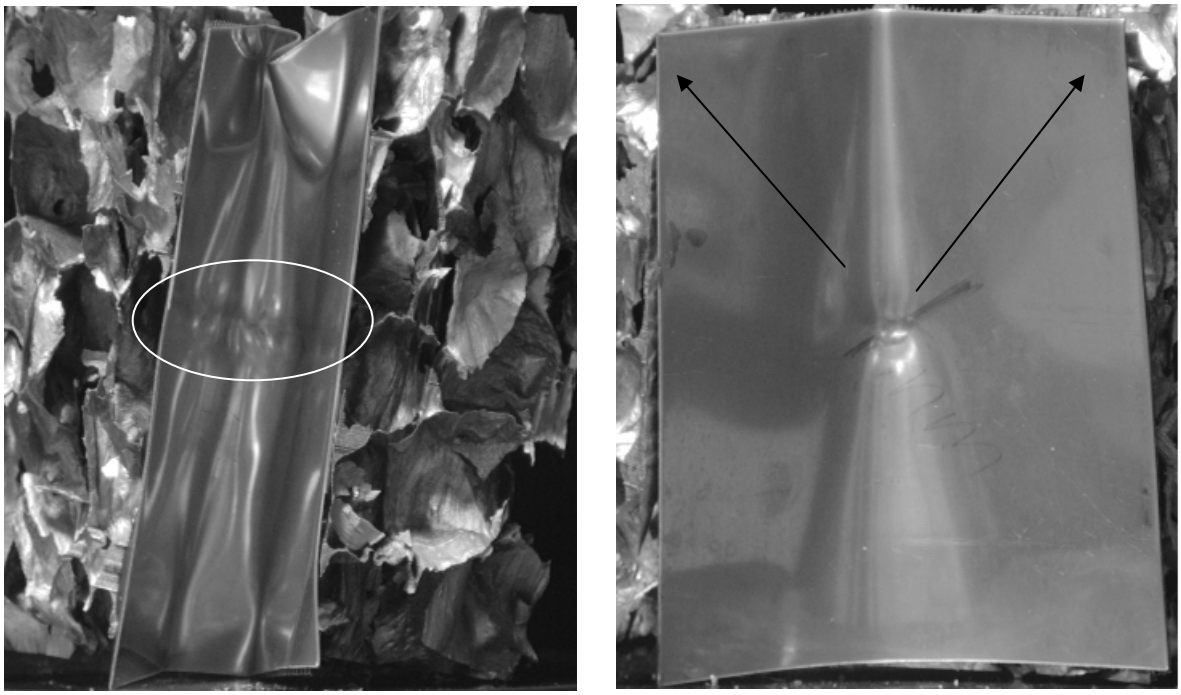

(e) (f)

Figure7.21 Top views of the impacted Cymat foam specimens without and with different face sheet (a) without face sheet, (b) 0.5 mm thick CFRP sheet, (c) 0.5 mm thick Al sheet, (d) 1.0 mm thick Al sheet, (e) 0.5 mm thick SS sheet, and (f) 1.0 mm thick SS sheet.

The rate of hardening in the case of SS face sheet is observed to be much higher than that of Al face sheet due to strain-hardening.

Further loading by impact produces more stretching, and due to this more foam cells start crumbling. This increases the resistance and maximizes as seen in the latter stage of load-displacement response, while this resistance was found to be absent in block with 1.0 mm SS sheet due to more strength of 1 mm SS sheet than 0.5 mm one. A small indent was found with little face sheet bending and stretching in block 40mm thick Cymat foam with 1mm SS sheet. Crumbling of complete foam core was not observed under quasi-static indentation flat punch because at lower strain rate face sheet strength was strong enough to resist the load applied to it.

Load increases up to a peak load in load- displacement response of Cymat foam blocks with CFRP face sheet. Few transverse cracks appear in the face sheet during impact of the foam block. The occurrence of these cracks is most likely due to the low transverse strength of these laminates as compared to the longitudinal strength. Face sheet punching was observed

ATTENTION: The Singapore Copyright Act applies to the use of this document. Nanyang Technological University Library

to be the final failure mechanism for this type of sample block; it can be seen in top view of the impacted specimen (shown in Figure 7.2 (b)). These blocks were found to have damage more locally because of high strain rate than blocks under quasi-static indentation as discussed in Chapter 6.

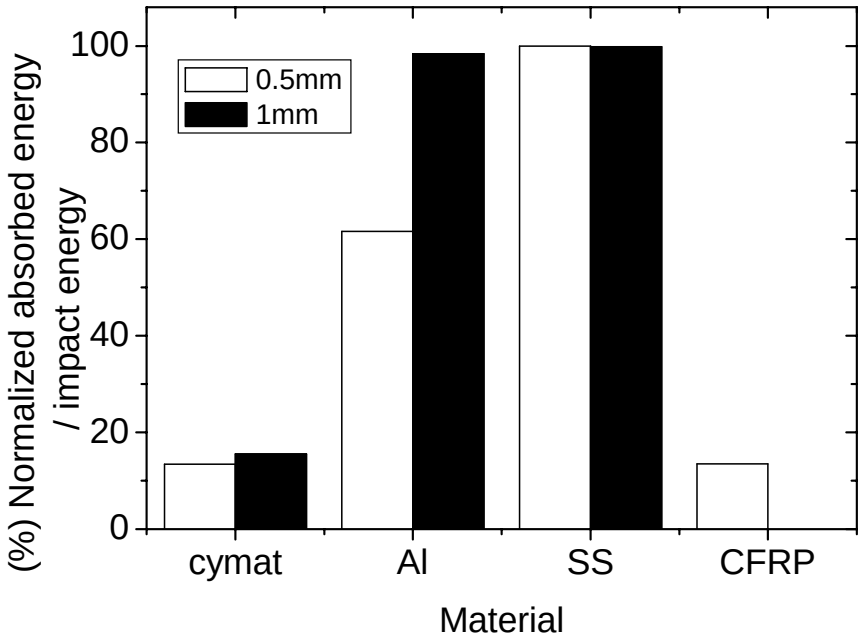

Figure7.22 Normalized absorbed energy vs. blocks of Cymat foam having thicknesses of 40 without and with different face sheet of 0.5mm and 1.0mm thicknesses under impact loading.

Absorbed energy was normalized by impact energy for Cymat foam block with various face sheets of both 0.5mm and 1mm are shown in Figure 7.22. Trend of normalized absorbed energy with impact energy of Cymat foam block with 0.5 mm thick face sheets was found to be similar with Alporas foam block with various face sheets of 0.5 mm thickness. Here, Cymat foam block with 1mm thick Al and both SS face sheet absorbed 100% of the energy. Energy absorbed by foam block with 0.5 mm thick CFRP sheet is found to be less than the foam block which indicates that the unidirectional laminate is not a good energy absorber. A large variation of cells in Cymat foam is the main reason for the deteriorated performance.

ATTENTION: The Singapore Copyright Act applies to the use of this document. Nanyang Technological University Library

Chapter -8

Sandwich structure of Al foam core with Al face sheet and Al tube under compression

8.1 Introduction

Sandwich structures are used as columns or tubes to support compression load in some engineering applications such as aircraft wings or car bumpers. For design purposes, it is necessary to investigate the failure behavior of sandwich columns under end compression to identify the competing failure modes. For the potential applications for protective energy absorption, the performance of these structures in terms of energy absorption should be studied. To achieve these two goals, work for this chapter is divided in two parts: firstly, the sandwich panels of Al foam core with Al sheets under compression, and secondly, the compression of rectangular Al tube filled with Al foam core.

For the first part, design formulae for failure load in different failure mechanisms are first provided. Then, limited experiments were carried out to investigate the failure mechanism in sandwich columns comprising Alporas foam core and Al face sheets under end compression. Finally, a failure mode map is constructed to show the overview of failure mechanism in terms of non-dimensional geometrical parameters and expressions for minimum weight design are deduced. For the second part, enhancement in the energy absorption capacity of rectangular Al tubes filled with Alporas foam is investigated experimentally. Energy absorption capacity of Al tubes and Al foams were investigated individually, and experiments were then performed on Al tubes filled with Al foam.

8.2. Analytical analysis of sandwich column under end compression

Consider a sandwich column of width b and length l, comprising of two identical face sheets of thickness, t and foam core of thickness, c. The column is subjected to end compression loading as shown in Figure 8.1: end load P is applied through loading platen and end tap were applied to prevent slippage.

ATTENTION: The Singapore Copyright Act applies to the use of this document. Nanyang Technological University Library

8.2.1. Estimation of failure loads

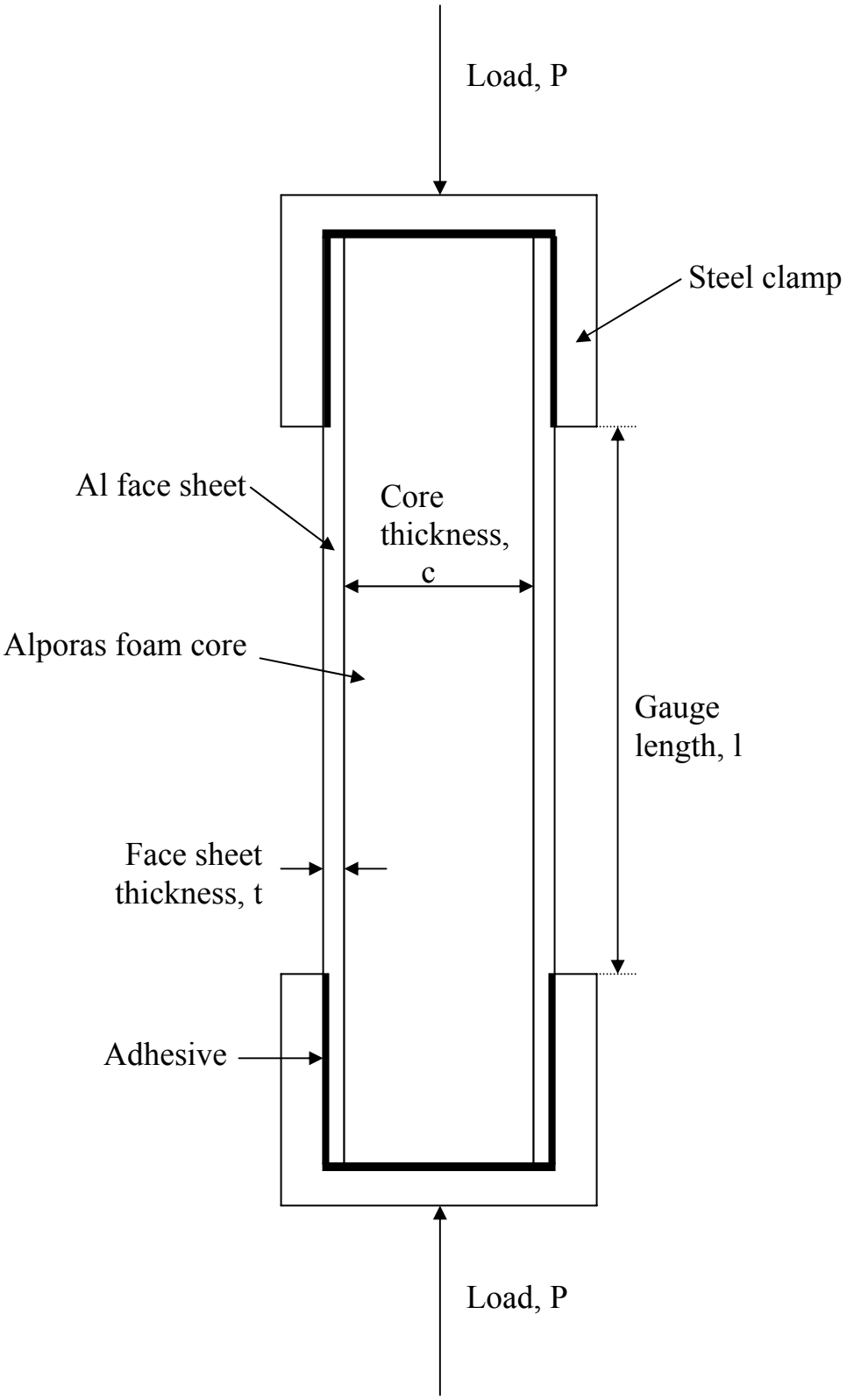

Figure8.1 A sandwich column consisting of Alporas foam core and Al face sheets under end compression.

ATTENTION: The Singapore Copyright Act applies to the use of this document. Nanyang Technological University Library

The analytical formulae for the different possible failure modes were discussed in the following paragraphs. During compression loading of the sandwich panel, the face sheets carry the uniaxial loads and the core bears the transverse shear forces.

A total of four possible mutually competing modes can occur for the sandwich column as shown in Figure 8.2: face sheet yielding, core shearing, elastic Euler macro-buckling, and face sheet wrinkling.

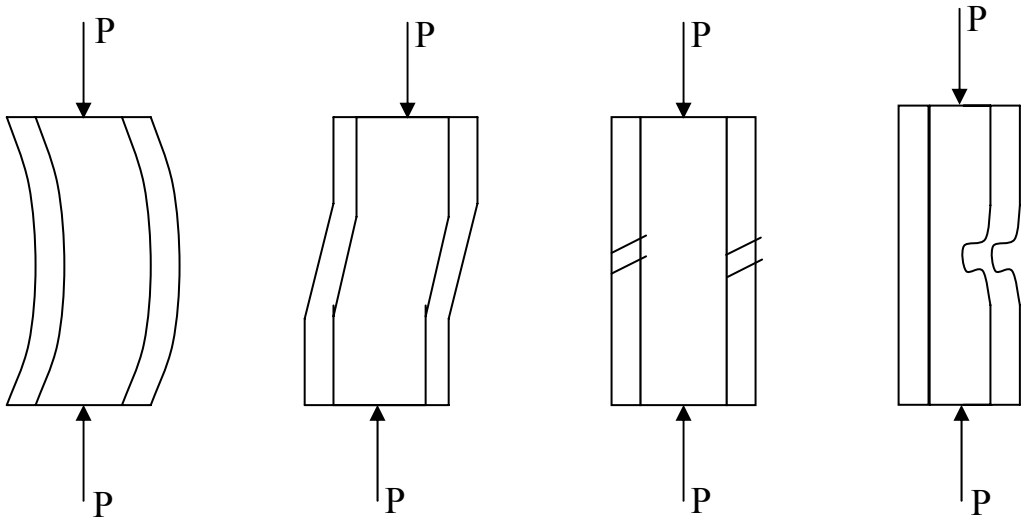

Figure8.2 Failure modes in sandwich columns subjected to end compression (a) Elastic Euler macro-buckling (b) Core shearing, (c) Face sheet yielding and, (d) Face sheet Wrinkling.

8.2.1.1 Euler macro-buckling

It was assumed that the sandwich column fails under Euler buckling when bending of the column starts with negligible rotation of column because fully constraints column with end tabs. Euler buckling failure load is estimated as

$$F_E = \frac{4\pi^2 (EI)_{eqv.}}{l^2} \tag{8.1}$$

$(EI)_{eqv.}$ is the equivalent flexural rigidity of the sandwich column and is given by

$$(EI)_{eq} = \frac{E_f btd^2}{2} + \frac{E_f bt^3}{6} + \frac{E_c bc^3}{12} \approx \frac{E_f btc^2}{2} \tag{8.2}$$

where $d = c + t$ is the spacing between the mid plane of the face sheets. E_f and E_c are the Young's moduli of the face sheet and foam core materials, respectively.

Combining equations (8.1 and 8.2) the failure load for Euler macro-buckling is given by

ATTENTION: The Singapore Copyright Act applies to the use of this document. Nanyang Technological University Library

$$F_E = \frac{2\pi^2 E_f btc^2}{l^2} \tag{8.3}$$

8.2.1.2 Core shear

It was assumed that the sandwich column fail under core shear when shearing of core start with negligible contribution of face sheet in resistance to rotation. Core shear failure load is estimated with shear stiffness of core is shown as

$$F_{CS} = (AG)_{eqv} = bcG_c \tag{8.4}$$

8.2.1.3 Face sheet yielding

It was assumed that the face sheet starts yielding when the face sheet of the sandwich column attains the failure strength of σ_y^f . With the assumption that the foam core is more compliant failure load for face sheet yielding is estimated as

$$F_{FSY} = 2bt\sigma_y^f \tag{8.5}$$

8.2.1.4 Face sheet wrinkling

Wrinkling is the short-wave length elastic buckling of the face sheets. It was assumed that the sandwich column fail under face sheet wrinkling, when a face sheet buckle with short wavelength as elastic beams supported upon a linear elastic foundation. The compressive stress in the face sheet for wrinkling is estimated with negligible stress in core given by

$$F_{FSW} = 0.5(E_f E_c G_c)^{1/3} \tag{8.6}$$

8.2.2. Experimental procedure for sandwich columns under end compression

Mechanical characterization of the materials (Alporas foam core and Al face sheets - Al 1050) involved in these sandwich columns were explained in Chapter 3. The practically possible geometries of the sandwich columns were tested with the help of Alporas foam and Al face sheets of different dimensions. In the present work, Al face sheets of thickness of 0.5 mm and 3.0 mm and Alporas core of 9.5% relative density with varying dimensions are employed to fabricate the columns. Fuller details of sandwich columns geometries are listed in Table 8.1. Sandwich columns of 20 mm width were prepared by bonding Al face sheets to Alporas foam core using Redux–322 adhesive* (as explained in details in chapter 4).

* supplied by Hexel Composites, Australia

ATTENTION: The Singapore Copyright Act applies to the use of this document. Nanyang Technological University Library

End compression test on sandwich columns were carried out according to ASTM STD. C-364 [152]. Specimens were bonded onto a U clamp with epoxy adhesive, in order to prevent slippage (which could occur in lengthy specimens such as geometry-1 Table-8.1), as shown in Fig. 8.1. Longitudinal strain on the face sheets was measured using strain gauges placed at mid length of the face sheets. Loading was applied at a displacement rate of 1 mm/sec. Precautions were taken to ensure that the sandwich column was flat and parallel. Snapshots of the loaded sandwich columns were taken at every significant change in the geometry.

Table8.1 Geometry of sandwich columns under end compression (all dimensions are in mm).

Specimen geometry	**Core thickness, *c mm***	**Face sheet thickness, *t mm***	**Column length, *l* mm**	**Expected failure mode**
EC 1	5	0.5	500	Euler buckling
EC 2	10	3.0	60	Core shear
EC 3	20	3.0	140	Face sheet yielding

8.2.3. Comparison of analytical and experimental results of end compression of sandwich columns with Al foams

A failure mechanism map is constructed that present an overview of the different failure mechanisms that can take place for these sandwich columns under end compression depending on various geometrical parameters. A total of three failure modes namely, Euler buckling, core shear and face sheet yielding were identified for sandwich columns consisting of Al face sheet and Alporas foam core. But only two competing modes, Euler buckling and core shear, were verified experimentally while face sheet yielding was not occurred due to failure of those columns from bond failure. In the following paragraphs, the experimentally measured load-displacement responses are compared with analytical predictions.

8.2.3.1 Failure mechanisms map for sandwich column under end compression

For a given sandwich column geometry and material system the dominating failure mode is the one which requires the lowest load to fail among all possible modes. A failure mechanism map (pioneered by Gibson and Ashby [10]) is drawn in Figure 8.3 in terms of non-dimensional parameters of core thickness normalized with columns length ($\bar{c} = c/l$) and face sheet thickness normalized with core thickness ($\bar{t} = t/c$) based on the analytical formulae

ATTENTION: The Singapore Copyright Act applies to the use of this document. Nanyang Technological University Library

presented in section 8.2.1 for a fixed material system **(**with fixed ratio of $\left(\frac{E_f}{\sigma_f^y}\right)$=627.27and $\frac{G_c}{\sigma_f^y}$=0.55).

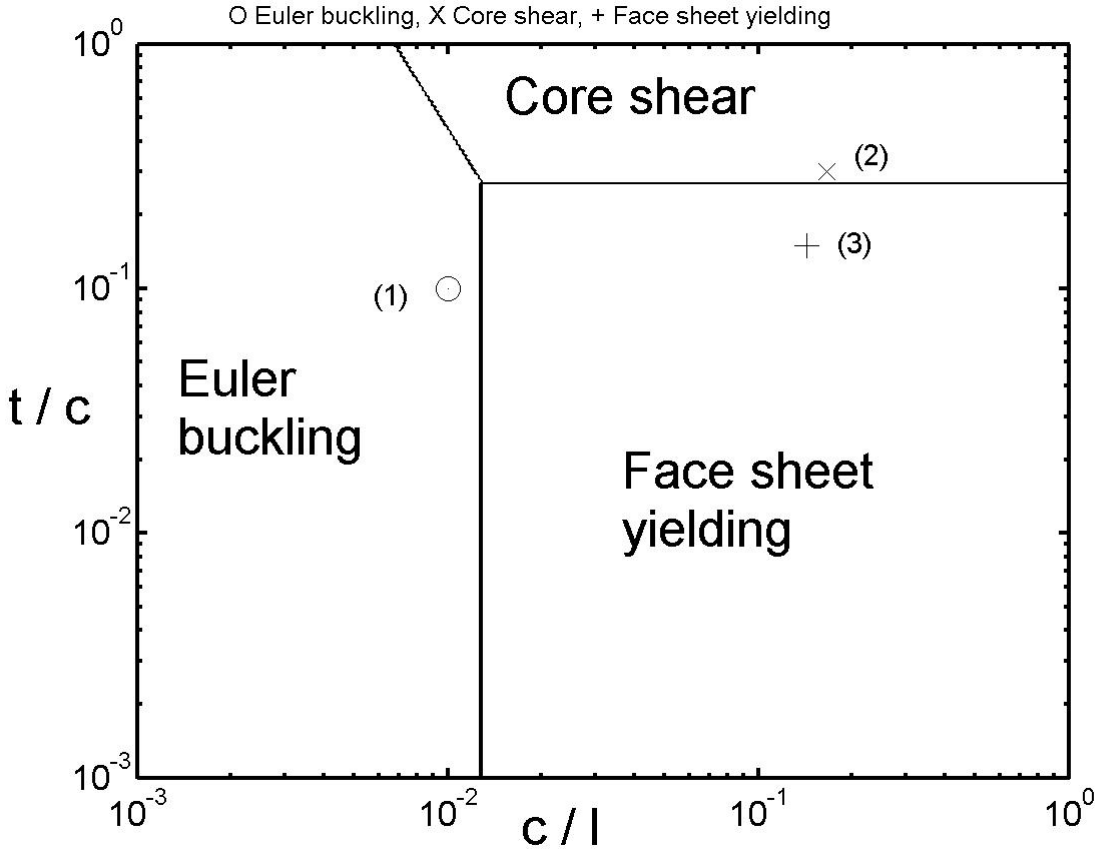

Figure8.3 Failure mechanisms map for sandwich column having Alporas foam core and Al face sheets showing all the possible failure modes (geometries of sandwich column are numbered according to Table-8.1) with fixed ratio of $\left(\frac{E_f}{\sigma_f^y}\right)$=627.27and $\frac{G_c}{\sigma_f^y}$=0.55.

Size ratio effect for shear failure was not incorporated in this map because the specimen in which shear failure was predicted analytically has normal shear strength (size ration is more than 2.67) [25]. It shows an overview of all the possible failure modes with the locations of the selected geometry of sandwich column in each region. Face sheet wrinkling failure was not observed in the present study due to higher face sheet wrinkling failure loads than other modes due to term of high young's modulus of face sheet (equation 8.6). The boundaries of the failure mechanisms are derived by equating failure load equations by taking two of them in each turn (equation 8.1, 8.2 and 8.5).

ATTENTION: The Singapore Copyright Act applies to the use of this document. Nanyang Technological University Library

It is clear from Figure 8.3 that Euler macro-buckling failure occurs for the column with very large lengths which turns into face sheet yielding if length is reduced or if there is increase in thickness of foam core. Core shear dominates for short columns with thick face sheets. In the present investigation, due to the practical constraints in the dimensions of the materials (such as making of foam core with length of more than 500 mm with low thickness of 5 mm), geometries of sandwich columns for experimentation are carefully chosen to cover the maximum possible competing failure mechanisms.

8.2.3.2 Results and discussion

The load versus displacement curve for sandwich column geometry-1 (Table 8.1), failed experimentally due to Euler macro-buckling was compared with analytical calculations as shown in Figure 8.4 (a). The load increases monotonically with displacement in a linear elastic manner up to a peak load and then start dropping smoothly. Analytical prediction (Equation 8.3) for failure was found to close with experimental observation. Euler buckling failure was identified by the overall deformation mode of the column. It is clear in the snapshot of sandwich column taken at failure as shown in Figure 8.5 (a) at a displacement of 7 mm.

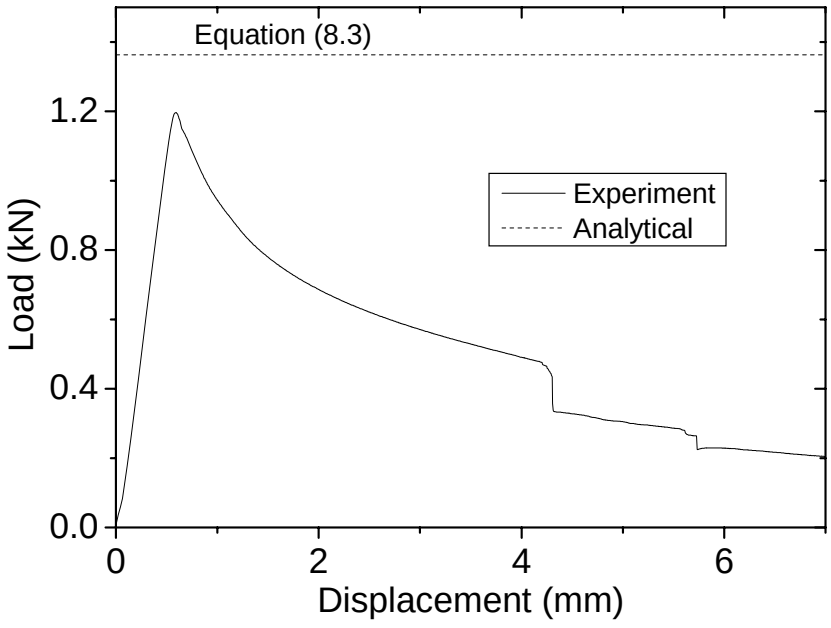

(a)

ATTENTION: The Singapore Copyright Act applies to the use of this document. Nanyang Technological University Library

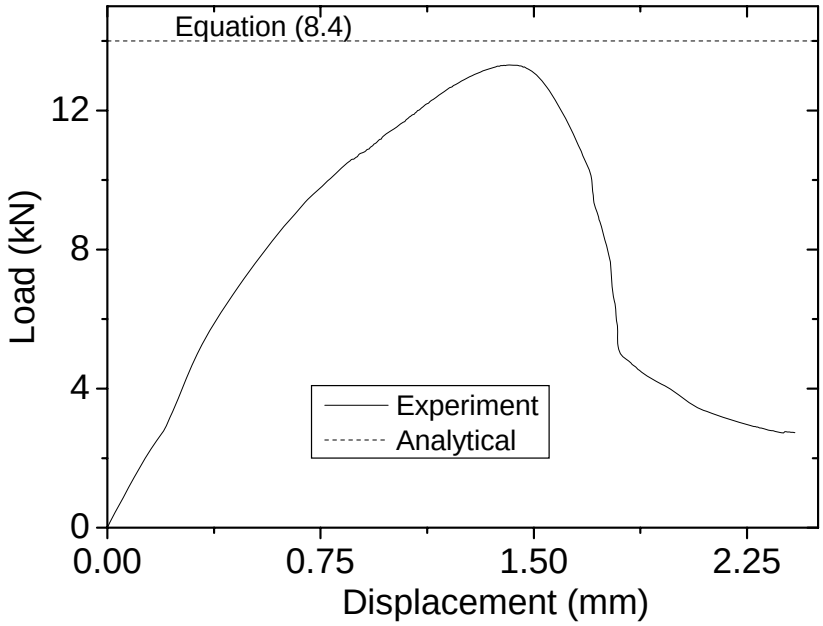

(b)

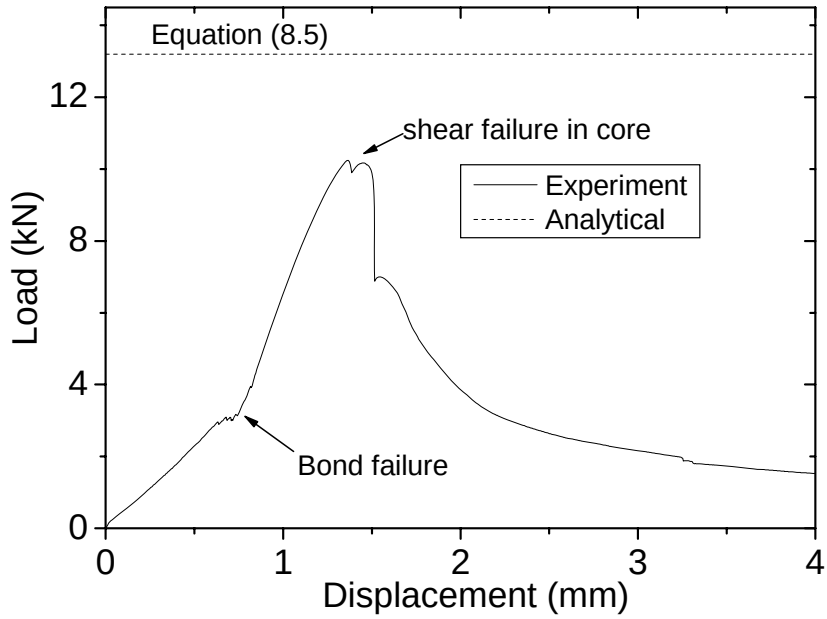

(c)

Figure8.4 Load and displacement curves derived from analytical and experimental observations for the sandwich column (a) Geometry no-1 (Table-8.1) failed under Euler macro-buckling (b) Geometry no-2 (Table-8.1) failed under core shear (c) geometry no-3 in Table-8.1 expected to fail under face sheet cracking but shearing occurs in foam core after bond failure.

The load versus displacement curve for sandwich column geometry - 2 (Table-8.1), failed experimentally by core shear was compared with analytical calculations as shown in Figure 8.4 (b). Load displacement response of the column failure under core shear is similar to

ATTENTION: The Singapore Copyright Act applies to the use of this document. Nanyang Technological University Library

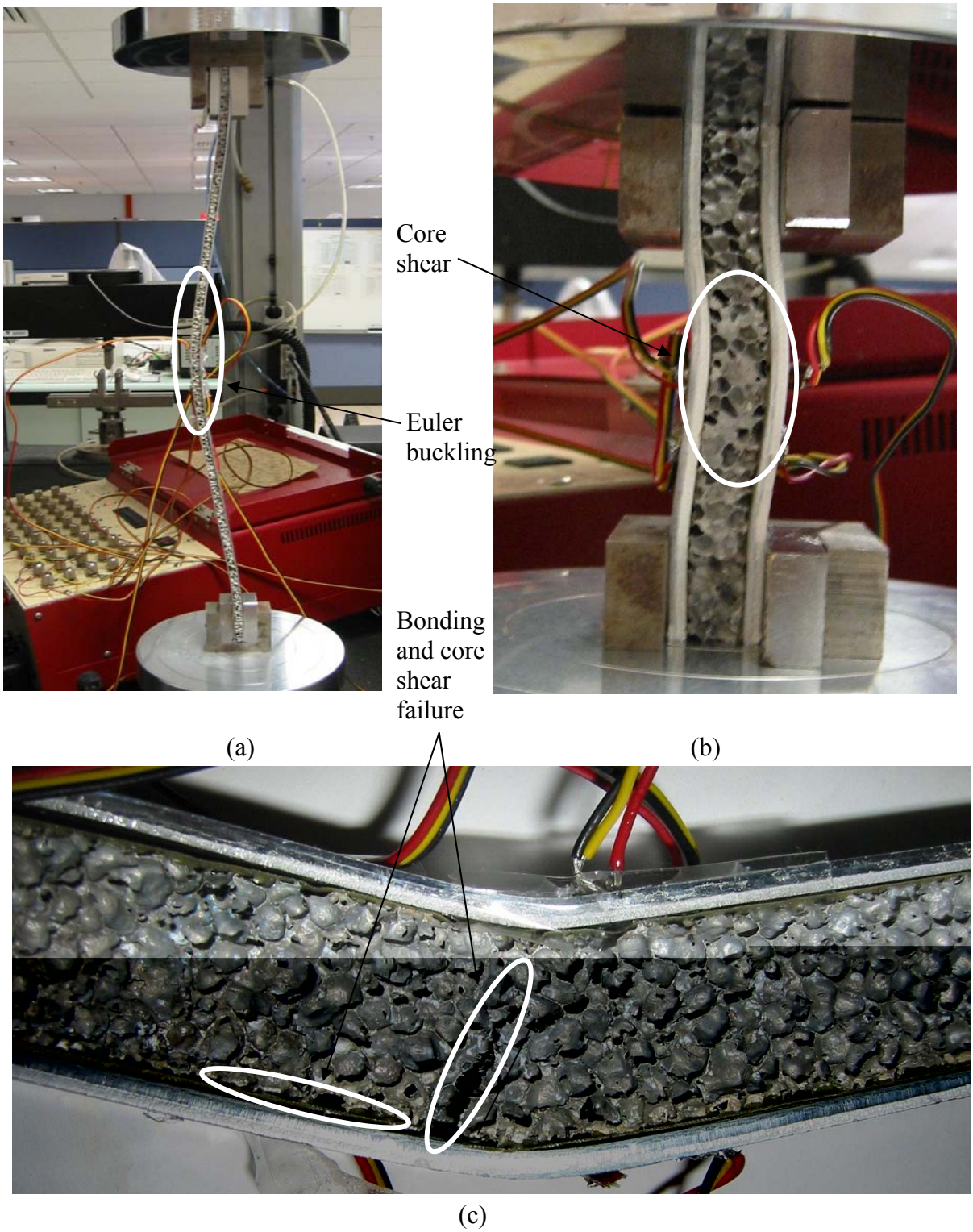

Figure8.5 Snap shots of the sandwich column specimens failed by different mechanisms (a) Euler macro-buckling failure for geometry – 1 (Table 8.1) at a displacement of 7 mm (b) core shear failure for geometry – 2 (Table-8.1) at a displacement of 2 mm (c) expected to fail under face sheet yielding for geometry –3 (Table-8.1) but shows shearing in foam core after bond failure at a displacement of 4mm.

ATTENTION: The Singapore Copyright Act applies to the use of this document. Nanyang Technological University Library

response observed for shear testing of Alporas foam core alone (Chapter-3). Load increased non-linearly with displacement to a maximum value and then dropped suddenly.

Here, the analytical prediction (Equation 8.4) for failure load is about 5% higher than the experimental measured value. Core shear failure was identified by initial deformation mode of the column similar to Figure 8.2 (b). It is clear in the snapshot of sandwich column as shown in Figure 8.5 (b) taken at a displacement of 2 mm.

The load-displacement response for sandwich column geometry - 3 (Table-8.1), expected to fail experimentally by face sheet yielding was compared with analytical calculations as shown in Figure 8.4 (c). All the columns with geometry-3 were failed by bond failure and that was the reason failure starts much earlier than the value expected by analytical solution. Shearing in Alporas foam core was started after bond failure between core and face sheet as shown in Figure 8.5 (c). The bond failure in the sandwich column occurred at around 0.7mm displacement as shown in the change of slope in the load-displacement response of this geometry as shown in Figure 8.4 (c). The sandwich column is also able to take more loads due to the foam core. It continued till the peak load where shearing of the core occurred and then the load dropped drastically. Another reason for this specimen to fail under core shear is that the geometry lies near to boundary of face sheet yielding and core shear in failure map as shown in Figure 8.3.

8.2.4 Minimum weight design

The structure should always be minimized to minimum weight for a given load-carrying capacity to minimize the cost and environmental impact. Minimum weight of the sandwich column can be found out for a given load carrying capacity as explained in Chapter 4. Non-dimensional terms such as face sheet thickness $\bar{t}$, core thickness $\bar{c}$, ratio of strength of core to face sheet $\overline{\sigma}$ and density ratio $\overline{\rho}$ are defined by equation 4.22 and 4.23 in Chapter 4.

Non-dimensional mass index ($\overline{M}$) and structural load index $\overline{F}$ of the sandwich column are also defined by equation 4.24 and 4.25 in Chapter 4.

The structural load index (non-dimensional form of load) for Euler buckling, core shear and face sheet yielding (considering equation 8.3, 8.4 and 8.5) can be expressed as

ATTENTION: The Singapore Copyright Act applies to the use of this document. Nanyang Technological University Library

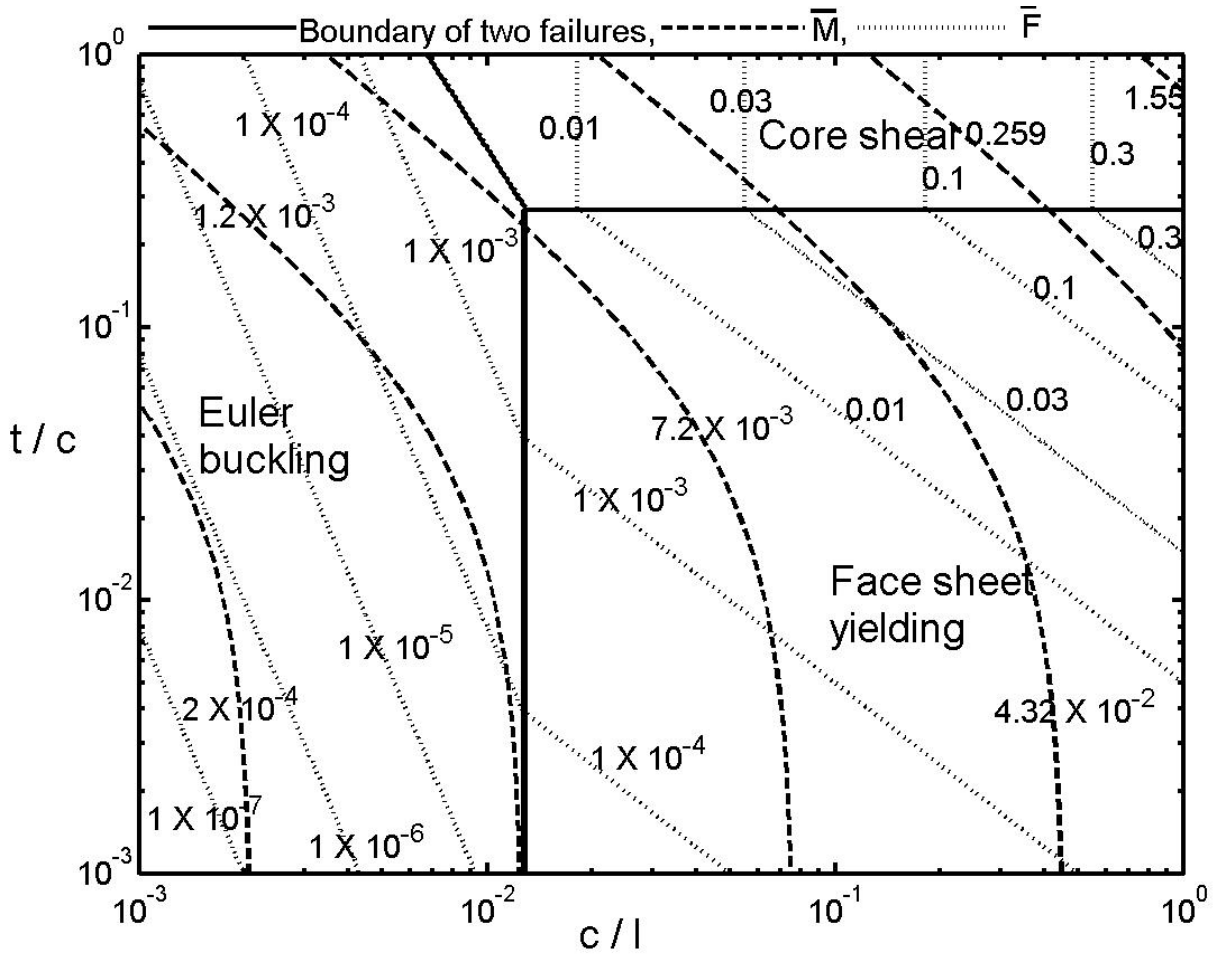

Figure8.6 Contours of the dimensionless mass index $\overline{M}$ and structural load index $\overline{F}$ in collapse mechanism map of sandwich column of Alporas foam core with Al face sheet having $\left(\frac{E_f}{\sigma_f^y}\right) = 627.27$, $\frac{G_c}{\sigma_f^y} = 0.55$ and $\overline{\rho} = 0.095$.

$$\overline{F}_E = 2\pi^2 \bar{t}\left(\bar{c}\right)^3 \left(\frac{E_f}{\sigma_f^y}\right) \tag{8.7}$$

$$\overline{F}_{CS} = \bar{c}\frac{G_c}{\sigma_f^y} \tag{8.8}$$

$$\overline{F}_{FSY} = 2\bar{c}\bar{t} \tag{8.9}$$

Optimum weight design can be defined with the selection of column geometry which minimizes the mass index $\overline{M}$ for a particular structural load index $\overline{F}$. Contours of $\overline{M}$ and $\overline{F}$ are added to the failure mechanism map in Figure 8.6 with collapse for sandwich column comprising Alporas foam core and Al face sheet with $\left(\frac{E_f}{\sigma_f^y}\right) = 627.27$, $\frac{G_c}{\sigma_f^y} = 0.55$ and $\overline{\rho}$ =

ATTENTION: The Singapore Copyright Act applies to the use of this document. Nanyang Technological University Library

0.095. Both these contours are increasing towards the leading diagonal of the map with increasing $\bar{t}$ and $\bar{c}$.

The analytical expression for minimum mass index of sandwich column can be found for each failure mode by the procedure that was explained in Chapter 4. By following the same steps, minimum mass index expression was obtained for each failure mode with optimum parameters ($\bar{c}$ and $\bar{t}$). Minimum mass index expression for core shear, face sheet yielding, Euler macro-buckling, core shear-Euler buckling, core shear-face sheet yielding and face sheet yielding-Euler macro-buckling is shown below:

$$\left(\overline{M}_{\min}\right)_{CS} = 0.1738\overline{F} \tag{8.10}$$

$$\left(\overline{M}_{\min}\right)_{FSY} = \overline{F} \tag{8.11}$$

$$\left(\overline{M}_{\min}\right)_{E} = 0.021\left(\overline{F}\right)^{1/3} \tag{8.12}$$

$$\left(\overline{M}_{\min}\right)_{CS-E} = \frac{4.805\times10^{-5}}{\overline{F}} + 0.173\overline{F} \tag{8.13}$$

$$\left(\overline{M}_{\min}\right)_{CS-FSY} = 1.173\overline{F} \tag{8.14}$$

$$\left(\overline{M}_{\min}\right)_{FSY-E} = 1.047\overline{F} \tag{8.15}$$

The minimum weight design is found by calculating the minimum mass index $\overline{M}_{\min}$ necessary to suppress all possible failures for a given structural load index $\overline{F}$. Therefore, the dominant mechanism or combination of mechanisms (at the boundary of two failures), is the one with the largest value of $\overline{M}_{\min}$ at each value of $\overline{F}$. To obtain a clear picture of minimum weight design, the largest $\overline{M}_{\min}$ for each value of $\overline{F}$ is plotted for each failure mode and

ATTENTION: The Singapore Copyright Act applies to the use of this document. Nanyang Technological University Library

combination of modes, which is shown in Figure 8.7 (a). This local minimum mass design map is valid only for $\left(\frac{E_f}{\sigma_f^y}\right) = 627.27$, $\frac{G_c}{\sigma_f^y} = 0.55$ and $\bar{\rho} = 0.095$.

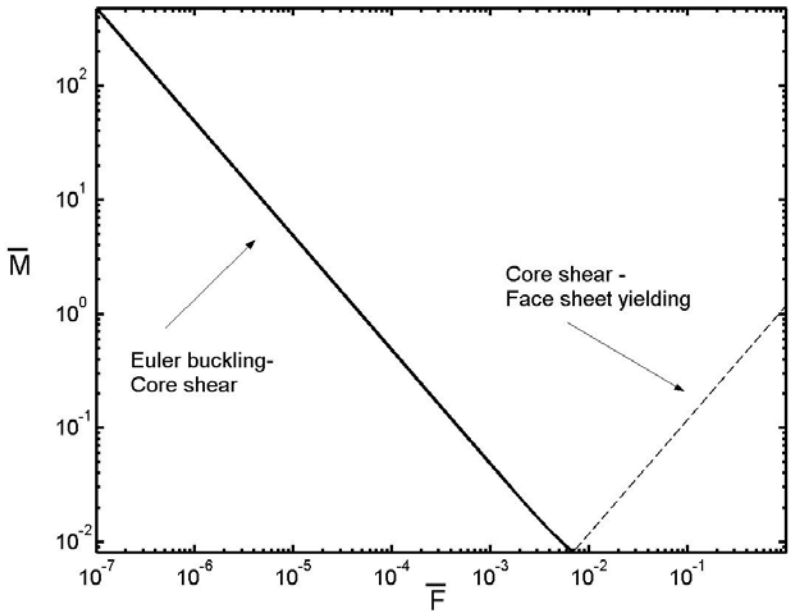

(a)

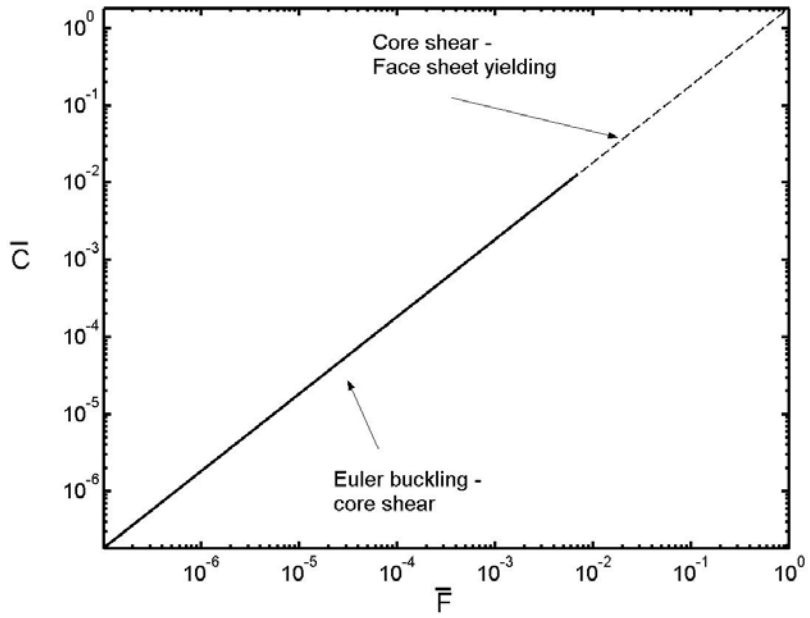

(b)

ATTENTION: The Singapore Copyright Act applies to the use of this document. Nanyang Technological University Library

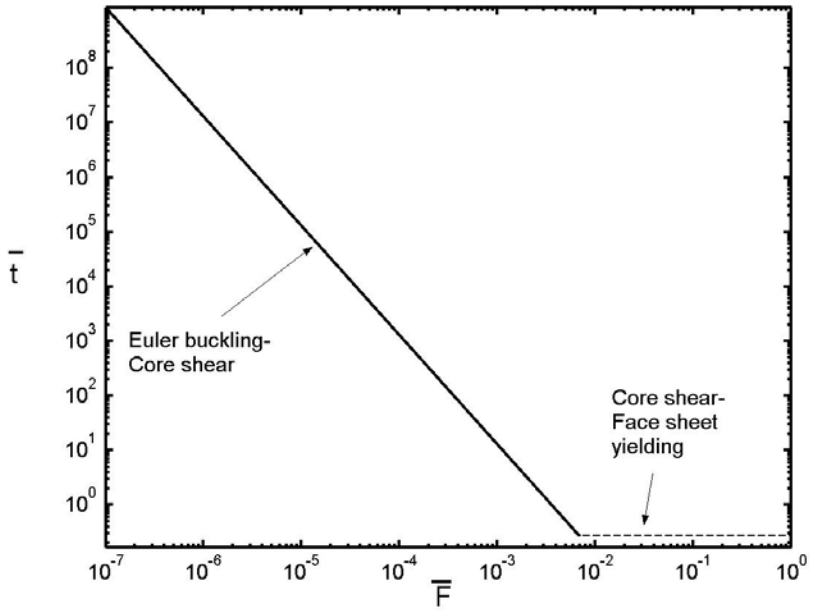

(c)

Figure8.7 Minimum weight design of sandwich column with Alporas foam core and Al face sheet with optimum geometrical parameters having $\left(\frac{E_f}{\sigma_f^y}\right) = 627.27$, $\frac{G_c}{\sigma_f^y} = 0.55$ and $\bar{\rho} = 0.095$ (a) Variation of minimum mass index $\bar{M}$ with structural load index $\bar{F}$ considering for all failure modes (b) Variation of $\bar{c}$ with structural load index $\bar{F}$ for minimum weight design of sandwich column (c) Variation of $\bar{t}$ with structural load index $\bar{F}$ for minimum weight design of sandwich column.

The trend of minimum weight design was found to be in a decreasing order with structural load index due to the denominator term of $\bar{F}$ in minimum mass design index expression for core shear-Euler buckling failure boundary. If these parameters will be changed then the values of the map will change but the trend would remain almost the same.

It was observed from the Figure 8.7 (a) that the minimum weight design is achieved at the boundary between Euler buckling and core shear for lower values of $\bar{F}$ and the boundary between core shear and face sheet yielding for higher values of $\bar{F}$ with constant values of $\left(\frac{E_f}{\sigma_f^y}\right) = 627.27$, $\frac{G_c}{\sigma_f^y} = 0.55$ and $\bar{\rho} = 0.095$. The associated optimum geometrical parameters ($\bar{c}$ and $\bar{t}$) are also plotted with structural load index as shown in Figure 8.7 (b) and (c). The trend of $\bar{c}$ was found to be always in an increasing linear manner with structural

ATTENTION: The Singapore Copyright Act applies to the use of this document. Nanyang Technological University Library

load index for both boundaries of failure loads while $\bar{t}$ was found to be in decreasing order with lower structural load index but remain constant for higher structural load index. Similarly, the global minimum weight design can also be constructed for the sandwich column having Alporas foam core with Al face sheet for various density ratio.

8.2.5 Compression of Alporas foam filled Al tubes

Here, energy absorption capacity of rectangular Al tubes filled with Alporas foam with failure analysis is discussed.

8.2.5.1 Experimental procedure

Experimental studies are divided into four groups according to specimens tested under compression, as shown in Table 8.2. According to the first group, compression testing was carried out only on empty Al rectangular tubes. In the second group, compression testing was performed on block of Al foams of same size. The effect of foam filling in those tubes was studied in third group with compression testing of those tubes with Al foam blocks of same size without any adhesive. Effect of adhesive in energy absorption for those tubes was studied in fourth group with compression testing of those tubes with Al foam blocks of same size with adhesive. Accordingly, a total of nine rectangular Alporas foam blocks of 10 cm X 5 cm X 4 cm and nine Al hollow tubes of 10 cm X 5.2 cm X 4.2 cm with wall thickness of 1.0 mm were cut.

Rectangular Alporas foam blocks of 10 cm X 5 cm X 4 cm were fitted tightly into the Al hollow tube of 10 cm X 5.2 cm X 4.2 cm (internal dimension) with wall thickness of 1.0 mm. Before putting adhesive, both inside walls of hollow tubes and outside of foam specimens were carefully degreased using acetone.

Table8. 2 Details of specimens tested under compression

Group	Number of specimens	Type of specimen
1	3	Al hollow tube
2	3	Alporas foam block
3	3	Un-bonded Al tube filled with Alporas foam block
4	3	Bonded Al tube filled with Alporas foam block

ATTENTION: The Singapore Copyright Act applies to the use of this document. Nanyang Technological University Library

Alporas foam blocks were wrapped with the Redux 322 adhesive thin layer and pushed gently to fit tightly into the Al hollow tube. Those Al foam filled tubes were put into the oven at temperature of 175^0 C for 1 hour for adhesive curing, as explained in Chapter 3.

Figure8.8 A bonded Al tube filled with Alporas foam during compression testing.

A load cell of capacity 50 kN was used to carry out those experiments and the loading was set to displacement control with an initial rate of 1.0 mm/min which is increased to 2.0 mm/min when the foam starts to collapse plastically. A typical setup of metal tube filled with Alporas foam during compression testing is shown in Figure 8.8.

Terminology used in tube compression is defined [153] as follows:
Total energy absorbed AE and mean force F_m are given by

$$AE(s) = \int_0^{cs} F(\overline{cs})d\overline{cs} \tag{8.16}$$

and

ATTENTION: The Singapore Copyright Act applies to the use of this document. Nanyang Technological University Library

$$F_m(cs) = \frac{AE(cs)}{cs} = \frac{\int_0^{cs} F(\overline{cs})d\overline{cs}}{cs} \tag{8.17}$$

where F is the applied compressive force and cs is the axial compressive displacement of the test rig (with integration variable $\overline{cs}$).

Assuming that the contribution due to elastic deformations is negligible, W can be regarded approximately as the energy dissipated by plastic deformation.

The stroke efficiency St_e is defined as

$$\mathrm{St_e} = \frac{S_{st}}{\mathrm{cl}} \tag{8.18}$$

where S_{st} means the stroke length (it is the length up to which the compression displacement is consider. There is no universal rule so far for considering this length. In the present study, it is considered as the displacement after plateau and at minimum load before steepness in the loading), and cl is the total length of the un-deformed crush element (which is the remaining uncrushed displacement of the tube; it is subtraction of stroke length from the total length of tube).

Mean force efficiency S_f show a comparison of the mass related mean force levels of crush elements which consist of different materials and is defined as

$$\mathrm{S_f} = \frac{F_m}{\sum \rho_i A_i} \tag{8.19}$$

Where ρ_i is density and A_i is cross-sectional area of different materials made crush element.

Specific mass energy absorption S_e, is a measure for the total energy absorption capacity per unit mass and is defined by

$$\mathrm{S_e} = \frac{W(S_{st})}{\mathrm{m_t}} \tag{8.20}$$

where m_t is the mass of the tube.

All these parameters depend upon the selection of 'cs', if it is considered as maximum (cs_{max}) then all the parameters such as AE, F_m will be considered as AE_{max}, and F_{max} respectively.

ATTENTION: The Singapore Copyright Act applies to the use of this document. Nanyang Technological University Library

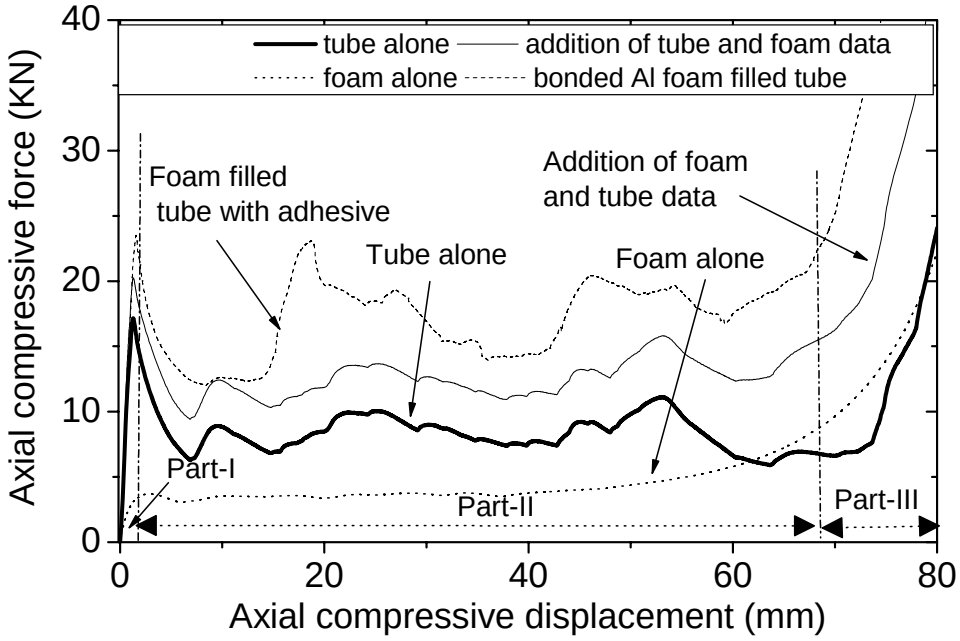

Figure8.9 Comparison of load-displacement response of bonded Al tube filled with Alporas foam under compression with response of individual constituents.

8.2.5.2 Energy absorption of Al foam with Al tube in compression

A comparison of load-displacement responses for rectangular Al hollow tubes with bonded Al tubes filled with Alporas foam under compression is made with individual constituents and presented in Figure 8.9. For all cases, the uniaxial compression stress-strain response is similar: it has three distinct parts as shown in Figure 8.9. First part of the response shows an elastic part representing linear increase in stress with strain. Second part of the response shows the long plastic collapse plateau region due to localized collapse of the tube or foam cells and the third part represents the densification region. A similar load-displacement behavior was observed in compression testing of different tubes with different Al foams by other researchers [117, 153].

The compression behavior of Al tube alone shows the initial linear response of load with displacement up to a peak. A sudden decrement in load-carrying capacity appears subsequently due to a localized failure of the tube initiated at the upper end due to folds as shown in Figure 8.10 (a). Then, the entire collapse of the tube occurs at almost a uniform load till the entire tube self-folded with short wavelengths. This essentially is the location of locking displacement (strain) at which the load increases enormously without much displacement.

ATTENTION: The Singapore Copyright Act applies to the use of this document. Nanyang Technological University Library

Folding mechanism was observed for compression of rectangular Al tubes as shown in Figure 8.10 (a). Lobes were formed through-out the deformation due to initial buckling pattern of the side walls of the tube. It is known as symmetric crushing mode which was observed for square Aluminum extrusions [114].

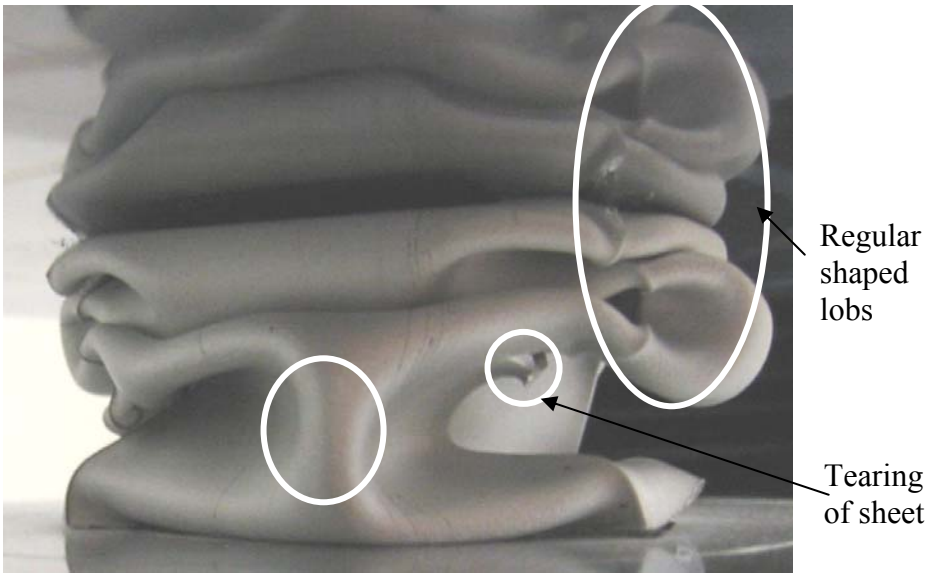

(a)

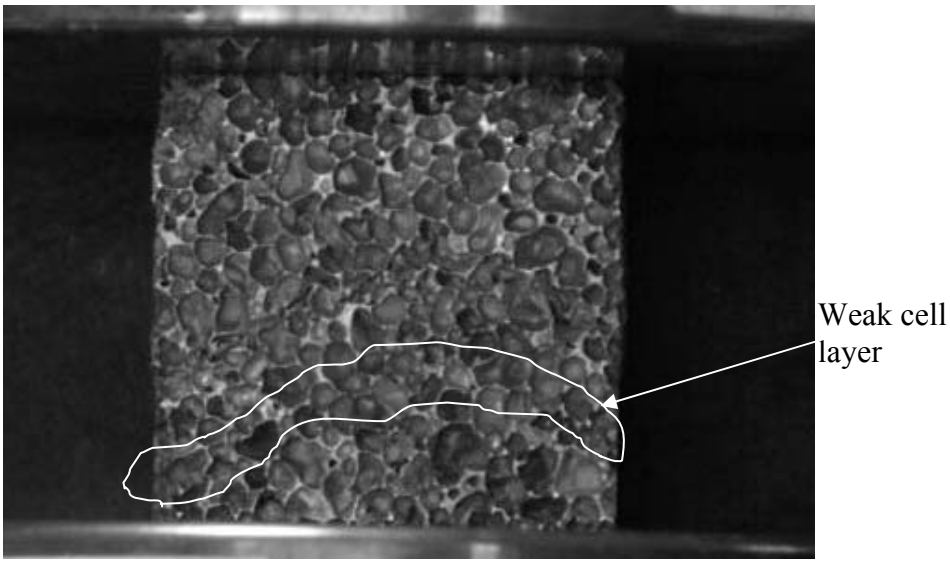

(b)

ATTENTION: The Singapore Copyright Act applies to the use of this document. Nanyang Technological University Library

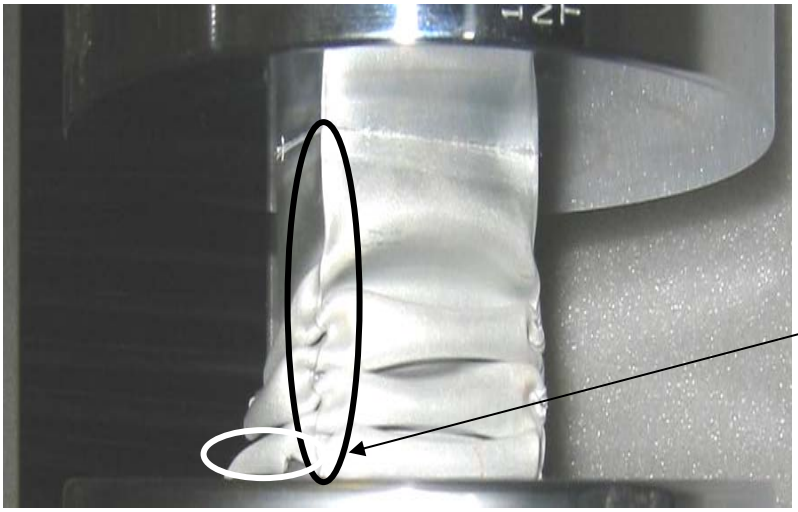

(c)

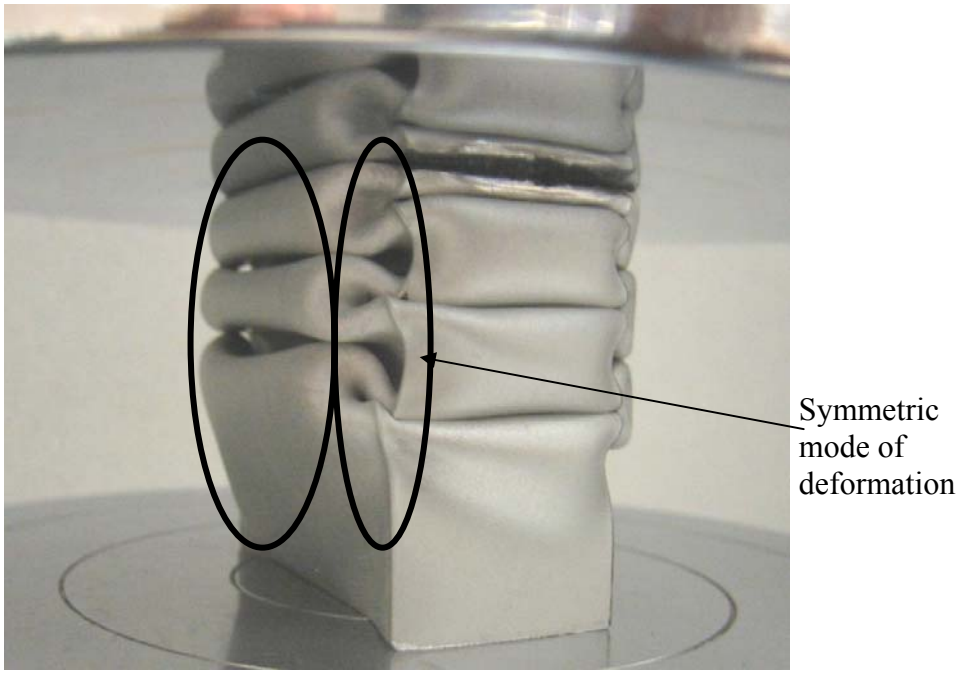

(d)

Figure8.10 Failure of specimens for various cases (a) failure of empty tube (b) failure of Alporas foam alone (c) failure of un-bonded Al tubes filled with Alporas foam (d) failure of bonded Al tubes filled with Alporas foam.

Here, the tearing off the bottom tube edge was observed as shown in Figure 8.10 (a), which occurred due to excessive localized deformation at that location in later stages of crushing. The compression behavior of Alporas foam block is shown in Figure 8.10 (b) and is similar to uniaxial compression of Alporas specimens which is explained in Chapter 3. Failure in

ATTENTION: The Singapore Copyright Act applies to the use of this document. Nanyang Technological University Library

terms of crushing of weak cell layer is shown in Figure 8.10 (b) with marking, this crushing leads to layer wise progressive failure of Alporas foam under compression.

Figure 8.9 also reveals the load-displacement behavior of bonded Al tube filled with Alporas foam. Clearly, there is an enhancement in the plateau stress level (in terms of load) with a slight decrease in locking strain. Because of the bond between Alporas foam and Al tube with the adhesive not only increase the plateau load level or the locking strain, but also increased significantly (around 23% compare to Al tube)the initial peak load at which first failure (by folding) in the tube occurred. The number of lobes was increased in the bonded tubes filled with Alporas foam in comparison to the empty Al tubes as shown in Figure 8.10 (a) and (d) because of reduction in buckling length as initial buckling is based on elastic type foundation. It agrees well for other Al foams in similar conditions [114].

Although theoretically, lobes of same shape should occurr in un-bonded Al tube filled with foam and empty Al tubes, experimentally, the lobes in un-bonded tubes filled with foam were found to be more irregular in shape than empty tubes as shown in Figure 8.10 (a) and (c). A symmetric mode of deformation was observed in bonded tubes filled with Alporas foam in comparison to the asymmetric mode of deformation for un-bonded tubes with foam as shown in Figure 8.10 (c) and (d).

The area under the uniaxial load-displacement curve is a measure of the energy absorbing capacity of the tube. So energy absorbed by different combinations as discussed above such as tube alone, tube with adhesive attach foam are measured and compared in Table-8.3 (where CS_{max} is consider as axial compressive displacement up to the starting of steepness in load in compression curves, its value is mention for each case in Table8.3).

It is clear from Table-8.3 that the specific mass energy absorption of the tubes is decreased by about 17 % with filling and bonding of Alporas foam of density ~ 9.5% with adhesive. This is due to the low specific mass energy absorption of Alporas foam of this density. Seitzberger et al [153] also found a similar response in their tests on steel tube filled with Alulight foam for certain densities. However, the overall absorption energy of the tube was increased due to the presence of foam. Actually a rigorous study on energy absorption with various densities of Alporas foam will find what density foam will be the best for increasing the specific mass energy absorption capacity of empty tubes.

ATTENTION: The Singapore Copyright Act applies to the use of this document. Nanyang Technological University Library

Table8.3 Experimental results of tubes compression in various combinations

Material	m_t **(g)**	F_{max} **(kN)**	CS_{max} **(mm)**	AE (CS_{max}) **(J)**	F_m (CS_{max}) **(kN)**	St_e **(%)**	S_f **(kJ/kg)**	S_e **(kJ/kg)**
Tube alone	49.68	17.15	70.00	589.48	8.42	70.00	16.95	11.87
Foam alone	51.20	9.65	70.00	303.86	4.34	70.00	8.48	5.935
Tube and foam addition	100.88	20.24	62.40	784.00	12.56	62.40	12.45	7.77
Foam filled tube without adhesive	100.88	18.28	49.74	670.98	13.49	49.74	13.37	6.65
Foam filled tube with adhesive	100.88	23.50	59.23	994.85	16.80	59.23	16.65	9.86

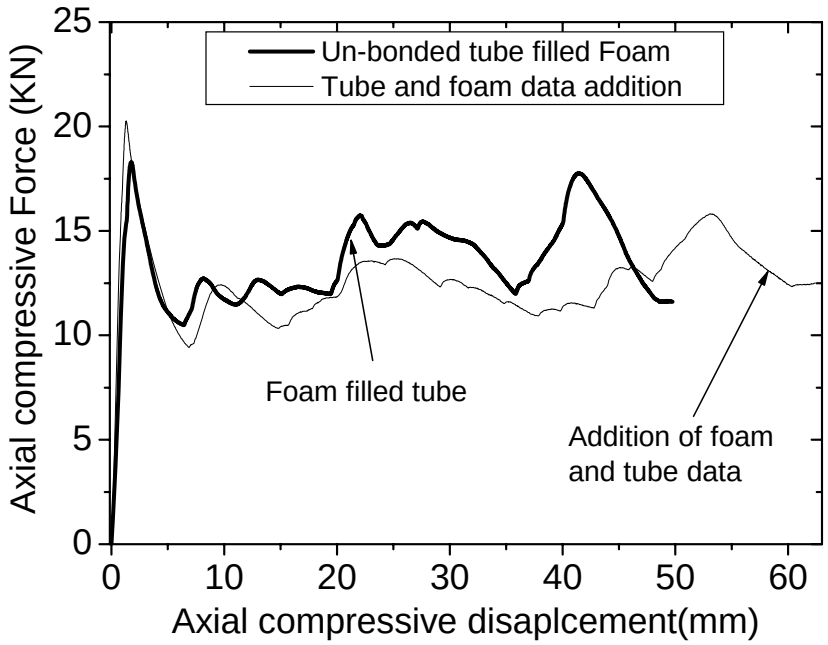

Figure8.11 Comparison of load-displacement response of un-bonded Al tube filled with Alporas foam under compression with response of summation of responses of Al tube and Alporas foam together.

ATTENTION: The Singapore Copyright Act applies to the use of this document. Nanyang Technological University Library

Interaction of the foam with the tube is seen in Figure 8.11, which shows the comparison of response of un-bonded Al tube filled with Alporas foam under compression with the response of summation of responses of Al tube and Alporas foam together. The first peak load was found to be slightly lower for un-bonded tube filled foam than the summation of foam and tube data but the plateau load was found to be higher.

Energy absorption (area under the curve) was found to be 10.5 % higher (up to 50 mm displacement) in un-bonded tubes filled with foam compare to summation data which reveal certain interaction between tube and foam as indicated on other foams by other researchers [9, 123].

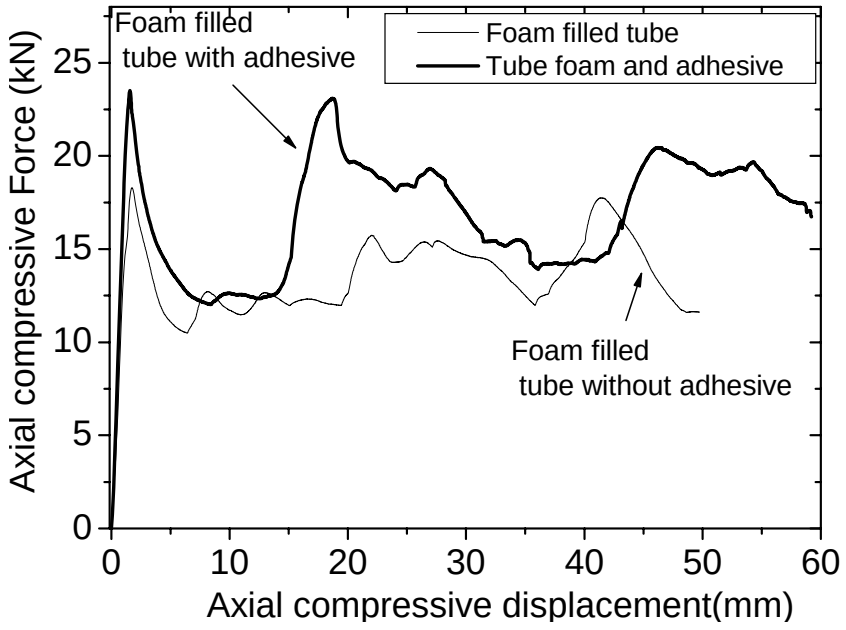

Figure8.12 Comparison of load-displacement response of bonded Al tube filled with Alporas foam under compression with response of un-bonded Al tube filled with Alporas foam.

The role of bonding between Al tube and Alporas foam was studied with the comparison of bonded tube with un-bonded tube as shown in Figure 8.12. It is clear from Figure 8.12 that because of bonding not only was the peak load increased but so was the plateau stress. It occurred due to efficient load transferring from tube to foam because of adhesive and many symmetric folds are seen in the bonded tubes. Additionally, this bond between tube and foam provide higher stiffness, so that the initiation of local buckling needs higher loads. Rupture of Al sheet at bottom tube corners was found in compression of un-bonded Al tubes filled with Alporas foam which could be due to poor contact between the tube and foam as shown with

ATTENTION: The Singapore Copyright Act applies to the use of this document. Nanyang Technological University Library

white ellipse in bottom of tube in Figure 8.10 (c). This tearing of tube with Alporas foam without adhesive is one factor involved in lowering down the locking strain value in comparison to bonded tube filled with Alporas foam.

ATTENTION: The Singapore Copyright Act applies to the use of this document. Nanyang Technological University Library

Chapter-9

Conclusions and Recommendations

9.1 Conclusions

On the basis of research work reported in the previous chapters the following conclusions are drawn:

1. Aluminum alloy foams namely Alporas of 9.5% relative density and Cymat foam of 4.7% relative density were used in the present study. The average cell size measured using Analytical Imaging Station (AIS) software was found to be 3.5 mm and 13.37 mm for Alporas and Cymat respectively. Strong hardening behavior was found in tensile testing of Alporas foam before peak stress. Similar behavior was observed under shear loading but the rate of hardening was low. Alporas foam was found to be crushed in bands in compression loading having weak cells in first band. Long plateaus were observed in both Alporas and Cymat foams under compression loading which indicate their usefulness in applications requiring energy absorption at uniform load. Tensile, compression and shear properties of Alporas foam are influenced by the size effect (ratio of specimen size to cell size). The size effect is negligible for Alporas foam under shear loading, when the specimen size exceeds the average foam cell size by 6 times. Alporas foam was also tested under four-point and three-point bending which shows little variation in bending strength and bending modulus with respect to the size ratio.

Mechanical characterization is carried out for materials used as face sheets of sandwich beams, columns and blocks tested in the present study under various loadings. Behavior of Al-1050 and Al-1100 sheets (used as face sheet for sandwich blocks and columns tested under indentation, impact and end compression loading) were found to be similar to pure Al of elastic perfectly plastic behavior under tensile loading. SS-314 sheet (used as a face sheet for sandwich blocks tested under indentation and impact loading) was found to be elastic–plastic strain hardening under tensile loading. Alumina sheets of various thicknesses (used as face sheet for sandwich beams tested under four-point bending) were found to have linear elastic-brittle behavior. Bending strength and modulus are fluctuated widely depending on

ATTENTION: The Singapore Copyright Act applies to the use of this document. Nanyang Technological University Library

the thickness of the sheet. CFRP sheet shows linear elastic–brittle failure under compression and tensile loading.

2. Sandwich beams comprising Alporas foam core and alumina face sheets with different geometries were tested under four point bending and three types of failure modes, namely face sheet cracking, core indentation and core shear were identified. Localized face sheet cracking was found in many specimens, in regions near to the indenters because the local stresses exceed the tensile strength of face sheet. Contact failure was not accounted for as a failure mode because even after exceeding this failure strength, the beam was able to take further load. The analytical equations for elastic stiffness and failure loads for various failure modes are in good agreement with the predictions by finite element simulation and experimentally measured values.

The failure mode map constructed in terms of non-dimensional geometrical parameters $(\bar{c}, \bar{t})$ of the sandwich beam for a given core and face sheet strength ratio will help to identify the expected failure mode for a given design geometry. As it predicts that the face sheet cracking will be the failure mode for the sandwich beams with larger span length *(l)* and small ratio of face sheet thickness, *t*, to core thickness, *c*. Local minimum weight design map for sandwich beam with Alporas foam core of fixed relative density and alumina face sheet of thickness 2 mm was constructed showing the overview of minimum weight of sandwich beam with optimal geometrical parameters for each possible failure mechanism as a function of structural load index.

3. Sandwich beams comprising Alporas foam core and carbon fiber reinforced laminate face sheets with different geometries have been investigated under three point bending. Core indentation, core shear and face sheet cracking were identified as three possible failure modes for failure of these sandwich beams. Localized cracking was absent in all sandwich beams with CFRP sheets due to high tensile strength of laminates as it was found in sandwich with alumina sheets. Predictions from analytical equations for elastic stiffness and load for failure of these beams for various failure modes were found to be in good agreement with the experimentally measured observations and numerically simulated responses.

An overview of these failure modes and their dependence on non-dimensional geometrical parameters $(\bar{c}, \bar{t})$ is provided in the form of a failure mode map. The dependence of core

ATTENTION: The Singapore Copyright Act applies to the use of this document. Nanyang Technological University Library

thickness is shown in terms of change over in domain of core shear and core indentation in failure mode map.

This work would allow the design engineer to choose the geometrical parameters for safe design of structure using sandwiches with Al foam core and brittle face sheets in real applications with enhanced load carrying capacity.

4. Alporas foam blocks with various face sheets were investigated under quasi-static indentation loading using flat and spherical punches. Foam core crushing below the indenter and tearing around the periphery of indenter were found to be the failure mechanism for samples without any face sheets. Various failure mechanisms were observed for the foam blocks with different face sheets under indentation loading, depending on factors such as face sheet constitutive property, thickness and indenter geometry. Different failure mechanisms appeared, such as face sheet bending in blocks with CFRP sheet, face sheet punching in blocks with Al sheet, core indentation in blocks with alumina sheet, bond failure in blocks with SS sheet etc. As precautions were taken for selecting the sizes of specimens and indenters, so load –displacement responses of the specimens and their associated failure mechanisms are not affected by size effects. But if different size ratios chosen which do not satisfied the size rule then the load-displacement response would be different with different failure mechanism compare to that in the present study. Here, constructing a failure map and showing the dependency of failure mode on various parameters such as face sheet thickness, its nature and core thickness was not carried out due to the complexity of failure mechanisms of these blocks having the additional factor of face sheet material. This comparison study enhances the understanding of designers for using light weight structure with metal foam where indentation type of loading is predominant.

5. Alporas and Cymat foam blocks with various face sheets including Al, SS, CFRP were studied under impact with a velocity of 6.7 m/sec, which is set to be guideline for assessing damage of any material for roll over crash in head on impact for automobiles. Blocks with SS face sheet of 0.5 mm thick absorbed almost all the impact energy especially the one with Alporas foam and proved to be best choice as energy absorber in comparison to blocks with other face sheets. The heavier weight of the SS sheet should be taken into account for comparison with other material when used as automobile parts.

ATTENTION: The Singapore Copyright Act applies to the use of this document. Nanyang Technological University Library

Foam core collapsing and tearing around the periphery of impactor were found as the failure mechanisms for samples of Alporas foam block without any face sheet under low velocity impact. Face sheet punching was found to be the only final failure mechanism (in addition to above mention foam failures) observed for the Alporas foam blocks having different face sheets except SS under impact, but the amount of energy absorption depends on the type of face sheet. Energy absorbing capacity was found to be higher with increased thickness of Alporas foam. The performance of blocks with CFRP sheets was found to be poor due to the low transverse strength of these laminates.

Foam core crumbing and face sheet bending were the failure mechanisms for block with Cymat foam and metal face sheets. However, large fluctuations were observed in their performance due to large size variations in the cells of Cymat foam. The performance of Alporas foam was found to be better than Cymat foam in terms of energy absorption. This study enhances the understanding of the selection criterion for usage of various sheets material as a face sheet of light weight sandwich structure with metal foam under low velocity impact.

6. Sandwich columns comprising Al foam core and Al face sheets with different geometries have been tested under end compression and three failure modes namely, Euler buckling, core shear and face sheet yielding were identified analytically. However, Euler buckling, core shear and bond failures were identified experimentally. The analytical equations for failure loads for these failure modes are in good agreement with experimentally measured values.

Similar to sandwich structure with brittle face sheets under bending, a failure mode map was constructed for the sandwich column for a given core and face sheet strength ratio. A design engineer can utilize the minimum weight design map constructed here for choosing the geometrical parameters for safe design of structure under compression loading such as wings of aircrafts or car bumpers.

7. Uniaxial compression tests were carried out on Al tubes of rectangular cross-section filled with Alporas foam in addition to measurement of responses from its all constituents to understand its behavior in depth. Folding of tube was found to be the final failure for each case under compression with different amount of cross-section of tube involved in folding with different fillings in tube such as Alporas foam alone, with adhesive or empty tube.

ATTENTION: The Singapore Copyright Act applies to the use of this document. Nanyang Technological University Library

Around 17% decrease in specific energy absorption was measured when bonded rectangular Al tubes filled with Alporas foam is compressed compared to empty Al tube. Increment in the plateau stress and decrease in locking strain was observed during the compression of un-bonded Al tube filled with Alporas foam over the combine responses of Al tube and Alporas foam. It indicates some interaction effect between the foam and tube. There is significant enhancement in the response of bonded Al tubes filled with Alporas foam: not only the first peak-stress for the tube-foam assembly increased by 28% but the plateau stress also increased by 20 %. This study shows the high potential of energy absorption of Alporas foam with rectangular tubes quantitatively.

9.2 Contributions

A series of analytical, numerical and experimental investigation have been carried out in order to achieve objectives of the study. The main contributions of this thesis are summarized as follows:

1. Development of failure mode map with non-dimensional geometrical parameters as variables for light weight sandwich beam comprising Al foam core and brittle face sheet under bending. This gave an overview of all the failures under which the beam can fail and the influence of sandwich geometry.
2. Determination of maximum possible failure modes for light weight sandwich column comprising Al foam core and Al face sheet under end compression loading. Development of minimum weight design map for specific strength ratio, for predicting the suitable geometry of sandwich column with Al foam core and Al face sheet under end compression and suitable geometry of sandwich beam with Al foam core and brittle face sheet under bending with maximum load carrying capacity.
3. Determination of maximum possible failure mechanisms under which a light weight sandwich structure with Al foam core and various face sheets under quasi-static indentation can fail.
4. Comparison of the performance of light weight Al foam sandwich structure with various face sheets under low velocity impact.
5. Determination of energy absorption capacity of Al rectangular tube filled with Al foam core under compression.

ATTENTION: The Singapore Copyright Act applies to the use of this document. Nanyang Technological University Library

Various novel things are carried out in this project which includes structural designing of hybrid sandwiches including metal foam core and especially with brittle materials as ceramic and carbon fiber reinforced plastics face sheet under bending. Another novel thing is the comparative study of structural behavior of Al foam sandwiches with various types of sheets (including elastic, elastic-perfectly plastic and elastic – plastic strain hardening) under indentation and low velocity impact which is very useful for designers to use foams for a variety of structures in various civil and defense applications.

9.3 Recommendations for future research scope

It is believed that research work on sandwich structures with brittle sheets such as composite or alumina will lead to investigations under various loading such as impact, blast protection and fatigue, in order to utilize the advantages of those structures over other in industrial applications. Failure analysis of multi- layered sandwiches comprising foam and various composites is worth for future work.

From the present study, it is clear that the type of indenter also plays an important role in the response of these foam structures under indentation. So responses from the conical indenter would be different in terms of failure mechanisms and load-displacement behavior. It is to be noted that the indentation response of foams especially Alporas depends upon the loading rate, which can differ by 34 % in plastic collapse strength and energy absorption [70]. Therefore, the failure mechanism appeared here could be different for another loading rate because the way in which the foam collapses is one factor contributing to the failure of the blocks. This research work on sandwich with different face sheets materials under indentation loading has future work scope on the changes of parameters such as size of the blocks, indentation depth, and type of foam, in order to have a more thorough understanding of foam indentation failures.

The performance of foam blocks with CFRP sheets under impact and indentation can be improved with multidirectional laminates of CFRP sheets or woven composites instead of unidirectional laminates. For a better understanding of energy absorption capacities of these foams, this work should continue for foam blocks with different thickness of face sheet under various low velocity impacts. Impact testing with different rates will help to understand the effect of loading rate on the failure of foam sandwiches with the selected geometry in

ATTENTION: The Singapore Copyright Act applies to the use of this document. Nanyang Technological University Library

addition to energy absorption. For indentation and impact problems, the indentor penetrates through the face sheet and the foam core. So, FEM study with cohesive zone elements with appropriate force-displacement (separation) law to model this punch through behavior is a good task for future for thorough understanding of this behavior.

The best density of foam for increasing the specific mass energy absorption capacity of empty tubes can be known with a rigorous study on the absorption of Alporas foam with various densities. For the better understanding of the energy absorption characteristics of Alporas foam, geometries with different cross-sections filled with Alporas foam with different tube wall materials can be selected for experimentation in the same way as shown in present study.

ATTENTION: The Singapore Copyright Act applies to the use of this document. Nanyang Technological University Library

References

[1] Banhart, J. (2003). Aluminum Foams: on the road to real applications. MRS bulletin, Vol. 28, pp. 290-295.

[2] Baumeister J., and Lehmhus D. (2003). Commercially available products made of PM aluminum foams-status and prospects. In: Proceedings of the 3rd International Conference on Cellular Metals and Metal Foaming Technology, Berlin, Germany, pp.13-18.

[3] Leyda, B. (2003). Applications for Open –cell metallic foams, MRS bulletin, Vol.28, pp. 292-293.

[4] Fuganti, A., Lorenzi L., Hanssen A.G., and Langseth M. (1999). Aluminum foam for automotive applications. In: Proceedings of the 1st International Conference on Metal foams and porous metal structures, Bermen, Germany, pp.5-13.

[5] Kretz, R., Hombergsmeier, E., and Eipper, K. (1999). Manufacturing and testing of aluminum foam structural parts for passenger cars demonstrated by example of a rear intermediate panel. In: Proceedings of the 1st International Conference on Metal foams and porous metal structures**,** Bermen, Germany, pp.23-29.

[6] Degisscher, Hans–Peter, and Kriszt, B. (Eds.)(2002).Handbook of cellular metals: production processing and applications, Wiley-Vch verilag GmbH, Weinheim.

[7] Banhart, J. (2001). Manufacture, characterization and application of cellular metals and metal foams. Progress in materials science, Vol.46, pp.559-632.

[8] Gibson L. J. (2003). Cellular solids. MRS bulletin, Vol.28, pp.270-271.

[9] Ashby, M.F., Evans, A.G., Fleck, N.A., Gibson, L.J., Hutchinson, J.W., and Wadley H.N.G. (2000). Metal foams: A design guide. Butterworth-Heinemann, Woburn.

[10] Gibson, L. J., and Ashby M.F. (1997). Cellular solids – structure and properties. 2nd edition, Cambridge: Cambridge university Press.

[11] Gibson, L. J. (2000). Mechanical Behavior of Metallic Foams. Annual Review Material Science, Vol.30, pp.191- 227.

[12] Chen, C., Harte, A-M, and Fleck, N. A. (2001). The plastic collapse of sandwich beams with a metallic foam core. International Journal of Mechanical sciences, Vol.43, pp.1483-1506.

ATTENTION: The Singapore Copyright Act applies to the use of this document. Nanyang Technological University Library

[13] Jessen, K., Fridrich B., and Rombach G. (2003). Al-foam production scrap-source for recyling. In: Proceedings of the 3rd International Conference on Cellular Metals and Metal Foaming Technology, Berlin, Germany, pp.543-548.

[14] Schnaik, A. Von, Reuter, M.A., and Nieuwkoop P. Van (2003). Secondary recovery of aluminum from aluminum foams. In: Proceedings of the 3rd International Conference on Cellular Metals and Metal Foaming Technology, Berlin, Germany, pp.549-555.

[15] C. Korner and R. F. Singer (2000). Processing of metal foams- challenges and opportunities. Advanced Engineering Materials, Vol.2, No. 4, pp.159-165.

[16] Simone, A.E., and Gibson L.J. (1998). Aluminum foams produced by liquid state processes. Acta Materillila, Vol.46, No. 9, pp.3109- 3123.

[17] www.metalfoam.net(latest by 22nd March, 2007).

[18] Miyoshi, T., Masao I., Akiyama, S., and Kitahara, A. (2000). ALPORAS aluminum Foam: Production Process, Properties and Applications. Advanced Engineering Materials, Vol.2, No. 4, pp.179- 183.

[19] Akiyama, S., Imagawa, K., Kitahara A., Nagata, S., Morimoto, K., Nishikawa, T. and Itoh, M. (1987). U.S. patent 4,713,277.

[20] Akiyama, S., Imagawa, K., Kitahara A., Nagata, S., Morimoto, K., Nishikawa, T. and Itoh, M. (1986). European patent Application 0,210,803 Al.

[21] Andrews, E., Sanders, W., and Gibson, L.J. (1999). Compressive and tensile behavior of aluminum foams. Materials Science and Engineering A, Vol. 270, pp.113-124.

[22] Miyoshi, T., Itoh, M., Mukai, T.,Kanahashi, H. , Kohzu, H., Tanabe, S. and Higashi, K. (1999). Enhancement of energy absorption in a closed-cell aluminum by the modification of cellular structures. Scripta Materillia, Vol. 41, No.10, pp.1055-1060.

[23] Kenesei, P., Kadar, Cs., Rajkovits, Zs., and Lendvai, J. (2004). The influence of cell-size distribution on the plastic deformation in metal foams. Scripta Materillia, Vol.50, pp.295– 300.

ATTENTION: The Singapore Copyright Act applies to the use of this document. Nanyang Technological University Library

[24] Onck, P.R., Andrews, E.W., and Gibson, L.J. (2001). Size effects in ductile cellular solids part I: Modeling. International Journal of Mechanical Sciences, Vol.43, pp.681-699.

[25] Andrews, E.W., Gioux, G., Onck, P., and Gibson, L.J. (2001). Size effects in ductile cellular solids part II: experimental results. International Journal of Mechanical Sciences, Vol.43, pp.701-713.

[26] Simone, A.E., and Gibson L.J. (1998). The effect of cell face curvature and corrugations on the stiffness and strength of metallic foams. Acta Materillia, Vol.46, No.11, pp.3929 – 3935.

[27] Simone, A.E., and Gibson L.J. (1998). Effects of solid distribution on the stiffness and strength of metallic foams. Acta Materillia, Vol.46, No.6, pp.2139 – 2150.

[27] Markaki, A.E., and Clyne, T.W. (2001). The effect of cell wall microstructure on the deformation and fracture of aluminum based foams. Acta Materilia, Vol.49, pp.1677-1686.

[28] Onck, P.R. (2003). Scale effects in cellular metals. MRS Bulletin, pp.279-283.

[29] Elmoutaouakkil, A., Salvo, L., Maire, E., and Peix, G. (2002). 2D and 3D characterization of metal foams using X-ray tomography. Advanced Engineering Materials, Vol.4, No. 10, pp.803- 807.

[30] Sugimura, Y., Meyer, J., He, M.Y., Bart-Smith, H., Grenstedt, J. and Evans, A.G. (1997). On the Mechanical properties of closed cell Al alloy foams. Acta Materillia, Vol.45, pp.5245 – 5239.

[31] McCULLOUGH, K.Y.G., Fleck, N.A., and Ashby, M.F. (1999). Uniaxial stress – strain behavior of Al Alloy Foams. Acta Materillia, Vol.47, No.8, pp.2323 – 2330.

[32] Fusheng, H., and Zhengang, Z. (1999). The mechanical behavior of foamed aluminum. Journal of Materials Science, Vol.34, pp.291-299.

[33] Bastawros, A-F, Bart-Smith, H., and Evans, A.G. (2000). Experimental analysis of deformation mechanisms in a closed- cell aluminum alloy foam. Journal of Mechanics and Physics of solids, Vol.48, pp.301-322.

[34] Olurin, O. B., Fleck, N. A., and Ashby, M. F. (2000). Deformation and fracture of aluminium foams. Materials Science and Engineering A, Vol.291, pp.136-146.

ATTENTION: The Singapore Copyright Act applies to the use of this document. Nanyang Technological University Library

[35] Motz, C., and Pippan, R. (2001). Deformation behavior of closed cell al foams in tension. Acta Materillia, Vol.49, pp.2463 – 2470.

[36] Kriszt, B., Foroughi, B., Faure, K. and Degischer, H.P.(2000).Behavior of Al foam under uniaxial compression. Materials Science and Technology, Vol.16, pp.792-796.

[37] Lu, T.J., and Ong, J.M. (2001). Characterization of closed celled cellular Al alloy. Journal of Materials Science, Vol.36, pp.2773-2786.

[38] Bart-Smith, H., Bastawros, A.-F., Mumm, D.R., Evans, A.G., Sypeck, D. J., and Wadley, H.N.G. (1998). Compressive deformation and yielding mechanisms in cellular Al alloys determined using X- Ray tomography and surface strain Mapping. Acta Materillia, Vol.46, No10, pp.3583– 3592.

[39] Bastawros, Ashraf-F, and Evans, A.G. (2000). Deformation heterogeneity in cellular al alloys. Advanced Engineering Materials, Vol.2, No. 4, pp.210-214.

[40] Ramamurthy, U., and Pual, A. (2004). Variability in mechanical properties of a metal foam. Acta Materiallia, Vol.52, No. 4, pp.869-876.

[41] Santosa, S. and Wierzbick, T. (1998). On the modeling of crush behavior of a closed-cell aluminum foam structure. Journal of the Mechanics and physics of solids, Vol.46, No. 4, pp.645-669.

[42] Pual, A., Seshacharyula T. and Ramamurthy, U. (1999). Tensile strength of a closed-cell al foam in the presence of notches and holes. Scripta Materillia, Vol.40, No.7, pp.809–814.

[43] Doyoyo, M. and Wierzbicki, T. (2003). Experimental studies on the yield behavior of ductile and brittle aluminum foams. International Journal of Plasticity, Vol.19, pp.1-19.

[44] Harte, A-M, Fleck, N.A., and Ashby, M.F. (2001). The fatigue strength of sandwich beams with an Al alloy foam core. International Journal of fatigue Vol.23, pp.499 – 507.

[45] Harte, A-M, Fleck, N.A., and Ashby, M.F. (1999). Fatigue failure of an open cell and a closed cell Al alloy foam. Acta Materillia, Vol.47, No. 8, pp.2511 – 2524.

ATTENTION: The Singapore Copyright Act applies to the use of this document. Nanyang Technological University Library

[46] Nieh, T. G., Higashi, K. and Wadsworth, J. (2000). Effect of cell morphology on the compressive properties of open-cell aluminum foams. Materials Science and Engineering A, Vol.283, pp.105-110.

[47] Fleck, N.A., Olurin,O.B., Chen, C. and Ashby,M.F. (2001). The effect of hole size upon the strength of metallic and polymeric foams. Journal of the Mechanics and Physics of Solids, Vol.49, pp.2015-2030.

[48] Deshpande, V.S., and Fleck, N.A. (2000). Isotropic constitutive models for metallic foams. Journal of the Mechanics and physics of solids, Vol.48, pp.1253-1283.

[49] Kesler, O., and Gibson, L.J. (2002). Size effects in metallic foam core sandwich beams. Materials science and Engineering A, Vol.326, pp.228-234.

[50] Bart-Smith, H., Hutchinson, J.W., Fleck, N.A., and Evans, A.G. (2002). Influence of imperfections on the performance of metal foam core sandwich panels. International Journal of Solids and Structures, Vol.39, pp.4999-5012.

[51] Chen, C., Fleck, N.A., and Shen, Y.P. (2003). Experimental and Micromechanical study of size effects in the constrained deformation of metallic foams. Key Engineering Materials, Vol.243-244, pp.421-426.

[52] Weaver, R. (1998). Ultrasonics in an aluminum foam. Ultrasonics, Vol.36, pp.435-442.

[53] Ji, Q., Le, L.H., Filipow, L.J., and Jackson, S.A. (1998). Ultrasonic wave propagation in water-saturated aluminum foams. Ultrasonics, Vol.36, pp.759-765.

[54] Fellah, Z.E.A., Depollier, C., Berger, S., Lauriks, W., Trompette, P., and Chepelon, J.-Y. (2003). Determination of transport parameters in air-saturated porous materials via reflected ultrasonic waves. Journal of the Acoustical Society of America, Vol.114, No.5, pp.2561-2569.

[55] Callister, W. D. (1994). Materials science and engineering an introduction, Third edition, john Wiley & sons, Inc.

[56] www.ms.ornl.gov/programs/energy/efcc/iof/chap21-2alo.pdf .

[57] http://en.wikipedia.org/wiki/Composite_material (latest by 22nd March 2007).

[58] Charambides, M. N., Hardouin, R., Kinloch, A.J., and Matthews, F.L. (1998). Adhesive-bonded repairs to fiber-composite materials I: Experimental. Composites Part A, Vol.29, pp.1371-1381.

ATTENTION: The Singapore Copyright Act applies to the use of this document. Nanyang Technological University Library

[59] www.baltek.com/products/info/sanwichp.html(latest by 22nd March 2007).

[60] Allen, H. G. (1969). Analysis and design of structural sandwich panels. Pergamon Press.

[61] Harte, A-M, Fleck, N.A., and Ashby, M.F. (2000). Sandwich panel design using Al alloy foam. Advanced Engineering Materials, Vol.2, No.4, pp.219- 222.

[62] McCormack, T.M., Miller, R., Kesler, O., and Gibson, L.J. (2001). Failure of sandwich beams with Metallic foam cores. International Journal of solids and structures, Vol.38, pp.4901-4920.

[63] Soden, P.D. (1996). Indentation of composite sandwich beams. Journal of strain analysis, Vol.31, No.5, pp.353-360.

[64] Wen, H.M., Reddy, T.Y., Reid, S.R., and Soden, P.D. (1998). Indentation, penetration and perforation of composite laminates and sandwich panels under quasi-static and projectile loading. Key Engineering Materials, Vol.141-143, pp.501-552.

[65] Bart-Smith, H., Hutchinson, J.W., Fleck, N.A., and Evans, A.G. (2001). Measurement and Analysis of the structural performance of cellular metal sandwich construction. International Journal of Mechanical Science, Vol.43, pp.1945-1963.

[66] Oliver, W. C., and Pharr, G.M. (2004). Measurement of hardness and elastic modulus by instrumented indentation: advances in understanding and refinements to methodology. Journal of Materials Research, Vol.19, No.1, pp.3-20.

[67] Kadar, C. Chmelk, F., Rajkovits, Z., and Lendvai, J. (2004). Acoustic emission measurements on metal foams, Journal of Alloys and Compounds, 378, pp.145-150.

[68] Olurin, O. B., Fleck, N. A., and Ashby, M. F. (2000). Indentation resistance of an Al foam. Scripta Materillia, Vol.43, pp.983– 989.

[69] Kadar,C., Maire, E., Borbely, A., Peix, G., Lendvai, J. and Rajkovits, Z.(2004). X-ray tomography and finite element simulation of the indentation behavior of metal foams. Materials Science and Engineering A, Vol.387-389, pp.321-389.

[70] Kumar, P.S., Ramachandra, S. and Ramamurhty, U. (2003). Effect of displacement – rate on the indentation behavior of an aluminum foam. Materials Science and Engineering A, Vol.347, pp.330-337.

ATTENTION: The Singapore Copyright Act applies to the use of this document. Nanyang Technological University Library

[71] Ramamurhty, U. and Kumaran, M. C. (2004). Mechanical property extraction through conical indentation of a closed-cell aluminum foam. Acta Materiallia, Vol.52, pp.181-189.

[72] Zenkert, D., Shipsha, A. and Persson, K. (2004). Static indentation and unloading response of sandwich beams. Composites: Part- B, Vol.35, pp.511-522.

[73] P. D. Soden, (1996). Indentation of composite sandwich plates. Journal of Strain Analysis, Vol.31, No.5, pp.353-360.

[74] Sburlati, R. (2002). The contact behavior between a foam core sandwich plate and a rigid indentor. Composites: Part-B, Vol.33, pp.325-332.

[75] Koissin, V., Shipsha, A. and Rizov, V. (2004). The inelastic quasi-static response of sandwich structures to local loading. Composite Structures, Vol.64, pp.129-138.

[76] Shuaeib, F.M. and Soden, P.D. (1997). Indentation failure of composite sandwich beams. Composites Science and Technology, Vol.57, pp.1249-1259.

[77] Rizov, V., Shipsha, A. and Zenkert, D. (2005). Indentation study of foam core sandwich composite panels. Composite Structures, Vol.69, pp.95-102.

[78] Rizov, V. I. (available online 11 April 2005).Elastic- plastic response of structural foams subjected to localized loads. Materials & Design.

[79] Rizov, V. I. (2006). Non-linear indentation behavior of foam core sandwich composite materials-A 2D approach. Computational Materials Science, Vol.35, No.2, pp.107-115.

[80] Miller, R.E. (2000). A continuum plasticity model for the constitutive and indentation behavior of foamed metals. International Journal of Mechanical Science, Vol.42, pp.729- 754.

[81] I. Sridhar and N.A. Fleck (unpublished work).

[82] Deshpande, V.S., and Fleck, N.A. (2000). High strain rate compressive behavior of aluminum alloys foams. International Journal of Impact Engineering, Vol.24, pp.277-298.

[83] Paul, A., and Ramamurthy, U. (2000). Strain rate sensitivity of a closed-cell aluminum foam. Materials Science and Engineering A, Vol.281, pp.1-7.

ATTENTION: The Singapore Copyright Act applies to the use of this document. Nanyang Technological University Library

[84] Mukai, T., Kanahashi, H., Miyoshi, T., Mabuchi, M., Nieh, T.G., and Higashi, K. (1999) .Experimental study of energy absorption in a closed-celled aluminum foam under dynamic loading. Scripta Materialia, Vol.40, No. 8, pp.921-927.

[85] Dannemann, K. A., and Lankford, Jr., J. (2000). High strain compression of closed-cell aluminum foams. Materials Science and Engineering A, Vol.293, pp.157-164.

[86] Kanahashi, H., Mukai, T., Yamada, Y., Shimojima, K., Mabuchi, M., Nieh, T.G. and Higashi, K. (2000). Dynamic compression of an ultra-low density aluminum foam. Materials Science and Engineering A, Vol.280, pp.349-353.

[87] Miyoshi, T., Itoh, M., Mukai, T., Kanahashi, H., Kanahashi, H., Kohzu, H., Tanabe, S. and Higashi, K. (1999). Enhancement of energy absorption in a closed-cell aluminum by the modification of cellular structures. Scripta Materialia, Vol.41, No.10, pp.1055-1060.

[88] Ramachandra, S., kumar , P. Sudheer, and Ramamurhty, U. (2003). Impact energy absorption in an Al foam at low velocities. Scripta Materialia, Vol.49, pp.741-745.

[89] Montanini, R. (2005). Measurement of strain rate sensitivity of aluminum foams for energy dissipation. International Journal of Mechanical Sciences, Vol.47, pp.26-42.

[90] Zhao H., Elnasri, I., and Abdennadher, S. (2005). An experimental study on the behavior under impact loading of metallic cellular materials. International Journal of Mechanical Sciences, Vol.47, pp.757-774.

[91] Tan, P. J., Harrigan, J. J., and Reid, S. R. (2002). Inertia effects in uniaxial dynamic compression of a closed cell aluminum alloy foam. Materials science and Technology, Vol.18, pp.480-488.

[92] Tan, P. J., Reid, S. R., Harrigan, J. J., Zou, Z. and Li, S. (2005). Dynamic compressive strength properties of aluminum foams. Part II- 'shock' theory and comparison with experimental data and numerical models. Journal of Mechanics and Physics of Solids, Vol.53, pp.2206-2230.

[93] Tan, P. J., Reid, S. R., Harrigan, J. J., Zou, Z., and Li, S. (2005). Dynamic compressive strength properties of aluminum foams. Part I- experimental data and observations. Journal of Mechanics and Physics of Solids, Vol.53, pp.2174-2205.

[94] Hall, I. W., Guden, M., and Yu, C.-J. (2000). Crushing of aluminum closed cell foams: density and strain rate effects. Scripta Materialia, Vol.43, pp.515-521.

ATTENTION: The Singapore Copyright Act applies to the use of this document. Nanyang Technological University Library

[95] Gassan, J., and Harwick, W. (2001). Behavior of aluminum foams under quasi-static and crash loadings. Journal of Materials Science Letters, Vol.20, pp.1047-1048.

[96] Mines, R.A.W., Worrall, C.M., and Gibson, A.G. (1994). The static and impact behavior of polymer composite sandwich beams. Composites, Vol.25, No. 2, pp.95-110.

[97] Mines, R.A.W. (1998). Impact energy absorption of polymer composite sandwich beams. Key Engineering Materials, Vol.141-143, pp.553-572.

[98] Bull, P.H., and Edgren, F. (2004). Compressive strength after impact of CFRP – foam core sandwich panels in marine applications. Composites, Part-B, Vol.35, pp.535-541.

[99] Kepler, J. (2004). Impact penetration of sandwich panels at different velocities – an experimental parameters study: part-I- parameters and results. Journal of Sandwich Structures and Materials, Vol.6, pp.357-374.

[100] Kepler, J. (2004). Impact penetration of sandwich panels at different velocities – an experimental parameters study: part-II- interpretation of results and modeling. Journal of Sandwich Structures and Materials, Vol.6, pp.379-397.

[101] Villanueva, G. R., and Cantwell, W. J. (2004). The high velocity impact response of composite and FML-reinforced sandwich structures. Composites Science and Technology, Vol.64, pp.35-54.

[102] Villanueva, G. R., and Cantwell, W. J. (2003). Low velocity impact response of novel fiber – reinforced aluminum foam sandwich structures. Journal of Materials Science Letters, Vol.22, pp.417-422.

[103] Kretz, R., Hausberger, K., and Gotzinger, B. (2002). Energy-absorption behavior of aluminum foams: head impact tests on the A-pillar of a car. Advanced Engineering Materials, Vol.4, No.10, pp.781-785.

[104] Yu, J.L., Wang, X., Wei, Z.G., and Wang, E. H. (2003). Deformation and failure mechanism of dynamically loaded sandwich beams with aluminum- foam core. International Journal of Impact Engineering, Vol.28, pp.331-347.

ATTENTION: The Singapore Copyright Act applies to the use of this document. Nanyang Technological University Library

[105] Gama, B. A., Bogetti, T. A., Fink, B. K., Yu, Chin-Jye, Claar, T.D., Eifert, H.H., and Jr. Gillespie, J.W. (2001). Aluminum foam integral armor: a new dimension in armor design. Composite Structures, Vol.52, pp.381-395.

[106] Hanssen, A.G., Enstock, L., and Langseth, M. (2002). Close – range blast loading of aluminum foam panels. International Journal Impact Engineering, Vol.27, pp.593-618.

[107] Destefanis, R., Schafer, F., Lambert, M., Faraud, M., and Schneider, E., (2003). Enhanced space debris shields for manned spacecraft. International Journal Impact Engineering, Vol.29, pp.215-226.

[108] Markaki, A. E. and Clyne, T. W. (2000) .Characterization of impact response of metallic foam/ceramic laminates, Materials Science and Technology. Vol.16, pp.785- 791.

[109] Hassen, A.G., Girard, Y., Olovsson, L., Berstad, T., and Langseth, M. (2006). A numerical model for bird strike of aluminum foam-based sandwich panels. International Journal Impact Engineering, Vol.32, pp.1127-1144.

[110] Fleck N.A., and Sridhar, I. (2002). End compression of sandwich columns. Composites: Part A, Vol.33, pp.353-359.

[111] Gdoutos, E.E., Daniel, I.M., and Wang, K.-A. (2003). Compression facing wrinkling of composite sandwich structures. Mechanics of Materials, Vol.35, pp.511-522.

[112] Vadakke, V., and Carlsson, L. A. (2004). Experimental investigation of compression failure of sandwich specimens with face/core debond. Composites: Part B, 35, pp.583-590.

[113] Roberts, J.C., Boyle, M.P., Wienhold, P.D., and White, G.J. (2002). Buckling, collapse and failure analysis of FRP sandwich panels. Composites: Part B, Vol.33, pp.315-324.

[114] Hassen, A. G., Langseth, M., and Hopperstad, O.S., (1999). Static crushing of square aluminum extrusions with aluminum foam filler. International Journal of Mechanical Sciences, Vol.41, pp.967-993.

ATTENTION: The Singapore Copyright Act applies to the use of this document. Nanyang Technological University Library

[115] Hassen, A. G., Langseth, M., and Hopperstad, O.S., (2002). Crash behavior of foam-based components: validation of numerical simulations. Advanced Engineering Materials, Vol.4, No.10, pp.771-776.

[116] Reyes, A., Hopperstad, O.S., Hassen, A. G., and Langseth, M., (2004). Modeling of material in foam-based components. International Journal of Impact Engineering, Vol.30, pp.805-834.

[117] Hassen, A. G., Langseth, M., and Hopperstad, O.S., (2000). Static and dynamic crushing of circular aluminum extrusions with aluminum foam filler. International Journal of Impact Engineering, Vol.24, pp.475-507.

[118] Santosa, S.P., Wierzbicki, T., Hassen, A. G., and Langseth, M. (2000). Experimental and numerical studies of foam-filled sections. International Journal of Impact Engineering, Vol.24, pp.509-534.

[119] Haberling, C., Haldenwanger, H.G., Bernard, T., Burzer, J., and Bergmann, H.W., (1999). Aluminum foams for energy absorbing structures under axial bending. In: Proceedings of the 1st International Conference on Metal foams and porous metal structures**,** Bermen, Germany, pp.37-44.

[120] Asavavisithchai, S., Slater, D., and Kennedy, A.R., (2004). Effect of tube length on the buckling mode and energy absorption of Al foam-filled tubes. Journal of Materials Science, Vol.39, pp.7395-7396.

[121] Asavavisithchai, S., Slater, D., and Kennedy, A.R., (2004). Effect of bonding strength on the energy absorption of Al foam-filled cylindrical tubes. Journal of Materials Science, Vol.39, pp.5873-5875.

[122] Claar, T.D., Yu, C.-J., Adkins, J.D., and Eifert, H.H. (2001). Properties and applications of aluminum foams: two case studies. In: Proceedings of the 2nd International Conference on cellular metals and metal foaming technology**,** Bermen, Germany, pp.37-42.

[123] Seitzberger, M., Rammerstorfer, F.G., Degischer, H.P., and Gradinger, R. (1997). Crushing of axially compressed steel tubes filled with aluminum foam. Acta Mechanica, Vol.125, pp.93-105.

[124] Hall, I.W., Guden, M., and Claar, T.D. (2002). Transverse and longitudinal crushing of aluminum-foam filled tubes. Scripta Materialia, Vol.46, pp.513-518.

ATTENTION: The Singapore Copyright Act applies to the use of this document. Nanyang Technological University Library

[125] Hall, I.W., Ebil, O., Guden, M., and Yu, C-J (2001). Quasi-static and dynamic crushing of empty and foam- filled tubes. Journal of Materials Science, Vol.36, pp.5853-5360.

[126] Sridhar, I. (2003). Plastic collapse of metal foam cored circular sandwich plates. In: proceedings of 1st International Conference on Design and analysis of protective structures against impact /impulsive/shock loads, Tokyo, Japan, pp.78-94.

[127] Deshpande, V.S., and Fleck, N.A. (2001). Collapse of truss core sandwich beams in 3-point bending. International Journal of Solids and Structures, Vol.38, pp.6175-6305.

[128] Budiansky, B. (1999). On the minimum weights of compression structures. International Journal of Solids and Structures, Vol.36, pp.3677-3708.

[129] Evans, A.G., Hutchinson, J.W., and Ashby, M.F. (1999). Multifunctionality of cellular metal systems. Progress in Materials Science, Vol.43, pp.171-221.

[130] Hanssen, A.G., Langseth, M., and Hopperstad, O.S. (2001). Optimum design for energy absorption of square aluminum columns with aluminum foam filler. International Journal of Mechanical Sciences, Vol.43, pp.153-176.

[131] Chen, W., Wierzbicki, T., and Santosa, S. (2002). Bending collapse of thin-walled beams with ultralight filler: numerical simulation and weight optimization. Acta Mechanica, Vol.153, pp.183-206.

[132] Kim, H.-S., Chen, W., and Wierzbicki, T. (2002). Weight and crash optimization of foam-filled three dimensional "S" frame. Computational Mechanics, Vol.28, pp.417-424.

[133] Reyes, A., Hopperstad, O.S., Berstad, T., Hanssen, A.G., and Langseth, M. (2003). Constitutive modeling of aluminum foam including fracture and statistical varialtion of density. European Journal of Mechanics A/Solids, Vol.22, pp.815-835.

[134] Hanssen, A.G., Hopperstad, O.S., Langseth, M., and Ilstad, H. (2002). Validation of constitutive models applicable to aluminum foams. International Journal of Mechanical Sciences, Vol.44, pp.359-406.

ATTENTION: The Singapore Copyright Act applies to the use of this document. Nanyang Technological University Library

[135] Onck, P.R. (2001). Application of a continuum constitutive model to metallic foam DEN-specimens in compression. International Journal of Mechanical Sciences, Vol.43, pp.2947-2959.

[136] Gioux, G., McCormacK, T.M., and Gibson, L.J. (2000). Failure of aluminum foams under multi axial loads. International Journal of Mechanical Science, Vol.42, pp.1097-1117.

[137] Abaqus Explicit manual Hibbit, Karlsson & Sorensen, Inc., USA, 2002.

[138] Abaqus theory manual, Hibbit, Karlsson & Sorensen, Inc., USA, 2002.

[139] Cymat foam technical manual.

[140] Instron testing machine user manual, Instron Singapore Pvt. Ltd.

[141] ASTM C-273. Standard Test Method for Shear Properties of Sandwich Core Materials. Technical report, ASTM, 2000.

[142] Popov, E. P. (1990). Engineering mechanics of solids. Prentice –Hall Inc.

[143] ASTM E8-04. Standard Test Methods for Tension Testing of Metallic Materials. Technical report, ASTM, 2004.

[144] Munro, R.G. (1997). Evaluated Material Properties for a Sintered alpha-Alumina. Journal of American Ceramic Society, Vol. 80, pp.1919–1928.

[145] Shakelford, J. F., and Alexander, W. (2001). CRC Materials science and Engineering handbook, (3rd edition) CRC press, U.S.

[146] Kumar S.B., PHD thesis, (submitted to Nanyang Technological University, Singapore in 2006).

[147] ASTM D3039/D3039M. Standard test methods for tensile properties of polymer matrix composite materials. Technical report, ASTM, 2001.

[148] Ashby, M.F., and Brechet, Y.J.M. (2003). Designing hybrid materials. Acta Materialia. Vol.51, No.19, pp.5801–5821.

[149] Steeves, C.A., and Fleck, N.A.(2004). Collapse mechanisms of sandwich beams with composite faces and a foam core, loaded in three-point bending. Part I: Analytical models and minimum weight design. International Journal of Mechanical Sciences. Vol.46, pp.561–583.

ATTENTION: The Singapore Copyright Act applies to the use of this document. Nanyang Technological University Library

[150] N. Tsuji and K. Kubomura. (1992). Non-linear compression stress-strain curve of pitchbased high modulus carbon fibre composites and structural responses. Journal of Materials Science, Vol. 27, pp 3782-3788.

[151] Steeves, C.A., and Fleck, N.A.(2004). Collapse mechanisms of sandwich beams with composite faces and a foam core, loaded in three-point bending. Part II: experimental investigation and numerical modeling. International Journal of Mechanical Sciences. Vol.46, pp.585–608.

[152] ASTM C364. Standard Test Method for Edgewise Compressive Strength of Sandwich Constructions . Technical report, ASTM, 1999.

[153] Seitzberger, M., Rammerstorfer, F.G., Gradinger, R., Degischer, H.P., Blaimschein, M., and Walch, C. (2000). Experimental studies on the quasi-static axial crushing of steel columns filled with Aluminum foam. International Journal of Solids and Structures, Vol.37, pp.4125-4147.

ATTENTION: The Singapore Copyright Act applies to the use of this document. Nanyang Technological University Library

Appendix A-1

FE modeling for one sandwich beam comprising Alporas foam core and alumina face sheet is described in here.

A1-1 FE Geometry and materials properties:

Alporas foam and alumina face sheets are modeled as rectangular blocks with their respective dimensions. Here, Alporas foam core was created in *Part module of ABAQUS/CAE as a 2D planar, deformable body with shell feature in 2D space with a dimensions of 135 mm X 20 mm. All the data were taken in only one unit system, MKS unit, in order to avoid aberrant output otherwise. Alumina face sheet was created in part module as a 2D planner, deformable body with shell feature in 2D space with a dimensions of 135 mm X 1 mm. Both upper and lower indenters were created as analytical rigid circular cylinder of radius 10 mm. Both indenters, being rigid bodies, are represented as a single reference point. Thickness of each part of the sandwich beam was assigned as 25 mm in the property module of ABAQUS/CAE. Material properties for Alporas foam core and alumina face sheet are listed in Table A1-1.

Table A1-1 Input data for Alporas (20 mm thick) and alumina sheet material (1 mm thick)

	Material	
Property	**Alporas foam**	**Alumina**
Elastic property		
Density (kg/m^3)	256	3960
Young's modulus (GPa)	0.50	467
Poisson's ratio	0.35	0.22
Bending strength (MPa)	-	306
Failure strain	-	0.000655
Plastic property		
Compression yield stress ratio	1.10	-
Plastic Poisson's ratio	0.03	-

Failure criterion for alumina face sheet was included in the "brittle cracking model" through input file. Failure criterion of Alporas foam was included through the "crushable foam hardening" option with the piecewise linear data of compression stress and strain of

ATTENTION: The Singapore Copyright Act applies to the use of this document. Nanyang Technological University Library

Alporas foam as obtained from the uniaxial compression experiments. Foam hardening data for 20mm thick Alporas foam core is shown in Table A1-2 from the compressive stress–strain data.

TableA1-2 Foam hardening data for Alporas foam(20 mm)

Yield stress (MPa)	Plastic strain
1.6300	0.000
1.6310	0.001
1.6318	0.002
1.6337	0.004
1.6356	0.006
1.6374	0.008
1.6393	0.010
1.6412	0.012
1.6430	0.014
1.6449	0.016
1.6468	0.018
1.6486	0.020
1.6767	0.500
1.6934	0.100
2.0973	0.500

A1-2 Contact interface:

When the sandwich is subjected to bending moment, the upper indenter attempts to compress it while the lower indenter tries to support it and the alumina face sheets and the foam block will impinge into each other. The appropriate constraints and contact interfaces between upper face sheet and foam block; the foam block and lower sheet; upper indenter and upper face sheet; lower indenter and lower face sheet have been defined in the ABAQUS software under “interaction module”.

ATTENTION: The Singapore Copyright Act applies to the use of this document. Nanyang Technological University Library

To model the constraints between face sheets and foam core "tie" option was used as it assumes perfect bonding between core and face sheets. To model the interactions between indenters and sheets contact surface (surface to surface contact) was used and the appropriate friction conditions were assigned for these interfaces. These contact (surface to surface contact) elements use a "master surface" and a "slave surface" to form a contact pair. This setting requires the surface with higher stiffness to be assigned as the master surface and with lower stiffness as the slave surface. The master surface is allowed to penetrate the slave surface but not the reverse. Therefore, two contact pairs were defined for indenter and alumina sheet contact as master surface and slave surface, respectively. Various contact condition; including sticking "frictionless" tangential behavior and "hard contact" normal behavior with no separation of contact surface were assigned for indenter and alumina face sheet.

A1-3 Loading and boundary conditions:

The boundary and loading conditions were defined by two steps: initial and Step-1, in the step module of ABAQUS/CAE. Boundary conditions were assigned in initial step while load was assigned under displacement control in Step-1.

In Step-1, EXPLICIT option was chosen as a solver because crushable foam model with isotropic hardening for Alporas and brittle cracking model for ceramic material are incorporated only in that solver. Here, there is no relation between the total step time and the calculated time by displacement. Initially, the simulation was run for high step time which was reduced slowly after analyzing the impact of reduction of step time each time. It is continued until a stage of optimization is achieved.

The geometrical and loading symmetry associated with four-point bending is exploited to reduce the computational time of the problem. In order to simulate the bending moment, the lower indenters (through reference point) was constraint by "encastre" option (U1 = U2 = U3 = UR1 = UR2 = UR3 = 0) such that all the degrees of freedom are set to zero as shown in Figure A1-1. In Step–1, upper indenter was displaced (through its reference point) by a magnitude of 5 mm (U2 = 0.005) to estimate the result under bending

ATTENTION: The Singapore Copyright Act applies to the use of this document. Nanyang Technological University Library

conditions. "smooth" amplitude option was chosen in order to simulate the smooth loading conditions.

The loading and supporting rollers are modeled as rigid-bodies. A contact algorithm within ABAQUS models the frictionless contact between the rollers and the sandwich beam. The multiaxial failure of metallic foams was investigated by Fleck and co-workers [48] and the failure surface can be approximated as

$$\phi \equiv \left[\frac{9}{9+\alpha^2}\right]\left[\sigma_e^2 + \alpha^2\sigma_m^2\right] - \left(\sigma_y^c\right)^2 = 0 \qquad \text{(A1-1)}$$

Where σ_y^c is the uniaxial compressive strength of foam, α is the aspect ratio of the elliptical yield surface (which is a function of foam plastic Poisson's ratio), σ_e is the Von-misses effective stress and σ_m is the mean stress.

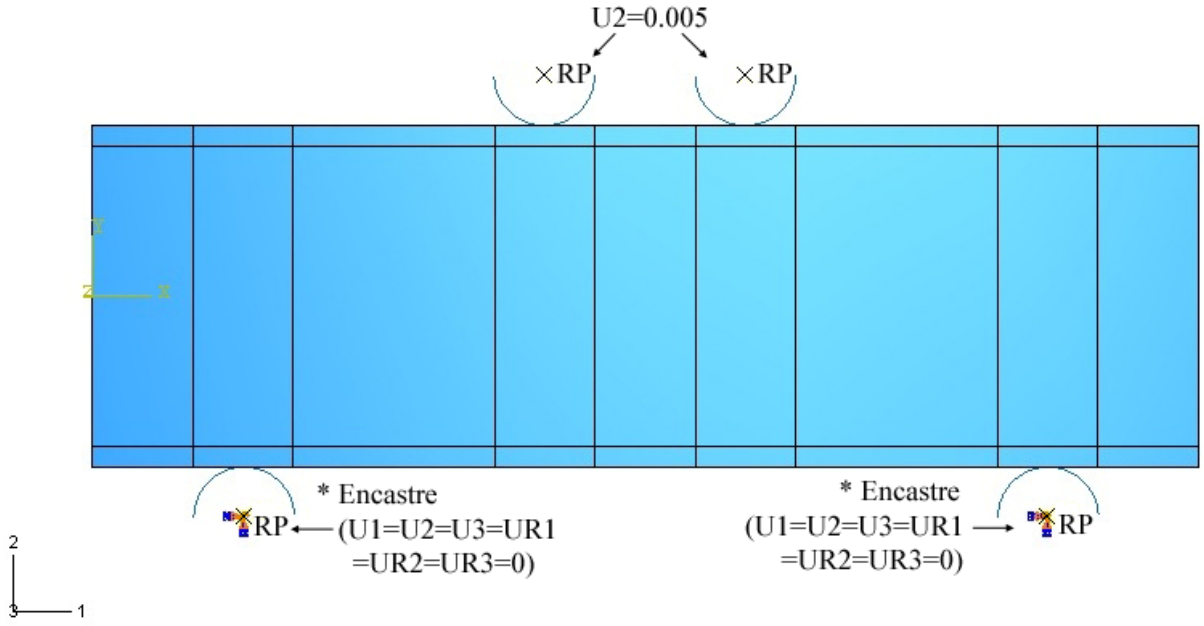

Figure A1-1 Loading of sandwich beam consisting of Alporas foam core and alumina face sheets having geometry no- 6 (Table4.1) with all boundary conditions.

A brittle cracking failure model is used to identify failure in the alumina face sheet. According to this model, a crack appears at any element only when the maximum principal tensile stress exceeds the material tensile strength in that region [138]. In the

ATTENTION: The Singapore Copyright Act applies to the use of this document. Nanyang Technological University Library

next load increment, the stresses applied to it are rotated normally for closing the crack in order to give same flexibility to study the behavior of brittle material which experiences crack opening and closing.

Both the metal foam constitutive model of Deshpande and Fleck [48] and brittle cracking model of alumina face sheet are in-built in ABAQUS explicit solver and hence it was used for simulation purposes.

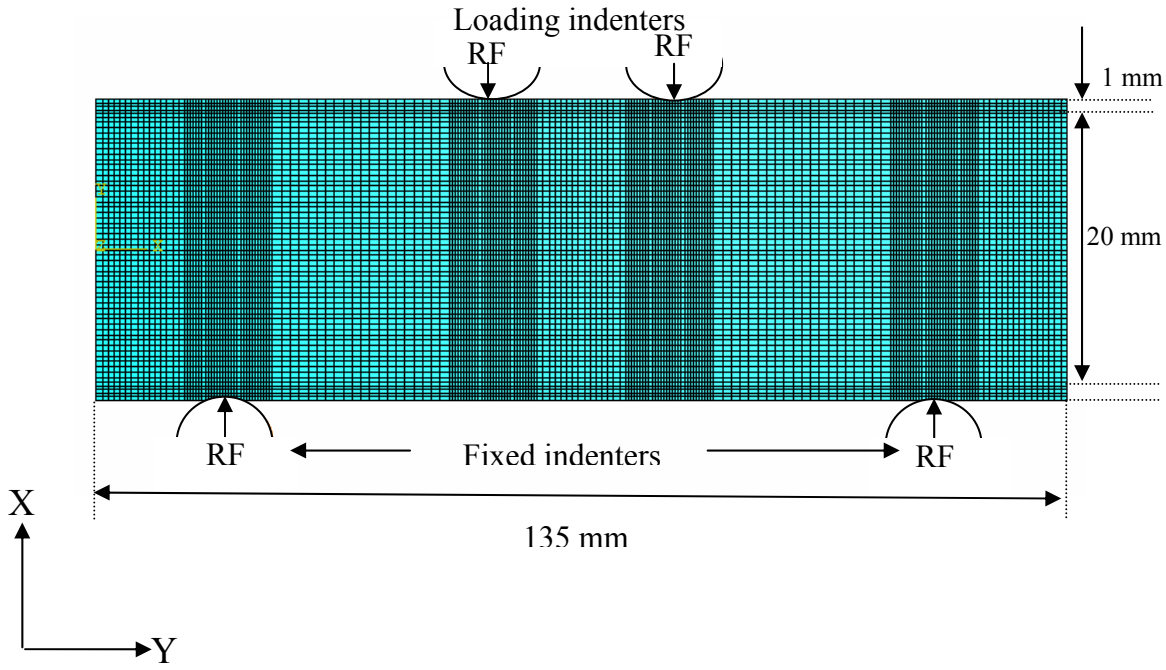

Figure A1-2 Typical finite elements mesh showing the geometry, loading and boundary conditions for geometry no-6 (Table-4.1).

A1-4 Mesh designing:

The foam core is completely constrained by the face sheets, also the face sheets are much wider than their thickness and hence a plane-strain analysis is justified on the sandwich beams. Four nodded bilinear plane strain quadrilateral elements with reduced integration (CPE4R) are used to discretize the sandwich beam geometry-6 (Table-4.1) as shown in Figure A1-2. In order to increase the accuracy of the iterations, second order accuracy was chosen in element control with enhancement of hourglass control. For accurate results, fine mesh is required in the region of high stress or strain gradient or in the contact region of the slave surface (deformable body) and master surface (analytical

ATTENTION: The Singapore Copyright Act applies to the use of this document. Nanyang Technological University Library

body). Elements of about 930 and nodes of about 1248 were created in each face sheet with 15500 elements and 15912 nodes in core of sandwich beam in the present model. Here, mesh refinement was carried out to verify the variation in the results and computational time. The results of several trial meshes were compared to select the final mesh. Figure A1-2. shows the meshing in the sandwich beam modeled with extra refining near the indenters. This mesh was found the most appropriate because further refinement barely affected the results of load-displacement response.

A1-5 Configuration of outputs:

The results of simulation of the sandwich assemblies have been viewed with the help of "Visualization Module" (ABAQUS/CAE). Results can be selected by "fieldoutput" and "historyouput" option of the "step" module of ABAQUS/CAE.

Different sets of results were created at important nodes or reference points, in order to save the results of stresses, load, deflections and strains at all those points. As the indenters were defined as analytical rigid body result in terms of load, deflection etc, cannot be requested in "field output" at representing reference points. So, results important to upper and lower indenters were requested in "history output". First few simulations were run to locate the failure region and therefore final simulations were run only after requesting different results in those regions by creating the necessary sets.

ATTENTION: The Singapore Copyright Act applies to the use of this document. Nanyang Technological University Library

List of Publications

1. Kapil Mohan, T. H. Yip and S. Idapalapati, "Failure of sandwich beams consisting of Alumina face sheet and an aluminum foam core", 3rd International conference on materials processing and performance (MP^3), Singapore, 24- 26 Nov. 2004.
2. Kapil Mohan, T. H. Yip, I. Sridhar and H. P. Seow, "Failure of sandwich beams consisting of alumina face sheet and aluminum foam core in bending", Materials Science and Engineering A-409 (2005), P 292-301.
3. Kapil Mohan, T. H. Yip and S. Idapalapati, "Failure of Sandwich Beams Consisting of Aluminum Foam Core and Carbon Fiber Reinforced Face Sheets", International symposium "Cellular Metals for structural and Functional Applications – CELLMET 2005" held in May 2005.
4. Kapil Mohan, T. H. Yip and S. Idapalapati, "Design of hybrid sandwich panel with aluminum foam core and carbon fiber reinforced plastic face sheets under three-point bending", Solid State Phenomena, Vol. 111, April 2006, pp. 63-66.
5. Kapil Mohan, T. H. Yip and S. Idapalapati, "Effect of Face sheet Material on the Indentation Response of Metallic Foams". Journal of Materials Science (Available online since 10th Feb 2007).